INVESTIGATION OF CELLULAR AND HUMORAL IMMUNE RESPONSES INDUCED BY SARS-CoV-2 VLP VACCINE IN PRE-CLINICAL AND CLINICAL STUDIES

A THESIS SUBMITTED TO

THE GRADUATE SCHOOL OF ENGINEERING AND SCIENCE

OF BILKENT UNIVERSITY

IN PARTIAL FULFILLMENT OF THE REQUIREMENTS FOR

THE DEGREE OF

MASTER OF SCIENCE

IN

MOLECULAR BIOLOGY AND GENETICS

By

Kadriye Tuğçe Bildik

August, 2022

Investigation of Cellular and Humoral Immune Responses Induced by SARS-CoV-2 VLP Vaccine in Pre-Clinical and Clinical Studies

By Kadriye Tuğçe Bildik

August, 2022

We certify that we have read this dissertation and that in our opinion it is fully adequate in scope and in quality, as a thesis for the degree of Master of Science.

İhsan Gürsel
(Advisor)

Murat Alper Cevher

Haluk Barbaros Oral

Approved for Graduate School of Engineering and Science

Orhan Arıkan
Director of the Graduate School of Engineering and Science

ABSTRACT

INVESTIGATION OF CELLULAR AND HUMORAL IMMUNE RESPONSES INDUCED BY SARS-COV-2 VLP VACCINE IN PRE-CLINICAL AND CLINICAL STUDIES

Kadriye Tuğçe Bildik

M.Sc. in Molecular Biology and Genetics

Advisor: İhsan Gürsel

August 2022

COVID-19 pandemic, caused by SARS-CoV-2, emerged in China in late 2019, and as of March 2020 has become a serious concern for the whole world due to severe progression of the disease especially in the elderly and high transmission rate of the virus. The ravages of pandemic on health sector, economy and social life accelerated the vaccine race as vaccination is the most critical measure to hamper the pace of the pandemic and the most important step for acquiring herd immunity. Various vaccine studies are registered by WHO most of which target Spike protein or a certain region of Spike protein, such as receptor binding domain (RBD) for inducing immune reactions. Alternatively, the use of virus-like particle (VLP) technology for vaccine development broadens the magnitude of immune responses as the four main structural proteins of the virus, Spike, Nucleocapsid, Membrane and Envelope, are incorporated. Therefore, we developed a VLP vaccine against SARS-CoV-2 and adjuvanted it using Alum and K3 CpG ODN. Herein, we investigated the humoral and cellular immune responses induced by SARS-CoV-2 VLP vaccine in pre-clinical and clinical studies. The results from pre-clinical experiments conducted on vaccinated BALB/c mice indicated that VLP vaccine triggered effective antibody response against Spike, Nucleocapsid, Wild Type RBD, Alpha RBD and Delta RBD proteins as shown by ELISA. Additionally, it was proven that the diminishing antibody responses can be boosted and a prolonged immune response was achieved by a third dose of VLP vaccine. For the clinical studies, the humoral and cellular immune responses of Phase II clinical trial volunteers were analyzed by employing ELISA and CBA methods respectively. The results obtained from ELISA demonstrated that the Phase II volunteers developed effective antibody titers against Spike, Nucleocapsid, Wild Type RBD, Alpha RBD and Delta RBD proteins. Analysis of the cellular immune responses by CBA showed that VLP vaccine induced a Th1-skewed immune reaction with coexistence of Th2-, Th17- and Treg related responses owing to its formulation with K3 CpG ODN and Alum. Taken together, our results indicated that SARS-CoV-2 VLP

vaccine triggered effective cellular and humoral immune reactions against Spike and Nucleocapsid along with RBD variants which proved the cross-protective response achieved. Elicitation of multi-functional immune response and adoptability of the VLP technology to newly emerging variants makes VLP vaccine a promising candidate for the future booster injections.

Key Words: COVID-19, SARS-CoV-2, Virus-like Particle, Vaccine, K3 CpG ODN, Humoral immune response Cellular immune response

ÖZET

SARS-COV-2 VLP AŞISINA KARŞI GELİŞTİRİLEN HÜMORAL VE HÜCRESEL İMMÜN YANITLARIN KLİNİK ÖNCESİ VE KLİNİK ÇALIŞMALARDA İNCELENMESİ

Kadriye Tuğçe Bildik

Moleküler Biyoloji ve Genetik, Yüksek Lisans

Danışman: İhsan Gürsel

Ağustos 2022

SARS-CoV-2 olarak adlandırılan bir virüsün sebep olduğu COVID-19 pandemisi, 2019'un sonlarında Çin'de ortaya çıkmış ve 2020'nin Mart ayı itibariyle, hastalığın özellikle yaşlılarda ciddi şekilde ilerlemesi ve virüsün bulaşma oranının yüksek olması nedeniyle tüm dünyayı ciddi bir endişe haline getirmiştir. Pandeminin sağlık sektörüne, ekonomiye ve sosyal hayata verdiği tahribat, aşılamanın pandeminin hızını kesmedeki en kritik önlem ve sürü bağışıklığı kazanma açısından en önemli adım olması nedeniyle aşı yarışını hızlandırdı. DSÖ tarafından, çoğu Spike proteinini veya Spike proteininin belirli bir bölgesini, örneğin reseptör bağlama alanı (RBD) gibi, hedef alarak bağışıklık sistemini harekete geçirmeyi hedefleyen çeşitli aşı çalışmaları kayıt altına alınmıştır. Alternatif olarak, aşı geliştirme için virüs benzeri parçacık (VLP) teknolojisinin kullanılması, virüsün dört ana yapısal proteini olan Spike, Nucleocapsid, Membrane ve Envelope dahil edildiğinden bağışıklık tepkilerini güçlendirmektedir. Bu nedenle, SARS-CoV-2'ye karşı bir VLP aşısı geliştirdik ve bu aşıyı Alum ve K3 CpG ODN kullanarak adjuvanladık. Bu tez çalışmasında, klinik öncesi ve klinik çalışmalarda SARS-CoV-2 VLP aşısının neden olduğu hümoral ve hücresel bağışıklık yanıtlarını araştırdık. Aşılanmış BALB/c fareleri üzerinde yürütülen klinik öncesi deneylerin sonuçları, VLP aşısının, ELISA ile gösterildiği gibi Spike, Nucleocapsid, Wild Type RBD, Alpha RBD ve Delta RBD proteinlerine karşı etkili antikor tepkisini tetiklediğini gösterdi. Ek olarak, üçüncü doz VLP aşısı ile azalan antikor tepkilerinin artırılabileceği ve uzun süreli bir bağışıklık tepkisi elde edilebileceği kanıtlandı. Klinik araştırmalar için, Faz II klinik deney gönüllülerinin hümoral ve hücresel bağışıklık tepkileri, sırasıyla ELISA ve CBA yöntemleri kullanılarak analiz edildi. ELISA'dan elde edilen sonuçlar, Faz II gönüllülerinin Spike, Nucleocapsid, Wild Type RBD, Alpha RBD ve Delta RBD proteinlerine karşı etkili antikor titreleri geliştirdiğini gösterdi. CBA ile değerlendirilen hücresel bağışıklık yanıtları, VLP aşısının, K3 CpG ODN ve Alum ile formülasyonu sayesinde Th2, Th17 ve Treg hücre yanıtlarıyla birlikte Th1-baskın bir bağışıklık reaksiyonunu indüklediğini gösterdi. Sonuç olarak, bu çalışma, SARS-CoV-2 VLP aşısının, Spike'a ve Nucleocapsid'e karşı etkili

hücresel ve hümoral bağışıklık reaksiyonlarını tetiklerken RBD varyantlarına karşı da yüksek antikor yanıtlarının oluşturulması ile aşının çapraz koruyucu etkisini kanıtlamaktadır. Çok işlevli bağışıklık tepkisinin ortaya çıkarılması ve VLP teknolojisinin yeni ortaya çıkan varyantlara kolayca uyarlanabilirliği, VLP aşısını gelecekteki rapel aşılar için umut verici bir aday haline getirmektedir.

Anahtar Sözcükler: COVID-19, SARS-CoV-2, Virus benzeri parçacık, Aşı, K3 CpG ODN, Humoral bağışıklık, Hücresel bağışıklık

ACKNOWLEDGEMENTS

I owe my deepest gratitude to my advisor Prof. İhsan Gürsel with whom I am honored to have worked with. With his endless support, encouragement, guidance and patience during my Master's degree studies, he has been not only my thesis advisor but also became a lifelong mentor for me whose support I will feel throughout my whole life. I also would like to extend my sincerest thanks Prof. Mayda Gürsel for her invaluable continuous support throughout this project. I feel very privileged to have had the chance of working with her and learning from her for the last two years.

I would like to appreciate my thesis jury members, Asst. Prof. Murat Alper Cevher and Prof. Haluk Barbaros Oral, for their collaboration, support and valuable suggestions.

I would like to thank members of THORLAB: Artun Bülbül, Tuğçe Yıldırım, Muzaffer Yıldırım, Yasemin Ceylan, İrem Abraş, Tolunay Ataç for their understanding and support during my studies. I would like to offer my special thanks to Ege Dedeoğlu, Oğuzhan Tarman, Pelin Ersan, Ünal Metin Tokat and Barış Küçükkaraduman for their valuable friendship over the last 3 years. Long-lasting lab hours would become unbearable if it weren't for the coffee breaks, dinners, lunch breaks and especially the meetings we had together. I would like to express my very great appreciation to Nilsu Turay, İrem Evcili, Bilgehan İbibik and Naz Bozbeyoğlu Özdemir for their invaluable friendship. I am very much grateful for all of the wonderful memories we had together.

I would like to express one of my deepest gratitude to Aslı Bartan and Berfu Saraydar. I cannot find enough words to describe how much thankful I am to have friends like you. With your unconditional support and love, you have been like my family in Ankara. We have shared so many memories full of both laughter and tears together and I hope we will have many more joyful years ahead of us. I feel so lucky to call you my friends.

My greatest thanks are for my family; my mother Nazan, my father Memet, my brother Can and my sister Zehra. Without their continuous love and faith, my achievements would not be possible. I will be forever in debt for their endless support.

Lastly, I would like to thank TÜBİTAK and Ministry of Industry and Technology for the financial support of my studies.

TABLE OF CONTENTS

ABSTRACT ii
ÖZET iv
ACKNOWLEDGEMENTS vi
TABLE OF CONTENTS vii
LIST OF FIGURES x
ABBREVIATIONS xii
INTRODUCTION 1
1.1. Immune System 1
1.1.1. Innate Immunity 1
1.1.1.1. Pattern Recognition Receptors (PRRs) 2
1.1.2. Adaptive Immunity 4
1.1.2.1. Cell Mediated Immunity 4
1.1.2.1.1. Differentiation of $CD4^+$ T Helper Cells & Th1/Th2 Responses 5
1.1.2.2. B-cell Mediated Immunity 7
1.1.2.2.1. Antibody (Immunoglobulin) Functions in Adaptive Immunity 8
1.2. COVID-19 9
1.2.1. Genomic and Structural Characteristics of SARS-CoV-2 9
1.2.2. Transmission Routes of SARS-CoV-2 10
1.2.3. Entry of SARS-CoV-2 into Host Cells and Pathogenesis 11
1.2.4. Immune Response Evoked by SARS-CoV-2 12
1.2.4.1. Innate Immune Response to SARS-CoV-2 12
1.2.4.2. Adaptive Immune Response to SARS-CoV-2 13
1.3. Vaccine Studies Against COVID-19 14
1.3.1. Virus-like Particle (VLP) Vaccines 15
1.3.2. VLP Vaccine Adjuvants 15
1.4. Clinical Trials 17

1.4.1. Phase I Clinical Trials 17
1.4.2. Phase II Clinical Trials 18
1.4.3. Phase III Clinical Trials 18
1.4.4. Phase IV Clinical Trials 18
1.5. Aims and Outline of the Study 19
MATERIALS AND METHODS 20
2.1. Materials 20
2.1.1. Cell Culture Media, Solutions and Buffers 20
2.1.2. ELISA Antibodies, Chemicals and Reagents 20
2.1.3. Kits 21
2.1.4. Equipment 21
2.1.5. Buffer, Media and Solution Contents 22
2.2. Methods 23
2.2.1. Cell Culture 23
2.2.1.1. Peripheral Blood Mononuclear Cells (PBMCs) and Plasma Isolation 23
2.2.1.2. Cell Counting 23
2.2.2. Production of Recombinant Proteins 23
2.2.3. Determination of Immune Responses from Sera 24
2.2.3.1. Determination of IgG Levels in Human Sera by Enzyme Linked Immunosorbent Assay (ELISA) 24
2.2.3.2. Determination of IgG Levels in Mice Sera by ELISA 25
2.2.3.3. Determination of IgG Levels in Human Sera by Corona Hunter Kit 25
2.2.3.4. Determination of Neutralizing Antibody Levels in Human Sera by SARS-CoV-IgG Quant 26
2.2.4. Assessment of T-Cell Immune Responses 26
2.2.4.1. Cytometric Bead Array (CBA) 26
2.2.5. *In Vivo* Experiments and Immunization Practices in Phase I & Phase II Clinical Trials 27
2.2.5.1. Immunization Studies on Mice 27
2.2.5.2. Vaccination Phase II Volunteers 27

RESULTS 29
3.1. Pre-Clinical Data 29
3.2. Clinical Data 35
3.2.1. Assessment of Humoral Immune Responses from Sera 35
3.2.2. Assessment of Cellular Immune Responses 45
DISCUSSION 51
BIBLIOGRAPHY 60
APPENDIX 72
COPYRIGHT PERMISSIONS 118

LIST OF FIGURES

Figure 1.1. TLR ligands and their signaling pathways. 3
Figure 1.2. Commitment factors for differentiation into Th cell subtypes and immunological functions of Th cells. 6
Figure 1.3. T-cell dependent and independent humoral immune responses. 8
Figure 1.4. Diagrams representing structural and genomic features of SARS-CoV-2. 10
Figure 1.5. Entry pathways of SARS-CoV-2 into host cells. 12
Figure 1.6. Development of humoral immune response against SARS-CoV-2. 14
Figure 3.1. Assessment of IgG responses of immunized mice against homemade recombinant trimeric Spike (S) protein (4 μg/ml) by ELISA. 30
Figure 3.2. Assessment of IgG responses of immunized mice against homemade recombinant nucleocapsid (N) protein (1 μg/ml) by ELISA. 31
Figure 3.3. Assessment of IgG responses of immunized mice against homemade recombinant receptor binding domain wild type (RBD WT) protein (4 μg/ml) by ELISA. 32
Figure 3.4. Assessment of IgG responses of immunized mice against commercial recombinant receptor binding domain UK (RBD UK) protein (1 μg/ml) by ELISA. 33
Figure 3.5. Assessment of IgG responses of immunized mice against commercial recombinant receptor binding domain Delta (RBD Delta) protein (1 μg/ml) by ELISA. 34
Figure 3.6. Determination of anti-Spike IgG titers of volunteers at days 0, 21, 35, 49 and 90 36
Figure 3.7. Determination of IgG titers of volunteers against homemade recombinant Nucleocapsid (N) (4 μg/ml) protein at days 0, 21, 35, 49 and 90 38
Figure 3.8. Determination of anti-RBD IgG titers of volunteers at days 35, 49 and 90 39
Figure 3.9. Quantification of neutralizing antibody levels of the serum and plasma samples using SARS-CoV-2 IgG Quant method performed via ARCHITECT i System. 42
Figure 3.10. Determination of anti-homemade recombinant Spike (S) (6 μg/ml) IgG titers of volunteers with no SARS-CoV-2 infection during the course of Phase II clinical trial at days 0, 21, 35, 49 and 90 43
Figure 3.11. Th1-related cytokine responses of PBMCs collected from vaccinated volunteers in Day 35 45
Figure 3.12. Th2-related cytokine responses of PBMCs collected from vaccinated volunteers in Day 35 46
Figure 3.13. Th17-based cytokine responses of PBMCs collected from vaccinated volunteers in Day 35 47

Figure 3.14. IL-6 and IL-10 cytokine responses of PBMCs collected from vaccinated volunteers in Day 35 48
Figure 3.15. The percent distribution of Th1, Th2, Th17, T-reg and IL-6 based immune responses are presented in a pie chart. 49

ABBREVIATIONS

ACE-2	Angiotensin Converting Enzyme-2
Alum	Aluminum Hydroxide
APC	Antigen Presenting Cells
BCR	B Cell Receptor
BSA	Bovine Serum Albumin
CBA	Cytometric Bead Array
CD	Cluster of Differentiation
CMI	Cell Mediated Immunity
COVID-19	Coronavirus Disease-19
CpG	Cytosine Phosphoguanosine
CV	Convoluted Vesicle
DAMP	Danger Associated Molecular Patterns
DC	Dendritic Cell
DMSO	Dimethyl Sulfoxide
DMV	Double Membrane Vesicle
DNA	Deoxyribonucleic Acid
DPBS	Dulbecco's Phosphate Buffer Saline
E	Envelope
ELISA	Enzyme-Linked ImmunoSorbent Assay
ELISpot	Enzyme-Linked Immune Absorbent Spot
ERGIC	Endoplasmic Reticulum-Golgi Intermediate Complex
FBS	Heat Inactivated Fetal Bovine Serum
FDA	Food and Drug Administration
FDC	Follicular Dendritic Cell
IFN	Interferon

Ig	Immunoglobulin
IL	Interleukin
IP-10	Interferon γ-Induced Protein 10
IRF	Interferon Regulatory Factor
LNP	Lipid Nanoparticles
LSM	Lymphocyte Separation Medium
M	Membrane
MERS	Middle East Respiratory Syndrome
MHC	Mahor Histocompatibility Complex
mRNA	Messenger Ribonucleic Acid
MyD88	Myeloid differentiation factor 88
N	Nucleocapsid
ODN	Oligodeoxynucleotide
ODN	Oligodeoxynucleotide
ORF	Open Reading Frame
PAMP	Pathogen Associated Molecular Patterns
PBMC	Peripheral Blood Mononuclear Cell
pDC	Plasmacytoid Dendritic Cells
PNPP	p-nitrophenyl phosphate
PRR	Pattern Recognition Receptors
RBD	Receptor Binding Domain
RTC	Replication and Transcription Complex
S	Spike
SARS-CoV-2	Severe Acute Respiratory Syndrome Coronavirus 2
STAT	Signal transducer and activator of transcription
TCR	T Cell Receptor
Th	Helper T Cell

TLR	Toll-like Receptor
TMPRSS2	Transmembrane Protease Serine 2
TNF-α	Tumor Necrosis Factor Alpha
Treg	Regulatory T Cell
TRIF	TIR domain-containing adaptor protein
VLP	Virus-Like Particle
WHO	World Health Organization

CHAPTER 1

INTRODUCTION

1.1. Immune System

Pathogens, non-pathogenic microbes, allergenic substances, and toxic materials exist all around the world exposing homeostasis of humans and other mammalians to constant danger. Therefore, a protective and defensive mechanism called immune system is evolved for detection and elimination of pathogens and toxins [1]. The basis of immune system relies on discrimination of self from non-self. Thus, it is crucial that the pathogens are targeted in a controlled manner without harming any of the host's tissues [2]. This imperativeness of making a clear distinction has evolved immune system to recognize a vast array of pathogens through various mechanisms. These mechanisms can be classified under two main headings called innate and adaptive immune responses depending on the rapidness and specificity of the response elicited [3]. The innate immune system sets the initial response against a detected pathogen through physical and chemical barriers, neutrophils, macrophages, complement system, cytokines and monocytes [4]. The reaction set by innate immune mechanism is not specific to antigens as the common microbial patterns are targeted [3]. However, the second arm of the immune system which consists of adaptive immune responses target pathogens based on antigen specificity thereby eliciting a stronger and more specific reaction [1]. If the innate immune mechanisms are not sufficient to clear infection, the adaptive immune system is triggered by cytokines and interaction of various immune cells. The adaptive branch of the immune system operates by cell-mediated responses through activation of T-cells and humoral immunity which involves production of antibodies by B-cells. These enable adaptive immune cells to generate a stronger and longer immune response with immunological memory so that in the case of reinfection, a quicker response can be elicited for the same antigen [2,5].

1.1.1. Innate Immunity

Innate immunity constitutes the first line of defense for body's response against pathogens and can be divided into two arms as constitutive and inducible mechanisms. The constitutive arm of the innate immune system can be further divided into two categories as chemical and physical barriers. The physical barriers include the skin, hair and cilia while the chemical barriers are mucus, stomach acid, digestive enzymes in mouth, urine flow, antimicrobial enzymes and etc. If the physical and chemical barriers of the innate immune system are breached by pathogens, the inducible arm involving innate immune cells is activated. The inducible immune mechanisms are

generated through activation of complement cascade or the stimulation of pattern recognition receptors (PRRs) by pathogen associated molecular patterns (PAMPs). The complement cascade mediated by plasma and cell surface proteins results in targeting of pathogens for lysis and phagocytosis by macrophages. Since microorganisms have evolved to evade host's immune defense mechanisms, pathogens can penetrate despite of anatomic barriers and complement system. In such cases, the innate immune cells containing PRRs are stimulated via PAMPs and the pathogens are targeted to be destroyed. If recognition of PAMPs and activation of effector cells though PRRs also fail then adaptive immune responses are induced in order to generate an amplified immune response with long term memory [2,3,6].

1.1.1.1. Pattern Recognition Receptors (PRRs)

PRRs are the receptors expressed in host's innate immune cells and recognize PAMPs or danger associated molecular patterns (DAMPs) which activate signaling cascades resulting in upregulation of certain genes' expressions, secretion of chemokines and cytokines and expression of immunoreceptors. Stimulation of PRRs not only facilitates destruction of pathogen by early immune response but also integrates innate immune responses into adaptive immunity [7]. There are different classes of PRRs and each member of these classes recognize a distinct type of PAMP leading to signaling by different pathways [8]. Toll-like receptors (TLRs) are one of the most widely studied class of PRRs. Reports indicate that humans and mice express 10 (TLR1-10) and 12 (TLR1-9 and TLR11-13) TLRs respectively [9]. Depending on the location of TLR it can be classified as cell surface or endosomal. While TLRs 1, 2, 4, 5, and 6 are expressed on the cell membrane TLRs 3, 7, 8, and 9 are expressed on the surface of endosomes. Based on recognition of similar PAMPs, TLRs can be divided into two groups as lipid-recognizing and nucleic acid-recognizing. It is demonstrated that TLR1, TLR2, TLR4 and TLR6 are activated by lipids while TLR3, TLR7, TLR8 and TLR9 bind to nucleic acids [7]. The signaling pathways for TLRs1-13 are depicted in Figure 1.1.

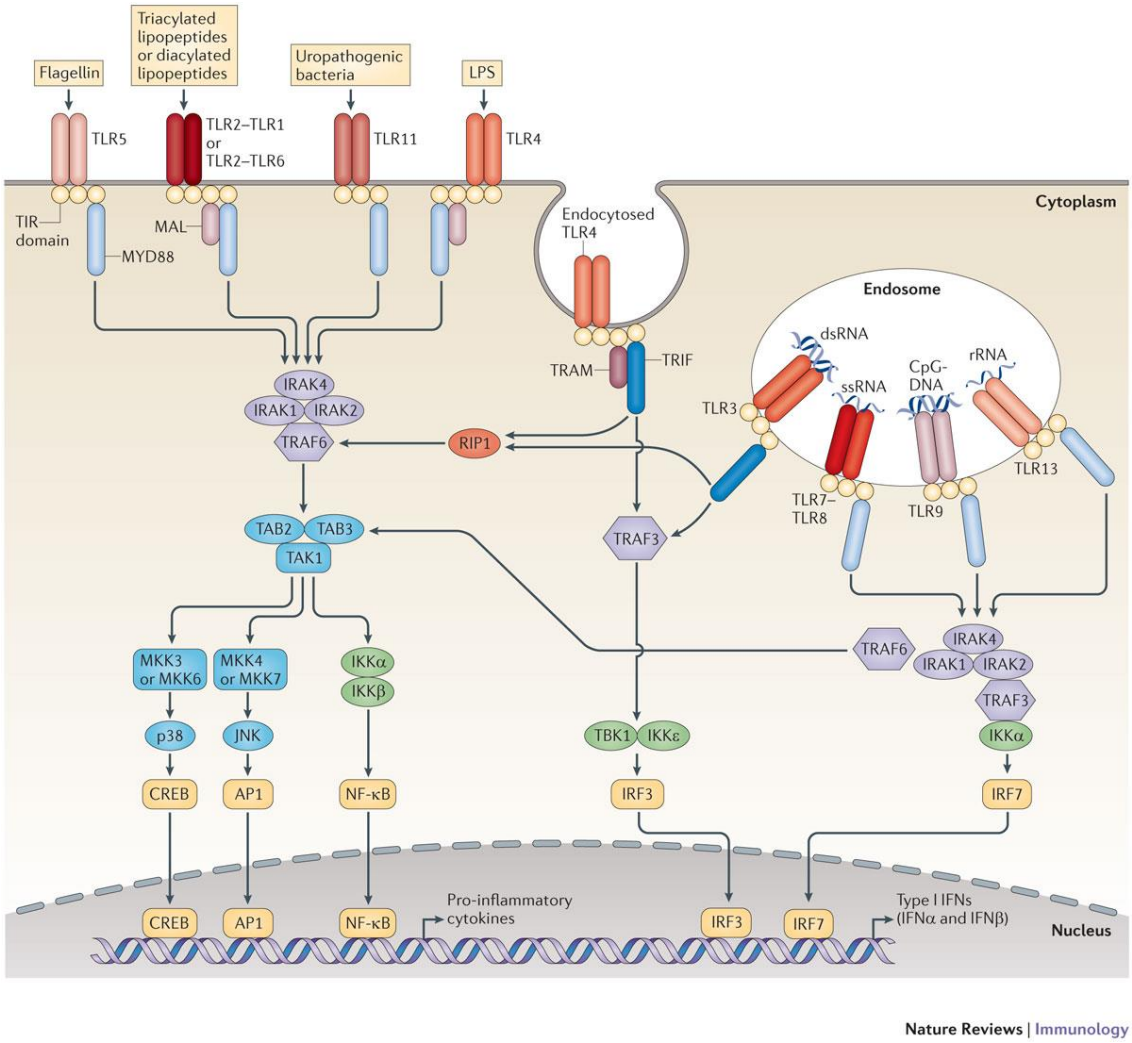


Figure 1.1. TLR ligands and their signaling pathways. Adopted from **[10]**.

TLR9 is an endosome associated receptor found in B cells, plasmacytoid dendritic cells eosinophils which interacts with unmethylated CpG sequences. The methylation of mammalian host DNA allows discrimination of self from non-self by TLR9 [11]. After CpG DNA is taken into cells via receptor-mediated endocytosis, endosome acidification takes place which is then followed by recognition of CpG DNA by TLR9 and activation of signal transduction. Many studies reported that TLR9 translocates from endoplasmic reticulum to Golgi apparatus and lysosomes as CpG DNA is moved within the cells [12]. The MyD88 and TRIF adaptor proteins are recruited by activated TLR9 and the signaling cascade eventuates in activation of multiple transcription factors, such as NF-kB, activating protein-1 (AP-1) and CREB which are involved in regulation of cytokine and chemokine related gene expressions. As a result of TLR9 signaling, expression of type I interferon genes is upregulated by transcription factors which leads to pro-inflammatory cytokine secretion. In macrophages, stimulation by CpG also culminates in secretion of IFN-ß, IP-10 and IL-10 [13]. The MyD88/IRF7 dependent pathway induces

polyclonal activation of B cells and paves the way for maturation of plasma and memory cells [13]. Overall, recognition of CpG by TLR9 promotes proliferation of B cells, activation of dendritic cells (DCs) and secretion of pro-inflammatory cytokines which together comprise a Th1-dominant immune response [1].

1.1.2. Adaptive Immunity

Evolution of adaptive immunity allows recognition of a broader range of pathogens and their annihilation through cell-mediated and humoral immune responses. Adaptive immune system cells are comprised of T lymphocytes and B lymphocytes which are involved in cell-mediated and humoral reactions respectively [15,16]. While T cell maturation takes place in thymus, B cell maturation takes place in bone marrow which are the two primary lymphoid organs [16]. The interaction between innate and adaptive immune responses are regulated by antigen presenting cells (APCs) which present antigens on surface major histocompatibility complex (MHC) molecules [17]. Antigen presentation by APCs results in maturation of naive T cells into $CD4^+$ and $CD8^+$ T cells [18]. The $CD8^+$ (cytotoxic) T cells are involved in destruction of infected cells while $CD4^+$ (helper) T cells take part in promotion of B cell activation and differentiation of T lymphocytes into various subtypes [19]. Stimulation of B cells culminates in production of antibodies which circulate in the blood and bind to pathogens leading to their inactivation and phagocytosis [20]. With the integrated action of cell-mediated and humoral adaptive immune responses a long-term and specific immunogenic response can be generated which underlie the basic principle of vaccination.

1.1.2.1. Cell Mediated Immunity

Cell mediated immunity (CMI) arm of the adaptive immune response is crucial for clearing of fungi, protozoa, intracellular bacteria and especially viruses [21]. Naïve circulating T-cells which have not encountered a specific antigen turn into armed effector T cells after being presented with antigens via MHC molecules [17]. MHC Class II molecules presenting antigens are recognized by T cell receptors (TCRs) on $CD4^+$ cells leading to their activation. The subsequent interaction between CD40 receptor, the costimulatory molecule B7 and cytokines, such as IL-12 eventuates in complete activation of $CD4^+$ cells and promotes their differentiation into Th1 helper T cells [21,22]. The $CD4^+$ Th1 cells secrete IFNγ which creates a positive feedback loop for more Th1 cell differentiation. Another vital function of IFNγ is activation of macrophages and enhancing microbicidal activity [23,24]. The activated macrophages can then induce stimulation of $CD8^+$ cytotoxic T cells via antigen presentation on MHC Class I molecules [21]. The role of $CD8^+$ cytotoxic T cells in cell mediated immune response is destruction of infected cells by inducing apoptosis. Apoptosis of the target cells can be achieved by either activation of granzyme-perforin mechanism or interaction of Fas and Fas ligand located on host cells and $CD8^+$ cells respectively

[25,26]. Apart from their role in $CD8^+$ T cell priming, $CD4^+$ Th1 cells are also involved in generation of high-affinity antibodies which will be further discussed in section 1.1.2.2 [27]. In addition, $CD4^+$ Th1 cells are reported to be functional in helping cytotoxic $CD8^+$ cells to gain their killing ability, production of $CD8^+$ memory T cells and clearing of infected host cells by granzyme-perforin mechanism induced by cytokines [21,22,23]. Following removal of the infection, the activated T cells are self-destroyed by apoptosis leaving a set of $CD4^+$ and $CD8^+$ memory T cells which can provide rapid response in the case of reinfection [28].

1.1.2.1.1. Differentiation of $CD4^+$ T Helper Cells & Th1/Th2 Responses

$CD4^+$ T helper (Th) cells play a key role in operation of cell mediated immune responses as mentioned in section 1.1.2.1. Upon recognition of antigen on MHC molecules located on APCs, naïve $CD4^+$ T cells which have fixed specificity can procure various effector functions [31]. The signals sent out by APCs and cytokine milieu are the factors contributing differentiation into subpopulations of Th cells [31]. Depending on the effector functions acquired and the set of cytokines secreted, Th cells can be classified as Th1, Th2, Th3, Th9, Th17, Treg, Tr1 and Tfh cells [33]. Differentiation of Th1 cells is driven by secretion of IL-12 and IFNγ from APC and they activate STAT4 and STAT1 transcription factors respectively [34,35]. This activation cascade results in expression of T-bet and secretion of IFNγ, TNF-α and IL-2 from Th1 cells [33]. It is reported that IFNγ activates macrophages, promotes IgG2a class switching, and provides an autocrine signaling pathway for differentiation of more Th1 cells while the T-bet transcription factor regulates IFNγ production [36,37]. Th2 cell differentiation is induced by IL-4 which controls activation of STAT6 transcription factor [35]. Downstream of IL-4 induced STAT6 activation, another key transcription factor named GATA-3 is expressed which take part in secretion of signature Th2 cytokine IL-4 [38]. In addition to IL-4, Th2 cells also produce IL-5, IL-9 and IL-13 [33,39]. Studies show that IL-4, IL-5 and IL-13 production by Th2 cells contributes to humoral immune responses via stimulating IgE production from B cells and activates eosinophils, basophils and mast cells [40,41]. Th17 cells are differentiated by the action of TGF-ß, IL-6 and IL-23 produced by antigen presenting cells in response to fungi or extracellular bacterial infection. As a consequence, STAT3 transcription factor is activated which controls downstream expression of ROR-γt. Activation of these transcription factors triggers secretion of IL-17 and IL-22 from Th17 cells [33,35]. IL-17 is known to be involved in recruitment of neutrophils and inducing inflammation while IL-22 facilitates epithelial cells to secrete antimicrobial peptides [42,43]. Regulatory T cell (Tregs) take part in suppression of the immune response in order to maintain the homeostasis. TGF-ß and IL-2 mainly drive differentiation of Th cells into Treg lineage. The activated Tregs are reported to secrete TGF-ß and IL-10 for regulation of immune responses [44]. IL-10 is an anti-inflammatory cytokine which prevents activation of macrophages while TGF-ß is shown to inhibit Th1 and Th2 related

responses and suppress immune system by inducing differentiation of more Tregs [45,46]. The differentiating factors and the cytokines secreted for the other Th cell subtypes are illustrated in Figure 1.2.

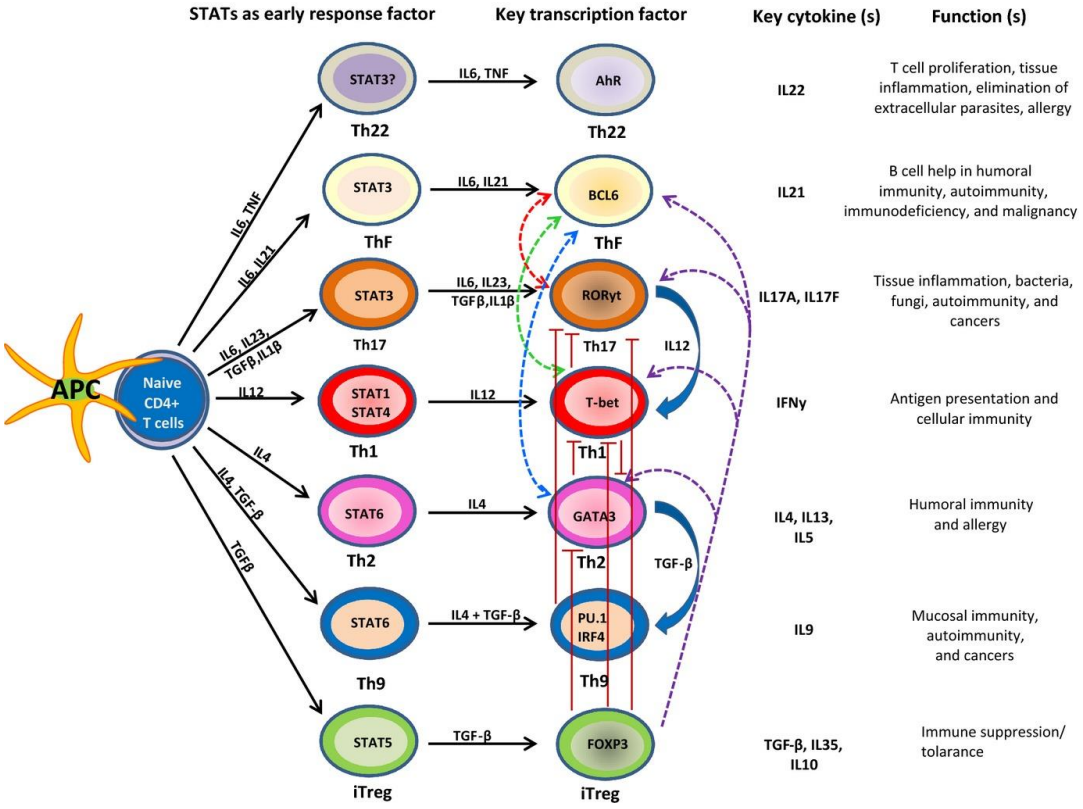


Figure 1.2. Commitment factors for differentiation into Th cell subtypes and immunological functions of Th cells. Adopted from **[47]**.

The Th1 and Th2 mediated immune responses oppose each other's functions through various ways. The two transcription factors T-bet and GATA3 involved in Th1 and Th2 differentiation respectively are proven to counteract each other. GATA3 has found to be suppressing Th1 inducing gene expression profiles and likewise T-bet is shown to be inhibiting genes related to Th2 differentiation [41,42]. Apart from the transcription factors, the source of infection also determines whether the Th cells are going to be primed for Th1 or Th2 subtypes. If the host is infected with intracellular bacteria or viruses then Th1 mediated immune response steps in. However, if the causative agent is helminth parasites or worm infections then Th2 mediated responses are engaged [30,34]. Additionally, strength of TCR signaling is shown to be affecting Th differentiation. While in the case of strong TCR stimulation Th1 differentiation is promoted, weak TCR stimulation results is Th2 differentiation [50]. The factors affecting priming of $CD4^+$ cells into Th1 cells results in orchestration of a proinflammatory immune response which is

balanced by anti-inflammatory cytokine producing Th2 cell response. Excess proinflammatory responses can cause serious damage in tissues in an uncontrolled way. Therefore, the counteracting immune mechanism generated by Th2 cells compensates Th1 mediated immune responses [51].

1.1.2.2. B-cell Mediated Immunity

The immune response induced by the activation of B-lymphocytes is also referred to as humoral immunity as it involves production of antibodies by B-cells [52]. Although mostly known for antibody production, B cells have a vast array of functions including antigen presentation, cytokine secretion, and ensuring proper development of lymphoid organs [53]. Once the B cells mature in bone marrow, they migrate to peripheral lymphoid organs where they encounter antigens and become activated [20]. Antigen presentation to the B cells can occur in two ways. The first way is recognition of small soluble antigens, such as bacterial polysaccharides which can directly filter through lymph node to be targeted by B cells. The cross-linking of B cell receptors with highly repetitive antigens results in activation of B-cells in a T-cell independent manner [54]. The T-cell independent mechanism of B-cell activation generates short-lived plasma cells but no memory cells. Therefore, it is considered that thymus-independent activation is crucial at the early stages of infections by bacterial pathogens [55]. The alternative way is presentation of larger antigen molecules by macrophages or dendritic cells. Antigens are presented by macrophages on surface MHC molecules which are recognized by B-cell receptors (BCR) located on B-lymphocytes [56]. The antigen is then internalized by the B-cell and exhibited on the cell surface on MHC Class II molecules for stimulation of helper T-cells [57]. Follicular dendritic cells (FDCs) are a subpopulation of dendritic cells which present antigens to B-cells via complement-mediated mechanism and through Fc receptors. The ability of FDCs to present antigens up to several days allows activation of B-cells for over longer period of times resulting in stronger immune response [58]. Once the antigen is internalized by B-cells, they are trafficked to T:B-cell border to encounter $CD4^+$ helper T cells. Upon recognition of the same antigen by $CD4^+$ T cells and B cells, CD40 ligand on $CD4^+$ cell binds to the CD40 receptor on the B-cell, starting a signaling cascade which culminates in activation of B-cells. Consequently, IL-4 is secreted and B-cell proliferation is promoted [53,59]. Following proliferation, B-cells can either differentiate into short-lived plasma cells to produce low-affinity antibodies or migrate into germinal centers for further maturation and generation of memory B cells and high-affinity antibody-producing plasma cells [59,60]. Proliferation of B cells through T-cell dependent and independent pathways are shown in Figure 1.3.

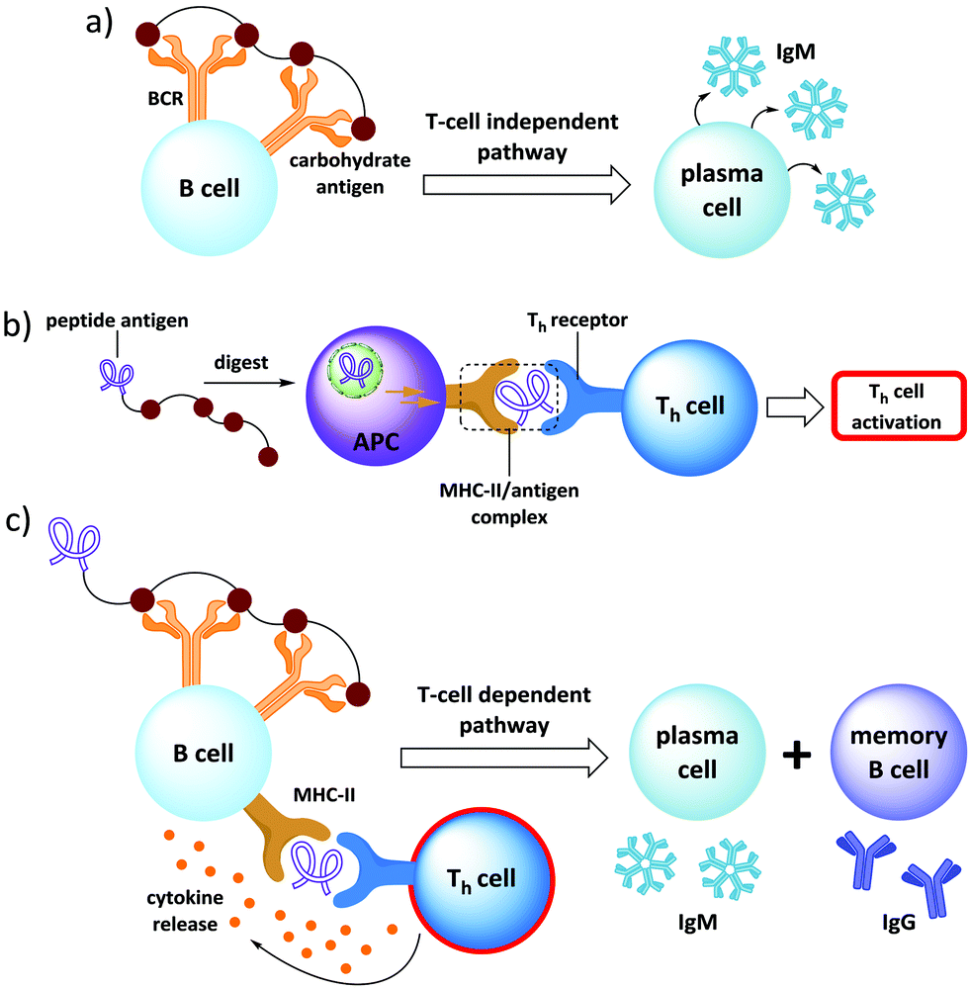


Figure 1.3. T-cell dependent and independent humoral immune responses. Adopted from **[61]**.

1.1.2.2.1. Antibody (Immunoglobulin) Functions in Adaptive Immunity

Antibodies also referred to as immunoglobulins (Ig) secreted by plasma cells are involved in defense against pathogens in different ways depending on their classes. Studies report that there are five main groups named as IgG, IgM, IgA, IgD and IgE which have different antigen targeting abilities by inducing distinct pathways [53]. It is proposed that there are three main ways through which antibodies can help clearing pathogens [52]. The first way is neutralization of the pathogens by coating of the pathogen surface with antibodies. This coating process prevents interactions between the surface proteins of the pathogens and the host cells. During viral infections, neutralizing antibodies are of vital importance since blockade of virus surface inhibits entry into host cells and thereby assembly of the viral proteins [62,63]. The second way antibodies utilize is opsonization which facilitates phagocytosis of the pathogen by the immune cells. Antibodies act as opsonins and bind to the surface of the pathogen with their variable regions marking the pathogen for phagocytosis. The Fc region of the antibodies are then recognized by

phagocytic cells such as neutrophils and monocytes by means of their Fc receptors. This can be followed by reinforcement of T-cell activities and robust immune response through antigen presentation by MHC molecules [62,64]. Antibodies are also known to be facilitating opsonization through activation of complement cascade. As a result of complement activation, complement proteins are deposited on the surface of the pathogen for opsonization and their targeting by phagocytic cells [65].

1.2. COVID-19

Coronavirus disease (COVID-19) caused by severe acute respiratory syndrome coronavirus 2 (SARS-CoV-2) led to an ongoing pandemic and resulted in infection and death of millions of people. The disease originated in Wuhan, China in December 2019, but in a short period of time, this highly transmissible virus has spread across continents and in March 2020, the World Health Organization announced that it became pandemic. Although in many cases the infected people are known to be asymptomatic, SARS-CoV-2 infection eventuates in different severity and disease progression from mild to severe symptoms among individuals. The manifestations of the disease include fever, dry cough and fatigue and it is shown that the severity of the symptoms vary depending on age, race, expression pattern of angiotensin converting enzyme-2 (ACE-2) and the immunogenic responses of the infected individuals. Despite the recovery rate from infection is high, mortality and hospitalization rates significantly increase in the elderly and immunocompromised individuals [66]. To prevent further transmission of the disease, as of December 2020, vaccination against COVID-19 has been started for the acquisition of herd immunity in addition to other preventive measures such as social distancing, wearing masks and disinfection of hands and etc.

1.2.1. Genomic and Structural Characteristics of SARS-CoV-2

SARS-CoV-2 possesses a positive-sense single-stranded RNA and belongs to the family of *Coronaviridae* and to the genus of *Betacoronavirus* [67]. The genomic comparisons proved that SARS-CoV-2 has 79% sequence similarity with SARS-CoV and 50% similarity with MERS-CoV which are the two zoonotic viruses that humankind suffered from in the recent past [68]. Being a member of *Coronaviridae*, the single stranded genome of SARS-CoV-2 is encapsulated with Nucleocapsid (N) which is packed within an envelope made up of Membrane protein (M), Envelope protein (E) and Spike protein (S) [69]. The diameter of the spherical or ellipsoidal shaped virion changes 100-116 nm and the size of the genome is 29.9 kilobases (kb) [69,70]. SARS-CoV-2 genome has 14 open reading frames (ORFs) which codes for non-structural proteins, accessory proteins and structural proteins [71]. Similar to other coronaviruses, the SARS-CoV-2 genome has a 5'-cap and a 3'-poly-A-tail so that it can be translated in the host due to its resemblance [71]. At the 5' end, ORF1a and ORF1b coding for 16 non-structural proteins

are located composing two thirds of the whole genome [72]. pp1a and pp1ab are encoded by ORF1a and a ribosomal frameshift of ORF1b respectively and they are further cleaved by viral proteases to generate 16 non-structural proteins (nsp1-nsp16) which are utilized in the cycle of infection [73]. On the 3' region, the 4 structural proteins S, M, E, N and 5 accessory proteins are encoded by the rest of the 13 ORFs [73]. The structural proteins are known to be majorly involved in packing of the genome by formation of the capsid and entry into host cells through receptors [66]. The genomic and structural features of SARS-CoV-2 are represented in more detail in Figure 1.4.

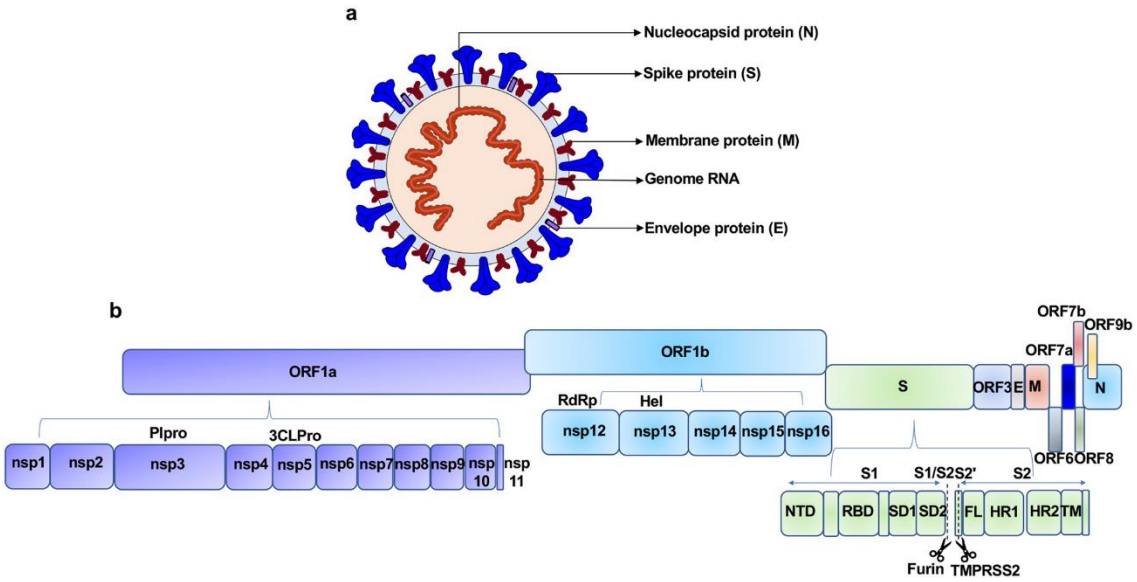


Figure 1.4. Diagrams representing structural and genomic features of SARS-CoV-2. Adopted from **[74]**.

1.2.2. Transmission Routes of SARS-CoV-2

For SARS-CoV-2, multiple transmission modes have been suggested such as aerosol, contamination of the surfaces, close contact, droplets, bloodborne transmission, fecal-oral route, mother to child and animal to human of which some of them are still a question of debate. Although some studies propose that no infectious airborne particles have been identified, some studies show evidence that viral RNA is detectable in the air around SARS-CoV-2 infected people. Therefore, more rigid evidence is required for aerosols to be regarded as one of the transmission routes of SARS-CoV-2 [67]. On the other hand, deposition of virus-laden droplets released from infected individuals can lead to formation of fomites on which the virus can remain several days depending on the conditions [67,75]. The most commonly encountered mode of transmission is close contact with a SARS-CoV-2 infected individual as the respiratory secretions expelled from the infected person can reach the people within 1 meter and cause infection [76].

The contribution of the other listed routes to transmission of SARS-CoV-2 remains elusive and requires further research for clarification [67]. In order to minimize transmission of SARS-CoV-2, cautionary measures such as wearing masks, social distancing, and frequent disinfection of the hands are suggested [77].

1.2.3. Entry of SARS-CoV-2 into Host Cells and Pathogenesis

SARS-CoV-2 enters the host cells through interaction of S protein with the N-terminal of ACE2 receptor which is followed by either fusion of the viral envelope and the cell membrane at the surface or fusion in the endosomal compartments after endocytosis [67,74]. The entry mechanism of SARS-CoV-2 into host cells depends on existence of sufficient transmembrane protease serine 2 (TMPRSS2) on the host cell membrane. If there are no TMPRSS2s or insufficient amount is expressed on the host cell surface, then the virus enters via clathrin-mediated endocytosis pathway [78]. After the S protein on the virus and the ACE2 receptor interacts, the virus is taken into the cell within a late endolysosome in which the S2' site is cleaved by a host cell protease called cathepsin-L. Subsequently, the membrane fusion of the endosome and the viral envelope takes place and the viral genome is released into plasma of the target cell to be further replicated [74,78]. Alternatively, if there is sufficient amount of TMPRSS2 on the target cell membrane, following binding of S protein to ACE2 receptor, the boundary between S1 and S2 subunits of the S protein is cleaved by host cell's protease called Furin. After cleavage of S1-S2 boundary, TMPRSS2 cleaves S2' site which leads to fusion of the viral envelope and the target cell membrane and release of the viral genome into host cell's plasma [78]. The entry routes of SARS-CoV-2 into host cells are illustrated in Figure 1.5. Upon entry through either of these two mechanisms, the genome of SARS-CoV-2 is released into cytosol and translation of ORF1a and ORF1b takes place to generate pp1a and pp1b. The post translational modifications of these two polyproteins lead to formation of replication and transcription complex (RTC). RTC enables constitution of double membrane vesicles (DMVs), convoluted membranes (CVs), and small open double membrane spherules (DMSs) which together create a microenvironment for the replication of SARS-CoV-2 genome. The structural and accessory proteins are then transferred to Endoplasmic reticulum-Golgi intermediate complex (ERGIC) for the final assembly of the virions. The newly synthesized virions are finally released from the host cell via exocytosis [67,79].

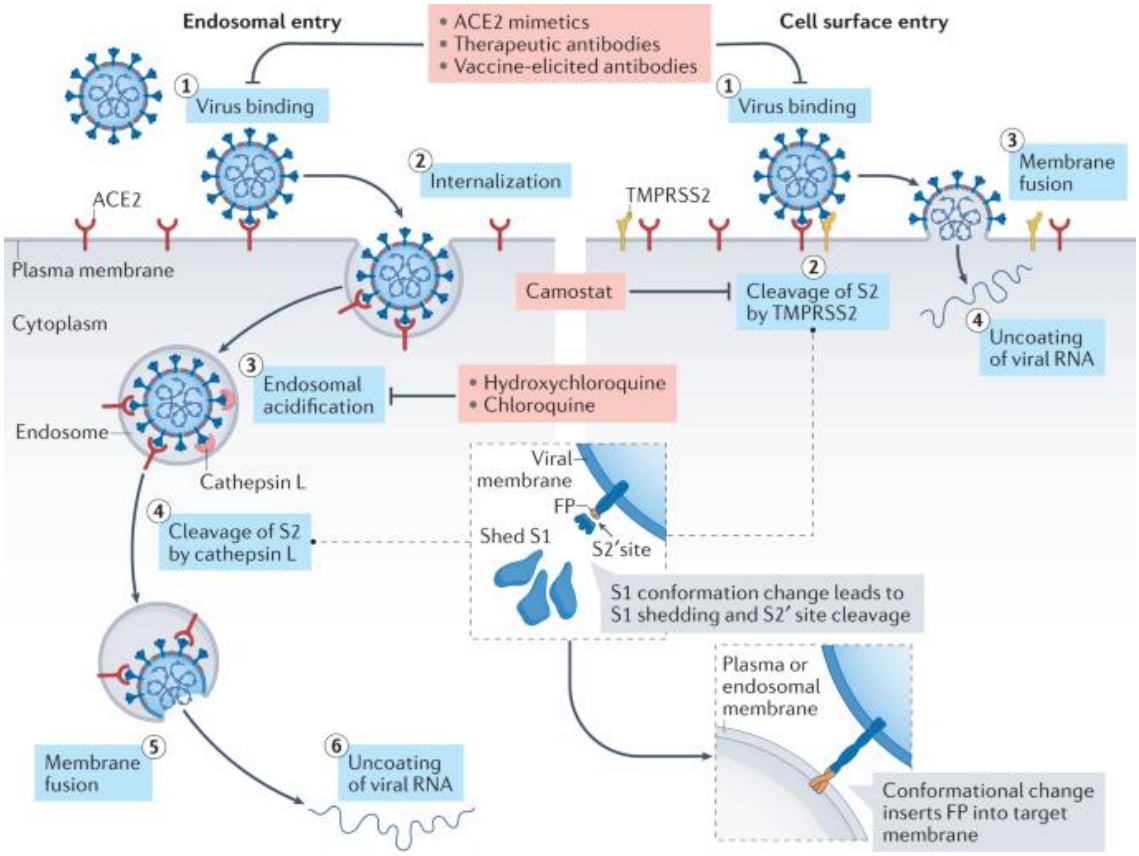


Figure 1.5. Entry pathways of SARS-CoV-2 into host cells. Adopted from **[78]**.

1.2.4. Immune Response Evoked by SARS-CoV-2

1.2.4.1. Innate Immune Response to SARS-CoV-2

Upon entry into host cells, SARS-CoV-2 is recognized by endosomal TLR3 and TLR7 or cytosolic retinoic acid-inducible gene 1 (RIG-I) and melanoma differentiation-associated protein 5 (MDA5) of the host's immune cells [80]. Stimulation of the TLRs by the viral components initiates a signaling cascade which results in activation of transcription factors NF-kB and IRF3. Activation of these transcription factors leads to secretion of pro-inflammatory cytokine, type I IFN, which sets the first line of defense against SARS-CoV-2. Induction of IFN signaling pathway culminates in synthesis of antiviral proteins via activation of JAK/STATs and expression of IFN-stimulated genes. Apart from type I IFNs, activation of NF-kB via TLR stimulation provides production of numerous inflammatory cytokines and chemokines including IL-6, IL-8, IL-10, TNF, CCL2, CCL3 and CXCL8 [81]. Studies indicate that expression of neutrophil chemoattractants are also upregulated leading to formation of neutrophil extracellular traps (NETs) in the lungs of SARS-CoV-2 infected people. However, NET formation is found to be harming for the host as it results in epithelial cells' death and lung damage [82]. NK cells are

involved in SARS-CoV-2 infection by secretion of IFN-II and TNF and destruction of the infected cells. Although it is reported that number of NK cells in the blood significantly decreases in SARS-CoV-2 infected people, the existing cells are shown to have elevated expression of granzyme B and perforin which mediate apoptosis of the target cells [80,83].

1.2.4.2. Adaptive Immune Response to SARS-CoV-2

The cellular immune response elicited against SARS-CoV-2 is comprised of $CD4^+$ and $CD8^+$ T cells [84]. Recent evidence suggests that $CD4^+$ T cells are more heavily involved in clearance and control of the virus during SARS-CoV-2 infection [85]. $CD4^+$ T cells that are presented with an antigen differentiate mostly into T helper (Th) cells upon stimulation with their specific cytokines. The cytokine milieu generated by Th cells is essential for stimulation of the B cells, recruitment of innate immune cells and helping $CD8^+$ T cells [84]. As it is mostly the case for viral infections, SARS-CoV-2 induces a Th1-biased immune response in the host's system. Therefore, IFNγ, TNF-α and IL-2 levels are shown to be elevated in patients [86]. In addition to T helper cells, $CD8^+$ T cells play an essential role with their killing ability, especially during acute phase of SARS-CoV-2 infection [87]. It is demonstrated that in response to Spike, Nucleocapsid and Membrane antigens present in the SARS-CoV-2 virus, $CD8^+$ T cells produce IFNγ, granzyme B and perforin which are necessary for execution of their cytotoxic activities [84,87].

Effective humoral response is an important arm of defense against COVID-19. Upon recognition of the SARS-CoV-2 antigens by naïve B cells, they can differentiate into short-lived or long-lived plasma cells or memory B cells [88]. Initially, anti-S and anti-N antibodies IgM and IgA are produced by B cells, which is followed by IgG production for long term protection. Antibody titers are directly correlated with severity of COVID-19. In severe patients, higher serum levels of antibodies against different antigens such as S and N proteins are widely observed. Neutralizing antibodies are also involved in defense against SARS-CoV-2 as they prevent interaction of the virus with the ACE2 receptor of the host cells [89]. Reports also indicate that there is a positive correlation between high neutralizing antibody titers and severity of SARS-CoV-2 infection, but the level of neutralizing antibodies decreases significantly after recovery [90].

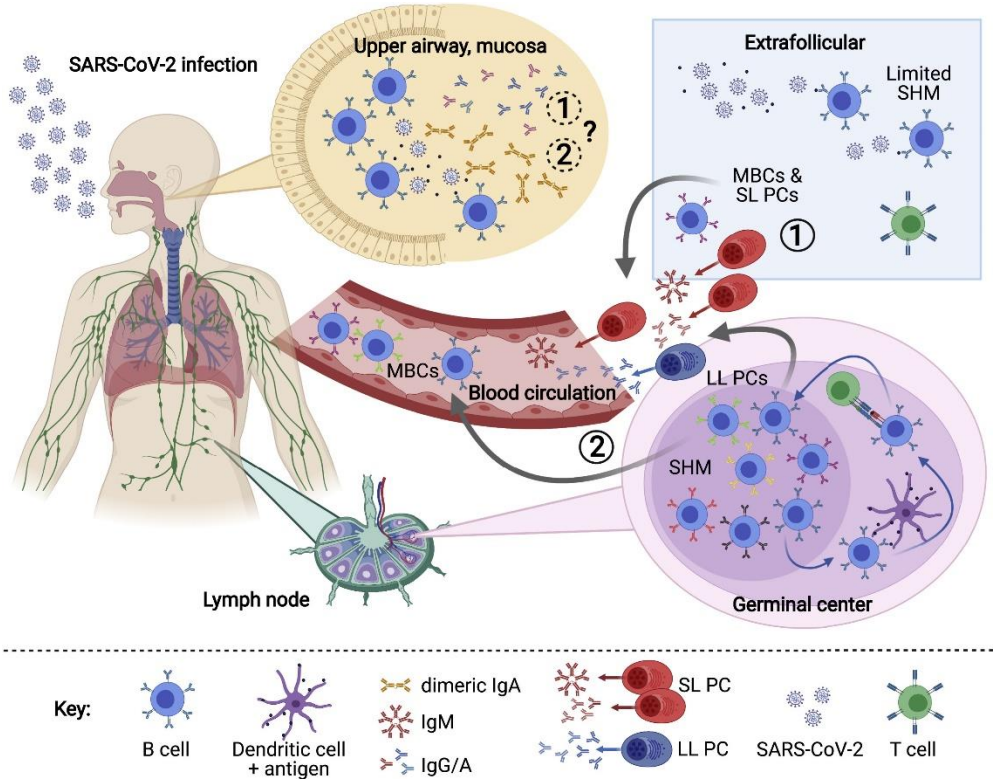


Figure 1.6. Development of humoral immune response against SARS-CoV-2. Adopted from **[88]**.

1.3. Vaccine Studies Against COVID-19

With the emergence of highly transmissible COVID-19 disease, vaccine development studies against SARS-CoV-2 have been accelerated in order to acquire herd immunity. Depending on the technology used, the vaccine studies can be divided into two major categories as classical and next-generation. The classical vaccine platforms consist of inactivated vaccines, live-attenuated vaccines, protein subunit vaccines and virus-like particle (VLP) vaccines. The next generation vaccine platforms include viral vector based vaccines, mRNA vaccines and DNA vaccines [91]. According to World Health Organization (WHO), as of August 15, 2022, there are 368 vaccine studies of which 198 are in pre-clinical development and 170 are in clinical development stage [92]. CoronaVac from Sinovac is a classical inactivated vaccine with reported efficacy rate of 51% [93]. BNT162b1/BNT162b2 from BioNTech/Pfizer and mRNA-1272 from Moderna are mRNA based vaccines which express a trimeric form of RBD and full length spike protein delivered via lipid nanoparticles (LNPs) respectively [94]. BioNTech/Pfizer and Moderna vaccines are considered 95% and 94.5% effective respectively.[95] ChAdOx1 nCoV-19 from AstraZeneca, Sputnik V from Gameleya and Ad26.COV2.S from Janssen/Johnson & Johnson are adenovirus vector based vaccines expressing full-length spike protein [94,95]. Assessment of neutralizing antibody levels indicated that efficacy rates for ChAdOx1 nCoV-19, Sputnik V and

Ad26.COV2.S are 62%, 91% and 66.9% respectively [95]. NVX-CoV2373 vaccine from Novavax is a classical protein subunit vaccine which delivers a recombinant full length spike protein for immunization. The neutralizing antibody titers demonstrate that NVX-CoV2373 is 89.7% effective against SARS-CoV-2 [95,96]. There are numerous vaccine studies against COVID-19 developed using different technologies, targeting different structures of the SARS-CoV-2 virus. However, efficacy rates of these vaccines are subject to type of the vaccine technology, dose of the vaccine, ages of the tested groups, type of adjuvants used and etc. In addition, the rapidly mutating genome of SARS-CoV-2 urges the need for reformulation and reconstruction of vaccines based on new mutations [72]. Therefore, although there are several on-going vaccine developments, immunization against SARS-CoV-2 is an area of serious concern as equal distribution of vaccines problem remains to be resolved, safety of the approved vaccines are still questioned, and the long term effectiveness is elusive [91].

1.3.1. Virus-like Particle (VLP) Vaccines

Virus-like particle (VLP) vaccines are recombinant protein vaccines containing the structural proteins of the virus and lacking the viral genomic material. Absence of viral genome renders VLP vaccines to be safer compared to inactive virus vaccines. VLP production can take place in different host systems, such as bacteria, yeast, insects, plant cells and mammalian cells. Under optimized circumstances, VLPs can be produced in large quantities making them a cheap and safe vaccine alternative. After production and purification processes, VLPs assemble in a structure which imitates the authentic virus creating a distinctive and repetitive entity that is highly pathogenic [97]. Compared to recombinant subunit vaccines, VLP vaccines offer a stronger immune response by stimulating both humoral and cellular immunity due to presence of different repetitive viral structures [98,99]. Several features of VLPs make them advantageous as potential vaccine candidates. First, APCs recognize and uptake VLPs more effectively since the multimeric components of innate humoral immune system can bind to repetitive structure of VLPs with high avidity. Second, the ability of VLPs to migrate into draining lymph nodes results in a more robust cellular and humoral immune response. Finally, the repetitive structure of VLPs enables formation of pathogen associated structural patterns (PASP) which leads to enhanced activation of B-cells and T-cell mediated immunity by lubricating B-cell receptor cross-linking [97,98]. Therefore, utilizing VLPs for vaccine development against SARS-CoV-2 can offer stronger activation of immune response. In this study the VLP vaccine is formulated with the 4 structural proteins of SARS-CoV-2 which are S, E, M and N to mimic the original virus.

1.3.2. VLP Vaccine Adjuvants

Adjuvants are agents used in vaccine formulations which promote enhanced immune response. Aluminum-salt based adjuvants which are also named alum, are one of the most commonly used

and oldest adjuvants employed in vaccine formulations. Although numerous adjuvants have demonstrated strong immunostimulatory effects, only a few of them are licensed for use in humans due to safety concerns [100]. Examples of licensed adjuvants include alum, AS01, AS03, AS04, cytosine phosphoguanosine (CpG), and MF59 [101]. Studies indicate that there are several mechanisms of action for adjuvants, and they can utilize more than one in order to trigger immune response [102]. Primarily, certain adjuvants can provide depot effect which is slow and sustained release of the antigen at the site of injection ensuring longer exposure [101,102]. Adjuvants have also been shown to upregulate cytokine and chemokine secretion which eventuates in recruitment of cells at the site of injection. Efficient T cell proliferation has also found to be promoted by the action of adjuvants as maturation of DCs is stimulated and expression of MHCs and other co-stimulatory molecules are found to be upregulated. Although not clear yet, the adjuvants are also thought to take part in increment of antigen uptake and presentation by the APCs. However, this topic needs further investigation for clarification. Lastly, adjuvants are shown to facilitate activation inflammasome complex which leads to a stronger and longer immune activity [102].

Despite VLP vaccines tend to induce stronger immune response compared to subunit vaccines, addition of adjuvants in vaccine formulations can accelerate the immune reaction and enhance stability of the vaccine [98]. In this study, the VLP vaccine against SARS-CoV-2 has been formulated with both aluminum hydroxide and K3 CpG ODN as adjuvants.

Although the exact molecular pathways through which Alum acts as an adjuvant remains to be resolved, it is proposed that alum can modulate immune response through different mechanisms. Aluminum hydroxide creates aggregates by adsorbing the antigen which triggers uptake of antigens by DCs. Alum also contributes to activation of Nlrp3 inflammasome complex which leads to release of pro-inflammatory cytokine IL-1ß. Reports demonstrate that Alum induces majorly $CD4^+$ T helper cell mediated activity and the response is more Th2-biased rather than Th1. Therefore, in the case of viral infections such as SARS-CoV-2, Alum might not be sufficient alone in terms of eliciting a strong immune response since Th1-biased immunity and activation of cytotoxic T lymphocytes are heavily required [98].

CpG oligodeoxynucleotides (ODNs) are single stranded, short DNA fragments containing unmethylated cytosine and guanine nucleotides which trigger immune response due to their resemblance to bacterial DNA. Four classes of CpG ODNs have been characterized based on their structural and biological features: K-type ODNs (B-type), D-type ODNs (A-type), C-type ODNs and P-type ODNs [98,103]. In this study, K-type CpG ODNs are used as a vaccine adjuvant along with aluminum hydroxide. K-type (B-type) CpG ODNs possess a phosphorothioate backbone coding for several CpG motifs [103]. The phoshorothioate backbone renders a longer *in vivo* half-life for CpG as it provides increased resistance against digestion by

nucleases.[104] Being TLR9 agonists, CpG ODNs are targeted at TLR9 expressing pDCs and B cells and mediate Th1-dominated immune responses [98]. After being internalized via endocytosis by the target cells, CpG activates TLR9 in B cells and pDCs leading to initiation of both innate and adaptive immune regulations. In B cells, the activation cascade leads to increased release of IL-6, IL-12, IP-10, Mig and I-TAC. Additionally, IgM production by B cells is also stimulated by secretion of IL-6. Consequently, the proliferation of activated B cells culminates in differentiation into plasma cells and memory B cells. On the other hand, stimulation of pDCs leads to their enhanced functionality through increased expression of MHC Class II molecules, and release of IL-1, IL-6, IL-12 and TNF-α, IFN-α, and IFN-β. Upregulation of these cytokines leads to the creation of a Th1-skewed immune response, enhanced antigen processing and presenting abilities of pDCs and robust activation of $CD8^+$ T cells [103,104]. Therefore, the ability of CpG ODNs to induce escalated humoral and cellular immune responses make them a promising candidate for VLP vaccine adjuvant.

1.4. Clinical Trials

Clinical research trials are performed to test safety and effectiveness of new drugs, drugs that are already approved, vaccine candidates, medical devices, new diagnostic assays and new surgical methods. Before the clinical trials start, pre-clinical studies, also called laboratory studies, are completed *in vitro* in cell cultures and *in vivo* animal models using a broad dose range of medical treatment to assess effectiveness, toxicity and pharmacokinetic dynamics. Depending on the success rate of the pre-clinical studies, the new treatment candidate then proceeds to clinical trial phases to be tested on human subjects with informed consent. There are four clinical trials that a new treatment must successfully pass in order to be classified as safe and effective by Food and Drug Administration (FDA). Generally, clinical trials have three main stages which are phase I, phase II, and phase III. However, in some studies an early trial step called phase 0 and phase IV, a final step after the treatment is licensed, are also included. For vaccine studies, the purpose of clinical trials is determination of safety, immune responses, and duration of immune response elicited [105–107].

1.4.1. Phase I Clinical Trials

Phase I clinical trials, also called dose-escalation studies or human pharmacology, are the initial steps for a medical treatment to be tested on a small group of human subjects with informed consent. The objective is to designate the optimum dose of the treatment without raising any safety concerns related to side effects. Phase I clinical trials are often conducted blind and placebo-controlled. The number of participants is generally 20-80 healthy or diseased volunteers. The medical treatments are generally performed in clinics where the volunteers can be monitored very closely after receiving the treatment for observation of any possible side effects. The first

volunteers receive the lowest dose of the treatment and if minor or no side effects are detected, the trial continues with escalating doses. If the clinical trial is for a vaccine, the dosage of adjuvants as well as the antigen are subject to investigation [105,107].

1.4.2. Phase II Clinical Trials

Phase II clinical trials, also referred to as therapeutic exploratory trials, are the second step of the clinical research. Phase II trials are conducted with 100-300 volunteers in order to assess the effectiveness, optimal dose, dose frequencies, and safety of the treatment. Comparison of efficiency of a new treatment to already existing ones, investigation of different doses and randomization of the volunteers to different arms of the study can also be achieved within the scope of phase II clinical trials. However, involvement of a limited number of volunteers necessitates performing phase III clinical trials for a more reliable evaluation of safety concerns, biological activity and effectiveness [105,107].

1.4.3. Phase III Clinical Trials

Phase III clinical trials aim to detect common side effects of the treatment as well as its effectiveness in a larger group of subjects consisting of 300-3000 individuals. Additionally, they can be conducted as comparative efficacy trials by which efficiency of the new treatment is compared with a standard therapy or as equivalency trials which purpose to demonstrate that the new treatment works similar to the standard treatment. Phase III trials are randomized controlled and can be multicentered allowing a broad variation range of volunteers. Despite the subject size is much more than phase I and phase II, it is still insufficient to identify less commonly encountered side effects. Therefore, generally more than one phase III trial is conducted for a new treatment so that a better statistical power can be obtained [105,108].

1.4.4. Phase IV Clinical Trials

Phase IV clinical trials, also named as post-marketing surveillance or drug monitoring trial, last for years after the medical treatment has been licensed by FDA. The two main objectives of phase IV clinical trials are to determine the less common or long-term side effects of the medical treatment and the effectiveness over long period of times. In the case of identifying any serious adverse effects, the treatment can be withdrawn or its usage can be restricted to certain groups of people that are considered eligible [105,109].

1.5. Aims and Outline of the Study

COVID-19 has become a serious concern of the world with its high transmission rate since March 2020. Up till today, to fight against SARS-CoV-2, various pharmacological approaches have been developed including drugs, interferon therapies, monoclonal antibodies and vaccines. Vaccines are an effector arm of fight against COVID-19 as they lubricate acquiring herd immunity and relieve symptoms after being infected. However, the race for development of the most effective and safest vaccine against COVID-19 has been an enormous challenge during pandemic. Defining the proper scientific formula, logistics of manufacturing process, administration of the dosage, storage and distribution of the vaccine have become the questions that are left to be resolved by the scientists. As of March 4, 2022, 147 vaccine candidates could manage these issues and have been reported to be in clinical stage according to WHO. SARS-CoV-2 VLP vaccine developed by our lab and Mayda Gürsel's lab from Middle East Technical University, Turkey, is among those candidates in clinical trial stage. The SARS-CoV-2 VLP vaccine formulation contains VLPs embodying HexaPro Spike along with Nucleocapsid, Membrane and Envelope proteins together with K3 CpG ODN and Alum as adjuvants. In this study, we aimed to analyze immunogenic responses of Phase II clinical trial volunteers elicited against SARS-CoV-2 VLP vaccine. Following immunization studies in mice, vaccination of Phase I volunteers were completed. After Phase I clinical trial was accomplished and the dosage was determined, Phase II clinical trial was pursued. The antibody titers from sera were analyzed with ELISA, the neutralizing antibody levels were determined and the T-cell responses were studied by CBA technique. These assessments provided understanding the efficiency and safety of SARS-CoV-2 VLP vaccine.

CHAPTER 2

MATERIALS AND METHODS

2.1. Materials

2.1.1. Cell Culture Media, Solutions and Buffers

Product	Company
RPMI-1640	Biological Industries, Beit-Haemek, Israel
Penicillin-Streptomycin	Biological Industries, Beit-Haemek, Israel
HEPES Buffer	Biological Industries, Beit-Haemek, Israel
Sodium Pyruvate	Biological Industries, Beit-Haemek, Israel
MEM Eagel Non-Essential Amino Acids	Biological Industries, Beit-Haemek, Israel
Heat Inactivated Fetal Bovine Serum (FBS)	Biological Industries, Beit-Haemek, Israel
Dulbecco's Phosphate Buffer Saline (DPBS)	Biological Industries, Beit-Haemek, Israel
Lymphocyte Separation Medium (LSM)	Capricorn, Ebsdorfergrund, Germany
Dimethyl Sulfoxide (DMSO)	Applichem, Germany

2.1.2. ELISA Antibodies, Chemicals and Reagents

Product	Company	Catalog No	Working Concentration
Goat Anti-Human IgG-AP	Southern Biotech, USA	2040-04	1:1000
Goat Anti-Mouse IgG-AP	Southern Biotech, USA	1030-04	1:1000
Homemade Recombinant SARS-CoV-2 Spike Protein	Bilkent University, Ankara, Turkey	-	Human: 6 μg/ml Mouse: 4 μg/ml
Homemade Recombinant SARS-CoV-2 Nucleocapsid Protein	Bilkent University, Ankara, Turkey	-	Human: 4 μg/ml Mouse: 6 μg/ml
Homemade Recombinant SARS-CoV-2 RBD Protein	Bilkent University, Ankara, Turkey	-	4 μg/ml
SARS-CoV-2 RBD of Spike protein (Wild Type)	ProteoGenix, France	PX-COVP046-100	1 μg/ml
SARS-CoV-2 RBD of Spike protein (UK Alpha Variant)	ProteoGenix, France	PX-COVP052-100	1 μg/ml

SARS-CoV-2 RBD of Spike protein (Indian Delta Variant)	ProteoGenix, France	PX-COVP061-100	1 µg/ml
Bovine Serum Albumin (BSA)	Capricorn, Ebsdorfergrund, Germany	BSA-1T	-
Sodium Chloride (NaCl)	Isolal, Wertheim, Germany	7647-14-5	-
Potassium Chloride (KCl)	Merck, Darmstandt, Germany	1.04936.1000	-
Sodium phosphate dibasic dihydrate ($Na_2HPO_4.2H_2O$)	Sigma Aldrich, St Louis, MO, USA	10028-24-7	-
Potassium Phosphate Monobasic (KH_2PO_4)	Sigma Aldrich, St Louis, MO, USA	7778-77-0	-
Tween-20	VWR, Radnor,PA, USA	97062-332	-
p-nitrophenyl phosphate (PNPP) Tablets	Thermo Fisher Scientific, Waltham, MA, USA	34047	1 tablet/5 ml
Substrate Buffer 5X	Thermo Fisher Scientific, Waltham, MA, USA	34064	1 ml/plate
Anti-SARSCoV-2 Verification Panel for Serology Assays	NIBSC, UK	20/B770	-
First WHO International Reference Panel for anti-SARS-CoV-2 immunoglubulin	NIBSC, UK	20/268	-
Convalescent Sera	Marmara University, İstanbul, Turkey	-	-

2.1.3. Kits

Product	Company	Catalog No
Corona Hunter ELISA Kit	Matriks Biotek, Ankara, Turkey	COR-QNS-IGG-STRIM
LEGENDplex™ HU Th Cytokine Panel (12-plex) w/ VbP V02 Kit	Biolegend, San Diego, CA, USA	741028
SARS-CoV-2 SMNO Peptide Pool	Mabtech, Nacka, Sweden	3622-1

2.1.4. Equipment

Device	Company
NovoCyte Flow Cytometer	ACEA Biosciences, San Diego, CA, USA
ThermoMax Microplate Reader	Molecular Devices, San Jose, CA, USA

2.1.5. Buffer, Media and Solution Contents

2% FBS Containing RPMI Medium:

- 500 ml RPMI-1640 Medium with L-Glutamine
- 10 ml heat inactivated FBS
- 5.32 ml Non-Essential Amino Acids
- 5.32 ml HEPES Buffer
- 5.32 ml Sodium Pyruvate
- 5.32 ml Penicillin-Streptomycin

10% FBS Containing RPMI Medium:

- 500 ml RPMI-1640 Medium with L-Glutamine
- 58.14 ml heat inactivated FBS
- 5.8 ml Non-Essential Amino Acids
- 5.8 ml HEPES Buffer
- 5.8 ml Sodium Pyruvate
- 5.8 ml Penicillin-Streptomycin

10X Phosphate Buffered Saline (PBS):

- 80 g NaCl
- 2 g KCl
- 15.2 g $Na_2HPO_4.2H_2O$
- 2 g KH_2PO_4
- Completed to 1 l by adding ddH_2O
- pH adjusted to 6.8
- Autoclaved

5% Blocking Buffer:

- 500 ml 1X PBS
- 25 g BSA
- 250 µl Tween-20

Wash Buffer:

- 500 ml 10X PBS
- 2.5 ml Tween-20
- 4.5 l ddH_2O

2.2. Methods

2.2.1. Cell Culture

2.2.1.1. Peripheral Blood Mononuclear Cells (PBMCs) and Plasma Isolation

Blood was collected from the Phase I and Phase II volunteers into BD Vacutainer EDTA blood collection tubes (BD Biosciences, USA) with informed consent. The blood tubes were inverted slowly a few times and diluted with 1X DPBS in 1:1 ratio. Diluted blood samples were gently layered onto the Lymphocyte Separation Medium (LSM-A, Capricorn, Germany) in 1:1.5 LSM:blood ratio. The tubes were centrifuged at 540 g for 30 minutes at 21°C and the deceleration was set to 0. After the centrifugation, the upper layer composes the plasma and the cloudy layer beneath the plasma contains the PBMCs. By using a sterile Pasteur pipette the plasma were collected into new falcon tubes and then centrifuged at 1500 g for 10 minutes in order to get rid of PBMCs. After the centrifuge, the plasma was collected into fresh falcon tubes making sure that no cells were contained. The plasma samples were then snap-freezed in liquid nitrogen and stored at -80°C for further use. The PBMC layer was collected into a separate falcon tube using a sterile Pasteur pipette, and RPMI-1640 medium containing 2% FBS is added onto the cells. The PBMCs were then centrifuged at 540 g for 10 minutes. This step was repeated for 2 times for efficient removal of the lymphocyte separation medium. After the second wash, the supernatant was aspirated, the PBMCs were resuspended in 500 µl FBS and then counted by using NovoCyte flow cytometer (ACEA Biosciences, San Diego, CA, USA) as described in section 2.2.1.2. After counting, the cells were frozen in 10% DMSO-FBS in 1:1 cell:DMSO-FBS ratio and stored at liquid nitrogen tanks until further use.

2.2.1.2. Cell Counting

For PBMC count, after the cells were resuspended in 500 µl FBS, 10 µl was transferred to an Eppendorf tube containing 990 µl RPMI-1640 with 2% FBS. For splenocyte count, after the cells were resuspended in 2 ml FBS, 20 µl was transferred into 5 ml isotonic solution (Beckmann Coulter, USA). Following dilution, 50 µl of PBMC samples and 100 µl of each splenocyte sample were counted using NovoCyte flow cytometer (ACEA Biosciences, San Diego, CA, USA) by employing a gate which disregards the apoptotic cells and the cell debris so that only the live cells of the total population were counted.

2.2.2. Production of Recombinant Proteins

HEK293-FT human embryonic kidney cell line was transfected with pVitro1-N and pVitro2-S constructs by employing PEIpro (Polyplus, France) transfection reagent. The details of the transient transfection process of the HEK293-FT cells can be found in İpekoğlu, E. M. (2022)

[110]. Following incubation of 96-120 hours, the medium was collected for further processing. The medium was first centrifuged at 500g for 10 minutes and then the supernatant was filtered using 0.22 µm microfilter (Sarstedt, Germany). The filtered medium was then treated with 200 U/ml of Denarase (c-LEcta, Germany) and left for incubation at 37°C for 2 hours. After that protein purification was performed using ÄKTA go fast protein liquid chromatography (Cytiva, USA). The detailed steps for purification of his-tagged proteins can be found in İpekoğlu, E. M. (2022) [110]. Shortly, HisTrap excel 1 mL pre-packed IMAM column was equilibrated using DPBS and this is followed by loading of the sample to the column. The fractions containing the recombinant spike and nucleocapsid proteins were collected during elution step using imidazole buffer. Following purification step, quantification of the recombinant proteins was done using Pierce BCA protein assay kit (Thermo Fisher Scientific, USA). Then the proteins were characterized by employing SDS-PAGE, Western Blotting, dot blotting and silver staining. The process of protein quantification and characterization are discussed in a more comprehensive way in İpekoğlu, E. M. (2022) [110].

2.2.3. Determination of Immune Responses from Sera

2.2.3.1. Determination of IgG Levels in Human Sera by Enzyme Linked Immunosorbent Assay (ELISA)

2HB ELISA plates (SPL Life Sciences, South Korea) were coated with 50 µl/well homemade recombinant Spike protein (6 µg/ml), homemade recombinant Nucleocapsid protein (4 µg/ml), commercial recombinant wild type RBD (ProteoGenix, France) (1 µg/ml), commercial recombinant Alpha RBD (ProteoGenix, France) (1 µg/ml), and commercial recombinant Delta RBD (ProteoGenix, France) (1 µg/ml) prepared in 1X PBS and incubated overnight at 4°C. The coating solutions were discarded and the plates were treated with 200 µl/well blocking buffer (5% BSA PBS-T) to be incubated at RT for 2 hours. The plates were then washed for 4 times with PBS-Tween (0.05% PBS-T), rinsed 2 times with dH_2O and dried. Human sera obtained from Phase II volunteers were prepared in 1:100 ratio and serially diluted sixfold for 2 times for spike and nucleocapsid plates and fourfold for 3 times for RBD variant plates. Following this, 50 µl of serially diluted sera were distributed to the plates and the plates were left for incubation overnight at 4°C. Next, the plates were washed for 4 times with PBS-Tween (0.05% PBS-T), rinsed 2 times with dH_2O and dried. ALP conjugated anti-human IgG (Southern Biotech, USA) was prepared in 1:1000 ratio in blocking buffer (5% BSA PBS-T) and distributed 50 µl/well to each plate to be incubated for 2 hours at RT. Then the washing step was repeated as before, and p-nitrophenyl phosphate (PNPP) (Thermo Scientific, USA) substrate solution was prepared following the instructions on the manufacturer's manual. The plates were treated with 50 µl/well PNPP

solution, and the optical density values were recorded at 405 nm in ThermoMax microplate reader (Molecular Devices, USA).

2.2.3.2. Determination of IgG Levels in Mice Sera by ELISA

2HB ELISA plates (SPL Life Sciences, South Korea) were coated with 50 µl/well homemade recombinant Spike protein (4 µg/ml), homemade recombinant Nucleocapsid protein (6 µg/ml), homemade recombinant WT RBD (4 µg/ml), commercial recombinant Alpha RBD (ProteoGenix, France) (1 µg/ml), and commercial recombinant Delta RBD (ProteoGenix, France) (1 µg/ml) prepared in 1X PBS and incubated overnight at 4°C. The coating solutions were discarded and the plates were treated with 200 µl/well blocking buffer (5% BSA PBS-T) to be incubated at RT for 2 hours. The plates were then washed for 4 times with PBS-Tween (0.05% PBS-T), rinsed 2 times with dH_2O and dried. Sera obtained from the immunized mice were prepared in 1:50 ratio and serially diluted fivefold for 8 times. Following this, 50 µl of serially diluted sera were distributed to the plates and the plates were left for incubation overnight at 4°C. Next, the plates were washed for 4 times with PBS-Tween (0.05% PBS-T), rinsed 2 times with dH_2O and dried. ALP conjugated goat anti-mouse IgG (Southern Biotech, USA) was prepared in 1:1000 ratio in blocking buffer (5% BSA PBS-T) and distributed 50 µl/well to each plate to be incubated for 2 hours at RT. Then the washing step was repeated as before, and PNPP (Thermo Scientific, USA) substrate solution was prepared following the instructions on the manufacturer's manual. The plates were treated with 50 µl/well PNPP solution and the optical density values were recorded at 405 nm in ThermoMax microplate reader (Molecular Devices, USA).

2.2.3.3. Determination of IgG Levels in Human Sera by Corona Hunter Kit

IgG responses of the volunteers against SARS-CoV-2 Spike protein were assessed by the employment of Corona Hunter Anti-SARS-CoV-2 SPIKE IgG ELISA kit (Matriks Biotek, Turkey). The protocol was executed according to the manufacturer's guidelines. Prior to start, the serum samples were diluted 1:100 ratio using Assay Buffer as diluent in a sterile 96-well plate (Sarstedt, Germany). Then, 100 µl Assay Buffer was distributed to each well of the previously coated 96-well plate provided by the manufacturer. 20 µl of the standards, high level control, low level control and the previously diluted samples were added to the respective wells of the plate. The plate was incubated at RT for 60 minutes. The plate content was discarded, wash step was performed for 3 times by pipetting 300 µl of Wash Buffer to each well and the plate was dried. 100 µl of Conjugate was added to each well and the plate was left to incubation at RT for 30 minutes. The plate was emptied and the wash step was performed as described above. Afterwards, 100 µl Substrate was pipetted into each well and the plate was incubated in the dark for 15 minutes at RT. The reaction was stopped 20 minutes later by adding 100 µl Stop Solution to each well

and the optical density values were recorded at 450 nm using ThermoMax microplate reader (Molecular Devices, USA).

2.2.3.4. Determination of Neutralizing Antibody Levels in Human Sera by SARS-CoV-IgG Quant

The neutralizing antibody levels of the sera obtained from the volunteers against receptor binding domain (RBD) of spike are quantified by SARS-CoV-2 IgG Quant method performed via ARCHITECT i System. This automated assay was performed by DEREN Laboratory (Ankara, Turkey). The procedure was carried out according to manufacturer's protocol. Basically, IgG levels were qualitatively and quantitatively determined by the chemiluminescent reaction resulting from the incubation of serum and the SARS-CoV-2 antigen coated paramagnetic microparticles. The results were assessed based on the cut off value which is 50.0 AU/ml.

2.2.4. Assessment of T-Cell Immune Responses

2.2.4.1. Cytometric Bead Array (CBA)

In preparation for the experiment, the PBMCs collected from the volunteers at day 35 (14 days post booster) were thawed, leaved for resting at 37°C for 1 hour in 10% FBS containing RPMI-1640 medium and then counted by using NovoCyte flow cytometer (ACEA Biosciences, San Diego, CA, USA) as described in section 2.2.1.2. 750,000/well PBMCs were incubated with SMNO peptide pool (Mabtech, Sweden) for 48 hours, the supernatant was collected and then the collective secretion of 12 different cytokines (IL-2, IL4, IL5, IL6, IL9, IL10, IL13, IL17A, IL17F, IL22, IFN-γ and TNF-α) were quantified using LEGENDplex™ HU Th Cytokine Panel (12-plex) w/ VbP V02 kit (Biolegend, USA). The instructions on the manufacturer's manual were followed. Prior to start, the beads, wash buffer and the human Th panel standard cocktail were prepared according to the guidelines in the kit protocol. For both standard and sample wells, 25 µl of assay buffer was loaded to corresponding wells of the 96-well V-bottom plate provided by the manufacturer. For standard and sample wells, 25 µl of standard solution and sample were added to corresponding wells respectively. Afterwards, 25 µl of mixed beads were added to each well. The plate was covered with aluminum foil and incubated in dark for 2 hours on a shaker rotating at 800 rpm. The plate was then centrifuged at 250 g for 5 minutes and the supernatant was discarded by inverting the plate. The plate was dried gently on a clean paper towel. Washing step was performed using 200 µl/well 1X wash buffer prepared previously, the plate was again centrifuged at 250 g for 5 minutes, the supernatant was removed by inverting the plate and the plate was dried. Then 25 µl of detection antibody was added to each well, the plate was covered with aluminum foil and incubated for 1 hours on a shaker rotating at 800 rpm. Following antibody incubation, 25 µl SA-PE was added to each well and the plate was left to incubate on a shaker set

to 800 rpm for 30 minutes after being covered with aluminum foil. After that the wash step was repeated as described previously. Lastly, 150 µl 1X wash buffer was added to each well in order to resuspend the beads and the samples were read on NovoCyte flow cytometer (ACEA Biosciences, San Diego, CA, USA). Data analysis was performed using LEGENDplex™ Data Analysis Software (Biolegend, U.S.A.).

2.2.5. *In Vivo* Experiments and Immunization Practices in Phase I & Phase II Clinical Trials

2.2.5.1. Immunization Studies on Mice

All animal experiments were conducted with the approval of Bilkent University Animal Ethics Committee (Bil-AEC). 6-8 weeks old female BALB/c mice were subcutaneously (s.c.) injected with 100 µl/mouse VLP vaccine. 7/mice group were used and there were 4 groups in total. In order to determine the best VLP vaccine formulation, mice were injected with different WT VLP, Alhydrogel (Alum) and K3-CpG ODN combinations. Vaccination was done at intervals of 2 weeks, on day 0 and day 14 and 2 months after the booster. The first group was placebo and injected with 100 µl/mice DPBS. For the second group, the injected vaccine formulation was 2.5 µg HexaPro WT VLP + 120 µg Alum + 60 µg K3-CpG. The third group was injected with 5 µg HexaPro WT VLP + 120 µg Alum + 60 µg K3-CpG formulation. Lastly, the fourth group was injected with 5 µg HexaPro WT VLP + 60 µg Alum + 30 µg K3-CpG. Mice were bled from the tail vein, one day before booster and 14 days post-booster. Blood samples were collected into BD microtainer blood collection tubes (BD Biosciences, USA). The tubes were centrifuged at 2500 g for 10 minutes at 21°C and the upper layer containing the serum was transferred to Eppendorf tubes which were stored at -20°C until further use.

2.2.5.2. Vaccination Phase II Volunteers

For Phase II clinical trial, 110 of total 330 volunteers were subcutaneously (s.c) injected with high dose HexaPro Wuhan (WT) VLP vaccine with the formulation of 40 µg HexaPro WT VLP + 600 µg Alum + 300 µg K3-CpG for 2 times with 21 days intervals. Vaccinations were done in Dr. Abdurrahman Yurtaslan Oncology Training and Research Hospital (Ankara, Turkey), Yedikule Chest Diseases and Thoracic Surgery Training and Research Hospital (Istanbul, Turkey) and Kocaeli Medical Hospital (Kocaeli, Turkey) with the approval of 2021-06/1231 ethics committee. Blood samples were collected from Phase II volunteers on day 0, 21, 35, 49, 90 and 180 into BD Vacutainer SST II Advance blood collection tubes (BD Biosciences, USA) and on Day 0 and Day 35 blood samples were also collected in BD Vacutainer EDTA blood collection tubes (BD Biosciences, USA) with informed consent. The SST tubes were centrifuged at 2500 g for 10 minutes at 21°C. The sera were collected from the upper layer of the tube and

transferred into Eppendorf tubes to be stored at -20°C until further use. The blood collected into EDTA tubes were used for PBMC and plasma isolation as described in section 2.2.1.1.

CHAPTER 3

RESULTS

3.1. Pre-Clinical Data

In order to determine the effect of different VLP and adjuvant amounts along with their alternative combinations on humoral antibody response, 7 female BALB/c mice/group were injected with three doses of the designated vaccine formulations. The first group was injected with 100 µl of 2.5 µg HexaPro WT VLP + 120 µg Alum + 60 µg K3-CpG, the second group was injected with 100 µl of 5 µg HexaPro WT VLP + 120 µg Alum + 60 µg K3-CpG and the third group was injected with 100 µl of 5 µg HexaPro WT VLP + 60 µg Alum + 30 µg K3-CpG. The mice were bled from the tail vein for four times to collect serum. The first bleeding corresponds to 15 days after primary injection, the second bleeding was performed 15 days after booster, the third bleeding was done 2 months after the booster and finally the fourth bleeding was carried out 15 days following the third injection.

In order to evaluate the humoral immune responses elicited in in mice immunized with different doses of VLP vaccine, ELISA was performed using serum samples collected on 15 days post primary injection, 15 days post booster, 2 months after booster, and 15 days post third injection were used. Due to being the main immunogens of SARS-CoV-2, IgG secretion against these proteins were assessed using in-house recombinant proteins. Additionally, with the aim of understanding the cross-protection achieved against the new variants of concern, IgG responses against in-house WT RBD, commercial UK RBD and commercial Delta RBD were tested.

The antibody responses against homemade Spike protein for all groups including placebo are presented in Figure 3.1 A, B and C respectively. Figure 3.1 illustrates that for all groups, there is a significant increase in IgG titers at 15 days post booster compared to placebo group. However, the IgG levels have shown to be significantly decreased at 2 months after the booster. Therefore, in order to re-boost the immune system, a third dose of the same formulation was injected to each group and the IgG titers were evaluated after 15 days. The results indicate that IgG levels detectably increased after the third dose and caught up the titers that were reached at second bleeding. When the three groups immunized with different vaccine formulations are compared to each other, it can be seen that the third group, presented in Figure 3.1C, yielded the highest humoral immune responses in terms of IgG titers. This is followed by the second group, Figure 3.1B, and the first group, Figure 3.1A, gave the lowest IgG titers. This suggests that the optimal

vaccine formulation to elicit a decent immune response in mice requires a minimum of 5 µg VLP content.

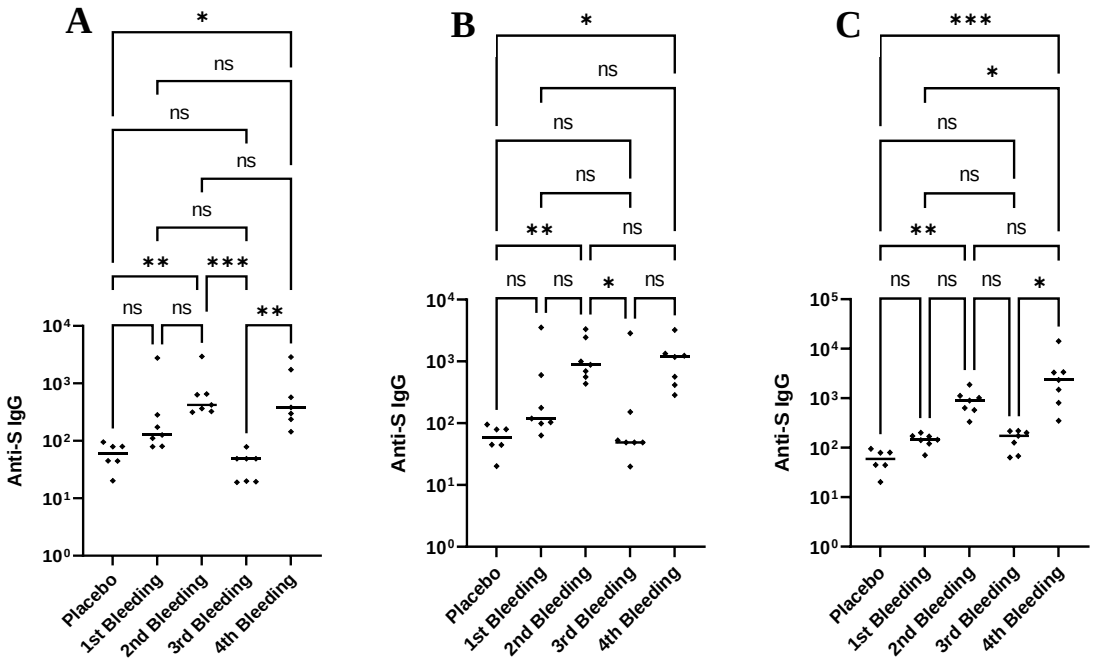


Figure 3.1. Assessment of IgG responses of immunized mice against homemade recombinant trimeric Spike (S) protein (4 µg/ml) by ELISA. 1st bleeding: 15 days post primary injection, 2nd bleeding: 15 days post booster, 3rd bleeding: 2 months after booster, 4th bleeding: 15 days post third injection. **(A)** Anti-spike IgG responses of 7 female BALB/c mice injected with 100 µl of 2.5 µg VLP + 120 µg Alum + 60 µg K3-CpG vaccine formulation. **(B)** Anti-spike IgG responses of 7 female BALB/c mice injected with 100 µl of 5 µg VLP + 120 µg Alum + 60 µg K3-CpG vaccine formulation. **(C)** Anti-spike IgG responses of 7 female BALB/c mice injected with 100 µl of 5 µg WT VLP + 60 µg Alum + 30 µg K3-CpG. Comparison of the IgG responses at indicated time points was done using one-way ANOVA with Dunnett's multiple comparisons test. *P < .05, **P < .01, ***P < .001.

In Figure 3.2. anti-homemade Nucleocapsid IgG titers of the previously mentioned experimental groups are presented. For all groups demonstrated in Figure 3.2A, B and C, anti-Nucleocapsid IgG titers of the immunized mice increase till 15 days post booster and remain at the peak level until 2 months after booster. When the serum samples are checked for IgG titers 15 days after the second booster (4th bleeding), the data show that the titers protected the peak values.

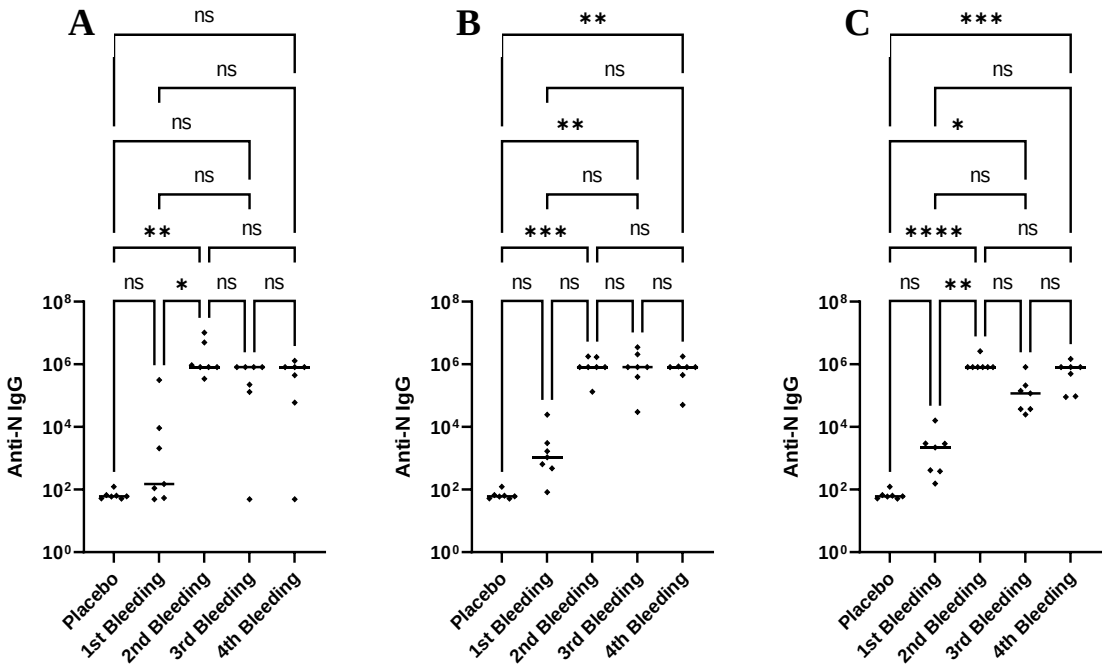


Figure 3.2. Assessment of IgG responses of immunized mice against homemade recombinant nucleocapsid (N) protein (1 μg/ml) by ELISA. 1st bleeding: 15 days post primary injection, 2nd bleeding: 15 days post booster, 3rd bleeding: 2 months after booster, 4th bleeding: 15 days post third injection. **(A)** Anti-nucleocapsid IgG responses of 7 female BALB/c mice injected with 100 μl of 2.5 μg VLP + 120 μg Alum + 60 μg K3-CpG vaccine formulation. **(B)** Anti-nucleocapsid IgG responses of 7 female BALB/c mice injected with 100 μl of 5 μg VLP + 120 μg Alum + 60 μg K3-CpG vaccine formulation. **(C)** Anti-nucleocapsid IgG responses of 7 female BALB/c mice injected with 100 μl of 5 μg WT VLP + 60 μg Alum + 30 μg K3-CpG. Comparison of the IgG responses at indicated time points was done using one-way ANOVA with Dunnett's multiple comparisons test. *P < .05, **P < .01, ***P < .001, ****P < .0001.

Studies prove that IgG production against receptor binding domain (RBD) of Spike protein is crucial as it is also directly correlated with generation of neutralizing antibodies against SARS-CoV-2 [111]. In Figure 3.3, anti-WT RBD IgG responses for all groups are demonstrated. Similar to anti-Spike antibody responses, the IgG titers increase significantly following 15 days after booster and there is a drop, although not significant, at 2 months after booster. When the IgG responses were re-assessed 15 days after the third dose, the data show that the levels increased slightly, but unlike in anti-Spike IgG levels, the responses acquired after the second bleeding could not be maintained. Although, for anti-WT RBD response the third dose could not boost the antibody levels as effectively as in anti-spike response, it can be seen that it is necessary in terms of retaining the IgG titers. Comparing IgG levels of the three vaccinated groups yields that the second group, presented in Figure 3.3B, elicited the highest humoral immune reaction in response to SARS-CoV-2 VLP vaccine.

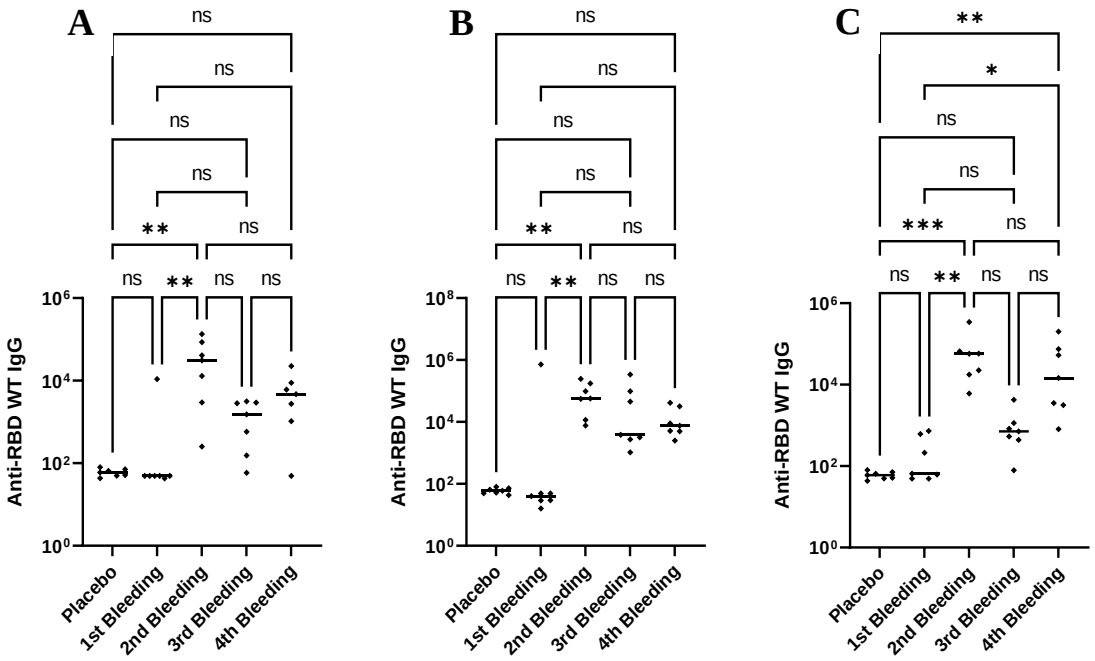


Figure 3.3. Assessment of IgG responses of immunized mice against homemade recombinant receptor binding domain wild type (RBD WT) protein (4 µg/ml) by ELISA. 1st bleeding: 15 days post primary injection, 2nd bleeding: 15 days post booster, 3rd bleeding: 2 months after booster, 4th bleeding: 15 days post third injection. **(A)** Anti-RBD WT IgG responses of 7 female BALB/c mice injected with 100 µl of 2.5 µg VLP + 120 µg Alum + 60 µg K3-CpG vaccine formulation. **(B)** Anti-RBD WT IgG responses of 7 female BALB/c mice injected with 100 µl of 5 µg VLP + 120 µg Alum + 60 µg K3-CpG vaccine formulation. **(C)** Anti-RBD WT IgG responses of 7 female BALB/c mice injected with 100 µl of 5 µg WT VLP + 60 µg Alum + 30 µg K3-CpG. Comparison of the IgG responses at indicated time points was done using one-way ANOVA with Dunnett's multiple comparisons test. *P < .05, **P < .01, ***P < .001.

Although all mice were immunized using vaccine containing the wild type VLP content, in order to test the effectiveness of VLP vaccine against other current variants, which are Alpha and Delta, the IgG production against these variants were also studied using recombinant Alpha and Delta RBD proteins.

There is a gradual increase in IgG titers against Alpha RBD in all groups presented in Figure 3.4 A, B, and C. Although there are conspicuous variations between the mice in the same group, IgG levels increase until 2 months after the booster and elevate upon injection with the third dose for all groups. Unlike the IgG responses generated against other recombinant proteins, anti-Alpha RBD IgG titers are observed to be higher at the third bleeding than second bleeding. When the data on Figure 3.4 is compared to Figure 3.3 it can be concluded that the IgG titers against WT RBD are higher than UK RBD for all vaccinated groups since the VLP vaccine is formulated with wild type VLP. However, unlike anti-WT RBD antibody responses, the results from anti-Alpha RBD IgG levels indicate that the highest antibody titers are obtained from the third group as it is presented in Figure 3.4C.

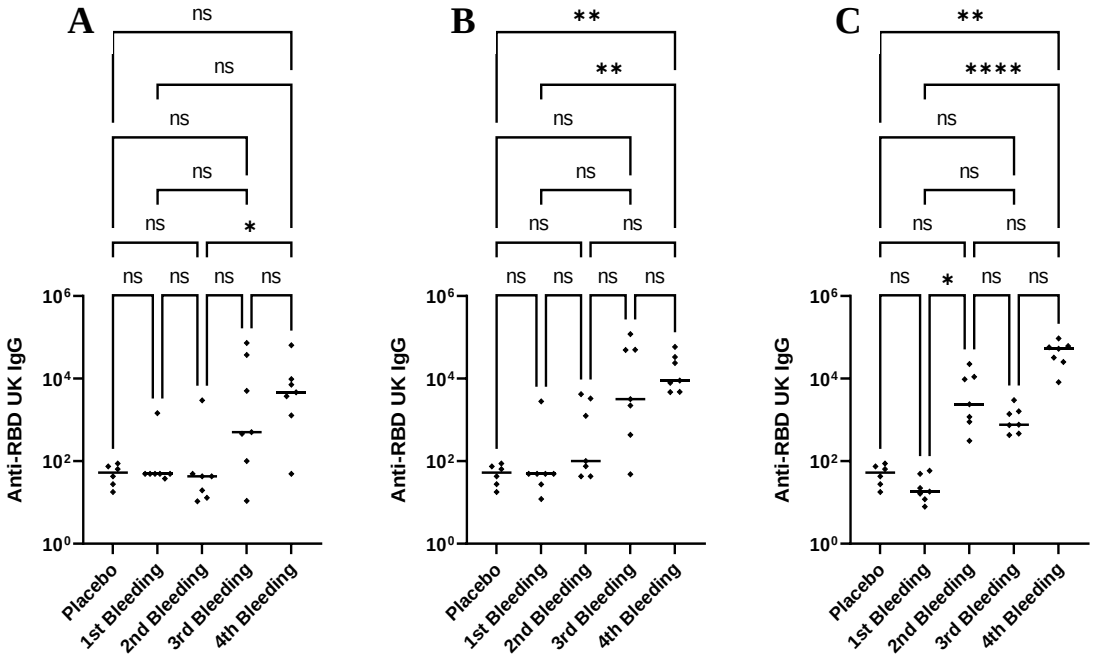


Figure 3.4. Assessment of IgG responses of immunized mice against commercial recombinant receptor binding domain UK (RBD UK) protein (1 µg/ml) by ELISA. 1st bleeding: 15 days post primary injection, 2nd bleeding: 15 days post booster, 3rd bleeding: 2 months after booster, 4th bleeding: 15 days post third injection. **(A)** Anti-RBD UK IgG responses of 7 female BALB/c mice injected with 100 µl of 2.5 µg VLP + 120 µg Alum + 60 µg K3-CpG vaccine formulation. **(B)** Anti-RBD UK IgG responses of 7 female BALB/c mice injected with 100 µl of 5 µg VLP + 120 µg Alum + 60 µg K3-CpG vaccine formulation. **(C)** Anti-RBD UK IgG responses of 7 female BALB/c mice injected with 100 µl of 5 µg WT VLP + 60 µg Alum + 30 µg K3-CpG. Comparison of the IgG responses at indicated time points was done using one-way ANOVA with Dunnett's multiple comparisons test. *P < .05, **P < .01, ***P < .001, ****P < .0001.

Finally, the IgG responses of the immunized mice against recombinant Delta RBD protein are presented in Figure 3.5. Similar to the results obtained against anti-UK RBD, the IgG titers gradually increase until the third bleeding. In the third group, demonstrated in Figure 3.5C, the effect of third injection on boosting the antibody responses is seen more clearly. The detected concentration of IgG against Delta RBD is lower compared to Alpha RBD and UK RBD. This may be because of the low detection capacity of the recombinant Delta RBD protein used. Similar to anti-UK RBD responses, the highest IgG production against recombinant Delta protein is achieved in the third group depicted in Figure 3.5C.

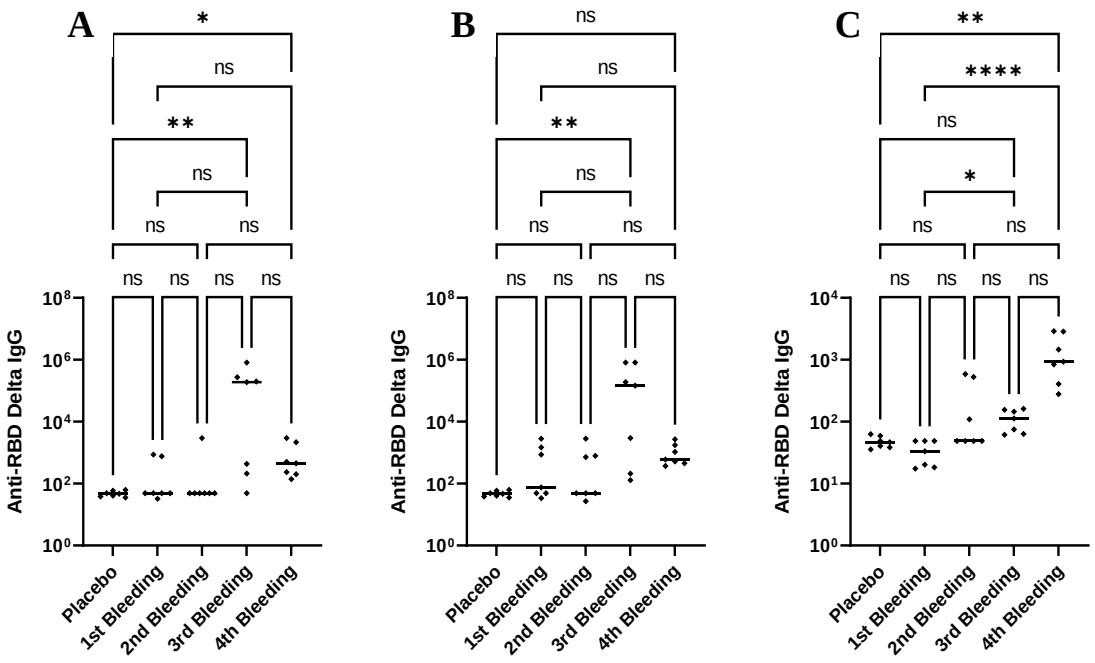


Figure 3.5. Assessment of IgG responses of immunized mice against commercial recombinant receptor binding domain Delta (RBD Delta) protein (1 µg/ml) by ELISA. 1st bleeding: 15 days post primary injection, 2nd bleeding: 15 days post booster, 3rd bleeding: 2 months after booster, 4th bleeding: 15 days post third injection. (A) IgG responses of 7 female BALB/c mice injected with 100 µl of 2.5 µg VLP + 120 µg Alum + 60 µg K3-CpG vaccine formulation. (B) IgG responses of 7 female BALB/c mice injected with 100 µl of 5 µg VLP + 120 µg Alum + 60 µg K3-CpG vaccine formulation. (C) IgG responses 7 female BALB/c mice injected with 100 µl of 5 µg WT VLP + 60 µg Alum + 30 µg K3-CpG. Comparison of the IgG responses at indicated time points was done using one-way ANOVA with Dunnett's multiple comparisons test. *P < .05, **P < .01, ***P < .001, ****P < .0001.

Overall, the pre-clinical results suggest that the vaccine formulation that elicited the highest humoral immune response contains 5 µg HexaPro WT VLP + 60 µg Alum + 30 µg K3-CpG which is injected to the third group containing 7 female BALB/c mice. When the antibody responses against Spike, Nucleocapsid and RBD variant proteins are evaluated based on ELISA results depicted in Figure 3.1-5, it can be deduced that the seropositivity increases 15 days after first booster, but the antibody levels start to decline until 2 months after booster. Hence, it is considered that a third dose of vaccine containing the same formulation would be necessary for boosting the humoral immune response. Evaluation of the results demonstrated that IgG titers increased 15 days after the third dose and fetched up the levels reached 15 days post booster. These data help to substantiate the necessity of third dose of vaccination for humans by presenting evidence about boosted IgG titers against Spike, Nucleocapsid and RBD variants.

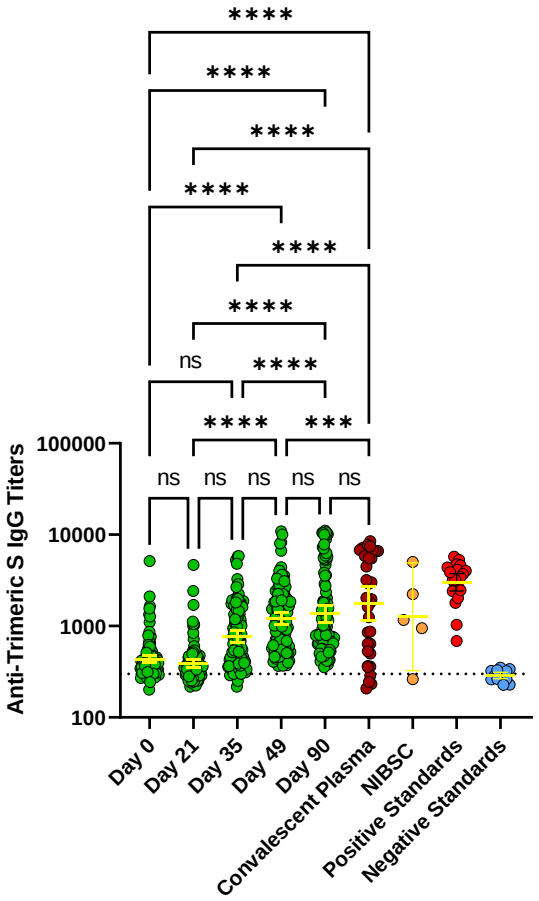
3.2. Clinical Data

3.2.1. Assessment of Humoral Immune Responses from Sera

Spike (S) and Nucleocapsid (N) proteins are among the four essential structural proteins of coronaviruses and studies prove that they act as the main immunogens during infection. Being a member of *Coronaviridae* family, SARS-CoV-2 is shown to induce IgG secretion against Spike, Nucleocapsid and receptor binding domain (RBD) of Spike for long term protection [112,113]. Therefore, in this study, the sera from volunteers immunized with two doses of VLP vaccine were collected at days 0, 21, 35, 49 and 90 and the immune responses were evaluated based on IgG production against Spike, Nucleocapsid, RBD WT, RBD UK, and RBD Delta antigens by employing ELISA method. In order to be able to evaluate and compare the IgG titers obtained from the volunteers, SARS-CoV-2 Verification Panel (containing 23 positive standards and 14 negative standards), International Reference Panel for SARS-CoV-2 (NIBSC) and 35 convalescent plasma samples from Marmara University were also studied.

In Figure 3.6 IgG titers of volunteers at days 0, 21, 35, 49 and 90 were determined against trimeric Spike protein by using homemade recombinant Spike protein (Figure 3.6A) and commercial Corona Hunter Spike IgG ELISA kit (Figure 3.6B). The serum samples were run together with the aforementioned standards and convalescent plasma samples for a valid comparison of the results. Figure 3.6A presents the anti-Spike IgG responses of the volunteers at the indicated days after first injection. The area under the curve values were calculated by drawing the OD405nm graph of every volunteer at each time point and are included in Appendix A. The negative sample of the NIBSC standards, indicated with the lowest value, sets the threshold for IgG titers. The results demonstrate that there is a gradual increase in IgG levels from Day 0 to Day 90 and the IgG responses are above the threshold. When the anti-Spike IgG titers at days 35, 49 and 90 are compared to negative standards, it can be seen that the antibody titers at the indicated time points are significantly higher. On the contrary, comparison of the IgG levels measured at days 35, 49 and 90 are not significantly lower than the positive standards. These results suggest that SARS-CoV-2 VLP vaccine can induce efficient humoral response against Spike protein in the long term.

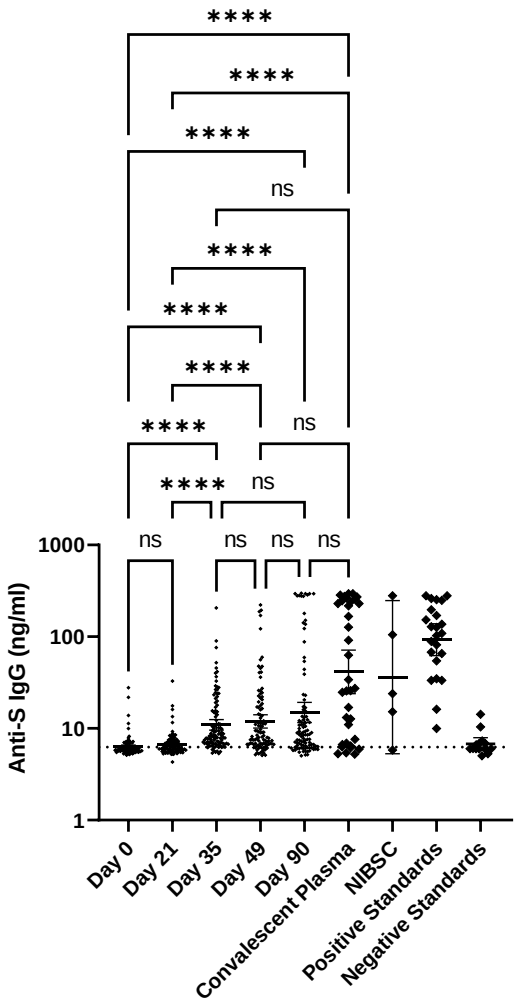
A



	Day 0	Day 21	Day 35	Day 49	Day 90	Convalescent Plasma	NIBSC	Positive Standards	Negative Standards
Number of values	105	106	106	109	98	35	5	23	14
Geometric mean	432.6	389.7	760.0	1217	1361	1756	1264	3015	287.8
Geometric SD factor	1.623	1.655	2.163	2.236	2.800	3.485	2.987	1.663	1.148
Lower 95% CI of geo. mean	393.9	353.6	655.0	1045	1107	1143	324.8	2420	265.8
Upper 95% CI of geo. mean	475.1	429.4	881.8	1418	1673	2696	4919	3756	311.7

Figure 3.6. Determination of anti-Spike IgG titers of volunteers at days 0, 21, 35, 49 and 90 compared to convalescent plasma samples, NIBSC reference panel for anti-SARS-CoV-2, positive standards and negative standards by ELISA. **(A)** IgG titers of the serum samples from the volunteers at days 0, 21, 35, 49, and 90, convalescent plasma samples, NIBSC International Reference Panel, positive standards and negative standards against homemade recombinant trimeric spike (S) protein (6 μg/ml). The dots represent area under the curve values for each volunteer. The IgG response comparisons for the samples was done using one-way ANOVA with Dunnett's multiple comparisons test. *P < .05, **P < .01, ***P < .001, ****P < .0001.

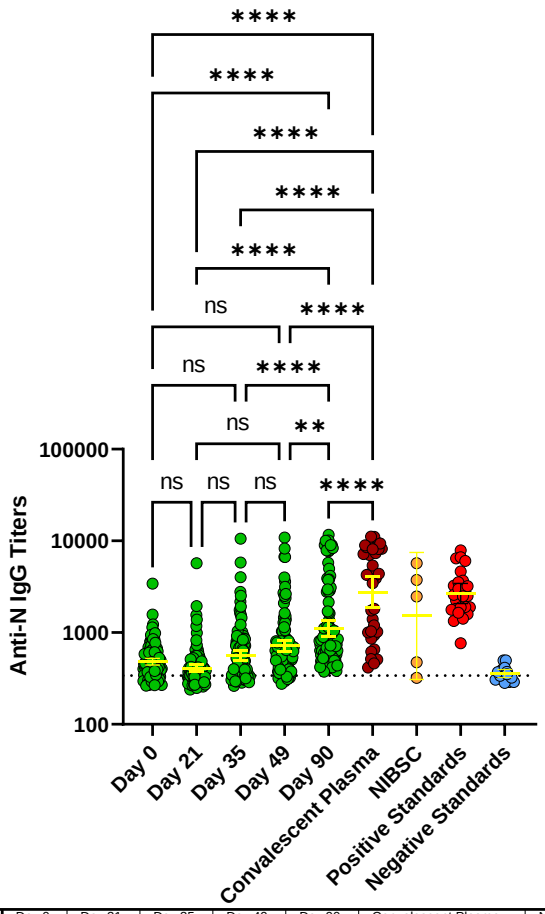
B



	Day 0	Day 21	Day 35	Day 49	Day 90	Convalescent Plasma	NIBSC	Positive Standards	Negative Standards
Geometric mean	6.312	6.666	10.95	11.91	14.93	41.35	36.15	92.78	6.768
Geometric SD factor	1.268	1.295	1.988	2.358	3.577	4.945	4.700	2.511	1.316
Lower 95% CI of geo. mean	6.035	6.348	9.599	10.08	11.59	23.88	5.293	62.31	5.775
Upper 95% CI of geo. mean	6.602	7.000	12.49	14.06	19.22	71.61	247.0	138.1	7.931

Figure 3.6. (B) IgG titers of serum samples from the volunteers at days 0, 21, 35, 49, and 90, convalescent plasma samples, NIBSC International Reference Panel, positive standards and negative standards against trimeric spike protein were assessed using Corona Hunter Kit. The IgG response comparisons for the samples was done using one-way ANOVA with Dunnett's multiple comparisons test. *P < .05, **P < .01, ***P < .001, ****P < .0001.

The anti-trimeric Spike IgG titers of the volunteers are further validated by using Corona Hunter Anti-SARS-CoV-2 Spike IgG ELISA kit. Like in Figure 3.6A, the negative specimen of the NIBSC reference panel designates the threshold for the IgG titers. The results obtained in Figure 3.6A are supported since IgG levels against trimeric Spike protein elevate in days 35,49 and 90 and they are higher than the negative standards. When the antibody production at days 35, 49 and 90 are compared with the convalescent plasma samples, it can be proposed that there is no significant difference between them. Increment in the level of antibodies until 3 months after the first dose proves the efficacy of the VLP vaccine in terms of its triggering of humoral immune responses and inducing long term protection.

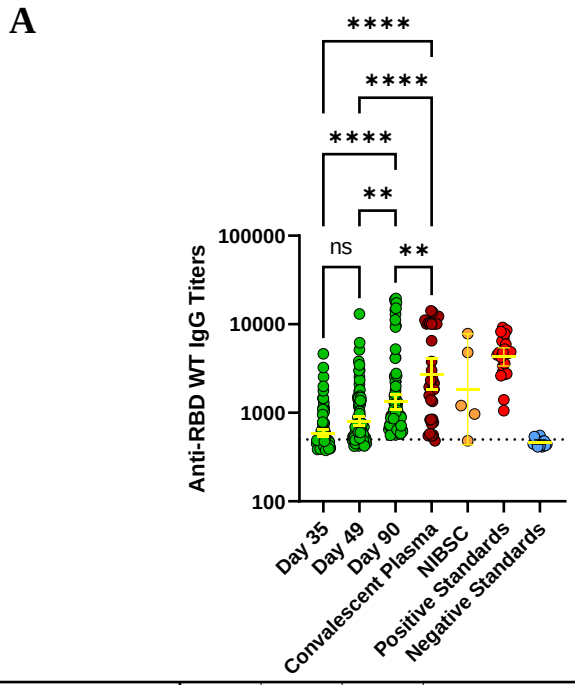


	Day 0	Day 21	Day 35	Day 49	Day 90	Convalescent Plasma	NIBSC	Positive Standards	Negative Standards
Number of values	105	106	106	106	97	35	5	23	14
Geometric mean	481.3	407.1	565.1	716.2	1116	2770	1519	2668	357.5
Geometric SD factor	1.522	1.592	1.971	2.155	2.659	3.054	3.610	1.793	1.200
Lower 95% CI of geo. mean	443.7	372.2	495.9	617.7	916.6	1887	308.5	2073	321.8
Upper 95% CI of geo. mean	522.1	445.3	644.0	830.4	1360	4064	7476	3434	397.2

Figure 3.7. Determination of IgG titers of volunteers against homemade recombinant Nucleocapsid (N) (4 µg/ml) protein at days 0, 21, 35, 49 and 90 compared to convalescent plasma samples, NIBSC reference panel for anti-SARS-CoV-2, positive standards and negative standards by ELISA. The dots represent area under the curve values for each volunteer. The IgG response comparisons for the samples was done using one-way ANOVA with Dunnett's multiple comparisons test. *P < .05, **P < .01, ***P < .001, ****P < .0001.

IgG responses of the volunteers, convalescent plasma samples, NIBSC International Reference Panel, positive standards and negative standards against homemade recombinant Nucleocapsid protein are depicted in Figure 3.7. The area under the curve values were calculated by drawing the OD405nm graph of every volunteer at each time point and are included in Appendix A. The baseline level of IgG is determined by the negative specimen of the NIBSC International Reference Panel and introduced as a dashed line on the graph. Similar to anti-Spike responses, there is an elevation in IgG titers from Day 0 to Day 90 especially following booster on Day 21. The IgG titers of the volunteer serum samples are higher than that of negative standards.

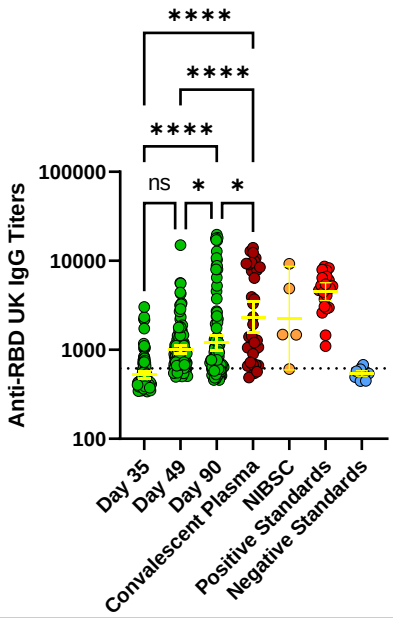
However, when compared to convalescent plasma samples and positive standards which yielded antibody responses very close to each other, volunteer serum samples seem to have lower IgG titers. When a comparison is made between anti-trimeric Spike and anti-Nucleocapsid IgG responses, presented in Figure 3.6A and Figure 3.7 respectively, it can be concluded that detected level of antibodies against Nucleocapsid protein is lower. In literature, it is proposed that antibody detection against Nucleocapsid is more sensitive than antibody detection against Spike [113,114]. However, according the results obtained, the sensitivity against-Spike antibodies is higher. This can be explained by the use of homemade recombinant Spike and Nucleocapsid proteins produced in our laboratory. The impurities in recombinant Spike protein used for coating may cause non-specific binding which leads to background signaling and higher OD405 values resulting in higher IgG titer profile.



	Day 35	Day 49	Day 90	Convalescent Plasma	NIBSC	Positive Standards	Negative Standards
Number of values	109	106	100	35	5	23	14
Geometric mean	587.3	804.0	1336	2719	1843	4282	466.8
Geometric SD factor	1.605	1.930	2.693	3.235	3.198	1.726	1.099
Lower 95% CI of geo. mean	536.9	708.4	1097	1817	435.2	3382	441.9
Upper 95% CI of geo. mean	642.5	912.5	1626	4070	7807	5421	493.1

Figure 3.8. Determination of anti-RBD IgG titers of volunteers at days 35, 49 and 90 compared to convalescent plasma samples, NIBSC reference panel for anti-SARS-CoV-2, positive standards and negative standards by ELISA. **(A)** IgG titers of the indicated serum and plasma samples against commercial recombinant RBD WT protein (1 µg/ml). The dots represent area under the curve values for each volunteer. The IgG response comparisons for the samples was done using one-way ANOVA with Dunnett's multiple comparisons test. *P < .05, **P < .01, ***P < .001, ****P < .0001.

B

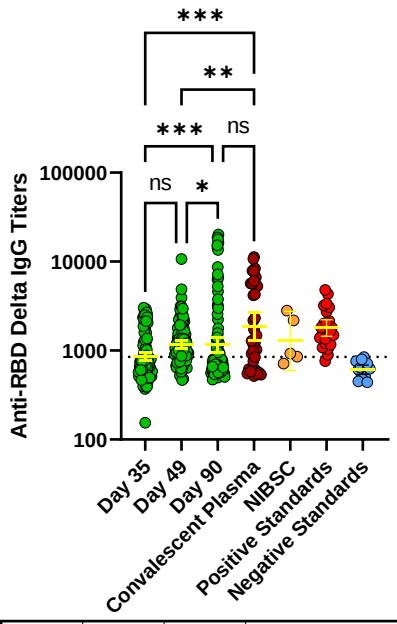


	Day 35	Day 49	Day 90	Convalescent Plasma	NIBSC	Positive Standards	Negative Standards
Number of values	109	111	104	35	5	23	14
Geometric mean	522.2	1008	1206	2325	2270	4514	542.4
Geometric SD factor	1.550	1.834	2.739	3.193	2.940	1.700	1.135
Lower 95% CI of geo. mean	480.5	899.3	991.4	1560	594.9	3589	504.3
Upper 95% CI of geo. mean	567.5	1130	1467	3465	8661	5677	583.5

Figure 3.8. (B) IgG titers of volunteers at days 35, 49 and 90 compared to convalescent plasma samples, NIBSC reference panel for anti-SARS-CoV-2, positive standards and negative standards against commercial recombinant RBD UK protein (1 µg/ml). The dots represent area under the curve values for each volunteer. The IgG response comparisons for the samples was done using one-way ANOVA with Dunnett's multiple comparisons test. *P < .05, **P < .01, ***P < .001, ****P < .0001.

In Figure 3.8 IgG titers of volunteers, convalescent plasma samples, NIBSC reference panel for anti-SARS-CoV-2, positive standards and negative standards against variants of receptor binding domain (RBD) of Spike are shown. The area under the curve values were calculated by drawing the OD405nm graph of every volunteer at each time point and are included in Appendix A. The threshold levels for the IgG titers against all variant recombinant proteins are specified according to the negative sample of the NIBSC International Reference Panel and shown as the dashed line on the graphs. When the IgG profiles of the abovementioned samples are investigated against wild type (WT) (Figure 3.8A) RBD, Alpha (UK) RBD (Figure 3.8B) and Delta RBD (Figure 3.8C), it can be concluded that the seropositivity against those three recombinant RBD proteins increases from Day 35 to Day 90. IgG titers against recombinant WT RBD increases more compared to UK RBD and Delta RBD, and the titers are not below the threshold level at Day 35 unlike the other two variants. Formulation of the vaccine with WT VLP is shown to favor anti-WT RBD responses more compared to other two variants.

C

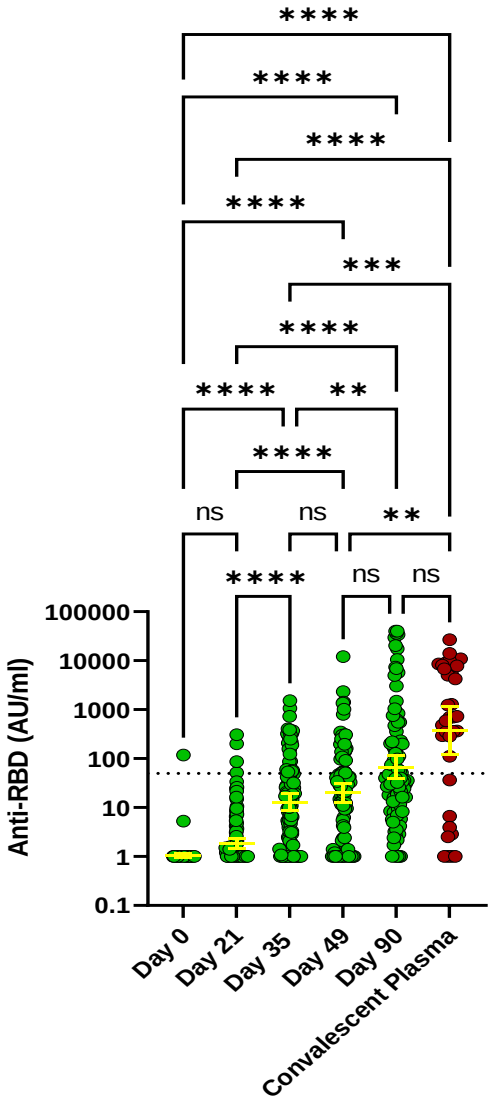


	Day 35	Day 49	Day 90	Convalescent Plasma	NIBSC	Positive Standards	Negative Standards
Number of values	109	106	100	35	5	23	14
Geometric mean	856.3	1176	1157	1874	1283	1795	609.6
Geometric SD factor	1.820	1.696	2.810	2.884	1.852	1.636	1.231
Lower 95% CI of geo. mean	764.2	1063	942.3	1303	596.6	1451	540.6
Upper 95% CI of geo. mean	959.4	1302	1420	2697	2758	2221	687.4

Figure 3.8. (C) IgG titers of volunteers at days 35, 49 and 90 compared to convalescent plasma samples, NIBSC reference panel for anti-SARS-CoV-2, positive standards and negative standards against commercial recombinant RBD UK protein (1 μg/ml). The dots represent area under the curve values for each volunteer. The IgG response comparisons for the samples was done using one-way ANOVA with Dunnett's multiple comparisons test. *P < .05, **P < .01, ***P < .001, ****P < .0001.

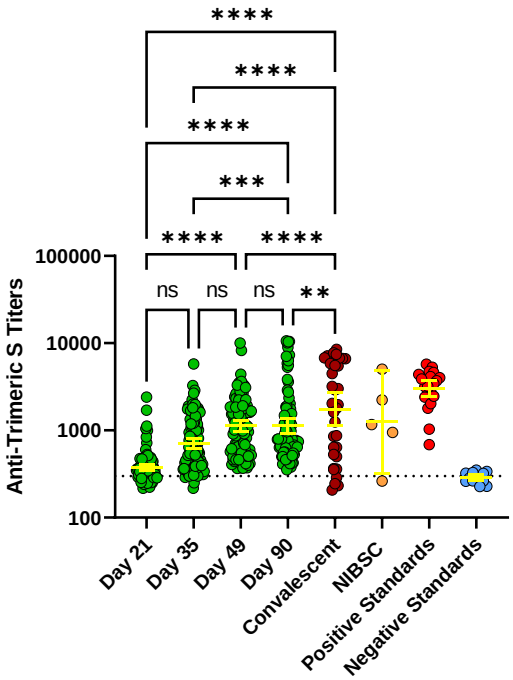
Neutralizing antibody production is vital during SARS-CoV-2 infection as it helps to minimize interaction of the viruses with the ACE-2 receptor expressing cells and elicits stronger and longer lasting immune response [115,116]. Studies show that the neutralizing antibodies against receptor binding domain (RBD) of Spike protein are produced after SARS-CoV-2 infection [115]. Therefore, the serum samples from the volunteers collected at days 0, 21, 35, 49 and 90 and the convalescent plasma samples were analyzed for the presence of neutralizing antibodies against RBD by Deren Laboratory, Ankara, Turkey. For quantification SARS-CoV-2 IgG Quant method was performed with Abbott kit by using the ARCHITECT i System. The results of the neutralizing anti-RBD antibody titers are presented in Figure 3.9 for the indicated sample set. According to the manufacturer's protocol, the cut off value was determined as 50 AU/ml. Data from Figure 3.9 demonstrate that although anti-RBD neutralizing antibody titers are below the cut of value, there is a progressive increase in the antibody titers from Day 21 to Day 90 while almost all the titers at Day 0 are below the threshold value and significantly lower than Day 35,

Day 49 and Day 90 titers. This once more validates the seronegativity of the samples prior to vaccination. Additionally, at Day 90, the titer reaches the cut off value of 50 AU/ml. When the antibody titers at Day 90 are compared to that of convalescent plasma samples, it can be seen that there is no significant difference which proves the long-term protection provided by the VLP vaccine.



	Day 0	Day 21	Day 35	Day 49	Day 90
Number of values	106	110	109	103	96
Geometric mean	1.063	1.833	12.90	19.78	67.27
Geometric SD factor	1.632	3.369	8.034	9.648	15.50
Lower 95% CI of geo. mean	0.9670	1.457	8.683	12.70	38.60
Upper 95% CI of geo. mean	1.168	2.306	19.16	30.80	117.2

Figure 3.9. Quantification of neutralizing antibody levels of the serum and plasma samples using SARS-CoV-2 IgG Quant method performed via ARCHITECT i System. This automated assay was performed by DEREN Laboratory (Ankara, Turkey). The comparisons for the samples were done using one-way ANOVA with Dunnett's multiple comparisons test. *P < .05, **P < .01, ***P < .001, ****P < .0001.



	Day 21	Day 35	Day 49	Day 90	Convalescent	NIBSC	Positive Standards	Negative Standards
Number of values	102	102	103	88	35	5	23	14
Geometric mean	374.9	711.4	1131	1131	1756	1264	3015	287.8
Geometric SD factor	1.503	2.020	2.088	2.481	3.485	2.987	1.663	1.148
Lower 95% CI of geo. mean	346.1	619.6	979.5	932.7	1143	324.8	2420	265.8
Upper 95% CI of geo. mean	406.2	816.7	1306	1371	2696	4919	3756	311.7

Figure 3.10. Determination of anti-homemade recombinant Spike (S) (6 µg/ml) IgG titers of volunteers with no SARS-CoV-2 infection during the course of Phase II clinical trial at days 0, 21, 35, 49 and 90 compared to convalescent plasma samples, NIBSC reference panel for anti-SARS-CoV-2, positive standards and negative standards by ELISA. The dots represent area under the curve values for each volunteer. The IgG response comparisons for the samples was done using one-way ANOVA with Dunnett's multiple comparisons test. *P < .05, **P < .01, ***P < .001, ****P < .0001.

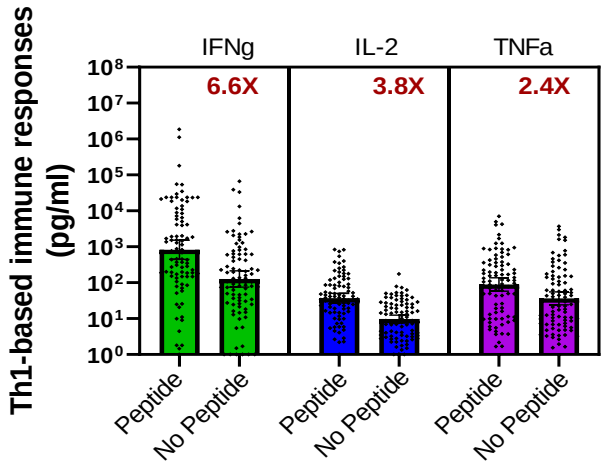
Over the course of Phase II clinical trial, 16 out of 110 volunteers vaccinated with 2 doses of WT VLP vaccine were infected with SARS-CoV-2. According to the information obtained, all the volunteers infected with SARS-CoV-2 were asymptomatic or showed mild symptoms. It is reported that the mild cases survived COVID-19 with flu-like symptoms without need of hospitalization or use of medication. In order to prove that presence of infected volunteers in the data doesn't affect efficacy of the VLP vaccine, in Figure 3.10 the SARS-CoV-2 infected individuals are omitted from the graph and the antibody titers against Spike protein are presented for the indicated sample set. Comparison of the IgG levels of the serum samples in Figure 3.10 to the results in Figure 3.6A indicates that efficacy of the VLP vaccine doesn't decrease when the infected volunteers are ruled out from the data.

Overall, evaluation of the antibody responses from sera shows that humoral immune response is triggered in vaccinated volunteers against Spike and Nucleocapsid proteins starting from Day 21 and continues to increase until Day 90. The assessments to quantify the efficacy of the VLP vaccine against current variants along with the authentic virus demonstrate that VLP vaccine is can effectively induce antibody production against recombinant WT RBD, Alpha RBD and Delta RBD proteins. Although the anti-Alpha RBD and anti-Delta RBD IgG titers are lower than that of anti-WT RBD, the IgG levels are above the determined cut-off values particularly in Day 49 and Day 90. The long-term protection provided by the VLP vaccine is further supported by presentation of the neutralizing antibody titers which is similar to the pattern observed in RBD variants which increases starting from Day 21 and reaches the highest titer in Day 90.

3.2.2. Assessment of Cellular Immune Responses

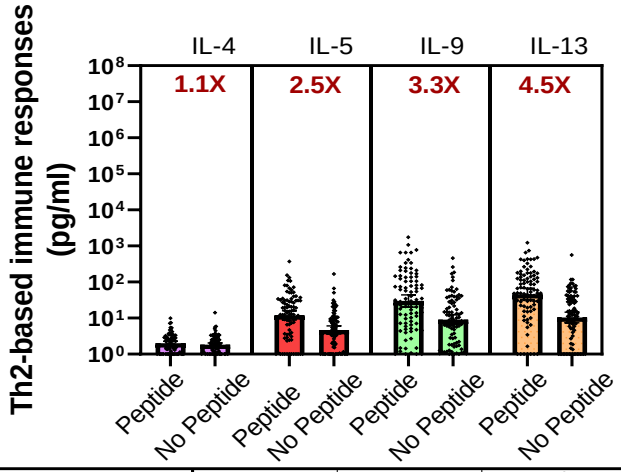
The adaptive arm of immune system takes part a crucial role during a viral infection with the help of T helper cells and the cytokine milieu generated [117]. Previous studies indicate that in the case of SARS-CoV and MERS-CoV infections, activation of Th1 arm of adaptive immunity is vital for effective clearance of the virus and control of the disease [118]. Similarly, SARS-CoV-2 infection is proven to elicit enhanced activation of $CD4^+$ T cells and cytokine production resulting in increased level of Th1 cells in COVID-19 patients [119]. Therefore, during the development of SARS-CoV-2 VLP vaccine, besides humoral immunity, triggering cellular immune responses was also aimed. To assure elevated cellular activation, VLP vaccine was formulated with Alum and K3 CpG ODN as adjuvants. Adjuvantation of the VLP vaccine with Alum favors a more Th2-biased immunity while formulation with K3 CpG ODN provides a Th1-skewed immune reaction as required for the viral clearance [98,103].

In order to evaluate the T cell responses of the vaccinated volunteers, PBMCs isolated from the Day 35 blood samples were stimulated with SARS-CoV-2 SMNO peptide pool and the production of 12 cytokines (IL-2, IL4, IL5, IL6, IL9, IL10, IL13, IL17A, IL17F, IL22, IFN-γ and TNF-α) were assessed using LEGENDplex™ HU Th Cytokine Panel (12-plex) kit. The dot plot overlays for each volunteer are provided in Appendix A.



	IFNg		IL-2		TNFa	
	A:1	A:2	B:1	B:2	C:1	C:2
Number of values	88	88	88	88	88	88
Geometric mean	825.8	126.0	37.30	9.724	89.26	36.72
Geometric SD factor	18.43	11.74	4.212	3.318	7.392	6.990
Lower 95% CI of geo. mean	445.4	74.79	27.51	7.542	58.43	24.32
Upper 95% CI of geo. mean	1531	212.4	50.59	12.54	136.4	55.45

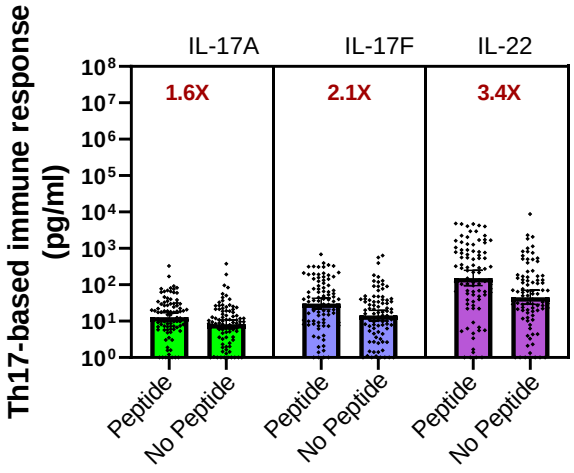
Figure 3.11. Th1-related cytokine responses of PBMCs collected from vaccinated volunteers in Day 35 are shown. Production of IFN-γ, IL-2 and TNF-α cytokines are presented for the SMNO peptide pool treated and the nontreated PBMCs. The fold induction values are demonstrated at the top of each cytokine column.



	IL-4		IL-5		IL-9		IL-13	
	A:1	A:2	B:1	B:2	C:1	C:2	D:1	D:2
Number of values	88	88	88	88	88	88	88	88
Geometric mean	2.009	1.823	11.85	4.677	29.88	9.066	46.25	10.38
Geometric SD factor	1.772	1.750	4.200	3.346	6.361	4.590	5.403	4.943
Lower 95% CI of geo. mean	1.780	1.620	8.743	3.621	20.19	6.565	32.35	7.398
Upper 95% CI of geo. mean	2.268	2.053	16.06	6.041	44.23	12.52	66.12	14.56

Figure 3.12. Th2-related cytokine responses of PBMCs collected from vaccinated volunteers in Day 35 are shown. Production of IL-4, IL-5, IL-9 and IL-13 cytokines are presented for the SMNO peptide pool treated and the nontreated PBMCs. The fold induction values are demonstrated at the top of each cytokine column.

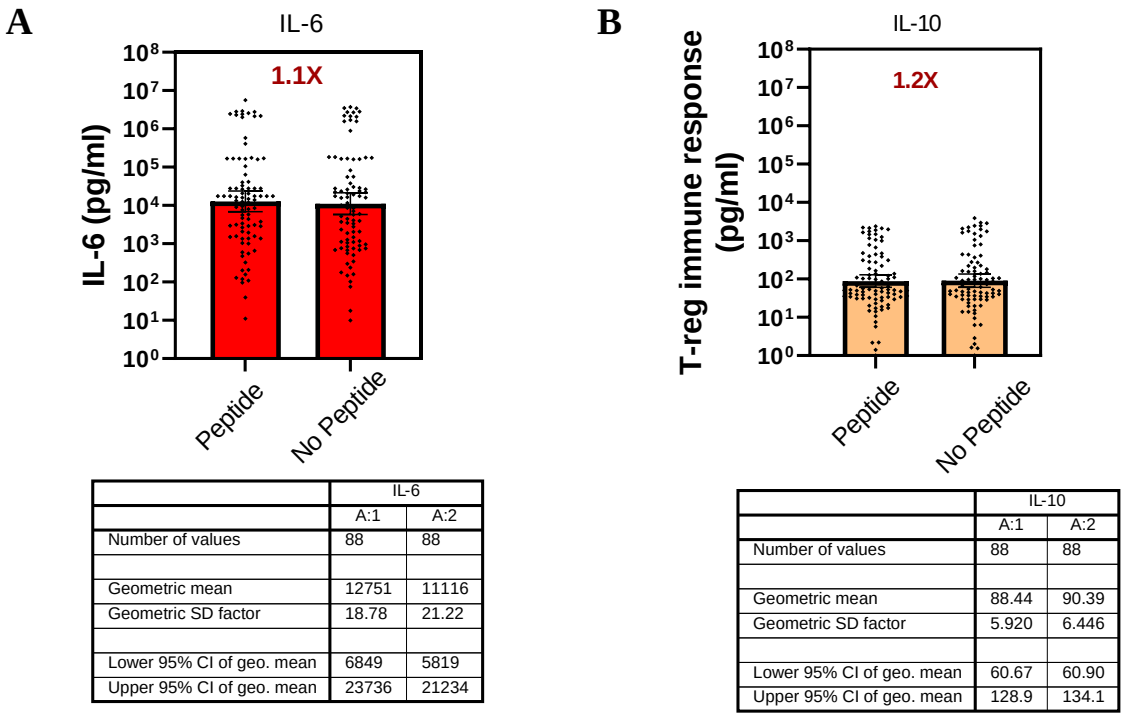
In Figure 3.11 secretion of Th1-type cytokines are shown for the peptide pool treated and the nontreated PBMCs. It can be seen that the cytokine secretion is highest for IFN-γ which is followed by IL-2 and TNF-α. The fold induction values provided for each cytokine show that production of IFN-γ, IL-2 and TNF-α increased after treatment with SMNO peptides proving the Th1-biased reaction facilitated by formulation with K3 CpG ODN. The levels of IL-4, IL-5, IL-9 and IL-13, presented in Figure 3.12, demonstrate the Th2-associated cytokine production. The data presented in Figure 3.12 suggest that production of all Th2-related cytokines increased after treatment with SARS-CoV-2 SMNO peptide pool. IL-13 level increased the most with a fold induction value of 4.5X while the increase in IL-4 level is the least with the fold induction value of 1.1X. It can be seen that utilization of Alum as the second adjuvant in VLP vaccine formulation favors Th2-type cytokine secretion. However, when the fold induction values presented in Figure 3.11 and Figure 3.12 are compared, it can be deduced that the increment in the level of Th1-associated cytokines is higher than that of Th2-based cytokines which is more advantageous during viral infections.



	IL-17A		IL-17F		IL-22	
	A:1	A:2	B:1	B:2	C:1	C:2
Number of values	88	88	88	88	88	88
Geometric mean	12.89	8.247	30.38	14.28	153.0	45.03
Geometric SD factor	3.641	3.583	5.079	4.685	9.812	8.179
Lower 95% CI of geo. mean	9.806	6.293	21.53	10.30	94.31	28.85
Upper 95% CI of geo. mean	16.96	10.81	42.87	19.81	248.2	70.28

Figure 3.13. Th17-based cytokine responses of PBMCs collected from vaccinated volunteers in Day 35 are shown. Production of IL-17A, IL-17F and IL-22 cytokines are presented for the SMNO peptide pool treated and the nontreated PBMCs. The fold induction values are demonstrated at the top of each cytokine column.

With the aim of analyzing other T helper cell subsets induced by VLP vaccine, Th17-associated cytokine levels were also assessed. During SARS-CoV-2 infection, inflammatory response is generated by Th17 through secretion of cytokines. Recent evidence suggests that elevated level of Th17 response results in suppression of Treg responses, downregulation of Th1 differentiation and induction of Th2-biased reaction [120]. Figure 3.13 demonstrates IL-17A, IL-17F and IL-22 productions for the peptide pool treated and nontreated PBMCs. According to the result, secretion of all three cytokines increased following treatment with peptide pool. However, comparing the data to the results in Figure 3.11 shows that the increase in Th1-associated cytokines is higher than that of Th17-type cytokines. These data verify the efficacy of VLP vaccine in terms of eliciting a Th1-dominant immune response together with inducing other helper T cell subsets for robust activation.



	IL-6	
	A:1	A:2
Number of values	88	88
Geometric mean	12751	11116
Geometric SD factor	18.78	21.22
Lower 95% CI of geo. mean	6849	5819
Upper 95% CI of geo. mean	23736	21234

	IL-10	
	A:1	A:2
Number of values	88	88
Geometric mean	88.44	90.39
Geometric SD factor	5.920	6.446
Lower 95% CI of geo. mean	60.67	60.90
Upper 95% CI of geo. mean	128.9	134.1

Figure 3.14. IL-6 and IL-10 cytokine responses of PBMCs collected from vaccinated volunteers in Day 35 are shown. **(A)** Production of IL-6 cytokine is presented for the SMNO peptide pool treated and the nontreated PBMCs. **(B)** Production of IL-10 cytokine is presented for the SMNO peptide pool treated and the nontreated PBMCs. The fold induction values are demonstrated at the top of each cytokine column.

Evidence suggests that excessive IL-6 secretion during viral infections restrains differentiation of Th1 cells and favors polarization into Th2 cells through suppression of IFN-γ secretion [121]. Additionally, IL-6 is involved in regulation of immune responses mediated by Th17 and Treg cells. While IL-6 is shown to be required for differentiation into Th17 subset, its presence is reported to inhibit generation of Treg cells which are involved in prohibition of autoimmune responses [122]. Therefore, IL-6 production after immunization with VLP vaccine was evaluated and the results are presented in Figure 3.14A. The data indicate that there is a very low increase in IL-6 production for the peptide treated PBMCs. Since there is no significant increase in IL-6 secretion, it can be concluded that Th1-associated response is not inhibited due to elevated level of IL-6. In order to interpret Treg cell activation, IL-10 secretion, which has anti-inflammatory activity, was quantified and the results are demonstrated in Figure 3.14B. The graph shows that there is no significant increase in IL-10 production for the peptide treated and the nontreated groups which implies that there is no significant differentiation into Treg cells.

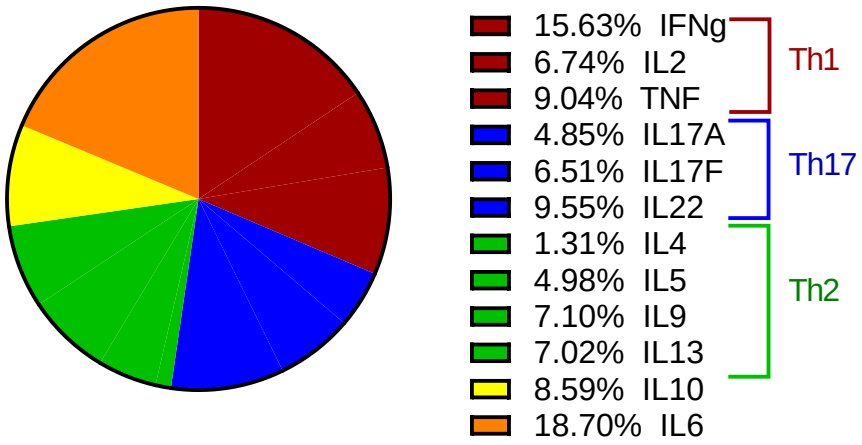


Figure 3.15. The percent distribution of Th1, Th2, Th17, T-reg and IL-6 based immune responses are presented in a pie chart.

Finally, in Figure 3.15 the percent distributions of each cytokine and the associated T cell subset responses are presented. The graph shows that the immune response induced by Th1, Th2, Th17 and Treg cells comprise 31.4%, 20.4%, 20.9% and 8.6% of the total cellular immune responses respectively. All in all, Figure 3.15 once more validates the observation that cellular immune response triggered against SARS-CoV-2 VLP vaccine is Th1-biased rather than Th2 as it was aimed by the utilization of K3 CpG ODN as adjuvant. This is followed by Th2-associated response which is favored due to use of Alum in the vaccine formulation.

CHAPTER 4

DISCUSSION

As of March 2020, COVID-19 pandemic, caused by SARS-CoV-2, has become one of the main concerns of the whole world. The high transmission rate of the virus, absence of an effective drug treatment or vaccine and the severe symptoms and death rates especially observed in elderly paved the way for cautionary measures such as lockdowns, social distancing, frequent disinfection of hands, wearing masks and etc. The devastating blows of pandemic to the health sector, economy and social life accelerated the global race to find a vaccine against SARS-CoV-2 for acquisition of herd immunity. Up until now, 147 vaccine studies employing different technologies are reported to be in clinical development stage according to WHO [92]. Among those 147 vaccines, the majority are designed for generation of antibody response against Spike protein of the SARS-CoV-2 virus due to interaction of the Spike protein with human ACE2 receptor [123]. The vaccines targeting Spike protein or a certain region of Spike protein are developed by utilizing various technologies including inactivated viruses, live attenuated vaccines, recombinant proteins, replication-incompetent vectors, DNA vaccines, RNA vaccines and etc. [94]. An alternative approach for vaccine development against SARS-CoV-2 is employment of VLPs containing the four structural proteins of the virus, Spike (S), Nucleocapsid (N), Membrane (M) and Envelope (E), which forms the basis of this project. Although some of the current vaccines in the clinical use induce high antibody production in the immune system, growing body of evidence points out that VLPs are effective in terms of eliciting robust cellular and humoral responses which is vital in the case of SARS-CoV-2 infection since neutralizing antibody titers are shown to diminish over time [124,125]. In addition to several advantages of VLPs mentioned in section 1.3.1, the use of VLP technology for SARS-CoV-2 vaccines can render it to become more effective against the newly emerging variants of serious concern such as Alpha, Delta and Omicron compared to other vaccines targeting only the Spike protein [126]. It has been reported that utilization of M and N proteins in vaccine formulation contributes to enhancement of the immune response via activation of $CD4^+$ and $CD8^+$ T cells [85,126]. Moreover, generation of non-neutralizing antibodies against Nucleocapsid protein can favor cross-immunity so that infection with new variants will result in a stronger immune reaction [126,127]. In this study, we aimed to analyze the humoral and cellular immune responses triggered by SARS-CoV-2 VLP vaccine formulated with the four structural proteins of the virus along with the adjuvants K3 CpG ODN and Alum.

Following manufacturing process of the vaccine as detailly described in İpekoğlu, E. M. (2022), pre-clinical studies are carried out in BALB/c mice. The experiment design consisted of 4 groups each containing 7 mice and each group was immunized with a different vaccine formulation in order to determine the optimum antigen and adjuvant doses. The first group was injected with 100 µl of 2.5 µg HexaPro WT VLP + 120 µg Alum + 60 µg K3-CpG, the second group was injected with 100 µl of 5 µg HexaPro WT VLP + 120 µg Alum + 60 µg K3-CpG, the third group was injected with 100 µl of 5 µg HexaPro WT VLP + 60 µg Alum + 30 µg K3-CpG and the fourth group was placebo. Throughout the pre-clinical and clinical practices, we used HexaPro (6p) VLP as our previous studies proved that it is more stable and induces a stronger immunogenic response compared to other variants such as two proline (2p) VLP [126].

Assessment of anti-Spike immune responses yielded that for all vaccinated groups, IgG levels slightly increase after first injection, but the boost in antibody titers is actually observed 15 days after the booster injection which corresponds to the 2nd bleeding. However, as evidenced in literature, a decline in IgG levels is expected to be observed after three months and the titers obtained after the third bleeding are in line with this argument [128]. In order to boost the immune reaction, mice were injected with a third dose of the vaccine and the results indicate that anti-Spike antibody titers are significantly elevated following booster for all groups.

Next, to evaluate the effect of VLP vaccine on humoral immune responses in mice, antibody production against the other main immunogen which Nucleocapsid was tested. Ortega et al. stated in their article that decay of anti-Nucleocapsid antibodies are faster compared to the decay of anti-Spike antibodies [128]. Therefore, for the third bleeding, we expected the anti-Nucleocapsid IgG titers to be lower than the anti-Spike IgG levels. However, according to our data, the trend in antibody titers against Nucleocapsid was unexpected. The results show that the antibody titers slightly increase after the first injection, but after the second injection, the antibody levels elevate significantly. Even at the third bleeding the IgG titers were observed to remain at the same level and there was no increase after the second booster. This can be explained by the use of in-house recombinant Nucleocapsid protein for ELISA. This batch of recombinant Nucleocapsid produced in our lab was rich in degradation product and impurities. Thus, the signal to background ratio was low and the signal obtained was not only due to Nucleocapsid specific antibodies but also because of impurities. By utilizing a commercial recombinant Nucleocapsid protein for ELISA, the results can be further verified and the effect of second booster injection on antibody levels can be comprehended more clearly.

As stated previously, interaction of RBD of Spike protein with the ACE2 receptors facilitates entry of the virus into the host cells and the anti-RBD antibody titers are directly correlated with neutralizing antibody levels [111]. Since for the animal experiments neutralization assay was not

performed, evaluation of anti-RBD antibody titers may give an idea about the neutralizing antibody response induced by VLP vaccine. To this end, we analyzed immunogenic responses elicited against WT RBD together with UK RBD and Delta RBD which are the newly emerging variants. For anti-WT RBD responses, it can be deduced that the trend in antibody levels is similar to anti-Spike titers. The IgG levels increase until the second bleeding, there is a decline 2 months after the booster and the second booster enhanced the titers. However, for the UK RBD and Delta RBD antibody titers, unexpectedly, antibody levels continued to increase until 2 months after the booster. Despite this, the third injection elevated the IgG responses. Among the RBD variants, the immunogenic response was triggered most effectively against the WT RBD as expected. The breadth of immune response elicited by VLP vaccine can be further expanded by formulating the third dose with the new variants of concern so that a cross-protective reaction can be triggered and the antibody titers obtained against different RBD variants could be higher.

As mentioned earlier the aim of pre-clinical experiments was also to establish the optimum dose for the clinical trials. In literature it was proven that VLP vaccines can induce a stronger immune response compared to subunit vaccines, but employment of the correct adjuvant with the optimum dose is also shown to reinforce the immune reaction triggered. It is vital to determine the optimum amount of Alum in vaccine formulation as it is known to cause destabilization of antigen structure [98]. When the three vaccinated groups are compared, it is decided that the third group which was injected with 5 μg HexaPro WT VLP + 60 μg Alum + 30 μg K3-CpG vaccine formulation developed most efficient humoral immune response with the balance of antigen to adjuvant and Alum to CpG ratio.

In our previous studies, we performed CBA in order to demonstrate the cellular immune response induced by VLP vaccine and the results proved that VLP vaccine triggers a Th1-skewed immune response after 2 doses [126]. Within the scope of this study CBA was not performed for the pre-clinical experiments. The boosting effect of the third dose only on the humoral immune response is shown with ELISA. However, performing CBA after the third dose could give a better insight on the enhanced T-cell responses and would substantiate the necessity of third injection for the prolonged immune reaction.

After the pre-clinical studies are completed using BALB/c mice, the clinical Phase I trial was conducted with 36 volunteers to determine the optimal dose for the VLP vaccine and to make sure no serious side effects are caused by the vaccination process. For Phase II volunteers, the vaccine formulation was determined as 40 μg HexaPro WT VLP + 600 μg Alum + 300 μg K3-CpG and the volunteers were vaccinated 2 times with 21-day intervals. In order to evaluate the immune responses induced by VLP vaccine, first the humoral immune responses of the volunteers against Spike, Nucleocapsid, WT RBD, UK RBD and Delta RBD proteins were assessed by

ELISA. Spike protein is considered to be the main immunogen of SARS-CoV-2 since the virus entry depends on the interaction between the ACE2 receptor of the host and the RBD unit of Spike protein [129]. It has been demonstrated that being among the four structural proteins of the virus, Spike and Nucleocapsid are considered to be the main immunogens, and patients infected with SARS-CoV-2 generate effective antibody responses against these proteins. Hence, in this study, we aimed to detailly analyze IgG production against Spike and Nucleocapsid proteins and RBD subunit.

For analysis of anti-Spike antibody production, ELISA was performed by utilizing in-house Spike protein produced in our lab and a commercial kit called Corona Hunter. Results obtained from both experiments validate that VLP vaccine induces a gradual increase in the IgG levels starting from Day 21 until Day 90 which is a proof of long-term protection. Evidence from literature asserts that IgG secretion against Spike protein can be detected 14 days after the symptoms observed [130]. Similarly, in our study, we observed that the antibody titers remain very close to the cut-off value until Day 35. Since Day 35 onwards, which corresponds to 14 days after second injection, the titers exceed the cut-off value and an increasing trend is observed until Day 90. When the IgG levels of convalescent plasma samples and Day 90 sera are compared, it can be observed that the results are very close to each other. This suggests that VLP vaccine yields similar antibody production as SARS-CoV-2 infection. However, at Day 90, the increment is less compared to Day 35 or Day 49. Since anti-Spike antibodies start to decay in the long run, if the experiment was conducted with serum samples from Day 180, a significant decline in the antibody titers would be expected. To avoid this, a third injection can be done three months after the first injection. Evidence from our pre-clinical studies prove the boosting effect of third dose of VLP vaccine on humoral responses of mice. Similarly, for mRNA vaccines, the boost in the antibody responses is clearly observed after the third dose according to Gruell et al. [131]. Thus, third injection must be under consideration for the VLP vaccine. For the booster injections, formulation of the vaccine with the newly emerging variants should be intended as the virus is mutating really fast and a prolonged immune response can be provided if the boosters are formulated with the current variants. In this scenario, using VLP technology for the vaccine becomes advantageous once again as the formulation can be easily adapted to new variants only by the change of one plasmid construct.

Assessment of antibody responses against Nucleocapsid was done by employing in-house Nucleocapsid protein produced in our lab. Studies indicate that antibody secretion against Spike and Nucleocapsid proteins of the virus generally occurs between Day 8 and Day 14 after the symptoms appear [130]. Data show that antibody levels increase from Day 21 to Day 90 and the titers exceed the baseline after Day 35 which is similar to anti-Spike IgG responses. Although in some studies it is found that Nucleocapsid antibodies are detected earlier than Spike antibodies,

in this thesis it is shown that detection of anti-Nucleocapsid and anti-Spike antibodies are observed to be around the same time point as they both exceed the cut-off value after Day 35. Brochot et al. has demonstrated in their article that compared to Spike, detection of Nucleocapsid and RBD proteins of the virus is more specific [113]. However, this study has certain limitations for evaluation of this argument. First of all, for the assessment of anti-Nucleocapsid IgG titers, in-house recombinant Nucleocapsid protein was utilized for the ELISA. Even though the protein was tried to be purified with the highest efficiency, the assays performed to understand the quality of the final product showed that the final recombinant protein was rich in degradation products and impurities. Following this, the optimization experiments proved that there was low signal to background ratio which resulted in low detection capacity. Therefore, in the case of anti-Nucleocapsid antibodies, it cannot be assured that the signal detected is purely due to the antibody response generated against Nucleocapsid antigen. It is also likely that the signal obtained is because of impurities and non-specific binding. In order to eliminate this possibility, the anti-Nucleocapsid IgG titers can be reassessed by employing a commercial recombinant Nucleocapsid protein and the signals can be compared for further verification of the results. Second, it is proposed that cross-reactivity with common cold human coronaviruses (hCoV), especially with alpha-hCoV, is also possible [132]. Hence, the antibody levels for Nucleocapsid antigen may not possibly be reflecting the titers solely induced by VLP vaccine. Considering the contribution of cross-reactive antibodies to Nucleocapsid-specific immune responses and the decay of antibodies, a third of the VLP vaccine can help boosting of the humoral immunity and ensures prolonged protection against the virus.

Due to emergence of new variants over the course of VLP vaccine studies, we tested efficacy of our vaccine against these new variants by measuring anti-UK RBD and anti-Delta RBD IgG responses together with anti-WT RBD IgG levels. Antibodies targeting RBD of the Spike protein are proven to inhibit the interaction of the virus with the ACE2 receptor of the host cells [133]. Hence, increase in the level of anti-RBD antibodies is related with increasing neutralizing antibody titers thereby promises a more comprehensive immune response against the virus. In this study, the results from all three RBD variants indicate that anti-RBD IgG titers increase from Day 35 to Day 90. Although the VLP vaccine was formulated with HexaPro WT VLP, the antibody responses against RBD UK and RBD Delta proteins are very close to IgG levels obtained against RBD WT. The increasing antibody levels against all three variants prove that a cross-protective immune response is achieved by VLP vaccine and the humoral response elicited against RBD can be an indicator of effective neutralizing antibody titers.

Neutralizing antibody production against SARS-CoV-2 is vital as they prevent interaction of RBD domain with ACE2 receptors of the host. In literature, it is shown that neutralizing antibody production during after vaccination is observed between days 14 and 20 after the first injection

but the titers display variability between individuals [116,134]. Therefore, for quantification of neutralizing antibody titers, SARS-CoV-2 IgG Quant method was performed via ARCHITECT i System by DEREN Laboratory (Ankara, Turkey). The neutralizing antibody titers are expected to be in correlation with the anti-RBD IgG titers. When the results are interpreted, it can be noticed that the increasing trend of antibody titers from Day 35 to Day 90 obtained in RBD variants is maintained in neutralizing antibody levels as anticipated. Unlike anti-RBD antibody titers, nearly half of the neutralizing antibody titers are observed to be under the cut-off value of 50 AU/ml. Despite of this, there is a clear elevation of neutralizing antibodies, and especially at Day 90 the average titer passes the baseline and reaches the NAb level generated by the convalescent plasma samples. In order to boost the neutralizing antibody response and achieve a long-term protection by delaying decay of the antibodies, a third dose of VLP vaccine must be injected to individuals 3 months after the first injection as recent evidence suggests that boosting injections for mRNA vaccines generate an increased neutralizing response in the serum [131]. The breadth of neutralizing antibody response can be further augmented by having a third booster injection formulated with the new emerging variants of SARS-CoV-2, such as Alpha and Delta so that enhanced cross-neutralizing activity can be generated against the new variants.

After studying the humoral immunity from sera, the cellular immune responses are evaluated. To this end, secretion of 12 cytokines from the supernatant of PBMCs stimulated with antigens was measured by employing CBA method. The results obtained showed that adjuvantation of SARS-CoV-2 VLP vaccine with K3 CpG ODN induces a Th1-dominated immune response as aimed. It has been shown that there is an increase in the production of Th1-associated cytokines, which are IFN-γ, IL-2 and TNF-α, following treatment with the SMNO peptide pool. IFN-γ, one of the signature cytokines for Th1-biased immunity, has shown the highest elevation compared to IL-2 and TNF-α with a fold induction value of 6.6X. In literature, it is proven that IFN-γ secretion creates a positive feedback loop for differentiation of more Th1 cells which eventuates in production of even more IFN-γ [135]. Therefore, observing IFN-γ as the cytokine with the highest increment can be explained by this pheomenon. IL-2 and TNF-α are also involved in antimicrobicidal avtivity and viral clearance [136]. Hence, their secretion has shown to be elevated as presented by the fold induction values of 3.8X and 2.4X respectively. Perez et al. indicated that IL-2 production is also related to expansion of humoral immune responses as IL-2 is found to be promoting IgG secretion against Spike 1, Nucleocapsid and RBD [137]. For this reason, the elevation of antibody titers against Spike, Nucleocapsid and the RBD variants can be also explained by the induction of escalated cellular immune responses. It is reported that effective Th1-dominant cellular response is observed in the less severe cases of COVID 19. Our results demonstrate that SARS-CoV-2 VLP vaccine successfully achieved induction of Th1-skewed immune response owing to its formulation with CpG ODN [136].

Although Th1-biased immune response was primarly intended with the SARS-CoV-2 vaccine formulation, Th2-rel responses were also expected to be observed to some extent due to formulation with Alum as the second adjuvant. The importance of Th1/Th2 balance in COVID-19 patients is signified in various studies since excessive Th1-biased response can lead to cytokine storm which may trigger excess Th2-dependent activities resulting in a more severe form of the SARS-CoV-2 infection for the patient [136]. Conversely, in Pavel et al. it is indicated that imbalance between Th1 and Th2-mediated responses and especially shift of immune rection towards a Th2-biased response increases mortality rates [138]. In our study, we evaluated the effect of VLP vaccine on Th2-associated responses by measuring secretion of IL-4, IL-5, IL-9 and IL-13. Treatment of the PBMCs with SMNO peptide pool yielded 1.1X, 2.5X, 3.3X and 4.5X increase in the secretion of listed cytokines respectively. Among Th2-related cytokines, IL-13 is observed to have the greatest increment but not more than that of IFN-γ which is one of the main cytokines for the Th1-mediated immunity. The anti-inflammatory cytokines IL-4, IL-5 and IL-13 can be counteractive for the Th1-associated responses if their levels are too high. Therefore, in the case of excess production, effective viral clearance and protection conducted by Th1 cells will be delayed which may result in a more severe progression of infection [136,139]. The change in the level of IL-9 after treatment with SMNO peptide pool was investigated and the results are included under Th2 subtype although Th9 cells are also known to produce IL-9[140]. Several studies have demonstrated that IL-9 is secreted by Th2 cells, but when TGF-β is present in the environment, it promotes differentiation of Th2 cells into Th9 lineage [129, 130]. Therefore, in this thesis, it is studied under Th2-mediated response. Among Th2-related cytokines, IL-9 has the second highest fold change value with 3.3X. It has been proven that IL-9 promotes secretion of IL-4 mediated IgG [142]. Hence, the 3.3X increase in the level of IL-9 may have triggered elevated antibody responses in the volunteers and contributed to humoral immune activities as well as Th2-associated response. Unlike IL-13 and IL-9, IL-4 and IL-5 demonstrated less increment in response to peptide pool treatment. Having the lowest fold induction value for the IL-4 favors the Th1-dependent response induced by the VLP vaccine since IL-4 is known to prevent differentiation into Th1 cells [143]. Wurtz et al. has proven in their study that for developing Th1 cells IL-4 induces commitment into Th2 lineage while for the effector Th1 cells IL-4 transiently inhibits IFN-γ secretion [143]. Regarding the data in our study, since IL-4 secretion remains very low after stimulation with peptide pool, IFN-γ production increases without being significantly inhibited. When the increment in IFN-γ level is compared to other cytokine levels investigated, it can be clearly seen that it has the highest fold induction value among 12 cytokines. This once again indicates that VLP vaccine triggers immune responses in a Th1-dominated way. However, as mentioned previously, for an efective an healthy immune reaction to be induced, Th1 and Th2 responses must coexist. Analyzing percent distributions of Th-cell immune responses shows that Th1-mediated reactions comprise 31.4% of the total

cellular immune responses while Th2-meadiated responses comprise 20.4%. This validates that VLP vaccine initiates both Th1 and Th2-related responses, but as aimed during formulation, it is rather Th1-biased for effective viral clearance and protection.

Th17 cells play a vital role during SARS-CoV-2 infection as they are not only involved in secretion of various cytokines, but also take part in triggering of Th2-mediated responses, suppresison of Th1-biased reactions and inhibiton of commitment into Treg cell lineage [120]. In order to assess Th17-related immune responses, levels of IL-17A, IL-17F and IL-22 were measured. The fold change values were calculated to be 1.6X, 2.1X and 3.4X respectively for the cytokines. Evidence suggests that in severe COVID-19 patients, the level of Th17-linked cytokines are extremely elevated and Th17/Th1 imbalance is significanly increased which lead to a more severe form of lung pathology and poor prognosis [127, 133]. According to the data obtained, Th17-related responses comprise 20.9% of the total cellular responses which is almost equal to reaction induced by Th2 cells. Similarly, when the percent distributions of Th1 and Th17 cell activities are compared, it can be seen that they constitute 30.1% and 20.9% of the total cellular activities respectively which points out to a Th1-dominated immune response with coexistence of Th17 cellular reactions. All in all, it can be concluded that SARS-CoV-2 VLP vaccine induces a balanced immune response by triggering each arm of the immune system in a balanced way so that a healthy and prolonged protection can be achieved against the virus.

The role of IL-6 in prognosis of SARS-CoV-2 infection has been established in various studies. It is explained that IL-6 is one of the leading cytokines giving rise to cytokine storm and disease exacerbation [121,145]. Although IL-6 is known to be involved in host's immune response in different ways such as favoring IgG secretion, promoting differentiation of B cells, it is also shown that IL-6 may hinder efficient viral clearance mechanism by restraining Th1-biased immune response through suppression of IFN-γ production [121]. Considering that IL-6 can both protective and fatal depending on its level during the course of COVID-19, we aimed to assess the change in its secretion. According to the results obtained, the fold change value for IL-6 is 1.1X. Even though no significant change was detected after treatment with SMNO peptide pool, the response is observed to be high when compared to IFN-γ level. When the percent distribution of IL-6 based response to total cellular reaction was calculated, 18.7% contribution was obtained. Therefore, it can said that IL-6 response induced by VLP vaccine helps to enforce the immune reaction induced by host, but doesn't avert the induction of Th1-biased response.

Finally, in order to evaluate Treg cell responses, secretion of IL-10 was investigated. Treg cells are involved in maintaining the homeostasis of the immune responses through suppression of immune reactions [146,147]. The anti-inflammatory cytokine IL-10, secreted by Treg cells, is proven to inhibit functioning of effector cells. Therefore, elevation of its levels is correlated with

increasing disease severity [148]. Tan et al. and Julia et al. demosntrated in their studies that the number of Treg cells elevate together with the amount of IL-10 secreted which may point out to immunosuppression and inefficient response by the host [149,150]. When the data from our study is evaluated, it can be said that the Treg responses remain in the minimum level with a fold change value of 1.2X. When the percentage of Treg cell responses was calculated, it was observed that the contribution of Treg-based response to total cellular response is 8.6%. Considering that various studies refer to inhibitory role of Tregs on Th17 cell functioning and inflammatory response, it can be said that the Treg response induced by VLP vaccine is sufficient to prevent excessive anti-inflammatory response, but doesn't restrain the Th1-biased response for viral clearance [146].

In conclusion, we investigated immune reactions induced by SARS-CoV-2 VLP vaccine in pre-clinical and clinal studies and proved the efficacy of VLP vaccine in terms of eliciting humoral and cellular immune responses. The high-antibody titers yielded against Spike, Nucleocapsid, WT RBD, Alpha RBD and Delta RBA proteins, increasing level of neutralizing antibodies and induction of Th1-biased immunity in coexistence of Th2, Th17 and Treg-related responses demonstrated the multi-functional protection achieved via immunization with VLP vaccine in both mice and human subjects. Although not proven in clinical trials yet, the boosting effect of the third injection in mice has shown the elevation in antibody titers and substatiates the necessity of third injections for retaining immune responses and protection. In addition to various advantages of using VLP technology, the feasiblity of shipment and storage conditions of VLP vaccines and adoptability of the VLP technology to new vairants of concern makes it a suitable candidate for the future booster injections.

BIBLIOGRAPHY

[1] Chaplin DD. Overview of the Immune Response. *J Allergy Clin Immunol*. 2010;125(2 Suppl 2):S3-23. doi:10.1016/j.jaci.2009.12.980

[2] Kenneth M, Weaver C. *Janeway's Immunobiology*. Vol 1. 9th ed. Garland Science, Taylor & Francis Group, LLC; 2017.

[3] Vivier E, Malissen B. Innate and adaptive immunity: specificities and signaling hierarchies revisited. *Nat Immunol*. 2005;6(1):17-21. doi:10.1038/ni1153

[4] Parkin J, Cohen B. An overview of the immune system. *The Lancet*. 2001;357(9270):1777-1789. doi:10.1016/S0140-6736(00)04904-7

[5] Kellie S, Al-Mansour Z. Chapter Four - Overview of the Immune System. In: Skwarczynski M, Toth I, eds. *Micro and Nanotechnology in Vaccine Development*. Micro and Nano Technologies. William Andrew Publishing; 2017:63-81. doi:10.1016/B978-0-323-39981-4.00004-X

[6] Paludan SR, Pradeu T, Masters SL, Mogensen TH. Constitutive immune mechanisms: mediators of host defence and immune regulation. *Nat Rev Immunol*. 2021;21(3):137-150. doi:10.1038/s41577-020-0391-5

[7] Mogensen TH. Pathogen Recognition and Inflammatory Signaling in Innate Immune Defenses. *Clin Microbiol Rev*. 2009;22(2):240-273. doi:10.1128/CMR.00046-08

[8] Akira S, Uematsu S, Takeuchi O. Pathogen Recognition and Innate Immunity. *Cell*. 2006;124(4):783-801. doi:10.1016/j.cell.2006.02.015

[9] Li D, Wu M. Pattern recognition receptors in health and diseases. *Sig Transduct Target Ther*. 2021;6(1):1-24. doi:10.1038/s41392-021-00687-0

[10] O'Neill LAJ, Golenbock D, Bowie AG. The history of Toll-like receptors — redefining innate immunity. *Nat Rev Immunol*. 2013;13(6):453-460. doi:10.1038/nri3446

[11] Ohto U, Ishida H, Shibata T, Sato R, Miyake K, Shimizu T. Toll-like Receptor 9 Contains Two DNA Binding Sites that Function Cooperatively to Promote Receptor Dimerization and Activation. *Immunity*. 2018;48(4):649-658.e4. doi:10.1016/j.immuni.2018.03.013

[12] Latz E, Schoenemeyer A, Visintin A, et al. TLR9 signals after translocating from the ER to CpG DNA in the lysosome. *Nat Immunol*. 2004;5(2):190-198. doi:10.1038/ni1028

[13] Takeshita F, Gursel I, Ishii KJ, Suzuki K, Gursel M, Klinman DM. Signal transduction pathways mediated by the interaction of CpG DNA with Toll-like receptor 9. *Seminars in Immunology*. 2004;16(1):17-22. doi:10.1016/j.smim.2003.10.009

[14] TLR9 - an overview | ScienceDirect Topics. Accessed March 12, 2022. https://www.sciencedirect.com/topics/neuroscience/tlr9

[15] Alberts B, Johnson A, Lewis J, Raff M, Roberts K, Walter P. The Adaptive Immune System. *Molecular Biology of the Cell 4th edition*. Published online 2002. Accessed March 13, 2022. https://www.ncbi.nlm.nih.gov/books/NBK21070/

[16] Bonilla FA, Oettgen HC. Adaptive immunity. *Journal of Allergy and Clinical Immunology*. 2010;125(2, Supplement 2):S33-S40. doi:10.1016/j.jaci.2009.09.017

[17] Charles A Janeway J, Travers P, Walport M, Shlomchik MJ. T Cell-Mediated Immunity. *Immunobiology: The Immune System in Health and Disease 5th edition*. Published online 2001. Accessed March 13, 2022. https://www.ncbi.nlm.nih.gov/books/NBK10762/

[18] Liao S, von der Weid PY. Lymphatic system: An active pathway for immune protection. *Seminars in Cell & Developmental Biology*. 2015;38:83-89. doi:10.1016/j.semcdb.2014.11.012

[19] Castellino F, Germain RN. Cooperation between CD4+ and CD8+ T cells: when, where, and how. *Annu Rev Immunol*. 2006;24:519-540. doi:10.1146/annurev.immunol.23.021704.115825

[20] McHeyzer-Williams LJ, McHeyzer-Williams MG. Antigen-specific memory B cell development. *Annu Rev Immunol*. 2005;23:487-513. doi:10.1146/annurev.immunol.23.021704.115732

[21] Bhagavan NV, Ha C-E. Chapter 33 - Immunology. In: Bhagavan NV, Ha C-E, eds. *Essentials of Medical Biochemistry*. Academic Press; 2011:449-472. doi:10.1016/B978-0-12-095461-2.00033-3

[22] Xing Z, Zganiacz A, Wang J, Divangahi M, Nawaz F. IL-12-Independent Th1-Type Immune Responses to Respiratory Viral Infection: Requirement of IL-18 for IFN-γ Release in the Lung But Not for the Differentiation of Viral-Reactive Th1-Type Lymphocytes. *The Journal of Immunology*. 2000;164(5):2575-2584. doi:10.4049/jimmunol.164.5.2575

[23] Bevan MJ. Helping the CD8+ T-cell response. *Nat Rev Immunol*. 2004;4(8):595-602. doi:10.1038/nri1413

[24] Laidlaw BJ, Craft JE, Kaech SM. The multifaceted role of CD4+ T cells in CD8+ T cell memory. *Nat Rev Immunol*. 2016;16(2):102-111. doi:10.1038/nri.2015.10

[25] Price GE, Huang L, Ou R, Zhang M, Moskophidis D. Perforin and Fas cytolytic pathways coordinately shape the selection and diversity of CD8+-T-cell escape variants of influenza virus. *Journal of Virology*. 2005;79(13):8545-8559. doi:10.1128/JVI.79.13.8545-8559.2005

[26] Topham DJ, Tripp RA, Doherty PC. CD8+ T Cells Clear Influenza Virus by Perform or Fas-Dependent Processes. *Journal of Immunology*. 1997;159(11):5197-5200.

[27] Zajac AJ, Harrington LE. Immune Response to Viruses: Cell-Mediated Immunity☆. In: *Reference Module in Biomedical Sciences*. Elsevier; 2014. doi:10.1016/B978-0-12-801238-3.02604-0

[28] Jansen JM, Gerlach T, Elbahesh H, Rimmelzwaan GF, Saletti G. Influenza virus-specific CD4+ and CD8+ T cell-mediated immunity induced by infection and vaccination. *Journal of Clinical Virology*. 2019;119:44-52. doi:10.1016/j.jcv.2019.08.009

[29] Ahrends T, Spanjaard A, Pilzecker B, et al. CD4+ T Cell Help Confers a Cytotoxic T Cell Effector Program Including Coinhibitory Receptor Downregulation and Increased Tissue Invasiveness. *Immunity*. 2017;47(5):848-861.e5. doi:10.1016/j.immuni.2017.10.009

[30] Juno JA, van Bockel D, Kent SJ, Kelleher AD, Zaunders JJ, Munier CML. Cytotoxic CD4 T Cells—Friend or Foe during Viral Infection? *Front Immunol*. 2017;8. doi:10.3389/fimmu.2017.00019

[31] Jankovic D, Feng CG. CD4+ T Cell Differentiation in Infection: Amendments to the Th1/Th2 Axiom. *Frontiers in Immunology*. 2015;6. Accessed March 16, 2022. https://www.frontiersin.org/article/10.3389/fimmu.2015.00198

[32] Zhu J, Yamane H, Paul WE. Differentiation of Effector CD4 T Cell Populations. *Annu Rev Immunol*. 2010;28:445-489. doi:10.1146/annurev-immunol-030409-101212

[33] Martinez-Sanchez ME, Huerta L, Alvarez-Buylla ER, Villarreal Luján C. Role of Cytokine Combinations on CD4+ T Cell Differentiation, Partial Polarization, and Plasticity: Continuous Network Modeling Approach. *Frontiers in Physiology*. 2018;9. Accessed March 16, 2022. https://www.frontiersin.org/article/10.3389/fphys.2018.00877

[34] Hsieh C-S, Macatonia SE, Tripp CS, Wolf SF, O'Garra A, Murphy KM. Development of TH1 CD4+ T Cells Through IL-12 Produced by Listeria-Induced Macrophages. *Science*. 1993;260(5107):547-549. doi:10.1126/science.8097338

[35] Saravia J, Chapman NM, Chi H. Helper T cell differentiation. *Cell Mol Immunol*. 2019;16(7):634-643. doi:10.1038/s41423-019-0220-6

[36] Szabo SJ, Kim ST, Costa GL, Zhang X, Fathman CG, Glimcher LH. A Novel Transcription Factor, T-bet, Directs Th1 Lineage Commitment. *Cell*. 2000;100(6):655-669. doi:10.1016/S0092-8674(00)80702-3

[37] Swain SL, McKinstry KK, Strutt TM. Expanding roles for CD4+ T cells in immunity to viruses. *Nat Rev Immunol*. 2012;12(2):136-148. doi:10.1038/nri3152

[38] Zheng W, Flavell RA. The Transcription Factor GATA-3 Is Necessary and Sufficient for Th2 Cytokine Gene Expression in CD4 T Cells. *Cell*. 1997;89(4):587-596. doi:10.1016/S0092-8674(00)80240-8

[39] Cote-Sierra J, Foucras G, Guo L, et al. Interleukin 2 plays a central role in Th2 differentiation. *Proceedings of the National Academy of Sciences*. 2004;101(11):3880-3885. doi:10.1073/pnas.0400339101

[40] Deo SS, Mistry KJ, Kakade AM, Niphadkar PV. Role played by Th2 type cytokines in IgE mediated allergy and asthma. *Lung India*. 2010;27(2):66-71. doi:10.4103/0970-2113.63609

[41] Spencer LA, Weller PF. Eosinophils and Th2 immunity: contemporary insights. *Immunol Cell Biol*. 2010;88(3):250-256. doi:10.1038/icb.2009.115

[42] Chiang H-Y, Lu H-H, Sudhakar JN, et al. IL-22 initiates an IL-18-dependent epithelial response circuit to enforce intestinal host defence. *Nat Commun*. 2022;13(1):874. doi:10.1038/s41467-022-28478-3

[43] Xu S, Cao X. Interleukin-17 and its expanding biological functions. *Cell Mol Immunol*. 2010;7(3):164-174. doi:10.1038/cmi.2010.21

[44] Hoeppli RE, Wu D, Cook L, Levings MK. The Environment of Regulatory T Cell Biology: Cytokines, Metabolites, and the Microbiome. *Front Immunol*. 2015;6:61. doi:10.3389/fimmu.2015.00061

[45] O'Farrell AM, Liu Y, Moore KW, Mui AL. IL-10 inhibits macrophage activation and proliferation by distinct signaling mechanisms: evidence for Stat3-dependent and -independent pathways. *EMBO J*. 1998;17(4):1006-1018. doi:10.1093/emboj/17.4.1006

[46] Wan YY, Flavell RA. 'Yin-Yang' functions of TGF-β and Tregs in immune regulation. *Immunol Rev*. 2007;220:199-213. doi:10.1111/j.1600-065X.2007.00565.x

[47] Tripathi SK, Lahesmaa R. Transcriptional and epigenetic regulation of T-helper lineage specification. *Immunological Reviews*. 2014;261(1):62-83. doi:10.1111/imr.12204

[48] Ouyang W, Löhning M, Gao Z, et al. Stat6-Independent GATA-3 Autoactivation Directs IL-4-Independent Th2 Development and Commitment. *Immunity*. 2000;12(1):27-37. doi:10.1016/S1074-7613(00)80156-9

[49] Usui T, Preiss JC, Kanno Y, et al. T-bet regulates Th1 responses through essential effects on GATA-3 function rather than on IFNG gene acetylation and transcription. *J Exp Med*. 2006;203(3):755-766. doi:10.1084/jem.20052165

[50] Hwang J-R, Byeon Y, Kim D, Park S-G. Recent insights of T cell receptor-mediated signaling pathways for T cell activation and development. *Exp Mol Med*. 2020;52(5):750-761. doi:10.1038/s12276-020-0435-8

[51] Gereda J, Leung D, Thatayatikom A, et al. Relation between house-dust endotoxin exposure, type 1 T-cell development, and allergen sensitisation in infants at high risk of asthma. *The Lancet*. 2000;355(9216):1680-1683. doi:10.1016/S0140-6736(00)02239-X

[52] Charles A Janeway J, Travers P, Walport M, Shlomchik MJ. The Humoral Immune Response. *Immunobiology: The Immune System in Health and Disease 5th edition*. Published online 2001. Accessed March 13, 2022. https://www.ncbi.nlm.nih.gov/books/NBK10752/

[53] Merlo LMF, Mandik-Nayak L. Chapter 3 - Adaptive Immunity: B Cells and Antibodies. In: Prendergast GC, Jaffee EM, eds. *Cancer Immunotherapy (Second Edition)*. Academic Press; 2013:25-40. doi:10.1016/B978-0-12-394296-8.00003-8

[54] Vos Q, Lees A, Wu ZQ, Snapper CM, Mond JJ. B-cell activation by T-cell-independent type 2 antigens as an integral part of the humoral immune response to pathogenic microorganisms. *Immunol Rev*. 2000;176:154-170. doi:10.1034/j.1600-065x.2000.00607.x

[55] Defrance T, Taillardet M, Genestier L. T cell-independent B cell memory. *Current Opinion in Immunology*. 2011;23(3):330-336. doi:10.1016/j.coi.2011.03.004

[56] Carrasco YR, Batista FD. B Cells Acquire Particulate Antigen in a Macrophage-Rich Area at the Boundary between the Follicle and the Subcapsular Sinus of the Lymph Node. *Immunity*. 2007;27(1):160-171. doi:10.1016/j.immuni.2007.06.007

[57] Neefjes J, Jongsma MLM, Paul P, Bakke O. Towards a systems understanding of MHC class I and MHC class II antigen presentation. *Nat Rev Immunol*. 2011;11(12):823-836. doi:10.1038/nri3084

[58] Allen CDC, Cyster JG. Follicular dendritic cell networks of primary follicles and germinal centers: Phenotype and function. *Seminars in Immunology*. 2008;20(1):14-25. doi:10.1016/j.smim.2007.12.001

[59] Crotty S. Follicular Helper CD4 T Cells (TFH). *Annual Review of Immunology*. 2011;29(1):621-663. doi:10.1146/annurev-immunol-031210-101400

[60] Harwood NE, Batista FD. Antigen presentation to B cells. *F1000 Biol Rep*. 2010;2:87. doi:10.3410/B2-87

[61] Pifferi C, Berthet N, Renaudet O. Cyclopeptide scaffolds in carbohydrate-based synthetic vaccines. *Biomater Sci*. 2017;5(5):953-965. doi:10.1039/C7BM00072C

[62] Joller N, Weber SS, Oxenius A. Antibody – Fc receptor interactions in protection against intracellular pathogens. *European Journal of Immunology*. 2011;41(4):889-897. doi:10.1002/eji.201041340

[63] Hangartner L, Zinkernagel RM, Hengartner H. Antiviral antibody responses: the two extremes of a wide spectrum. *Nat Rev Immunol*. 2006;6(3):231-243. doi:10.1038/nri1783

[64] Hiemstra PS, Daha MR. Opsonization. In: Delves PJ, ed. *Encyclopedia of Immunology (Second Edition)*. Elsevier; 1998:1885-1888. doi:10.1006/rwei.1999.0475

[65] Dunkelberger JR, Song W-C. Complement and its role in innate and adaptive immune responses. *Cell Res*. 2010;20(1):34-50. doi:10.1038/cr.2009.139

[66] Kanimozhi G, Pradhapsingh B, Singh Pawar C, Khan HA, Alrokayan SH, Prasad NR. SARS-CoV-2: Pathogenesis, Molecular Targets and Experimental Models. *Frontiers in Pharmacology*. 2021;12. Accessed February 26, 2022. https://www.frontiersin.org/article/10.3389/fphar.2021.638334

[67] Harrison AG, Lin T, Wang P. Mechanisms of SARS-CoV-2 Transmission and Pathogenesis. *Trends in Immunology*. 2020;41(12):1100-1115. doi:10.1016/j.it.2020.10.004

[68] Hu B, Guo H, Zhou P, Shi Z-L. Characteristics of SARS-CoV-2 and COVID-19. *Nat Rev Microbiol*. 2021;19(3):141-154. doi:10.1038/s41579-020-00459-7

[69] Wang M-Y, Zhao R, Gao L-J, Gao X-F, Wang D-P, Cao J-M. SARS-CoV-2: Structure, Biology, and Structure-Based Therapeutics Development. *Frontiers in Cellular and Infection Microbiology*. 2020;10. Accessed March 1, 2022. https://www.frontiersin.org/article/10.3389/fcimb.2020.587269

[70] Hardenbrook NJ, Zhang P. A structural view of the SARS-CoV-2 virus and its assembly. *Current Opinion in Virology*. 2022;52:123-134. doi:10.1016/j.coviro.2021.11.011

[71] Mariano G, Farthing RJ, Lale-Farjat SLM, Bergeron JRC. Structural Characterization of SARS-CoV-2: Where We Are, and Where We Need to Be. *Frontiers in Molecular Biosciences*. 2020;7. Accessed March 1, 2022. https://www.frontiersin.org/article/10.3389/fmolb.2020.605236

[72] Kouhpayeh S, Shariati L, Boshtam M, et al. The Molecular Basis of COVID-19 Pathogenesis, Conventional and Nanomedicine Therapy. *Int J Mol Sci*. 2021;22(11):5438. doi:10.3390/ijms22115438

[73] Naqvi AAT, Fatima K, Mohammad T, et al. Insights into SARS-CoV-2 genome, structure, evolution, pathogenesis and therapies: Structural genomics approach. *Biochim Biophys Acta Mol Basis Dis*. 2020;1866(10):165878. doi:10.1016/j.bbadis.2020.165878

[74] Zhang Q, Xiang R, Huo S, et al. Molecular mechanism of interaction between SARS-CoV-2 and host cells and interventional therapy. *Sig Transduct Target Ther*. 2021;6(1):1-19. doi:10.1038/s41392-021-00653-w

[75] Chia PY, Coleman KK, Tan YK, et al. Detection of air and surface contamination by SARS-CoV-2 in hospital rooms of infected patients. *Nat Commun*. 2020;11(1):2800. doi:10.1038/s41467-020-16670-2

[76] Luo L, Liu D, Liao X, et al. Modes of contact and risk of transmission in COVID-19 among close contacts. Published online 2020. Accessed March 1, 2022. https://medrxiv.org/cgi/content/short/2020.03.24.20042606

[77] Transmission of SARS-CoV-2: implications for infection prevention precautions. Accessed March 1, 2022. https://www.who.int/news-room/commentaries/detail/transmission-of-sars-cov-2-implications-for-infection-prevention-precautions

[78] Jackson CB, Farzan M, Chen B, Choe H. Mechanisms of SARS-CoV-2 entry into cells. *Nat Rev Mol Cell Biol*. 2022;23(1):3-20. doi:10.1038/s41580-021-00418-x

[79] V'kovski P, Kratzel A, Steiner S, Stalder H, Thiel V. Coronavirus biology and replication: implications for SARS-CoV-2. *Nat Rev Microbiol*. 2021;19(3):155-170. doi:10.1038/s41579-020-00468-6

[80] Lowery SA, Sariol A, Perlman S. Innate immune and inflammatory responses to SARS-CoV-2: Implications for COVID-19. *Cell Host & Microbe*. 2021;29(7):1052-1062. doi:10.1016/j.chom.2021.05.004

[81] Blanco-Melo D, Nilsson-Payant BE, Liu W-C, et al. Imbalanced Host Response to SARS-CoV-2 Drives Development of COVID-19. *Cell*. 2020;181(5):1036-1045.e9. doi:10.1016/j.cell.2020.04.026

[82] Veras FP, Pontelli MC, Silva CM, et al. SARS-CoV-2–triggered neutrophil extracellular traps mediate COVID-19 pathologySARS-CoV-2 directly triggers ACE-dependent NETs. *Journal of Experimental Medicine*. 2020;217(12):e20201129. doi:10.1084/jem.20201129

[83] Natural killer cell immunotypes related to COVID-19 disease severity. Accessed May 6, 2022. https://www.science.org/doi/full/10.1126/sciimmunol.abd6832

[84] Sette A, Crotty S. Adaptive immunity to SARS-CoV-2 and COVID-19. *Cell*. 2021;184(4):861-880. doi:10.1016/j.cell.2021.01.007

[85] Grifoni A, Weiskopf D, Ramirez SI, et al. Targets of T Cell Responses to SARS-CoV-2 Coronavirus in Humans with COVID-19 Disease and Unexposed Individuals. *Cell*. 2020;181(7):1489-1501.e15. doi:10.1016/j.cell.2020.05.015

[86] Braun J, Loyal L, Frentsch M, et al. SARS-CoV-2-reactive T cells in healthy donors and patients with COVID-19. *Nature*. 2020;587(7833):270-274. doi:10.1038/s41586-020-2598-9

[87] Le Bert N, Tan AT, Kunasegaran K, et al. SARS-CoV-2-specific T cell immunity in cases of COVID-19 and SARS, and uninfected controls. *Nature*. 2020;584(7821):457-462. doi:10.1038/s41586-020-2550-z

[88] Röltgen K, Boyd SD. Antibody and B cell responses to SARS-CoV-2 infection and vaccination. *Cell Host & Microbe*. 2021;29(7):1063-1075. doi:10.1016/j.chom.2021.06.009

[89] Röltgen K, Powell AE, Wirz OF, et al. Defining the features and duration of antibody responses to SARS-CoV-2 infection associated with disease severity and outcome. *Sci Immunol*. 2020;5(54):eabe0240. doi:10.1126/sciimmunol.abe0240

[90] Pang NY-L, Pang AS-R, Chow VT, Wang D-Y. Understanding neutralising antibodies against SARS-CoV-2 and their implications in clinical practice. *Military Medical Research*. 2021;8(1):47. doi:10.1186/s40779-021-00342-3

[91] Karpiński TM, Ożarowski M, Seremak-Mrozikiewicz A, Wolski H, Wlodkowic D. The 2020 race towards SARS-CoV-2 specific vaccines. *Theranostics*. 2021;11(4):1690-1702. doi:10.7150/thno.53691

[92] COVID-19 vaccine tracker and landscape. Accessed March 7, 2022. https://www.who.int/publications/m/item/draft-landscape-of-covid-19-candidate-vaccines

[93] The Sinovac-CoronaVac COVID-19 vaccine: What you need to know. Accessed March 7, 2022. https://www.who.int/news-room/feature-stories/detail/the-sinovac-covid-19-vaccine-what-you-need-to-know

[94] Krammer F. SARS-CoV-2 vaccines in development. *Nature*. 2020;586(7830):516-527. doi:10.1038/s41586-020-2798-3

[95] Prüβ BM. Current State of the First COVID-19 Vaccines. *Vaccines*. 2021;9(1):30. doi:10.3390/vaccines9010030

[96] Zhao J, Zhao S, Ou J, et al. COVID-19: Coronavirus Vaccine Development Updates. *Frontiers in Immunology*. 2020;11. Accessed March 7, 2022. https://www.frontiersin.org/article/10.3389/fimmu.2020.602256

[97] Mohsen MO, Zha L, Cabral-Miranda G, Bachmann MF. Major findings and recent advances in virus–like particle (VLP)-based vaccines. *Seminars in Immunology*. 2017;34:123-132. doi:10.1016/j.smim.2017.08.014

[98] Cimica V, Galarza JM. Adjuvant formulations for virus-like particle (VLP) based vaccines. *Clinical Immunology*. 2017;183:99-108. doi:10.1016/j.clim.2017.08.004

[99] Ward BJ, Gobeil P, Séguin A, et al. Phase 1 randomized trial of a plant-derived virus-like particle vaccine for COVID-19. *Nat Med*. 2021;27(6):1071-1078. doi:10.1038/s41591-021-01370-1

[100] Pulendran B, S. Arunachalam P, O'Hagan DT. Emerging concepts in the science of vaccine adjuvants. *Nat Rev Drug Discov*. 2021;20(6):454-475. doi:10.1038/s41573-021-00163-y

[101] Ulmer J. Vaccine Adjuvants: Mode of Action. *Frontiers in Immunology*. 2013;4. Accessed March 7, 2022. https://www.frontiersin.org/article/10.3389/fimmu.2013.00214

[102] AWATE S, Babiuk L, Mutwiri G. Mechanisms of Action of Adjuvants. *Frontiers in Immunology*. 2013;4. Accessed March 7, 2022. https://www.frontiersin.org/article/10.3389/fimmu.2013.00114

[103] Bode C, Zhao G, Steinhagen F, Kinjo T, Klinman DM. CpG DNA as a vaccine adjuvant. *Expert Rev Vaccines*. 2011;10(4):499-511. doi:10.1586/erv.10.174

[104] Krieg AM. CpG motifs: the active ingredient in bacterial extracts? *Nat Med*. 2003;9(7):831-835. doi:10.1038/nm0703-831

[105] Umscheid CA, Margolis DJ, Grossman CE. Key Concepts of Clinical Trials: A Narrative Review. *Postgraduate Medicine*. 2011;123(5):194-204. doi:10.3810/pgm.2011.09.2475

[106] Commissioner O of the. Step 3: Clinical Research. *FDA*. Published online April 18, 2019. Accessed March 10, 2022. https://www.fda.gov/patients/drug-development-process/step-3-clinical-research

[107] Artaud C, Kara L, Launay O. Vaccine Development: From Preclinical Studies to Phase 1/2 Clinical Trials. In: Ariey F, Gay F, Ménard R, eds. *Malaria Control and Elimination*. Methods in Molecular Biology. Springer; 2019:165-176. doi:10.1007/978-1-4939-9550-9_12

[108] Walker E, Nowacki AS. Understanding Equivalence and Noninferiority Testing. *J Gen Intern Med*. 2011;26(2):192-196. doi:10.1007/s11606-010-1513-8

[109] Lasser KE, Allen PD, Woolhandler SJ, Himmelstein DU, Wolfe SM, Bor DH. Timing of new black box warnings and withdrawals for prescription medications. *JAMA*. 2002;287(17):2215-2220. doi:10.1001/jama.287.17.2215

[110] İpekoğlu EM. DEVELOPMENT AND IMMUNOLOGICAL EVALUATION OF SARS-COV-2 VIRUS-LIKE PARTICLES (VLP) EXPRESSING THE PREFUSION STABILIZED VARIANTS OF THE SPIKE PROTEIN. Published online January 2022.

[111] Iyer AS, Jones FK, Nodoushani A, et al. Dynamics and significance of the antibody response to SARS-CoV-2 infection. *medRxiv*. Published online July 20, 2020:2020.07.18.20155374. doi:10.1101/2020.07.18.20155374

[112] Gaebler C, Wang Z, Lorenzi JCC, et al. Evolution of antibody immunity to SARS-CoV-2. *Nature*. 2021;591(7851):639-644. doi:10.1038/s41586-021-03207-w

[113] Brochot E, Demey B, Touzé A, et al. Anti-spike, Anti-nucleocapsid and Neutralizing Antibodies in SARS-CoV-2 Inpatients and Asymptomatic Individuals. *Frontiers in Microbiology*. 2020;11. Accessed April 19, 2022. https://www.frontiersin.org/article/10.3389/fmicb.2020.584251

[114] Burbelo PD, Riedo FX, Morishima C, et al. Sensitivity in Detection of Antibodies to Nucleocapsid and Spike Proteins of Severe Acute Respiratory Syndrome Coronavirus 2 in Patients With Coronavirus Disease 2019. *The Journal of Infectious Diseases*. 2020;222(2):206-213. doi:10.1093/infdis/jiaa273

[115] Tea F, Stella AO, Aggarwal A, et al. SARS-CoV-2 neutralizing antibodies: Longevity, breadth, and evasion by emerging viral variants. *PLOS Medicine*. 2021;18(7):e1003656. doi:10.1371/journal.pmed.1003656

[116] Chvatal-Medina M, Mendez-Cortina Y, Patiño PJ, Velilla PA, Rugeles MT. Antibody Responses in COVID-19: A Review. *Frontiers in Immunology*. 2021;12. Accessed April 25, 2022. https://www.frontiersin.org/article/10.3389/fimmu.2021.633184

[117] Alipoor SD, Mortaz E, Jamaati H, et al. COVID-19: Molecular and Cellular Response. *Frontiers in Cellular and Infection Microbiology*. 2021;11. Accessed May 1, 2022. https://www.frontiersin.org/article/10.3389/fcimb.2021.563085

[118] Li CK, Wu H, Yan H, et al. T Cell Responses to Whole SARS Coronavirus in Humans. *J Immunol*. 2008;181(8):5490-5500.

[119] Chen Z, John Wherry E. T cell responses in patients with COVID-19. *Nat Rev Immunol*. 2020;20(9):529-536. doi:10.1038/s41577-020-0402-6

[120] Martonik D, Parfieniuk-Kowerda A, Rogalska M, Flisiak R. The Role of Th17 Response in COVID-19. *Cells*. 2021;10(6):1550. doi:10.3390/cells10061550

[121] Gubernatorova EO, Gorshkova EA, Polinova AI, Drutskaya MS. IL-6: Relevance for immunopathology of SARS-CoV-2. *Cytokine Growth Factor Rev*. 2020;53:13-24. doi:10.1016/j.cytogfr.2020.05.009

[122] Kimura A, Kishimoto T. IL-6: Regulator of Treg/Th17 balance. *European Journal of Immunology*. 2010;40(7):1830-1835. doi:10.1002/eji.201040391

[123] Kyriakidis NC, López-Cortés A, González EV, Grimaldos AB, Prado EO. SARS-CoV-2 vaccines strategies: a comprehensive review of phase 3 candidates. *npj Vaccines*. 2021;6(1):1-17. doi:10.1038/s41541-021-00292-w

[124] Noh JY, Jeong HW, Kim JH, Shin E-C. T cell-oriented strategies for controlling the COVID-19 pandemic. *Nat Rev Immunol*. 2021;21(11):687-688. doi:10.1038/s41577-021-00625-9

[125] García-Silva I, Colunga-Saucedo M, Almendarez-Rodríguez C, Miranda-López C, Rosales-Mendoza S, Comas-Garcia M. Chapter 10 - Virus-like particle-based vaccines against SARS-CoV-2. In: Rosales-Mendoza S, Comas-Garcia M, Gonzalez-Ortega O, eds. *Biomedical Innovations to Combat COVID-19*. Academic Press; 2022:173-192. doi:10.1016/B978-0-323-90248-9.00005-X

[126] Yilmaz IC, Ipekoglu EM, Bulbul A, et al. Development and preclinical evaluation of virus-like particle vaccine against COVID-19 infection. *Allergy*. Published online September 21, 2021:10.1111/all.15091. doi:10.1111/all.15091

[127] Viral nucleoprotein antibodies activate TRIM21 and induce T cell immunity. *The EMBO Journal*. 2021;40(5):e106228. doi:10.15252/embj.2020106228

[128] Ortega N, Ribes M, Vidal M, et al. Seven-month kinetics of SARS-CoV-2 antibodies and role of pre-existing antibodies to human coronaviruses. *Nat Commun*. 2021;12(1):4740. doi:10.1038/s41467-021-24979-9

[129] Zamorano Cuervo N, Grandvaux N. ACE2: Evidence of role as entry receptor for SARS-CoV-2 and implications in comorbidities. *eLife*. 9:e61390. doi:10.7554/eLife.61390

[130] Burbelo PD, Riedo FX, Morishima C, et al. Detection of Nucleocapsid Antibody to SARS-CoV-2 is More Sensitive than Antibody to Spike Protein in COVID-19 Patients. *medRxiv*. Published online April 24, 2020:2020.04.20.20071423. doi:10.1101/2020.04.20.20071423

[131] Gruell H, Vanshylla K, Tober-Lau P, et al. mRNA booster immunization elicits potent neutralizing serum activity against the SARS-CoV-2 Omicron variant. *Nat Med*. 2022;28(3):477-480. doi:10.1038/s41591-021-01676-0

[132] Dobaño C, Santano R, Jiménez A, et al. Immunogenicity and crossreactivity of antibodies to the nucleocapsid protein of SARS-CoV-2: utility and limitations in seroprevalence and immunity studies. *Transl Res*. 2021;232:60-74. doi:10.1016/j.trsl.2021.02.006

[133] Yang J, Wang W, Chen Z, et al. A vaccine targeting the RBD of the S protein of SARS-CoV-2 induces protective immunity. *Nature*. 2020;586(7830):572-577. doi:10.1038/s41586-020-2599-8

[134] Favresse J, Gillot C, Di Chiaro L, et al. Neutralizing Antibodies in COVID-19 Patients and Vaccine Recipients after Two Doses of BNT162b2. *Viruses*. 2021;13(7):1364. doi:10.3390/v13071364

[135] Curtsinger JM, Agarwal P, Lins DC, Mescher MF. Autocrine IFN-γ promotes naïve CD8 T cell differentiation and synergizes with IFN-α to stimulate strong function. *J Immunol*. 2012;189(2):659-668. doi:10.4049/jimmunol.1102727

[136] Aleebrahim-Dehkordi E, Molavi B, Mokhtari M, et al. T helper type (Th1/Th2) responses to SARS-CoV-2 and influenza A (H1N1) virus: From cytokines produced to immune responses. *Transpl Immunol*. 2022;70:101495. doi:10.1016/j.trim.2021.101495

[137] Pérez-Cabezas B, Ribeiro R, Costa I, et al. IL-2 and IFN-γ are biomarkers of SARS-CoV-2 specific cellular response in whole blood stimulation assays. Published online January 8, 2021:2021.01.04.20248897. doi:10.1101/2021.01.04.20248897

[138] Pavel AB, Glickman JW, Michels JR, Kim-Schulze S, Miller RL, Guttman-Yassky E. Th2/Th1 Cytokine Imbalance Is Associated With Higher COVID-19 Risk Mortality. *Frontiers in Genetics*. 2021;12. Accessed May 30, 2022. https://www.frontiersin.org/article/10.3389/fgene.2021.706902

[139] Donlan AN, Sutherland TE, Marie C, et al. IL-13 is a driver of COVID-19 severity. *medRxiv*. Published online March 1, 2021:2020.06.18.20134353. doi:10.1101/2020.06.18.20134353

[140] Chen J, Guan L, Tang L, et al. T Helper 9 Cells: A New Player in Immune-Related Diseases. *DNA Cell Biol*. 2019;38(10):1040-1047. doi:10.1089/dna.2019.4729

[141] Takami M, Love RB, Iwashima M. TGF-β converts apoptotic stimuli into the signal for Th9 differentiation. *J Immunol*. 2012;188(9):4369-4375. doi:10.4049/jimmunol.1102698

[142] Interleukin 9 - an overview | ScienceDirect Topics. Accessed May 31, 2022. https://www.sciencedirect.com/topics/medicine-and-dentistry/interleukin-9

[143] Wurtz O. IL-4-mediated inhibition of IFN- production by CD4+ T cells proceeds by several developmentally regulated mechanisms. *International Immunology*. 2004;16(3):501-508. doi:10.1093/intimm/dxh050

[144] Hotez PJ, Bottazzi ME, Corry DB. The potential role of Th17 immune responses in coronavirus immunopathology and vaccine-induced immune enhancement. *Microbes Infect*. 2020;22(4):165-167. doi:10.1016/j.micinf.2020.04.005

[145] Santa Cruz A, Mendes-Frias A, Oliveira AI, et al. Interleukin-6 Is a Biomarker for the Development of Fatal Severe Acute Respiratory Syndrome Coronavirus 2 Pneumonia. *Frontiers in Immunology*. 2021;12. Accessed June 2, 2022. https://www.frontiersin.org/article/10.3389/fimmu.2021.613422

[146] Wang H, Wang Z, Cao W, Wu Q, Yuan Y, Zhang X. Regulatory T cells in COVID-19. *Aging Dis*. 2021;12(7):1545-1553. doi:10.14336/AD.2021.0709

[147] Kondělková K, Vokurková D, Krejsek J, Borská L, Fiala Z, Ctirad A. Regulatory T cells (TREG) and their roles in immune system with respect to immunopathological disorders. *Acta Medica (Hradec Kralove)*. 2010;53(2):73-77. doi:10.14712/18059694.2016.63

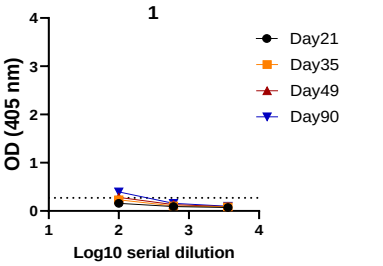
[148] Kubo T, Morita H, Sugita K, Akdis CA. Chapter 1 - Introduction to Mechanisms of Allergic Diseases. In: O'Hehir RE, Holgate ST, Sheikh A, eds. *Middleton's Allergy Essentials*. Elsevier; 2017:1-27. doi:10.1016/B978-0-323-37579-5.00001-5

[149] Tan M, Liu Y, Zhou R, et al. Immunopathological characteristics of coronavirus disease 2019 cases in Guangzhou, China. *Immunology*. 2020;160(3):261-268. doi:10.1111/imm.13223

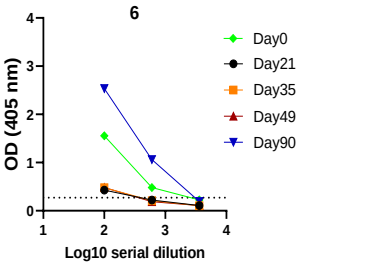
[150] Neumann J, Prezzemolo T, Vanderbeke L, et al. Increased IL-10-producing regulatory T cells are characteristic of severe cases of COVID-19. *Clin Transl Immunology*. 2020;9(11):e1204. doi:10.1002/cti2.1204

APPENDIX

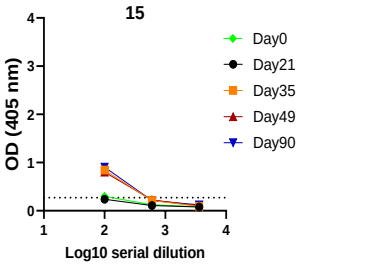
	Day21	Day35	Day49	Day90
Total Area	310.0	365.8	431.8	522.5



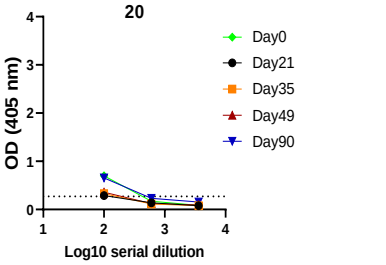
	Day0	Day21	Day35	Day49	Day90
Total Area	1571	654.3	643.0	608.0	2779



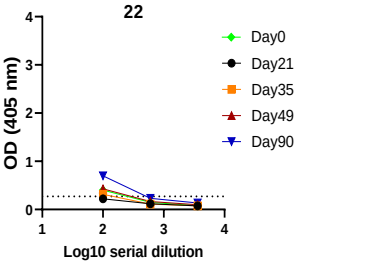
	Day0	Day21	Day35	Day49	Day90
Total Area	417.5	367.0	719.0	743.8	783.5



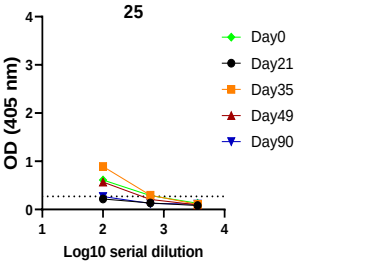
	Day0	Day21	Day35	Day49	Day90
Total Area	603.0	430.0	397.0	445.3	804.3



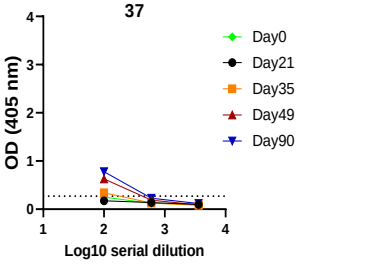
	Day0	Day21	Day35	Day49	Day90
Total Area	478.0	377.5	387.0	544.0	783.0



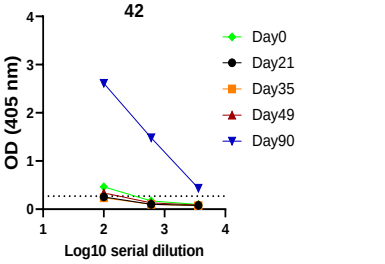
	Day0	Day21	Day35	Day49	Day90
Total Area	845.5	412.0	896.3	650.8	452.3



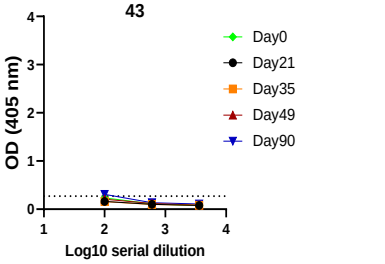
	Day0	Day21	Day35	Day49	Day90
Total Area	429.3	432.3	434.0	621.3	770.3



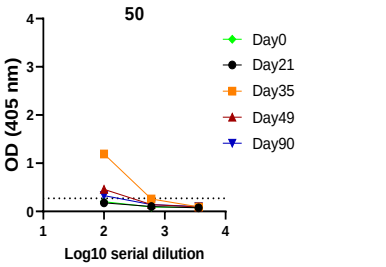
	Day0	Day21	Day35	Day49	Day90
Total Area	567.3	357.5	349.3	443.0	3899



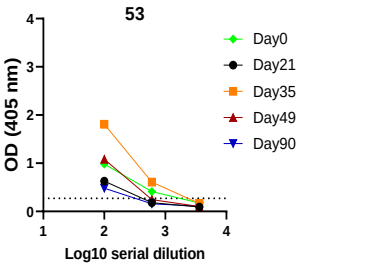
	Day0	Day21	Day35	Day49	Day90
Total Area	365.0	337.5	332.5	390.8	472.3



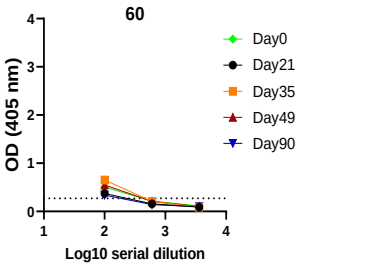
	Day0	Day21	Day35	Day49	Day90
Total Area	331.0	330.3	890.5	497.5	480.0



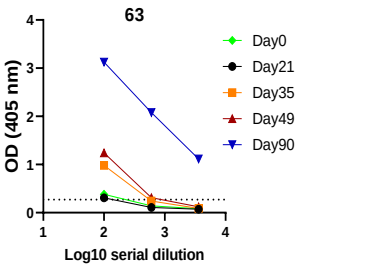
	Day0	Day21	Day35	Day49	Day90
Total Area	1227	611.8	1760	854.3	560.5



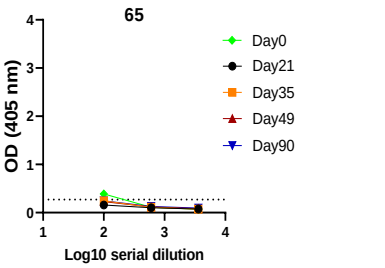
	Day0	Day21	Day35	Day49	Day90
Total Area	672.3	501.5	658.8	654.3	481.5



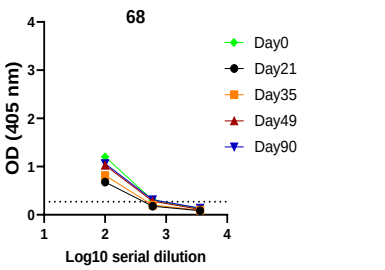
	Day0	Day21	Day35	Day49	Day90
Total Area	460.0	372.8	803.0	1035	6089



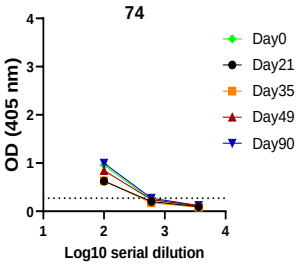
	Day0	Day21	Day35	Day49	Day90
Total Area	397.8	332.0	364.0	386.8	424.8



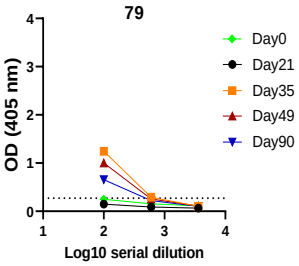
	Day0	Day21	Day35	Day49	Day90
Total Area	1024	609.0	698.0	920.0	1018



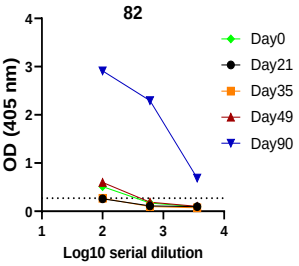
	Day0	Day21	Day35	Day49	Day90
Total Area	803.3	650.5	592.0	805.8	904.0



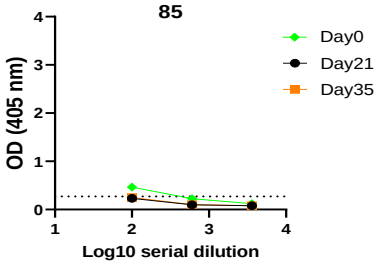
	Day0	Day21	Day35	Day49	Day90
Total Area	501.5	288.8	977.0	860.5	706.8



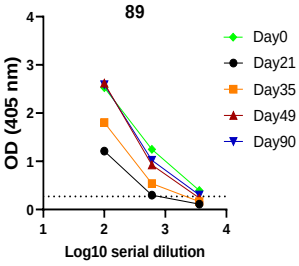
	Day0	Day21	Day35	Day49	Day90
Total Area	570.5	399.8	343.0	635.3	5776



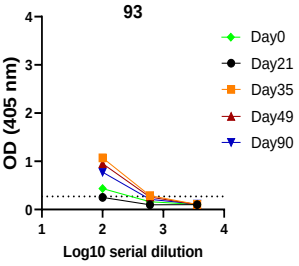
	Day0	Day21	Day35
Total Area	693.5	348.3	357.8



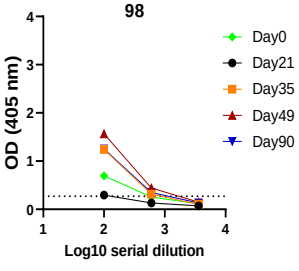
	Day0	Day21	Day35	Day49	Day90
Total Area	3410	993.3	1637	2631	2883



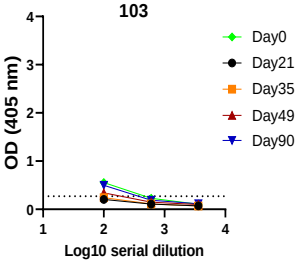
	Day0	Day21	Day35	Day49	Day90
Total Area	549.3	387.3	932.5	844.3	729.3



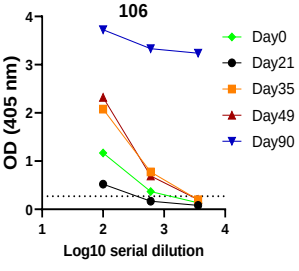
	Day0	Day21	Day35	Day49	Day90
Total Area	794.3	410.8	1013	1386	1122



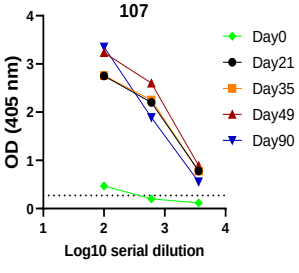
	Day0	Day21	Day35	Day49	Day90
Total Area	693.5	343.3	355.0	495.0	624.3



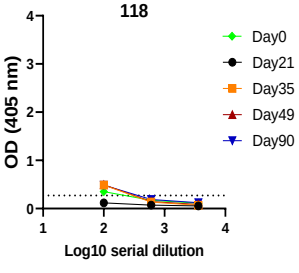
	Day0	Day21	Day35	Day49	Day90
Total Area	1137	546.3	2170	2090	11618



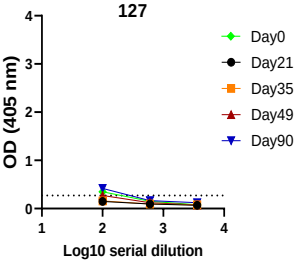
	Day0	Day21	Day35	Day49	Day90
Total Area	650.3	5711	5794	6700	4975



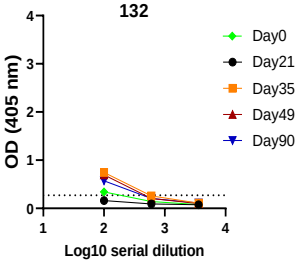
	Day0	Day21	Day35	Day49	Day90
Total Area	552.3	239.8	460.5	506.8	636.5



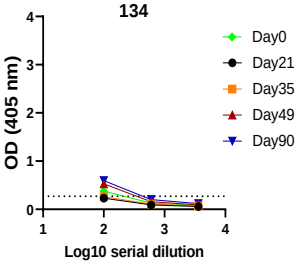
	Day0	Day21	Day35	Day49	Day90
Total Area	468.5	302.5	320.8	395.8	577.8



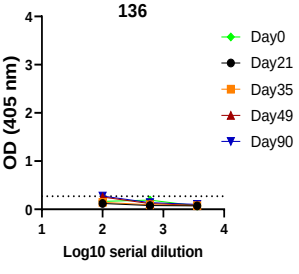
	Day0	Day21	Day35	Day49	Day90
Total Area	451.0	312.3	800.0	679.5	671.3



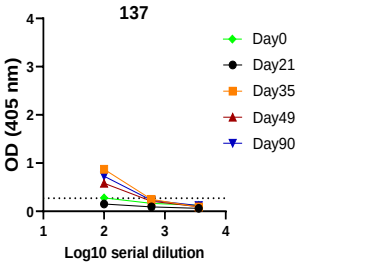
	Day0	Day21	Day35	Day49	Day90
Total Area	444.8	308.8	355.0	544.5	676.3



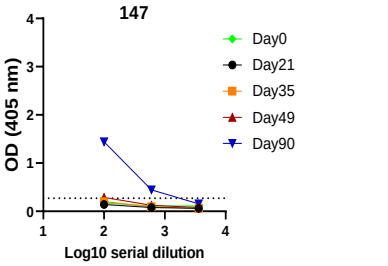
	Day0	Day21	Day35	Day49	Day90
Total Area	487.0	273.3	315.0	388.5	465.3



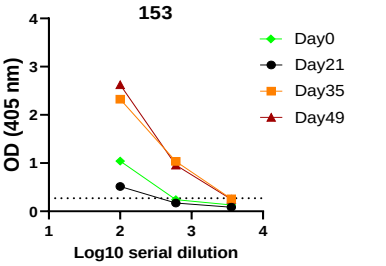
	Day0	Day21	Day35	Day49	Day90
Total Area	546.0	291.8	787.5	655.0	761.0



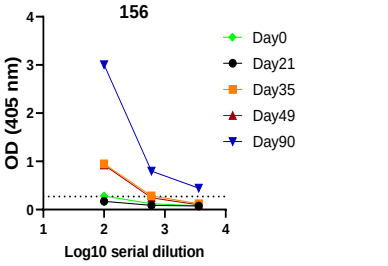
	Day0	Day21	Day35	Day49	Day90
Total Area	400.5	267.8	310.8	408.0	1375



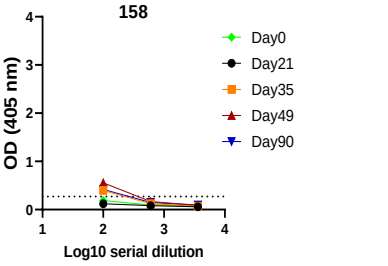
	Day0	Day21	Day35	Day49
Total Area	878.5	553.8	2779	2710



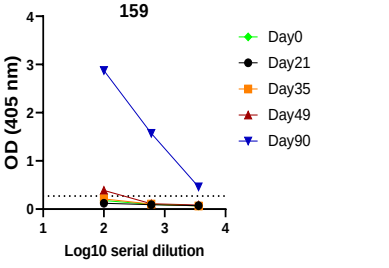
	Day0	Day21	Day35	Day49	Day90
Total Area	400.8	311.0	919.3	805.0	2815



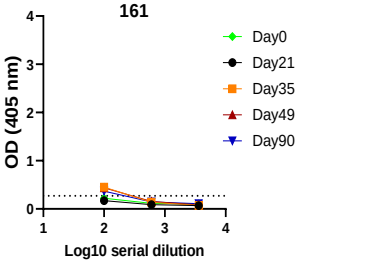
	Day0	Day21	Day35	Day49	Day90
Total Area	337.8	257.3	413.3	556.8	506.8



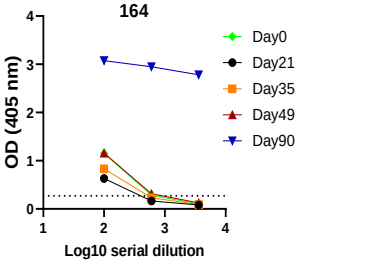
	Day0	Day21	Day35	Day49	Day90
Total Area	318.3	296.3	334.0	417.3	4158



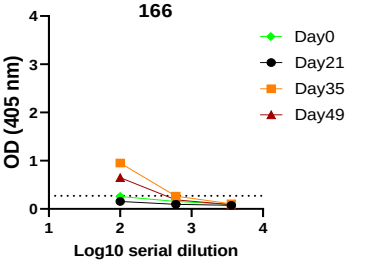
	Day0	Day21	Day35	Day49	Day90
Total Area	409.8	301.3	460.8	505.3	504.8



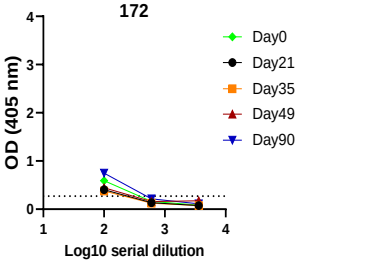
	Day0	Day21	Day35	Day49	Day90
Total Area	943.8	565.3	749.8	1025	10101



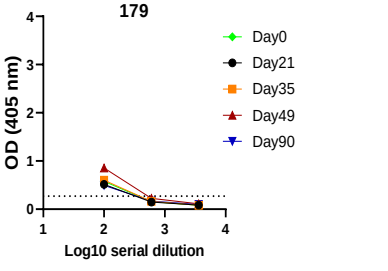
	Day0	Day21	Day35	Day49
Total Area	480.0	319.5	857.5	619.8



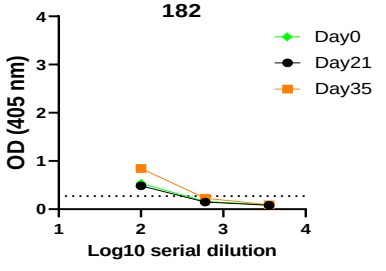
	Day0	Day21	Day35	Day49	Day90
Total Area	558.8	450.0	424.5	650.0	734.8



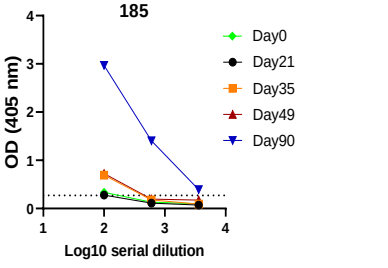
	Day0	Day21	Day35	Day49	Day90
Total Area	541.3	515.3	552.5	775.8	568.3



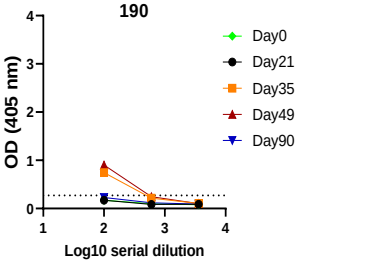
	Day0	Day21	Day35
Total Area	544.0	508.5	748.0



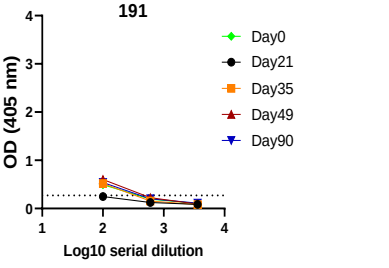
	Day0	Day21	Day35	Day49	Day90
Total Area	460.0	370.3	619.3	784.5	3789



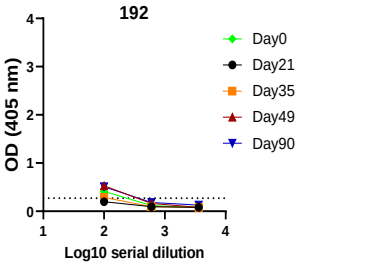
	Day0	Day21	Day35	Day49	Day90
Total Area	334.8	325.8	719.8	807.5	404.5



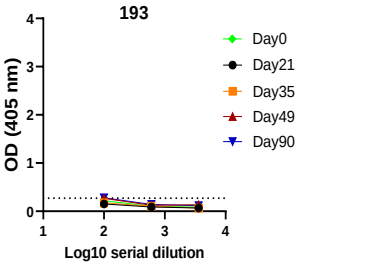
	Day0	Day21	Day35	Day49	Day90
Total Area	622.5	409.5	520.5	682.0	655.8



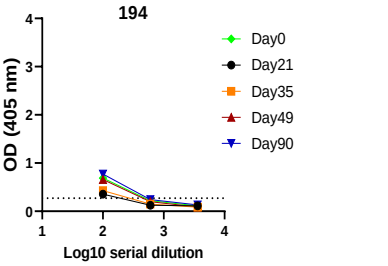
	Day0	Day21	Day35	Day49	Day90
Total Area	422.0	337.8	358.5	535.5	635.8



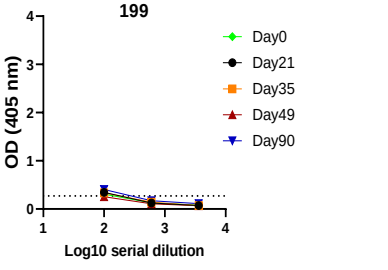
	Day0	Day21	Day35	Day49	Day90
Total Area	365.5	298.8	321.5	487.8	489.0



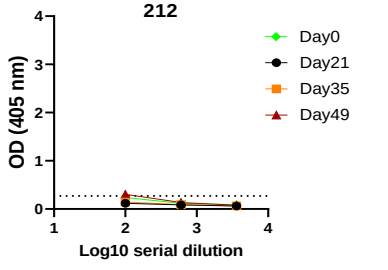
	Day0	Day21	Day35	Day49	Day90
Total Area	720.5	475.5	492.0	645.8	811.8



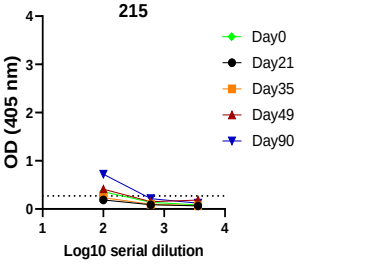
	Day0	Day21	Day35	Day49	Day90
Total Area	416.0	412.8	440.8	353.0	573.3



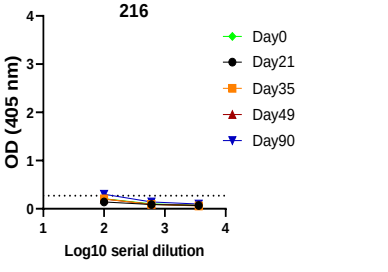
	Day0	Day21	Day35	Day49
Total Area	405.0	273.3	296.5	427.8



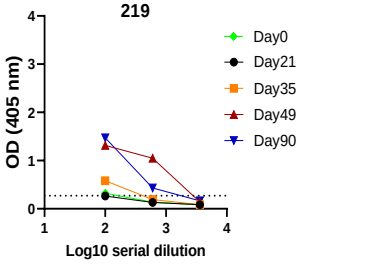
	Day0	Day21	Day35	Day49	Day90
Total Area	455.0	300.8	330.8	647.8	738.3



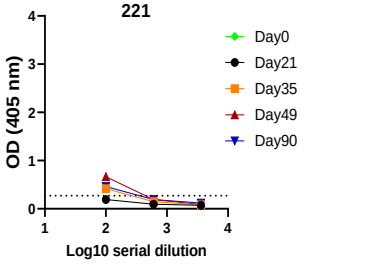
	Day0	Day21	Day35	Day49	Day90
Total Area	340.0	293.5	302.3	317.8	469.3



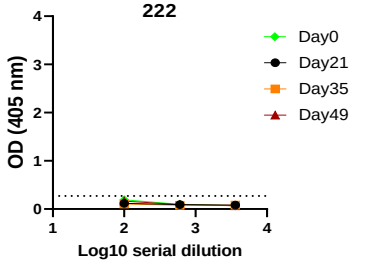
	Day0	Day21	Day35	Day49	Day90
Total Area	440.5	424.8	604.0	2372	1368



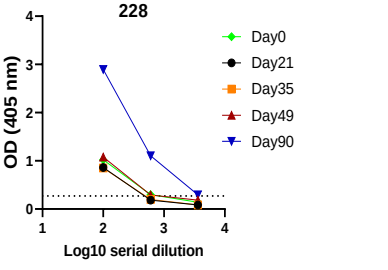
	Day0	Day21	Day35	Day49	Day90
Total Area		321.8	485.0	631.0	633.5



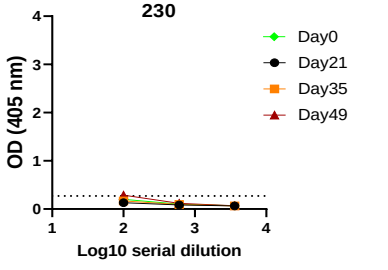
	Day0	Day21	Day35	Day49
Total Area	323.5	313.8	284.8	301.3



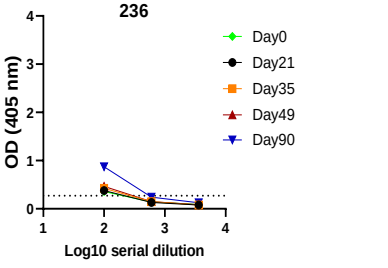
	Day0	Day21	Day35	Day49	Day90
Total Area	987.0	665.3	687.3	1060	3102



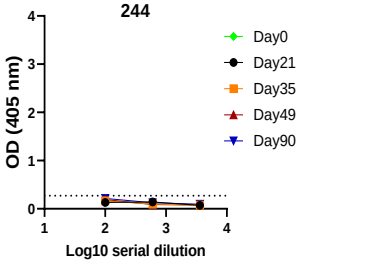
	Day0	Day21	Day35	Day49
Total Area	332.0	277.3	302.8	385.8



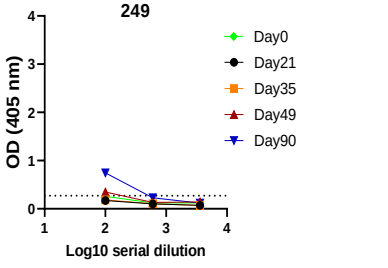
	Day0	Day21	Day35	Day49	Day90
Total Area	475.3	441.0	481.0	508.0	829.3



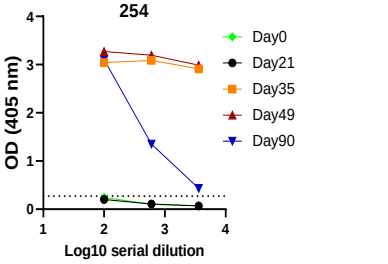
	Day0	Day21	Day35	Day49	Day90
Total Area	332.0	385.5	328.5	323.5	413.3



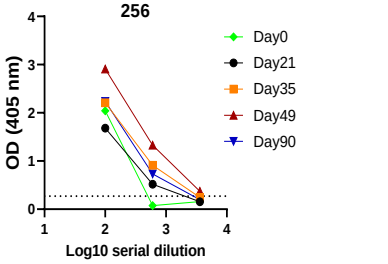
	Day0	Day21	Day35	Day49	Day90
Total Area	459.8	323.3	330.0	533.3	765.5



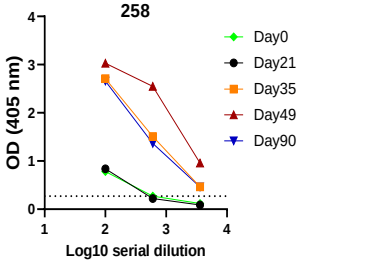
	Day0	Day21	Day35	Day49	Day90
Total Area	345.5	338.0	10534	10895	3790



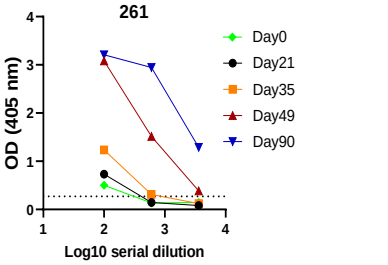
	Day0	Day21	Day35	Day49	Day90
Total Area	877.3	1556	2519	3609	2138



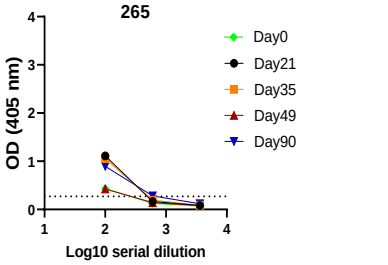
	Day0	Day21	Day35	Day49	Day90
Total Area	846.5	732.3	4017	6651	3745



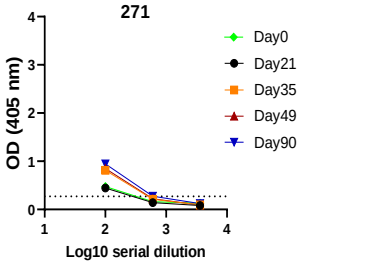
	Day0	Day21	Day35	Day49	Day90
Total Area	582.3	558.3	1038	3998	7889



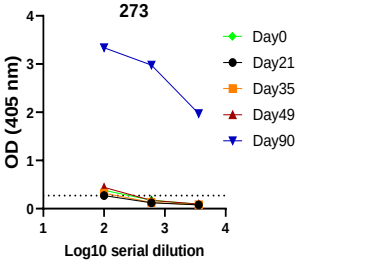
	Day0	Day21	Day35	Day49	Day90
Total Area	440.3	686.5	726.8	472.8	891.0



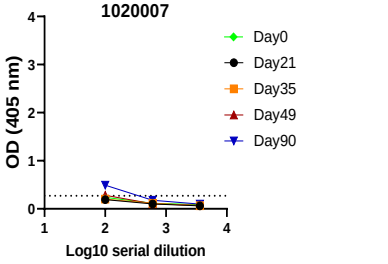
	Day0	Day21	Day35	Day49	Day90
Total Area	594.0	483.0	712.8	736.5	897.5



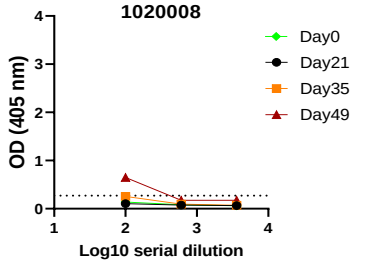
	Day0	Day21	Day35	Day49	Day90
Total Area	543.0	396.5	423.0	553.3	9001



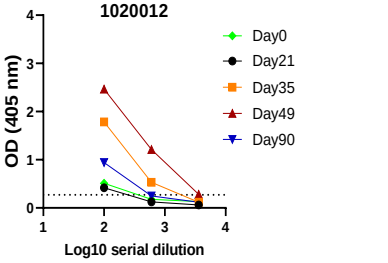
	Day0	Day21	Day35	Day49	Day90
Total Area	389.5	317.3	350.5	357.0	585.0



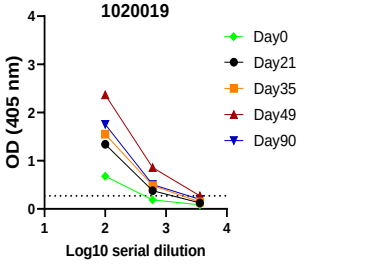
	Day0	Day21	Day35	Day49
Total Area	267.8	256.8	339.8	732.5



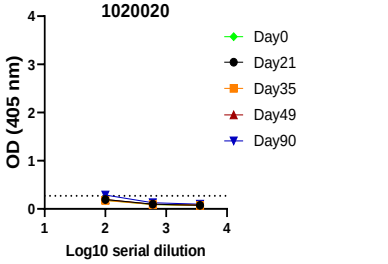
	Day0	Day21	Day35	Day49	Day90
Total Area	638.3	414.8	1553	3157	848.0



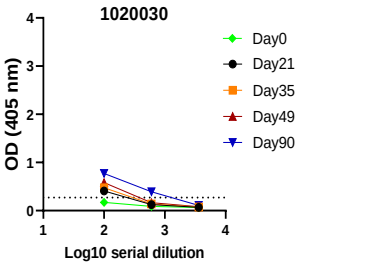
	Day0	Day21	Day35	Day49	Day90
Total Area	627.3	1181	1453	2500	1620



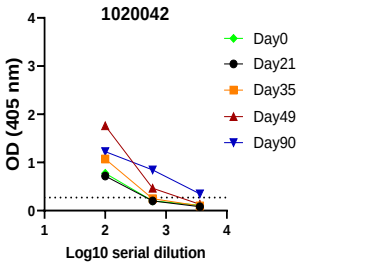
	Day0	Day21	Day35	Day49	Day90
Total Area	309.8	334.3	312.5	337.0	441.8



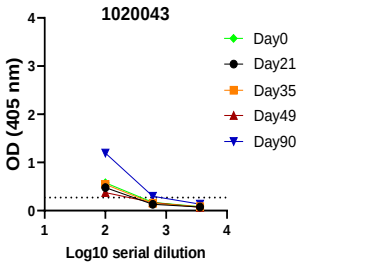
	Day0	Day21	Day35	Day49	Day90
Total Area	296.0	421.3	471.5	556.0	1041



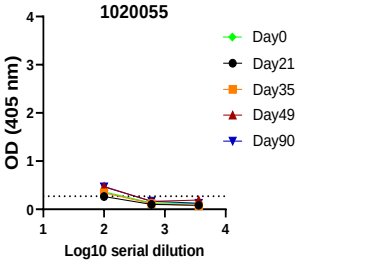
	Day0	Day21	Day35	Day49	Day90
Total Area	715.5	653.8	850.5	1454	2304



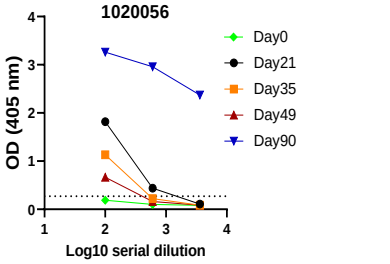
	Day0	Day21	Day35	Day49	Day90
Total Area	569.3	463.0	523.8	489.3	1019



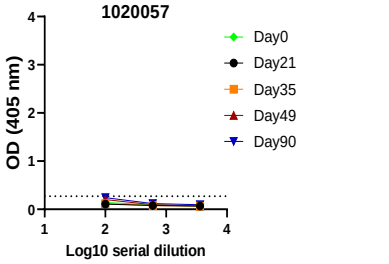
	Day0	Day21	Day35	Day49	Day90
Total Area	501.0	374.0	398.5	696.0	598.0



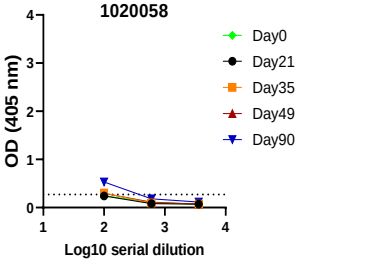
	Day0	Day21	Day35	Day49	Day90
Total Area	345.3	1381	796.0	579.3	9553



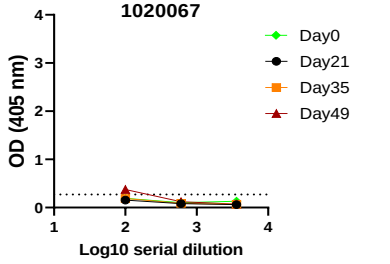
	Day0	Day21	Day35	Day49	Day90
Total Area	294.0	265.5	262.0	322.3	409.5



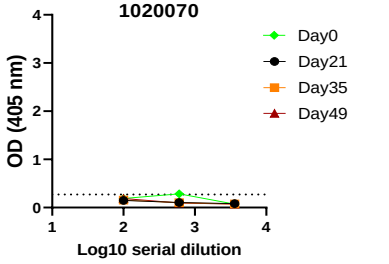
	Day0	Day21	Day35	Day49	Day90
Total Area	352.0	315.3	348.5	374.5	622.5



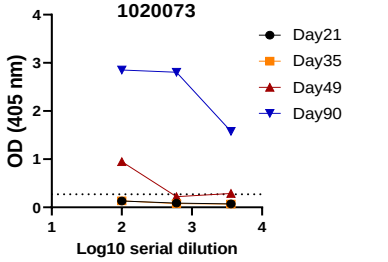
	Day0	Day21	Day35	Day49
Total Area	421.0	273.5	305.0	415.3



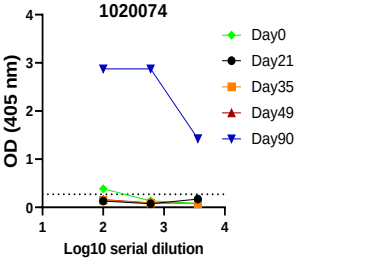
	Day0	Day21	Day35	Day49
Total Area	651.8	339.5	326.0	317.8



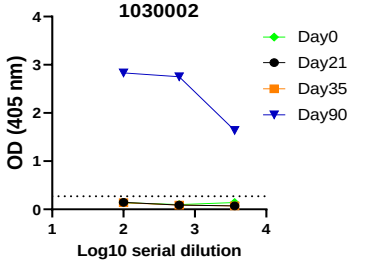
	Day21	Day35	Day49	Day90
Total Area	294.0	270.8	1058	7987



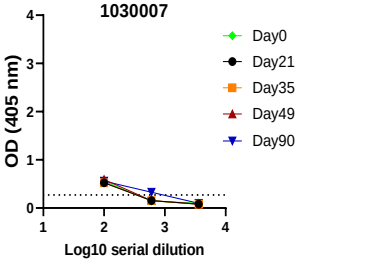
	Day0	Day21	Day35	Day49	Day90
Total Area	454.3	420.5	311.0	318.3	7886



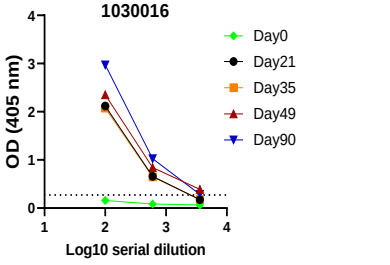
	Day0	Day21	Day35	Day90
Total Area	418.8	300.0	299.8	7977



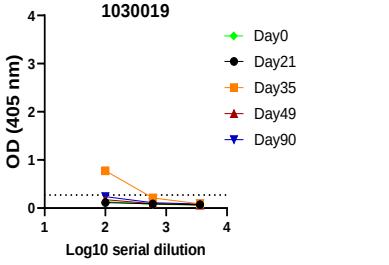
	Day0	Day21	Day35	Day49	Day90
Total Area	546.0	525.5	526.8	535.8	857.3



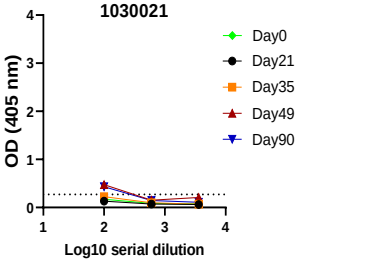
	Day0	Day21	Day35	Day49	Day90
Total Area	285.5	1944	1920	2642	2964



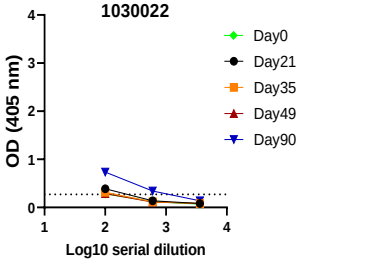
	Day0	Day21	Day35	Day49	Day90
Total Area	268.0	290.3	698.5	296.3	382.0



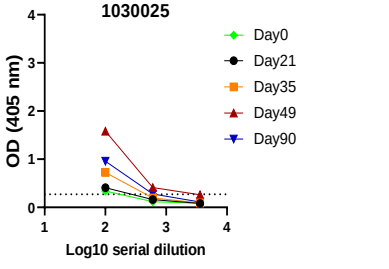
	Day0	Day21	Day35	Day49	Day90
Total Area	305.3	248.8	327.8	693.5	525.5



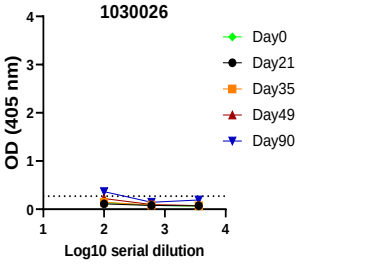
	Day0	Day21	Day35	Day49	Day90
Total Area	389.5	460.3	403.3	397.5	987.0



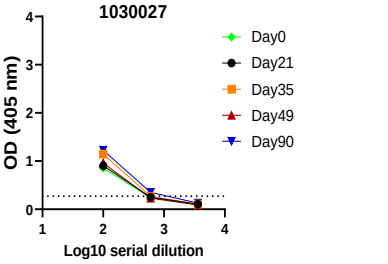
	Day0	Day21	Day35	Day49	Day90
Total Area	417.3	511.8	658.5	1512	892.3



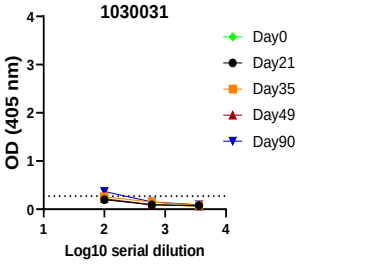
	Day0	Day21	Day35	Day49	Day90
Total Area	275.0	269.5	288.3	341.3	636.0



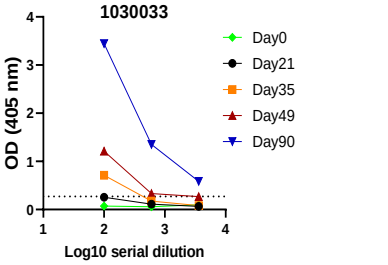
	Day0	Day21	Day35	Day49	Day90
Total Area	772.5	822.5	917.3	780.0	1114



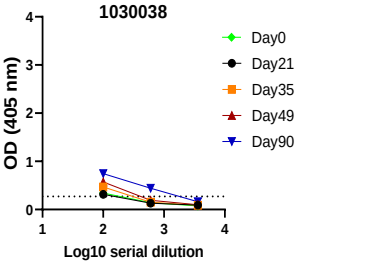
	Day0	Day21	Day35	Day49	Day90
Total Area	323.0	319.5	444.8	316.3	494.3



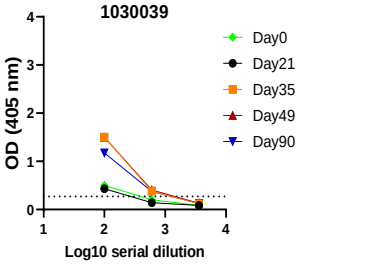
	Day0	Day21	Day35	Day49	Day90
Total Area	264.3	360.5	606.0	1283	4101



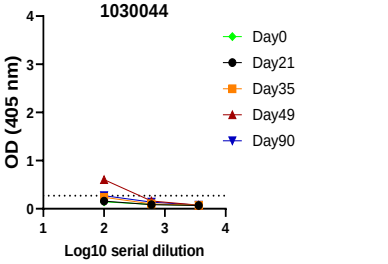
	Day0	Day21	Day35	Day49	Day90
Total Area	444.3	447.5	515.5	625.8	1204



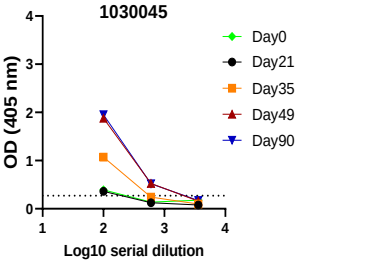
	Day0	Day21	Day35	Day49	Day90
Total Area	602.8	485.3	1218	1276	1142



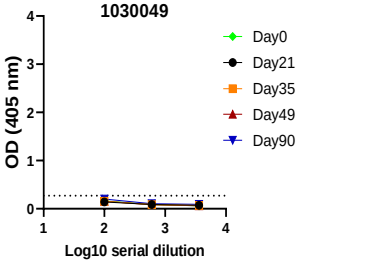
	Day0	Day21	Day35	Day49	Day90
Total Area	308.8	289.0	344.5	547.0	419.0



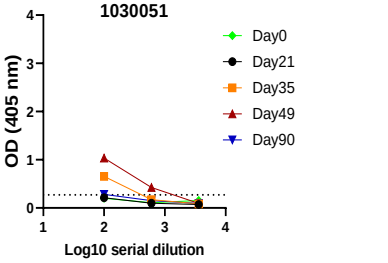
	Day0	Day21	Day35	Day49	Day90
Total Area	611.5	423.3	835.0	1624	1652



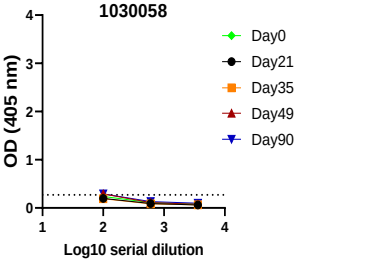
	Day0	Day21	Day35	Day49	Day90
Total Area	292.0	296.3	286.3	277.0	374.0



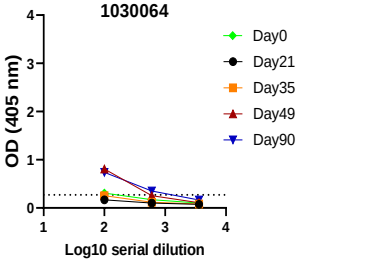
	Day0	Day21	Day35	Day49	Day90
Total Area	470.0	331.3	588.8	1145	480.0



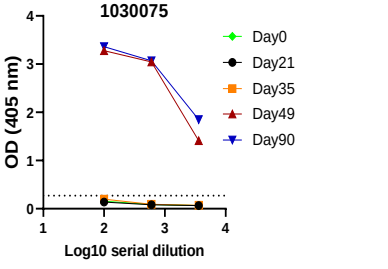
	Day0	Day21	Day35	Day49	Day90
Total Area	371.0	300.3	292.8	378.0	454.5



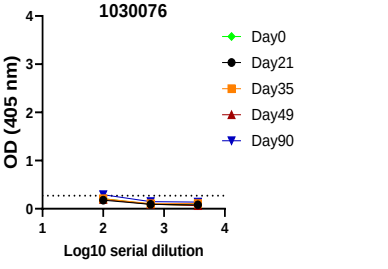
	Day0	Day21	Day35	Day49	Day90
Total Area	529.0	328.3	391.3	810.0	1050



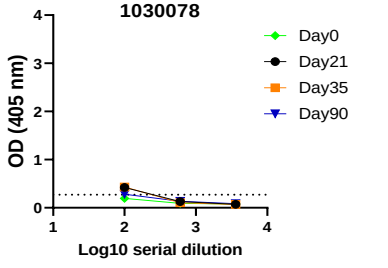
	Day0	Day21	Day35	Day49	Day90
Total Area	293.3	270.8	319.0	8266	8979



	Day0	Day21	Day35	Day49	Day90
Total Area	324.8	325.3	399.5	312.3	536.0



	Day0	Day21	Day35	Day90
Total Area	328.5	433.0	395.0	437.3



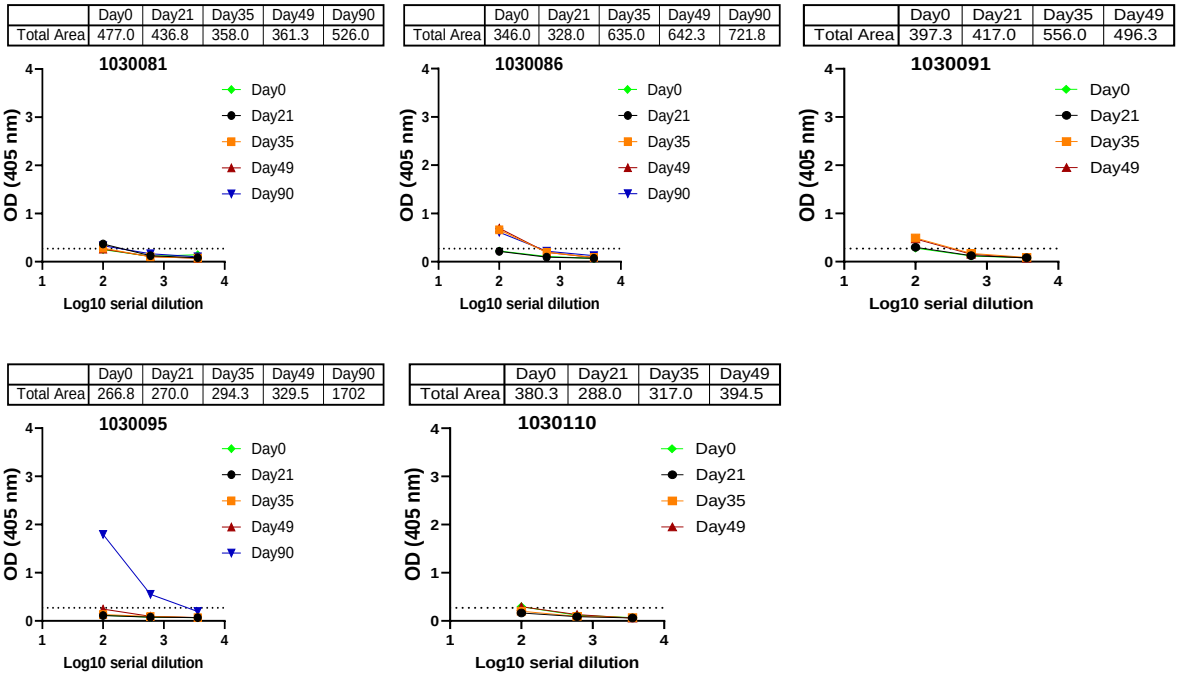
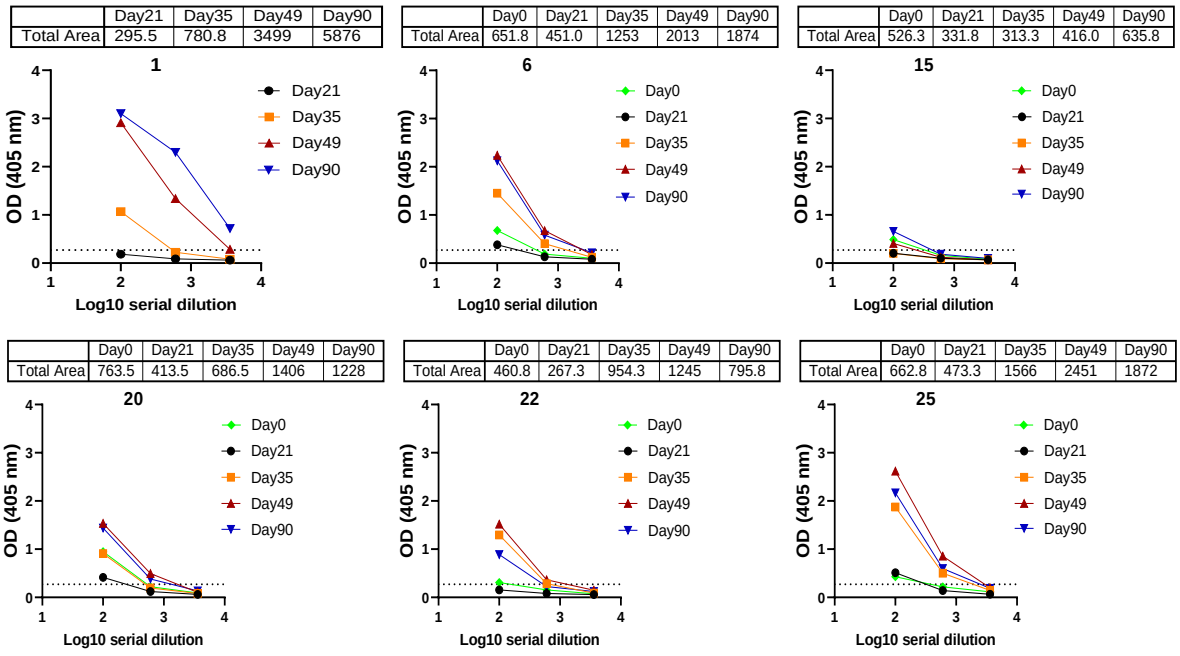
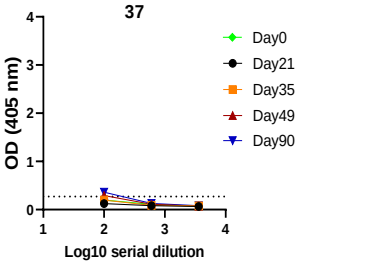


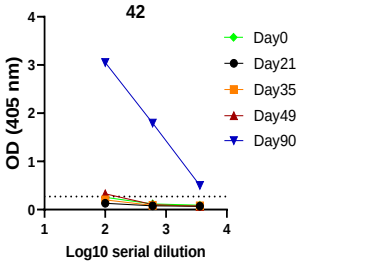
Figure A.1. The IgG responses of the volunteers against recombinant nucleocapsid protein were assessed by ELISA. 2HB ELISA plates were coated 1 ug/ml of recombinant nucleocapsid protein and following overnight incubation and blocking steps, the human sera collected at days 0, 21, 35, 49, and 90 were added to the wells. The sera were initially prepared in 1:100 ratio and then serially diluted sixfold for 2 times. After overnight incubation, the plates were treated with anti-human IgG prepared in 1:1000 ratio and the OD405 values were recorded following treatment with PNPP substrate solution. OD405 values for each volunteer are demonstrated in each graph with area under the curve values presented in the tables.



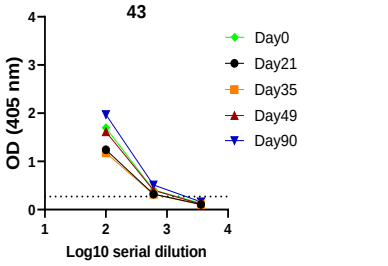
	Day0	Day21	Day35	Day49	Day90
Total Area	341.8	270.5	322.0	372.3	436.5



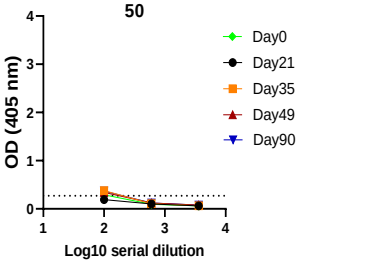
	Day0	Day21	Day35	Day49	Day90
Total Area	406.5	277.3	323.3	366.5	4658



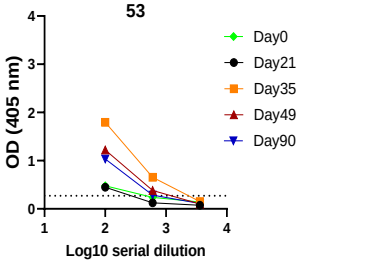
	Day0	Day21	Day35	Day49	Day90
Total Area	1334	1032	1006	1275	1636



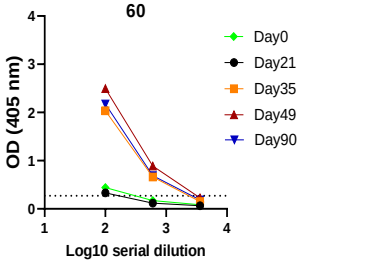
	Day0	Day21	Day35	Day49	Day90
Total Area	331.8	316.0	380.8	416.0	425.8



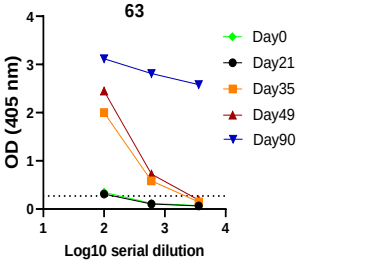
	Day0	Day21	Day35	Day49	Day90
Total Area	753.8	443.5	1821	1125	927.3



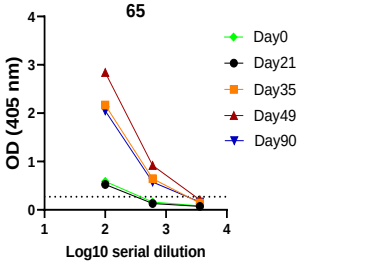
	Day0	Day21	Day35	Day49	Day90
Total Area	536.8	388.5	1895	2523	2029



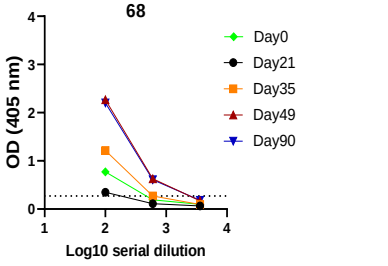
	Day0	Day21	Day35	Day49	Day90
Total Area	398.3	359.0	1749	2163	9574



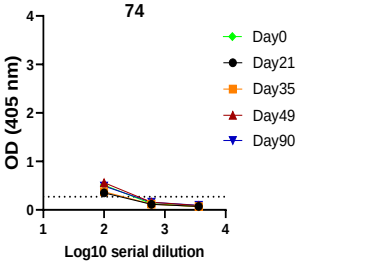
	Day0	Day21	Day35	Day49	Day90
Total Area	553.5	473.3	1881	2632	1763



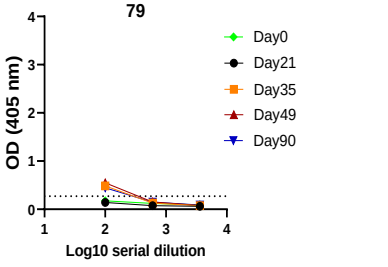
	Day0	Day21	Day35	Day49	Day90
Total Area	670.8	380.5	919.3	1923	1888



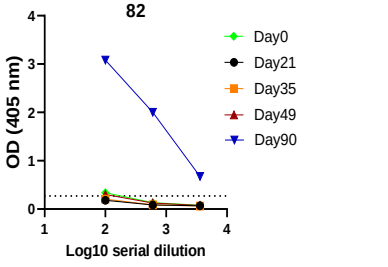
	Day0	Day21	Day35	Day49	Day90
Total Area	454.3	394.0	401.0	547.8	545.5



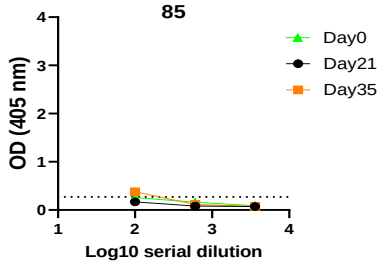
	Day0	Day21	Day35	Day49	Day90
Total Area	393.5	259.5	456.0	520.6	499.0



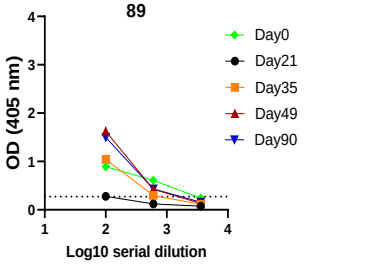
	Day0	Day21	Day35	Day49	Day90
Total Area	432.5	296.3	300.5	406.5	5287



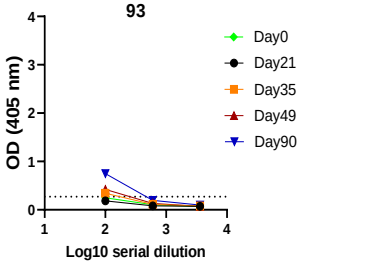
	Day0	Day21	Day35
Total Area	481.3	291.5	408.0



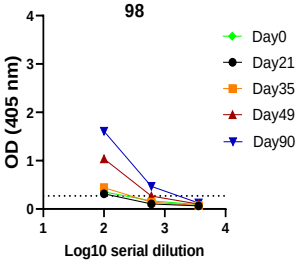
	Day0	Day21	Day35	Day49	Day90
Total Area	1650	398.5	949.5	1351	1364



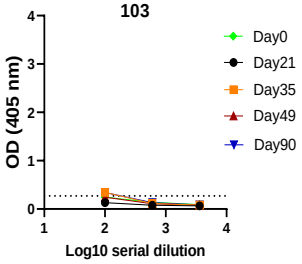
	Day0	Day21	Day35	Day49	Day90
Total Area	344.5	293.0	399.8	439.5	677.3



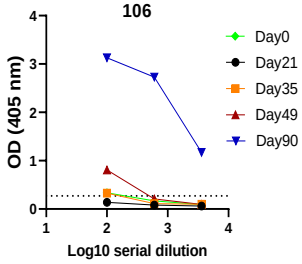
	Day0	Day21	Day35	Day49	Day90
Total Area	519.3	361.5	462.0	881.5	1410



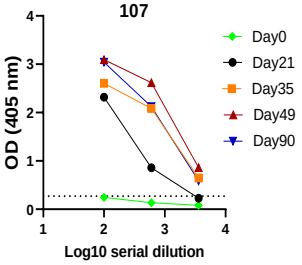
	Day0	Day21	Day35	Day49	Day90
Total Area	439.5	270.3	409.5	373.0	442.0



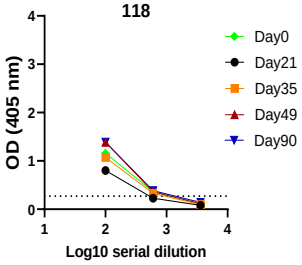
	Day0	Day21	Day35	Day49	Day90
Total Area	512.8	271.0	421.5	705.0	7316



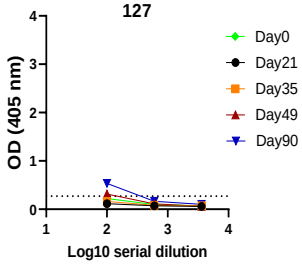
	Day0	Day21	Day35	Day49	Day90
Total Area	420.3	2425	5275	6652	5359



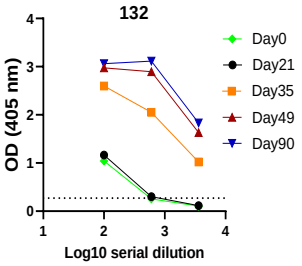
	Day0	Day21	Day35	Day49	Day90
Total Area	1102	719.3	988.8	1147	1236



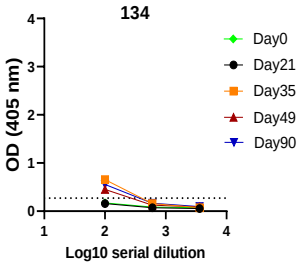
	Day0	Day21	Day35	Day49	Day90
Total Area	335.3	242.8	288.8	367.8	572.3



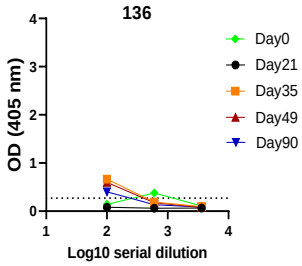
	Day0	Day21	Day35	Day49	Day90
Total Area	863.0	995.5	5775	8259	8963



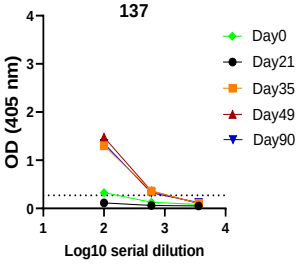
	Day0	Day21	Day35	Day49	Day90
Total Area	296.0	249.8	546.8	460.5	568.3



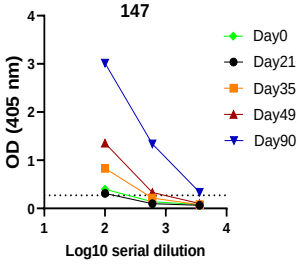
	Day0	Day21	Day35	Day49	Day90
Total Area	859.0	228.3	637.8	570.8	462.3



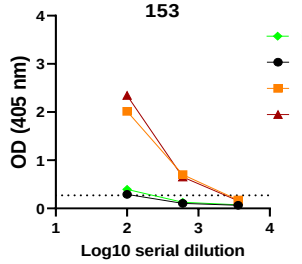
	Day0	Day21	Day35	Day49	Day90
Total Area	427.3	216.8	1118	1156	1089



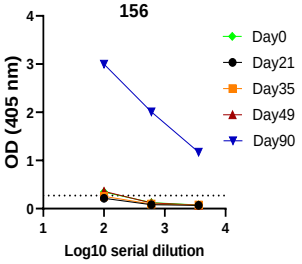
	Day0	Day21	Day35	Day49	Day90
Total Area	456.5	346.8	702.5	1071	3597



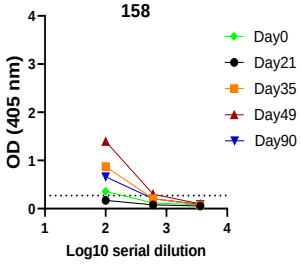
	Day0	Day21	Day35	Day49
Total Area	434.8	355.8	1996	1960



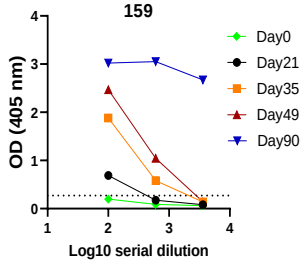
	Day0	Day21	Day35	Day49	Day90
Total Area	417.5	297.8	342.0	399.3	6020



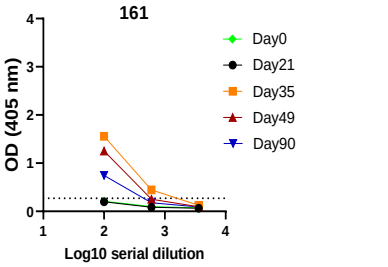
	Day0	Day21	Day35	Day49	Day90
Total Area	415.0	262.3	691.5	1021	654.5



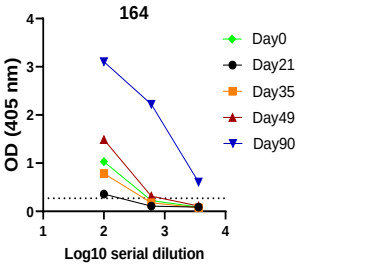
	Day0	Day21	Day35	Day49	Day90
Total Area	300.0	599.5	1697	2661	10104



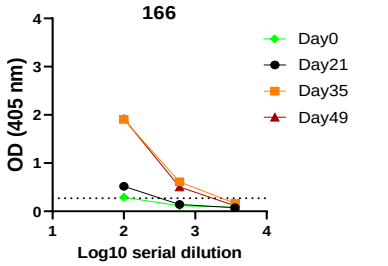
	Day0	Day21	Day35	Day49	Day90
Total Area	335.0	296.3	1356	891.8	636.0



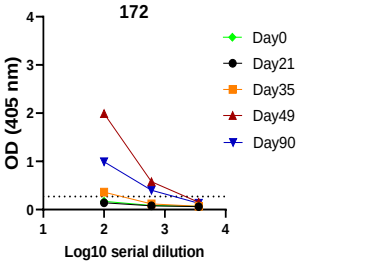
	Day0	Day21	Day35	Day49	Day90
Total Area	788.8	409.3	621.8	1090	5577



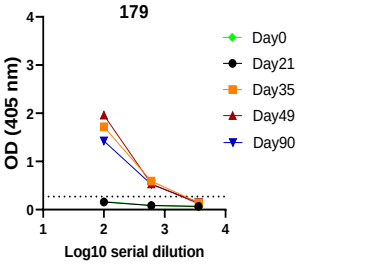
	Day0	Day21	Day35	Day49
Total Area	401.8	489.0	1792	1537



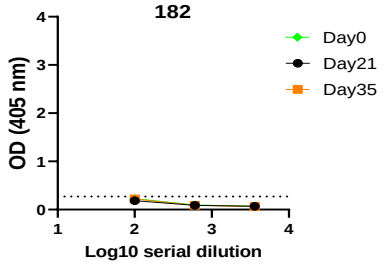
	Day0	Day21	Day35	Day49	Day90
Total Area	293.8	267.8	402.5	1737	1149



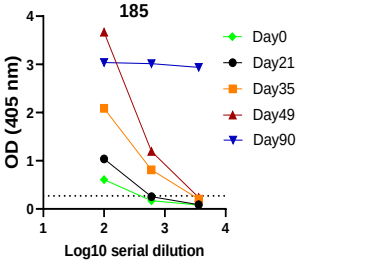
	Day0	Day21	Day35	Day49	Day90
Total Area	295.3	288.8	1681	1611	1500



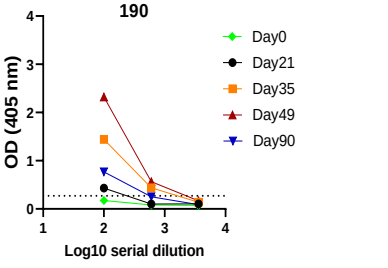
	Day0	Day21	Day35
Total Area	328.0	302.5	311.5



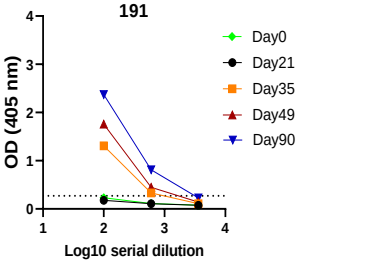
	Day0	Day21	Day35	Day49	Day90
Total Area	574.3	839.0	2250	3367	10446



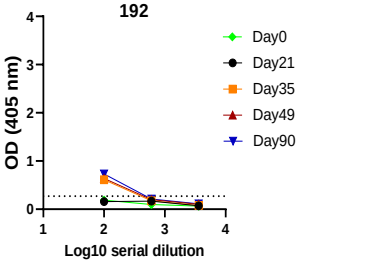
	Day0	Day21	Day35	Day49	Day90
Total Area	294.0	440.5	1334	1821	763.0



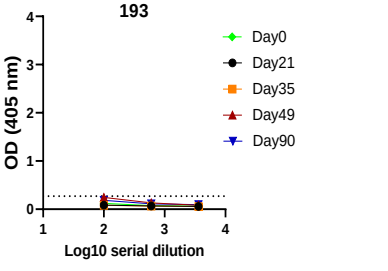
	Day0	Day21	Day35	Day49	Day90
Total Area	372.5	345.5	1067	1440	2353



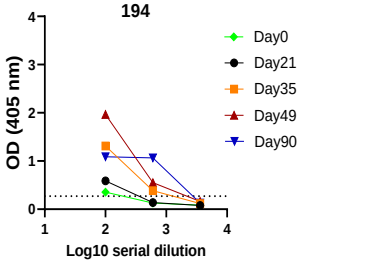
	Day0	Day21	Day35	Day49	Day90
Total Area	315.8	438.3	577.8	657.5	722.3



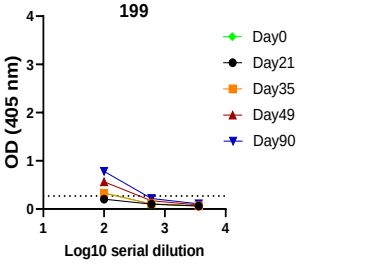
	Day0	Day21	Day35	Day49	Day90
Total Area	254.8	223.8	216.8	415.3	379.5



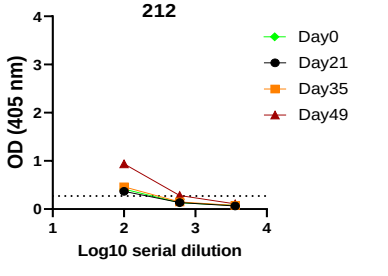
	Day0	Day21	Day35	Day49	Day90
Total Area	440.5	505.8	1177	1701	2327



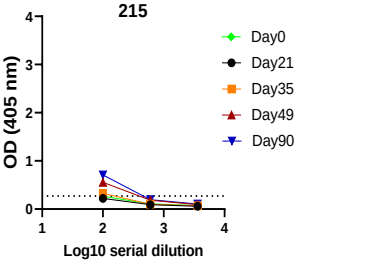
	Day0	Day21	Day35	Day49	Day90
Total Area	364.3	324.8	370.0	571.0	742.5



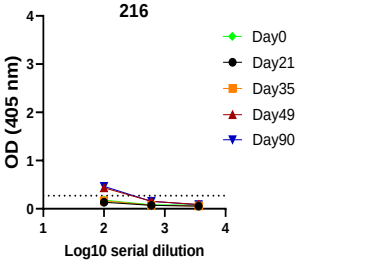
	Day0	Day21	Day35	Day49
Total Area	447.3	423.0	488.8	886.5



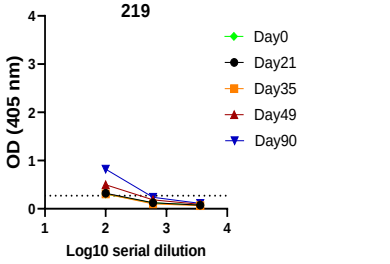
	Day0	Day21	Day35	Day49	Day90
Total Area	361.8	304.3	360.5	600.3	675.8



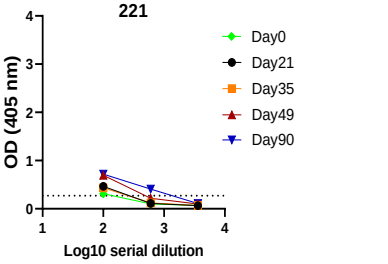
	Day0	Day21	Day35	Day49	Day90
Total Area	299.0	240.3	250.8	510.3	513.0



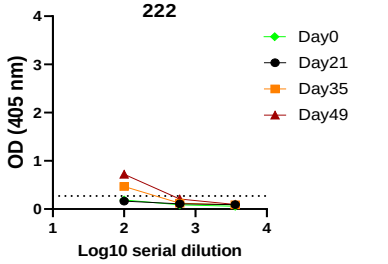
	Day0	Day21	Day35	Day49	Day90
Total Area	398.8	413.5	350.0	584.5	785.5



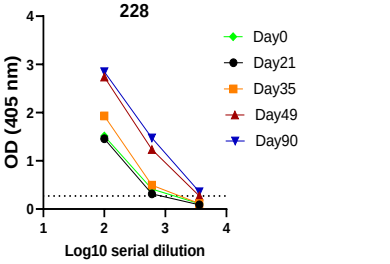
	Day0	Day21	Day35	Day49	Day90
Total Area	355.0	411.5	426.0	700.8	1052



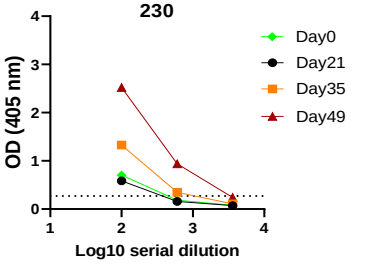
	Day0	Day21	Day35	Day49
Total Area	291.3	366.8	465.5	690.8



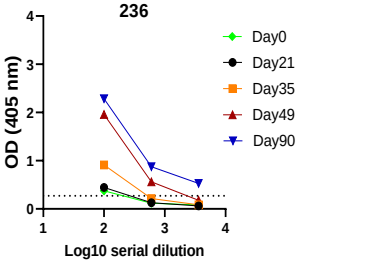
	Day0	Day21	Day35	Day49	Day90
Total Area	1272	1048	1523	3255	3831



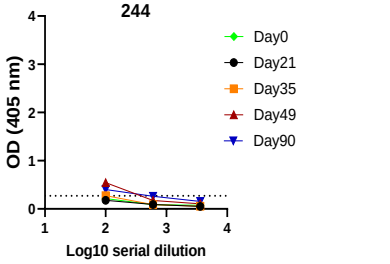
	Day0	Day21	Day35	Day49
Total Area	620.5	529.8	1104	2631



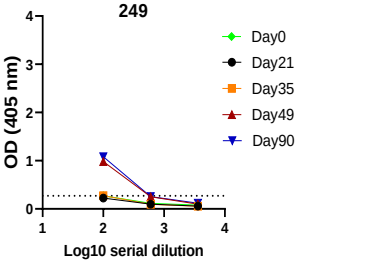
	Day0	Day21	Day35	Day49	Day90
Total Area	425.5	425.3	731.5	1740	2895



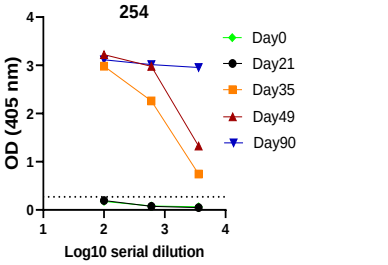
	Day0	Day21	Day35	Day49	Day90
Total Area	325.0	282.0	306.8	598.3	787.8



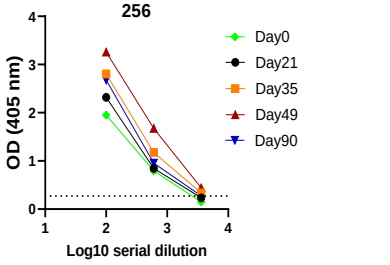
	Day0	Day21	Day35	Day49	Day90
Total Area	387.5	313.0	317.8	833.3	895.5



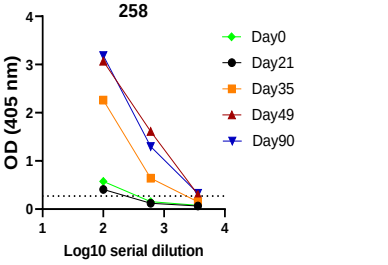
	Day0	Day21	Day35	Day49	Day90
Total Area	284.3	252.0	5822	8006	10489



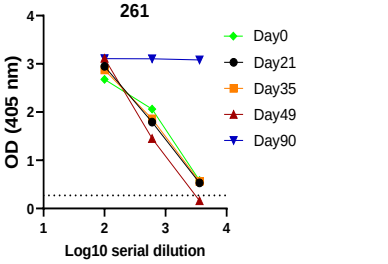
	Day0	Day21	Day35	Day49	Day90
Total Area	2106	2412	3258	4407	2754



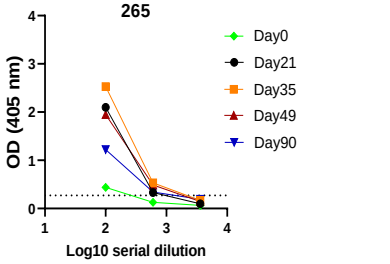
	Day0	Day21	Day35	Day49	Day90
Total Area	528.5	413.0	1917	4039	3558



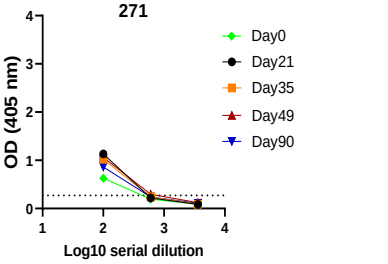
	Day0	Day21	Day35	Day49	Day90
Total Area	5151	4665	4812	3563	10831



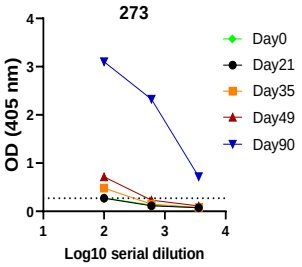
	Day0	Day21	Day35	Day49	Day90
Total Area	432.5	1251	1814	1561	1193



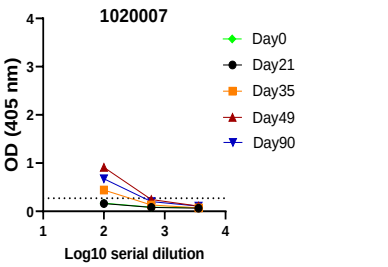
	Day0	Day21	Day35	Day49	Day90
Total Area	630.8	792.0	815.3	962.8	793.5



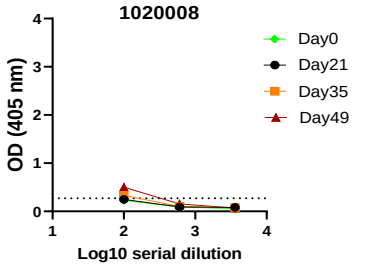
	Day0	Day21	Day35	Day49	Day90
Total Area	400.0	381.3	499.5	752.8	5921



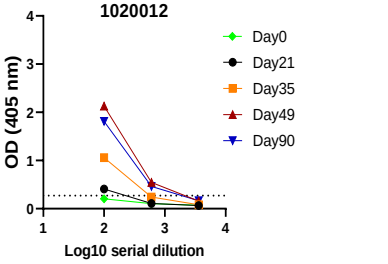
	Day0	Day21	Day35	Day49	Day90
Total Area	309.5	280.0	453.0	820.0	679.0



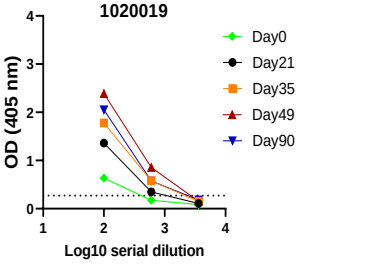
	Day0	Day21	Day35	Day49
Total Area	301.8	344.5	377.0	498.5



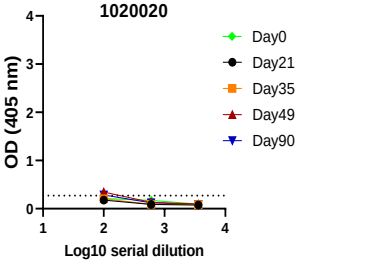
	Day0	Day21	Day35	Day49	Day90
Total Area	343.5	388.5	809.5	1724	1506



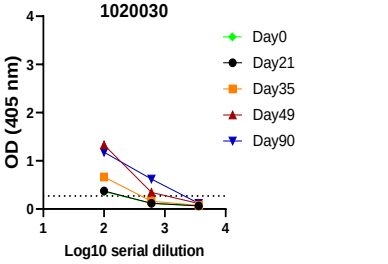
	Day0	Day21	Day35	Day49	Day90
Total Area	592.5	1117	1683	2324	1794



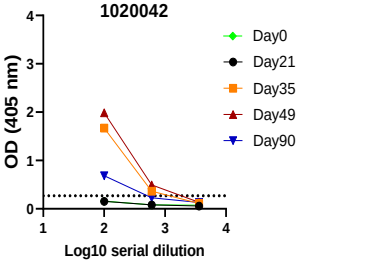
	Day0	Day21	Day35	Day49	Day90
Total Area	496.8	311.5	338.3	460.0	421.3



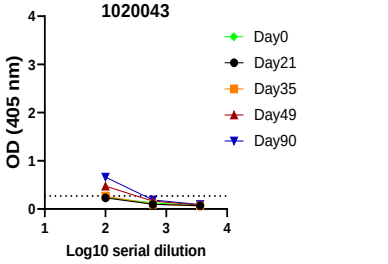
	Day0	Day21	Day35	Day49	Day90
Total Area	404.3	403.0	565.5	1109	1555



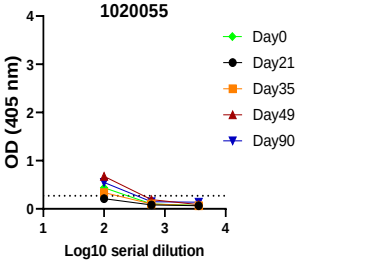
	Day0	Day21	Day35	Day49	Day90
Total Area	292.0	267.0	1227	1562	766.8



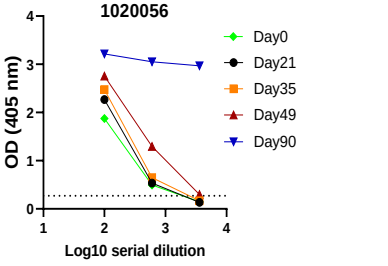
	Day0	Day21	Day35	Day49	Day90
Total Area	384.5	329.8	337.5	530.8	630.8



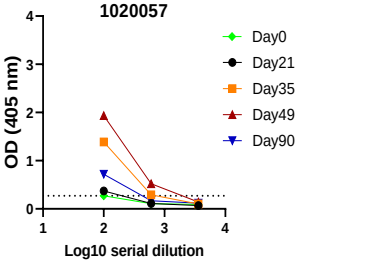
	Day0	Day21	Day35	Day49	Day90
Total Area	392.5	291.0	357.0	631.5	604.8



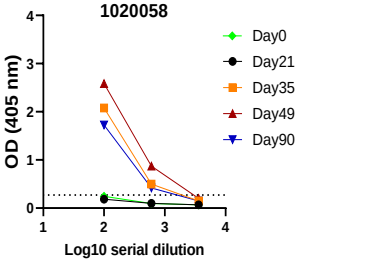
	Day0	Day21	Day35	Day49	Day90
Total Area	1556	1708	2005	3405	10597



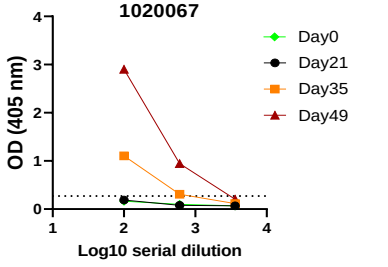
	Day0	Day21	Day35	Day49	Day90
Total Area	395.3	389.8	1008	1609	647.8



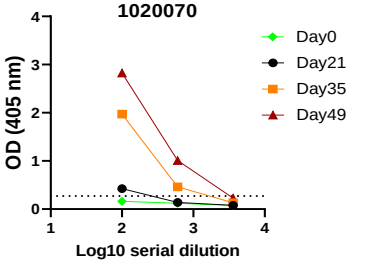
	Day0	Day21	Day35	Day49	Day90
Total Area	332.8	321.3	1613	2477	1392



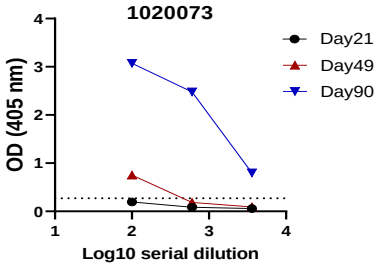
	Day0	Day21	Day35	Day49
Total Area	315.0	288.5	991.0	2685



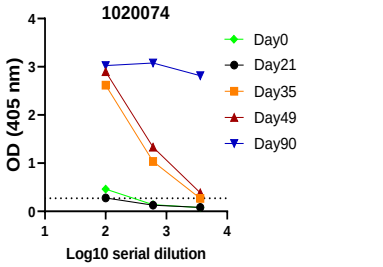
	Day0	Day21	Day35	Day49
Total Area	364.8	466.8	1501	2811



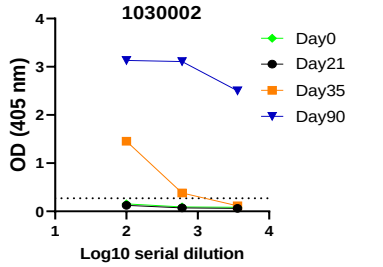
	Day21	Day49	Day90
Total Area	285.8	647.8	6304



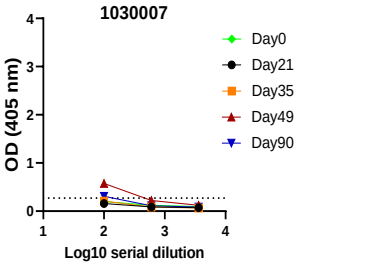
	Day0	Day21	Day35	Day49	Day90
Total Area	474.0	415.3	2868	3634	10367



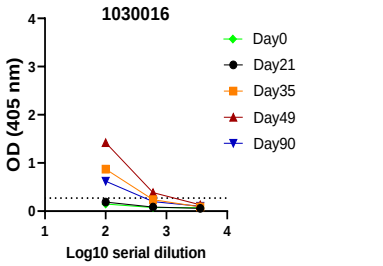
	Day0	Day21	Day35	Day90
Total Area	327.5	252.3	1205	9978



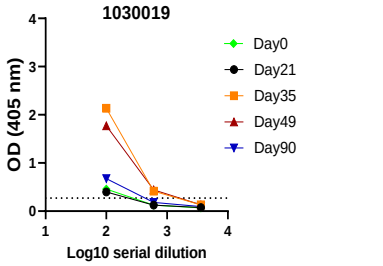
	Day0	Day21	Day35	Day49	Day90
Total Area	404.0	298.5	298.8	713.5	400.3



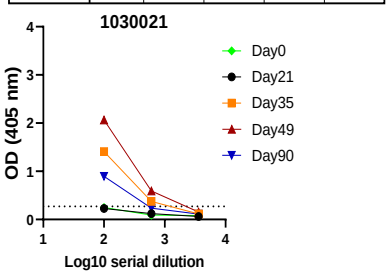
	Day0	Day21	Day35	Day49	Day90
Total Area	275.3	286.0	769.5	1227	653.3



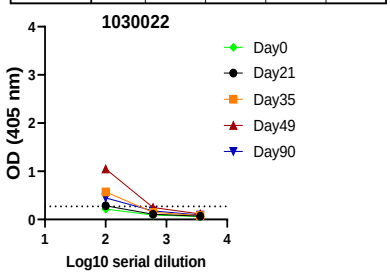
	Day0	Day21	Day35	Day49	Day90
Total Area	436.5	433.8	1457	1413	630.0



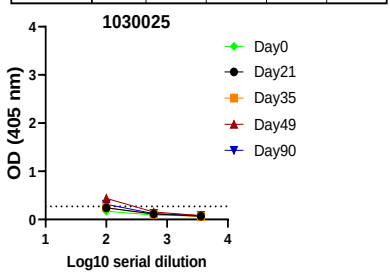
	Day0	Day21	Day35	Day49	Day90
Total Area	346.5	362.3	1182	1787	803.0



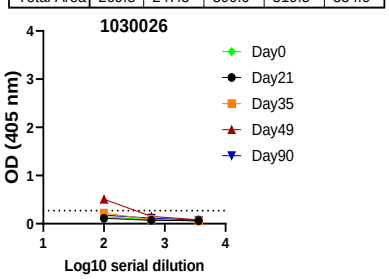
	Day0	Day21	Day35	Day49	Day90
Total Area	306.3	363.8	530.0	870.0	564.8



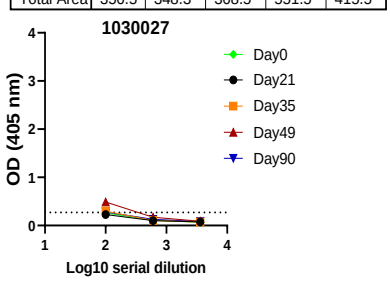
	Day0	Day21	Day35	Day49	Day90
Total Area	316.5	360.8	337.8	506.8	411.0



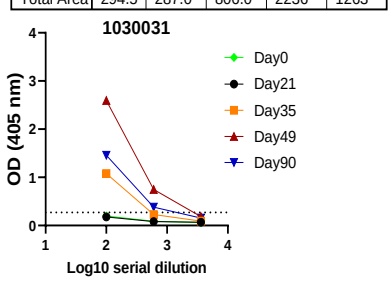
	Day0	Day21	Day35	Day49	Day90
Total Area	269.8	247.5	300.0	519.5	354.0



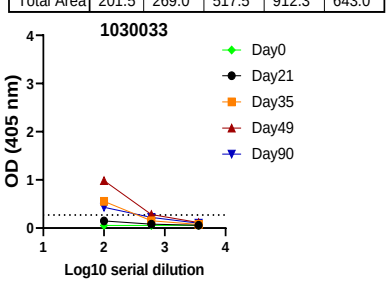
	Day0	Day21	Day35	Day49	Day90
Total Area	356.5	348.3	368.5	551.5	415.5



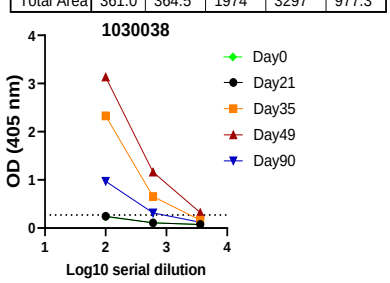
	Day0	Day21	Day35	Day49	Day90
Total Area	294.5	287.0	806.0	2236	1263



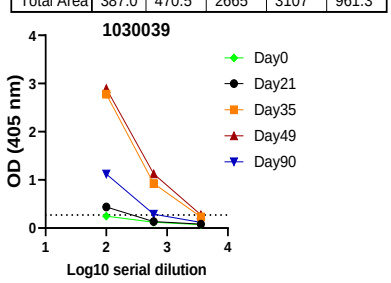
	Day0	Day21	Day35	Day49	Day90
Total Area	201.5	269.0	517.5	912.3	643.0



	Day0	Day21	Day35	Day49	Day90
Total Area	361.0	364.5	1974	3297	977.3



	Day0	Day21	Day35	Day49	Day90
Total Area	387.0	470.5	2665	3107	961.3



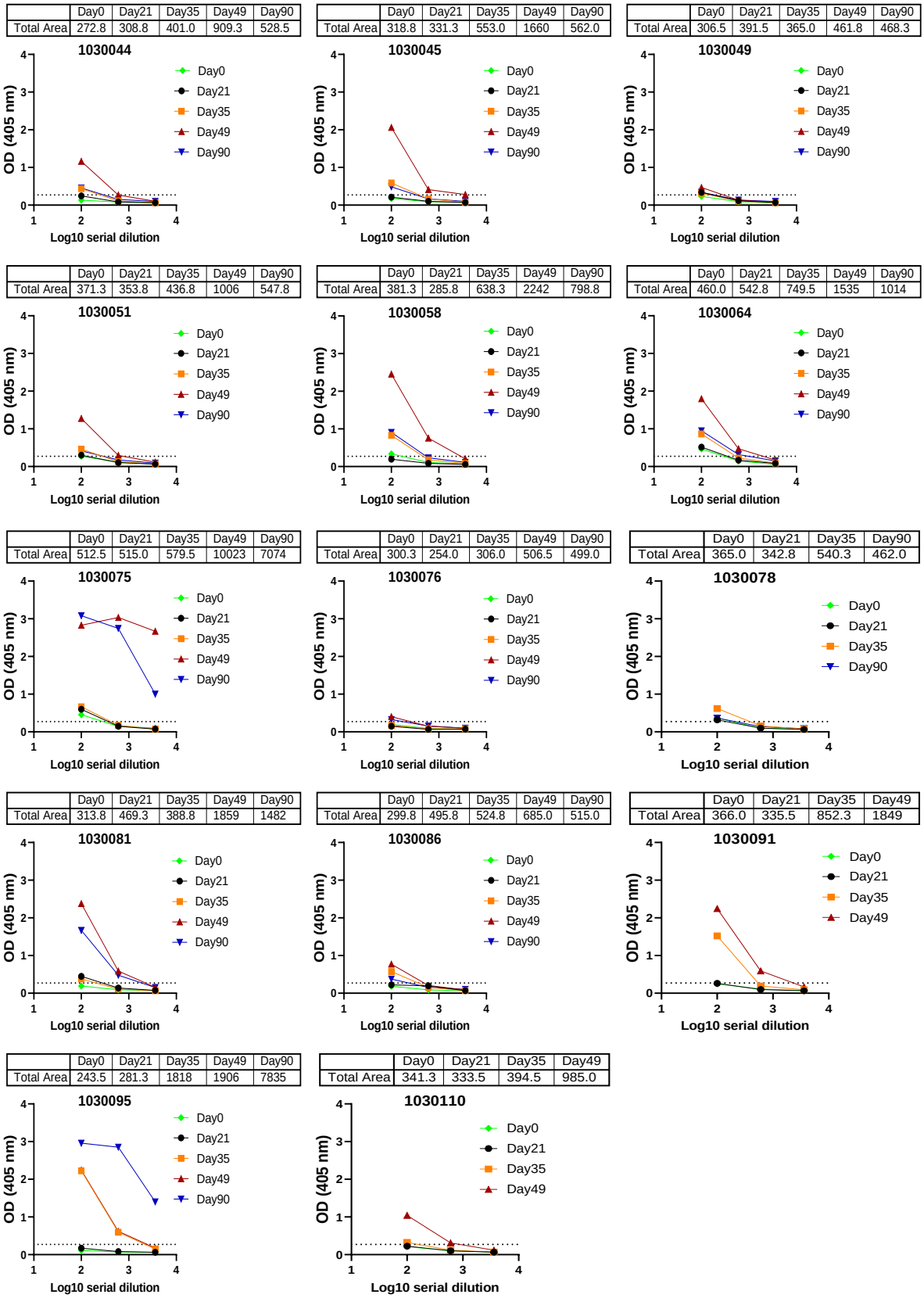
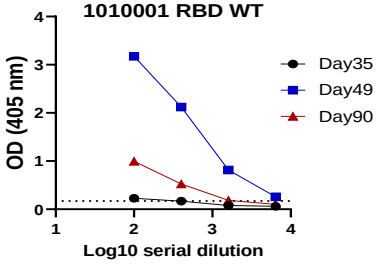
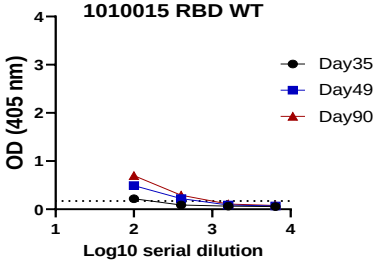


Figure A.2. The IgG responses of the volunteers against recombinant spike protein were assessed by ELISA. 2HB ELISA plates were coated 6 ug/ml of recombinant spike and following overnight incubation and blocking steps, the human sera collected at days 0, 21, 35, 49, and 90 were added to the wells. The sera were initially prepared in 1:100 ratio and then serially diluted sixfold for 2 times. After overnight incubation, the plates were treated with anti-human IgG and the OD405 values were recorded following treatment with PNPP substrate solution. OD405 values for each volunteer are demonstrated in each graph with area under the curve values presented in the tables.

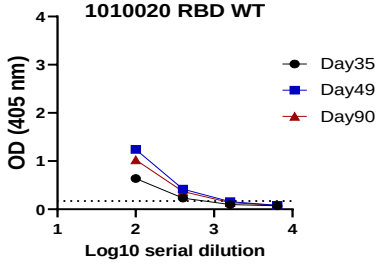
	Day35	Day49	Day90
Total Area	542.9	5132	1345



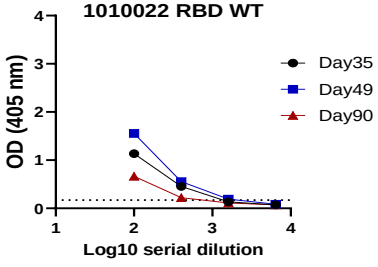
	Day35	Day49	Day90
Total Area	431.0	668.9	832.5



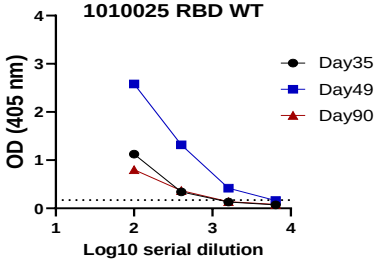
	Day35	Day49	Day90
Total Area	736.8	1168	1040



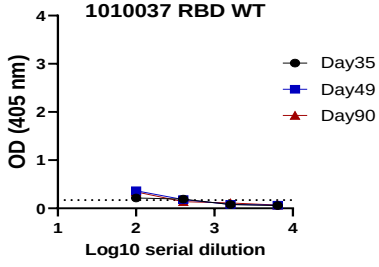
	Day35	Day49	Day90
Total Area	1088	1426	775.8



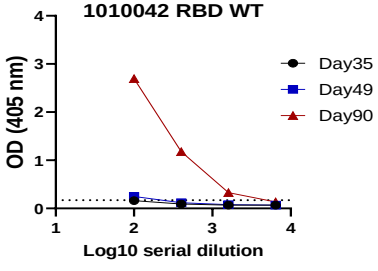
	Day35	Day49	Day90
Total Area	990.8	3023	1006



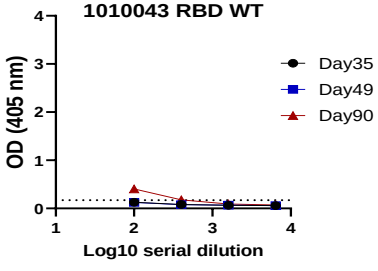
	Day35	Day49	Day90
Total Area	549.8	590.9	653.1



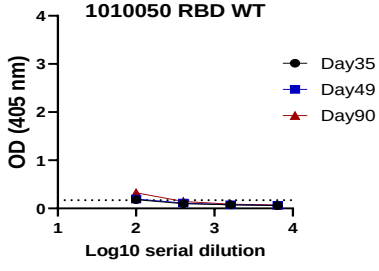
	Day35	Day49	Day90
Total Area	454.1	529.7	2593



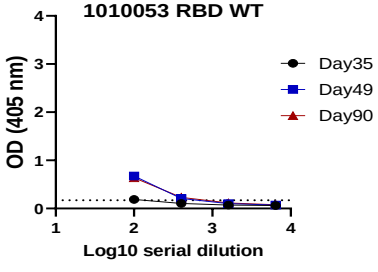
	Day35	Day49	Day90
Total Area	422.6	422.9	642.2



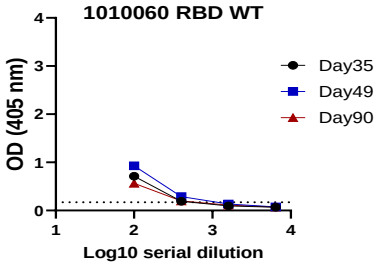
	Day35	Day49	Day90
Total Area	467.4	491.4	600.5



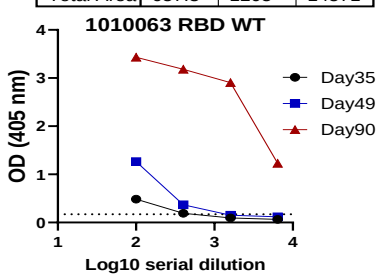
	Day35	Day49	Day90
Total Area	469.4	729.2	808.2



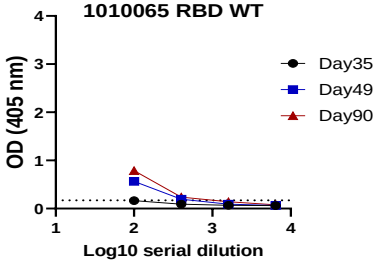
	Day35	Day49	Day90
Total Area	697.8	936.9	738.6



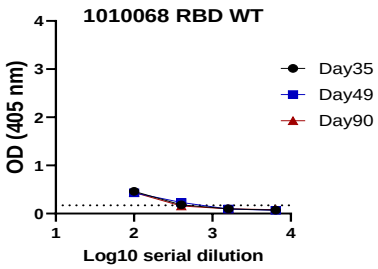
	Day35	Day49	Day90
Total Area	657.3	1205	14571



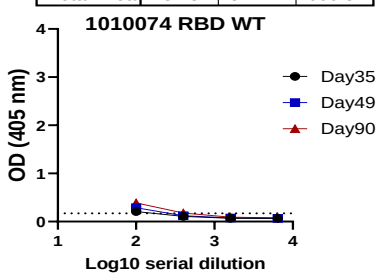
	Day35	Day49	Day90
Total Area	448.2	664.7	908.6



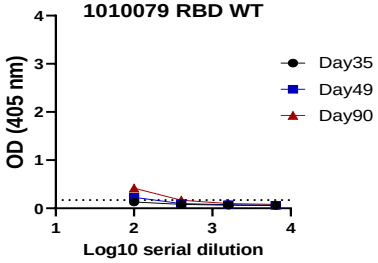
	Day35	Day49	Day90
Total Area	667.1	685.8	667.1



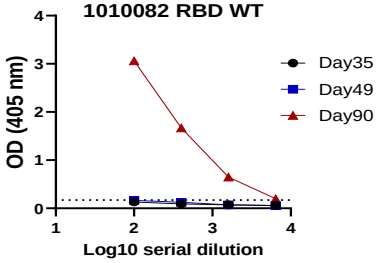
	Day35	Day49	Day90
Total Area	484.8	514.2	660.5



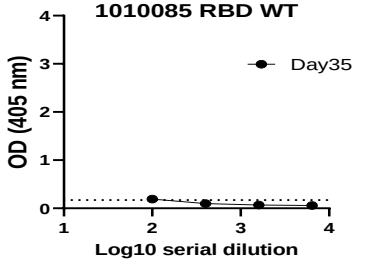
	Day35	Day49	Day90
Total Area	414.8	477.9	674.3



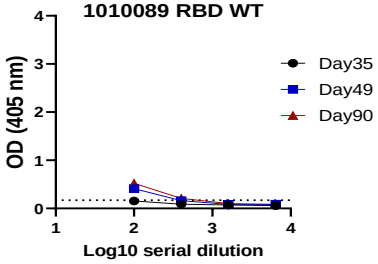
	Day35	Day49	Day90
Total Area	450.0	476.7	4129



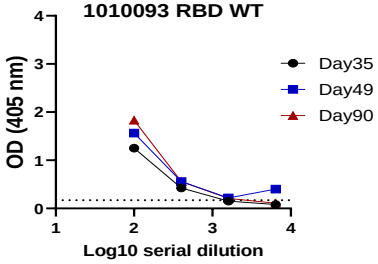
	Day35
Total Area	450.3



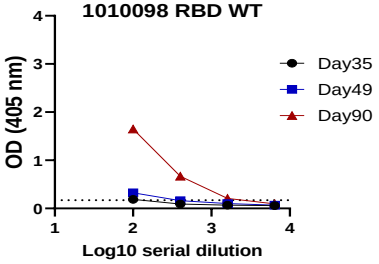
	Day35	Day49	Day90
Total Area	446.3	651.2	732.8



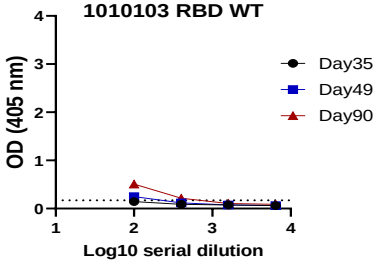
	Day35	Day49	Day90
Total Area	1159	2266	1579



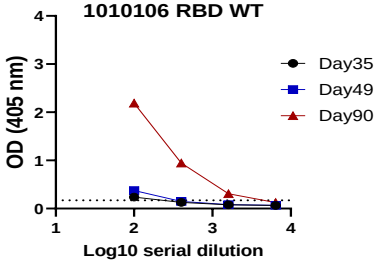
	Day35	Day49	Day90
Total Area	444.6	642.5	1598



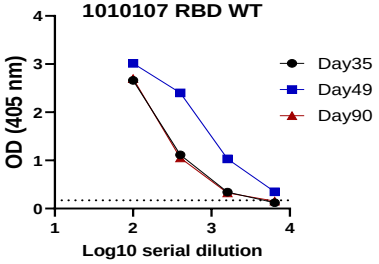
	Day35	Day49	Day90
Total Area	465.5	495.8	762.9



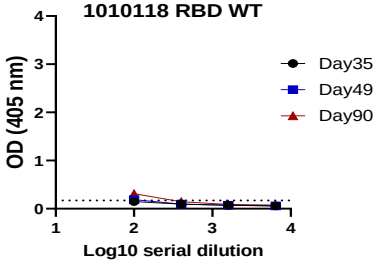
	Day35	Day49	Day90
Total Area	515.6	571.1	2262



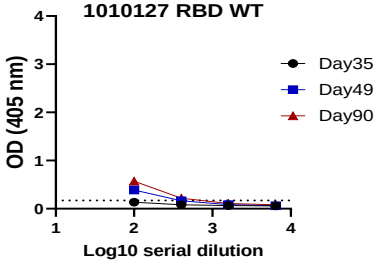
	Day35	Day49	Day90
Total Area	2548	6183	2539



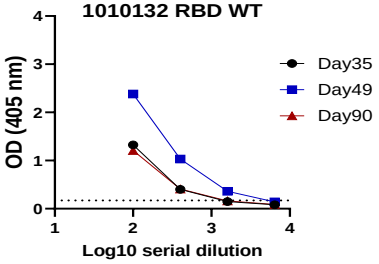
	Day35	Day49	Day90
Total Area	443.7	450.2	593.1



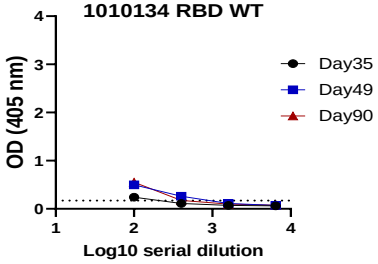
	Day35	Day49	Day90
Total Area	414.5	582.8	765.9



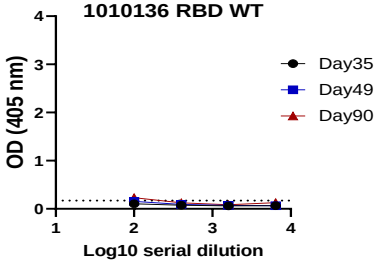
	Day35	Day49	Day90
Total Area	1139	2553	1180



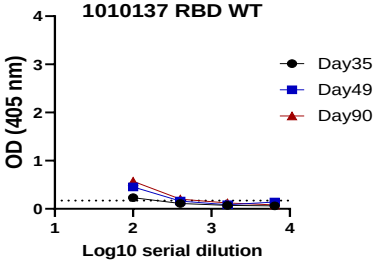
	Day35	Day49	Day90
Total Area	480.5	785.4	684.8



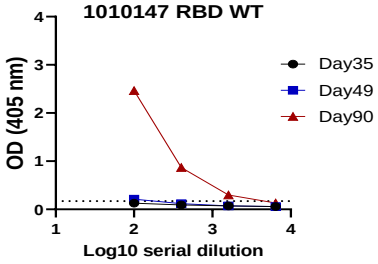
	Day35	Day49	Day90
Total Area	411.8	468.9	693.3



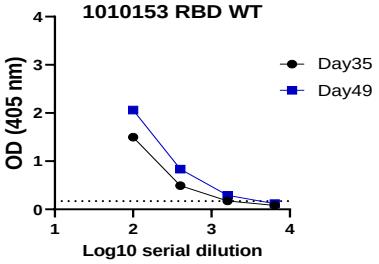
	Day35	Day49	Day90
Total Area	477.5	785.6	791.6



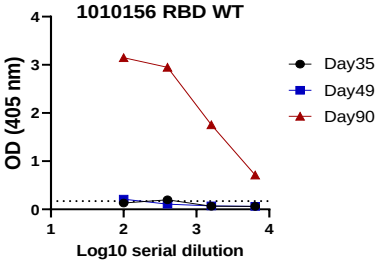
	Day35	Day49	Day90
Total Area	446.3	481.2	2233



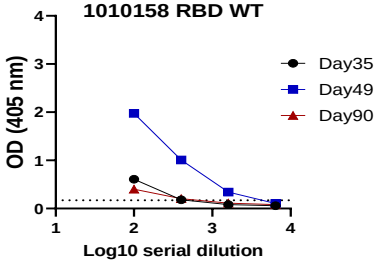
	Day35	Day49
Total Area	1308	2090



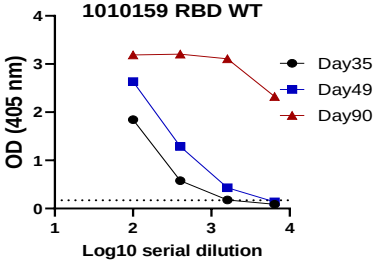
	Day35	Day49	Day90
Total Area	508.8	477.5	9656



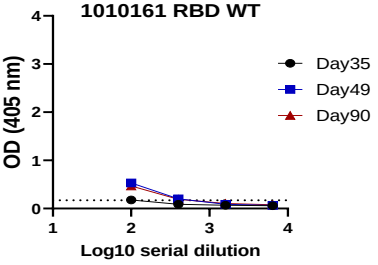
	Day35	Day49	Day90
Total Area	613.2	2331	742.5



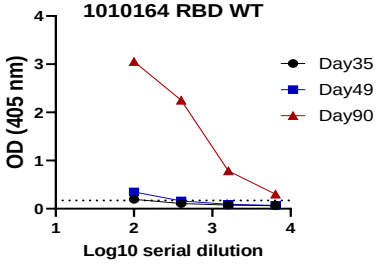
	Day35	Day49	Day90
Total Area	1455	2986	17783



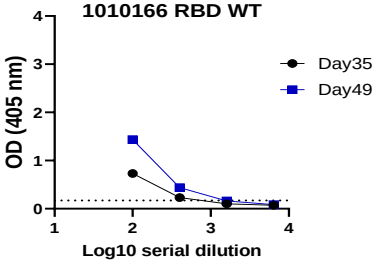
	Day35	Day49	Day90
Total Area	441.3	648.6	712.4



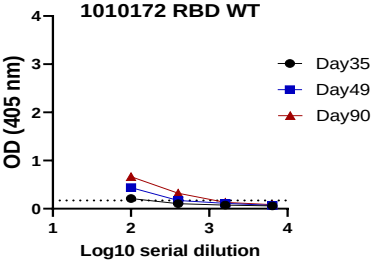
	Day35	Day49	Day90
Total Area	481.7	610.5	5225



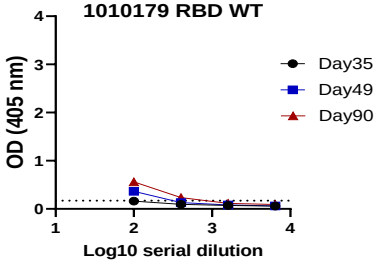
	Day35	Day49
Total Area	763.2	1235



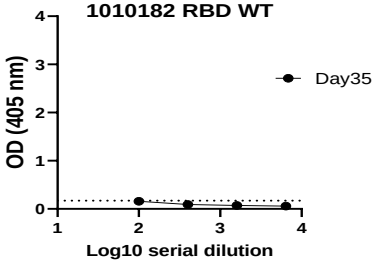
	Day35	Day49	Day90
Total Area	476.6	695.4	935.3



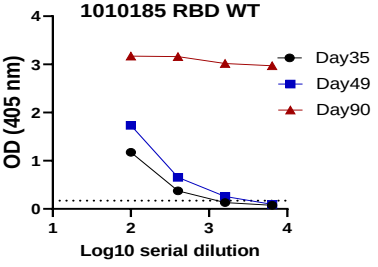
	Day35	Day49	Day90
Total Area	443.3	539.6	823.4



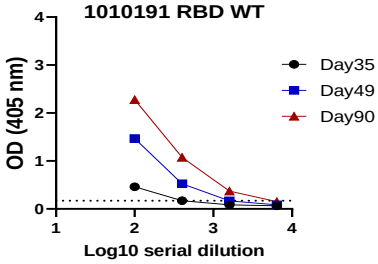
	Day35
Total Area	448.1



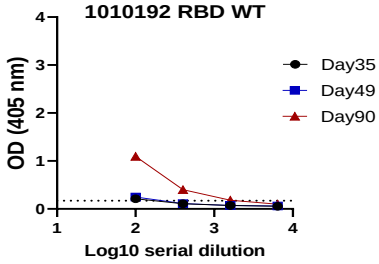
	Day35	Day49	Day90
Total Area	1034	1753	19033



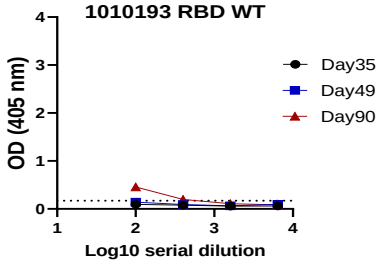
	Day35	Day49	Day90
Total Area	608.6	1324	2629



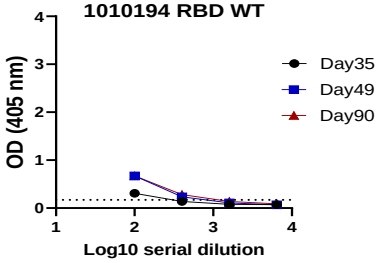
	Day35	Day49	Day90
Total Area	464.7	476.1	1242



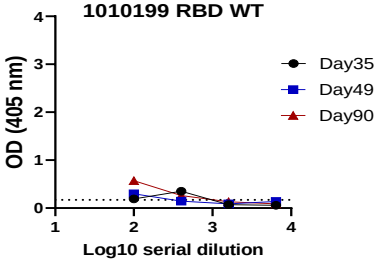
	Day35	Day49	Day90
Total Area	395.6	515.3	748.8



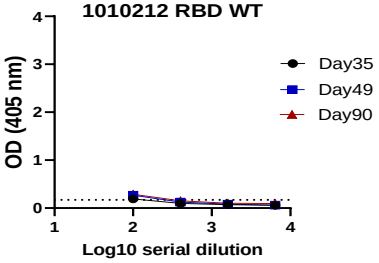
	Day35	Day49	Day90
Total Area	560.4	767.3	935.9



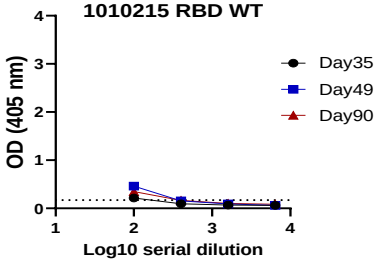
	Day35	Day49	Day90
Total Area	655.5	746.7	893.6



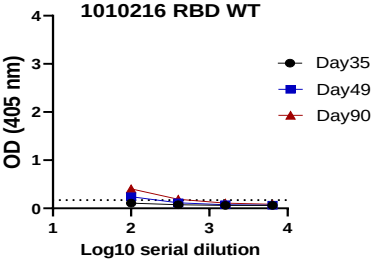
	Day35	Day49	Day90
Total Area	454.4	519.6	686.9



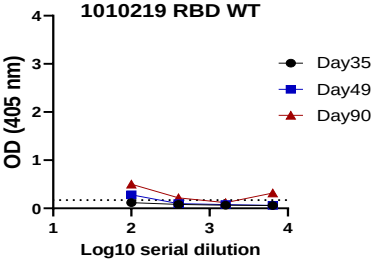
	Day35	Day49	Day90
Total Area	460.8	610.7	683.1



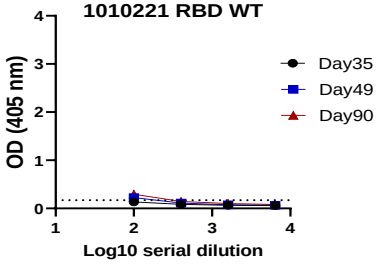
	Day35	Day49	Day90
Total Area	404.3	501.8	727.5



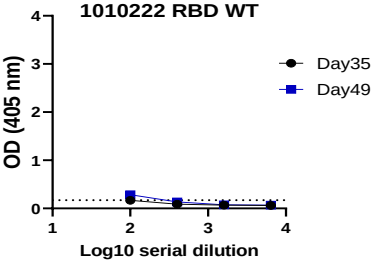
	Day35	Day49	Day90
Total Area	413.0	498.9	1356



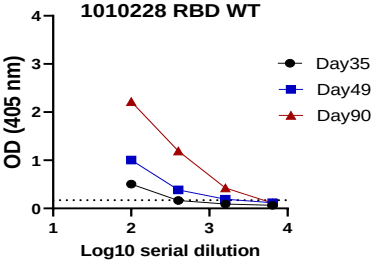
	Day35	Day49	Day90
Total Area	420.3	501.6	647.6



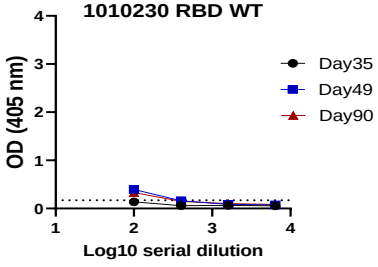
	Day35	Day49
Total Area	448.4	536.7



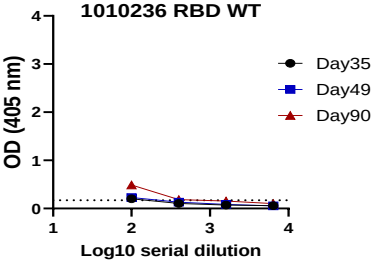
	Day35	Day49	Day90
Total Area	626.9	1299	2771



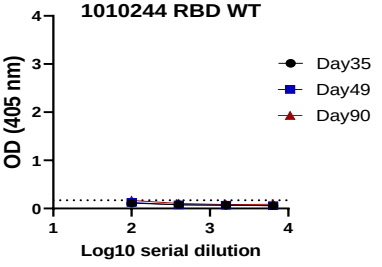
	Day35	Day49	Day90
Total Area	395.3	615.5	664.5



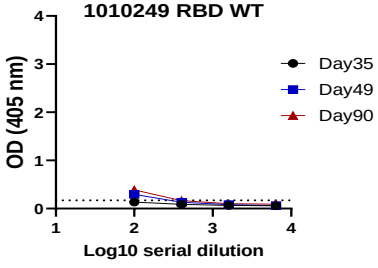
	Day35	Day49	Day90
Total Area	467.0	522.8	925.5



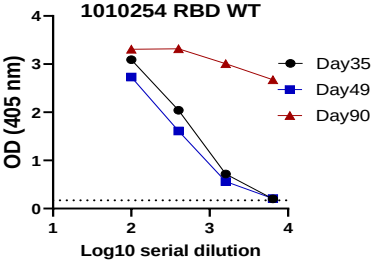
	Day35	Day49	Day90
Total Area	420.9	420.8	564.3



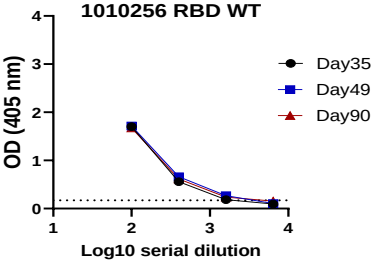
	Day35	Day49	Day90
Total Area	416.9	532.2	705.3



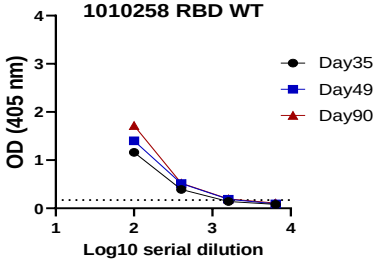
	Day35	Day49	Day90
Total Area	4633	3809	18425



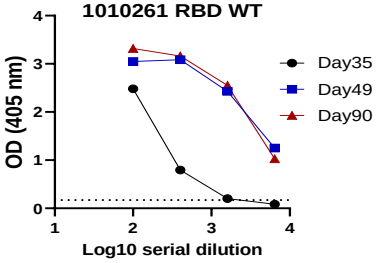
	Day35	Day49	Day90
Total Area	1459	1811	1793



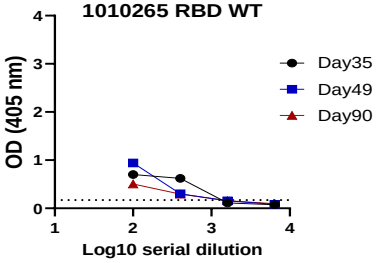
	Day35	Day49	Day90
Total Area	1094	1386	1494



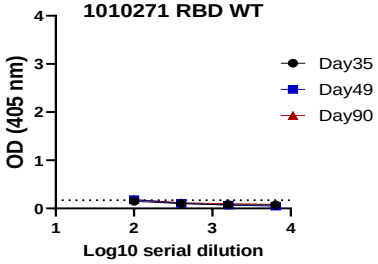
	Day35	Day49	Day90
Total Area	1776	13054	12989



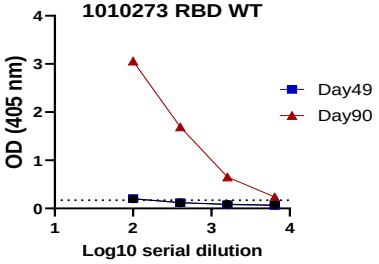
	Day35	Day49	Day90
Total Area	1086	1030	1005



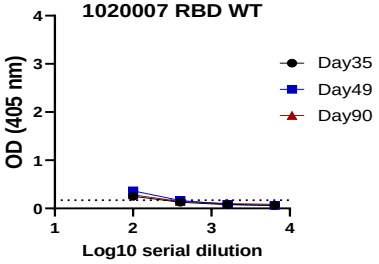
	Day35	Day49	Day90
Total Area	494.7	429.9	612.8



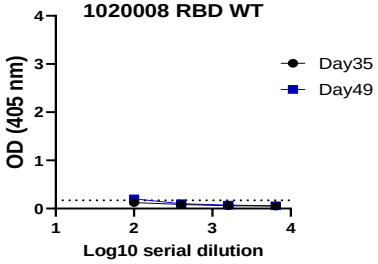
	Day35	Day49	Day90
Total Area	551.4	508.7	4246



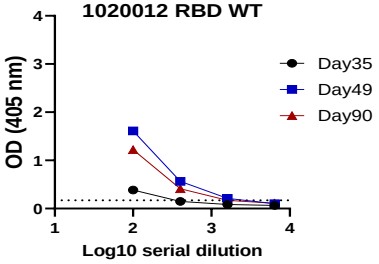
	Day35	Day49	Day90
Total Area	521.3	580.2	659.9



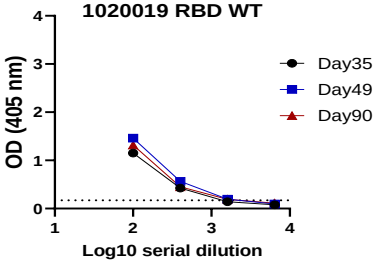
	Day35	Day49
Total Area	385.8	459.2



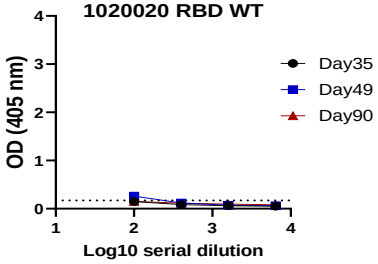
	Day35	Day49	Day90
Total Area	582.0	1545	1270



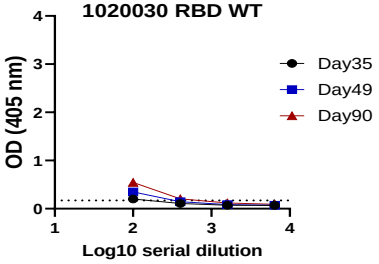
	Day35	Day49	Day90
Total Area	1102	1455	1373



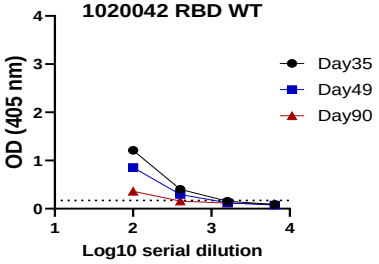
	Day35	Day49	Day90
Total Area	395.4	491.0	590.9



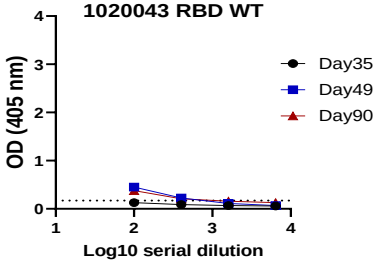
	Day35	Day49	Day90
Total Area	488.1	584.0	807.9



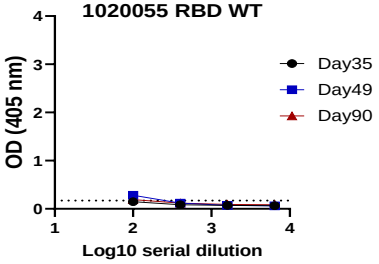
	Day35	Day49	Day90
Total Area	1160	890.9	735.6



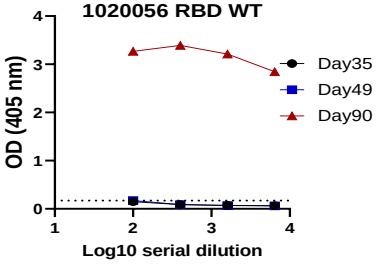
	Day35	Day49	Day90
Total Area	432.0	735.3	994.7



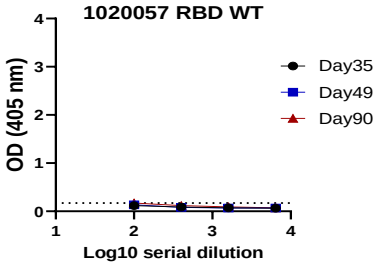
	Day35	Day49	Day90
Total Area	455.0	494.6	601.1



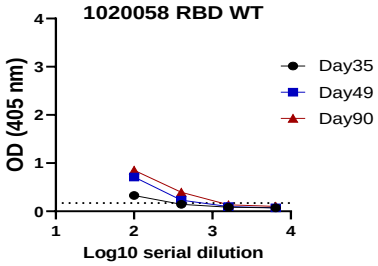
	Day35	Day49	Day90
Total Area	461.1	440.7	19499



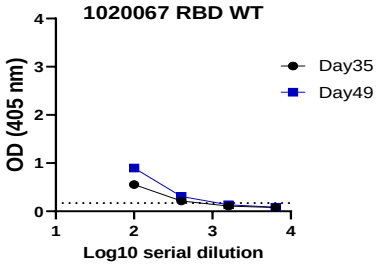
	Day35	Day49	Day90
Total Area	454.5	447.3	559.1



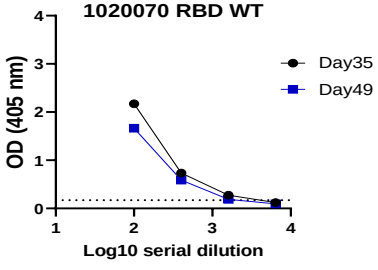
	Day35	Day49	Day90
Total Area	582.2	742.8	1076



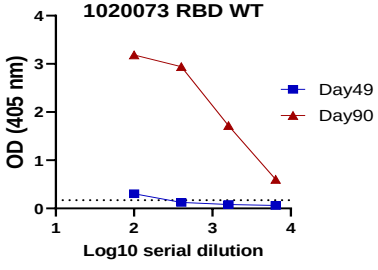
	Day35	Day49
Total Area	757.2	972.5



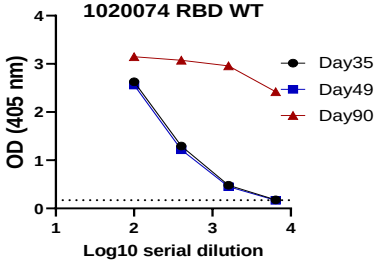
	Day35	Day49
Total Area	1995	1480



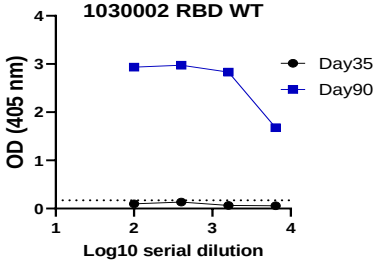
	Day49	Day90
Total Area	526.7	9288



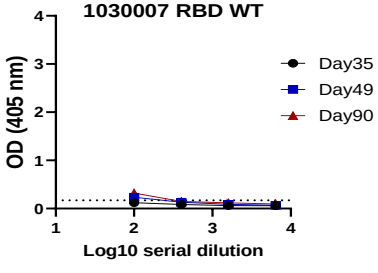
	Day35	Day49	Day90
Total Area	3243	3054	17460



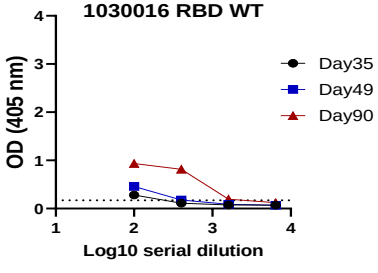
	Day35	Day90
Total Area	452.4	15189



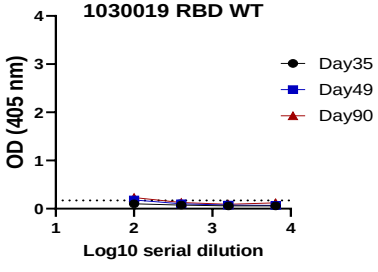
	Day35	Day49	Day90
Total Area	408.2	563.4	739.1



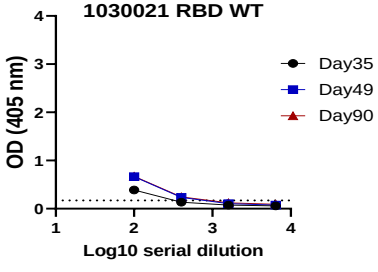
	Day35	Day49	Day90
Total Area	517.8	637.1	1631



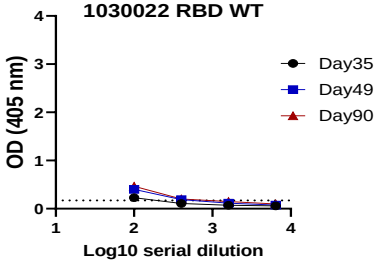
	Day35	Day49	Day90
Total Area	390.2	492.6	699.6



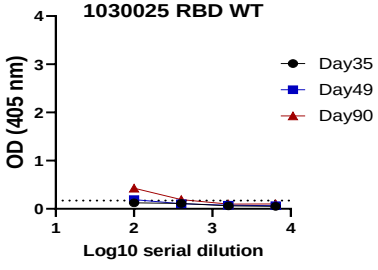
	Day35	Day49	Day90
Total Area	522.2	777.0	870.3



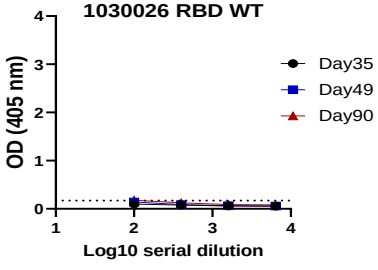
	Day35	Day49	Day90
Total Area	468.9	724.5	899.7



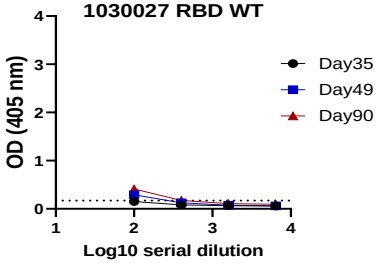
	Day35	Day49	Day90
Total Area	413.6	488.4	747.5



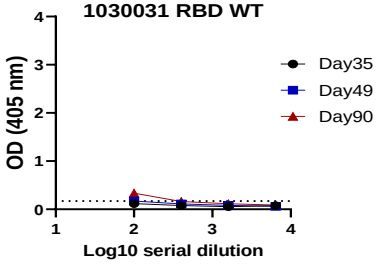
	Day35	Day49	Day90
Total Area	375.9	422.7	575.9



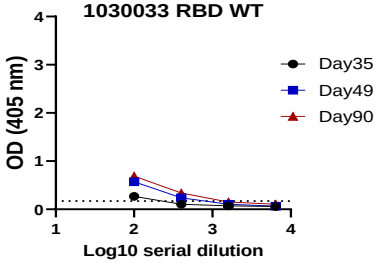
	Day35	Day49	Day90
Total Area	424.1	516.8	747.5



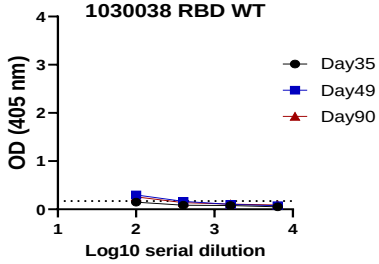
	Day35	Day49	Day90
Total Area	424.8	497.1	727.2



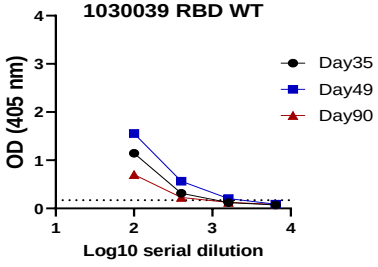
	Day35	Day49	Day90
Total Area	471.9	734.6	1060



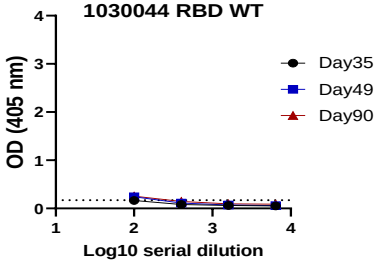
	Day35	Day49	Day90
Total Area	442.5	656.0	680.3



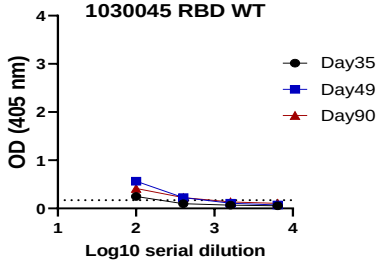
	Day35	Day49	Day90
Total Area	949.8	1481	858.5



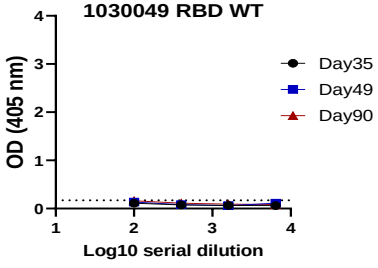
	Day35	Day49	Day90
Total Area	391.5	471.9	645.5



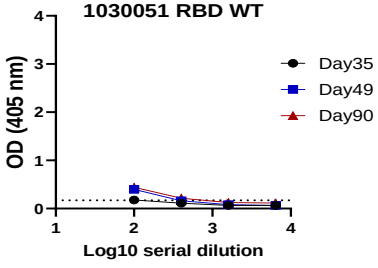
	Day35	Day49	Day90
Total Area	452.7	754.8	887.9



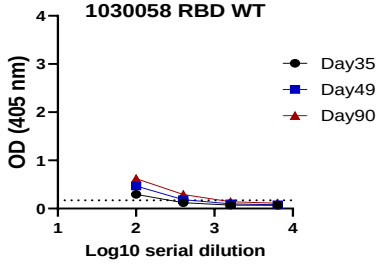
	Day35	Day49	Day90
Total Area	413.7	539.6	584.7



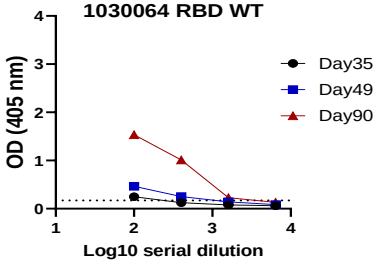
	Day35	Day49	Day90
Total Area	467.9	584.1	875.3



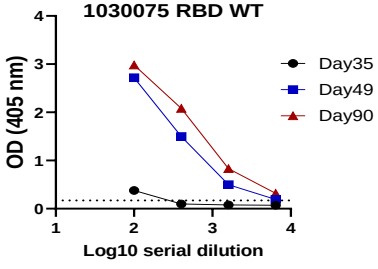
	Day35	Day49	Day90
Total Area	515.4	690.9	1011



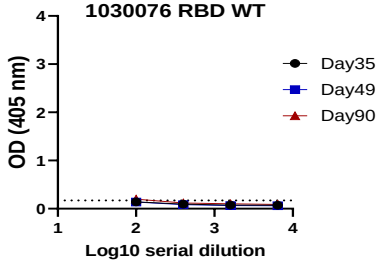
	Day35	Day49	Day90
Total Area	518.3	889.7	1990



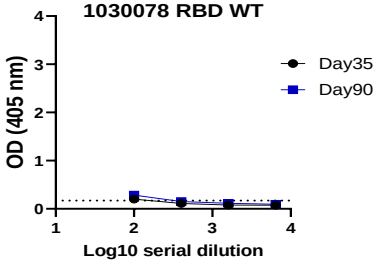
	Day35	Day49	Day90
Total Area	532.2	3477	5262



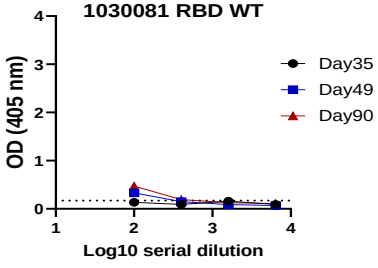
	Day35	Day49	Day90
Total Area	489.9	427.5	629.9



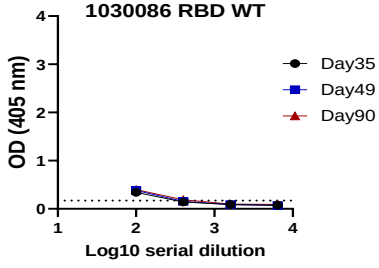
	Day35	Day90
Total Area	531.5	732.0



	Day35	Day49	Day90
Total Area	783.9	594.2	858.8



	Day35	Day49	Day90
Total Area	597.0	603.0	713.7



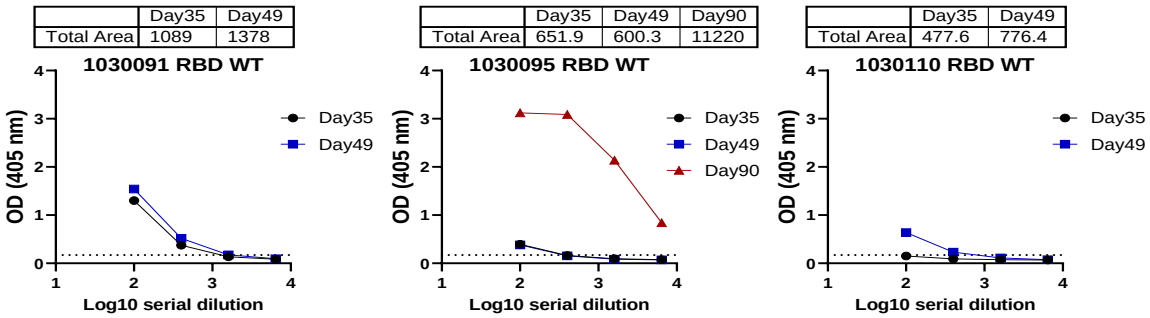
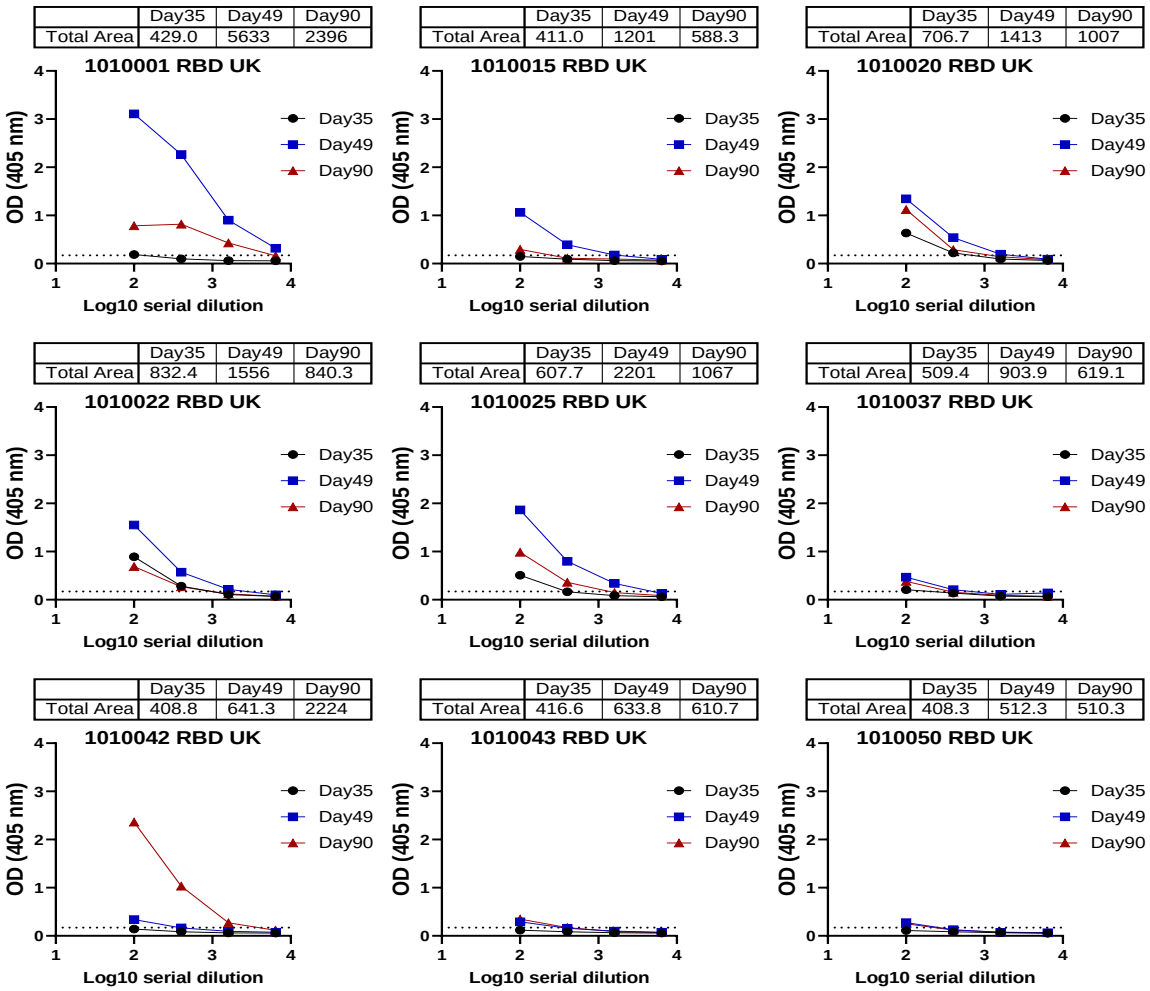
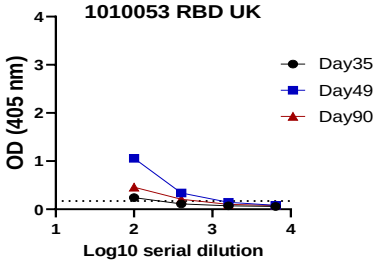


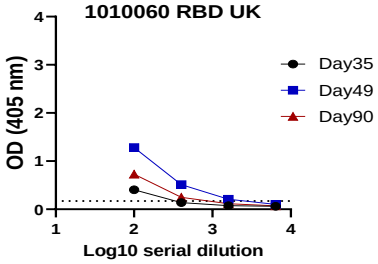
Figure A.3. The IgG responses of the volunteers against recombinant RBD wild type (WT) protein were assessed by ELISA. 2HB ELISA plates were coated 1 ug/ml of recombinant RBD WT protein and following overnight incubation and blocking steps, the human sera collected at days 35, 49, and 90 were added to the wells. The sera were initially prepared in 1:100 ratio and then serially diluted fourfold for 3 times. After overnight incubation, the plates were treated with anti-human IgG prepared in 1:1000 ratio and the OD405 values were recorded following treatment with PNPP substrate solution. OD405 values for each volunteer are demonstrated in each graph with area under the curve values presented in the tables.



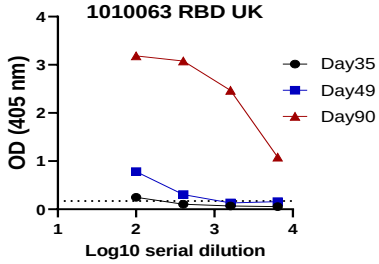
	Day35	Day49	Day90
Total Area	466.5	1049	714.9



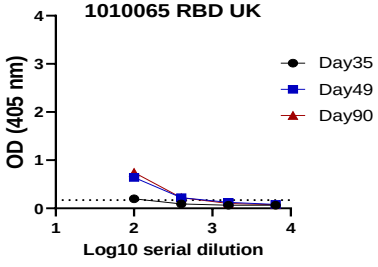
	Day35	Day49	Day90
Total Area	539.0	1442	810.0



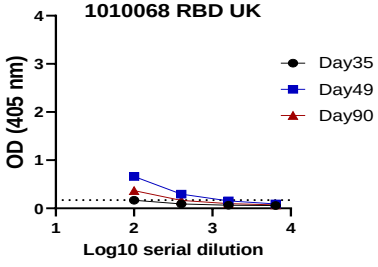
	Day35	Day49	Day90
Total Area	449.7	1113	12780



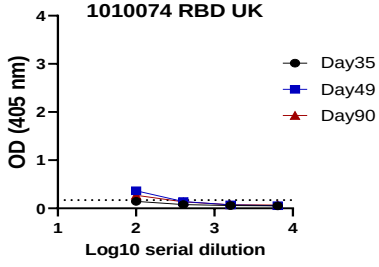
	Day35	Day49	Day90
Total Area	449.1	835.4	764.3



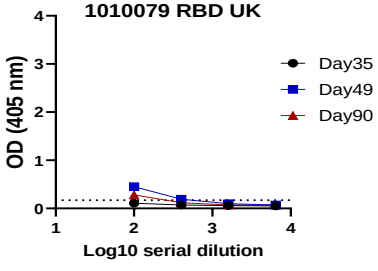
	Day35	Day49	Day90
Total Area	431.6	1006	644.3



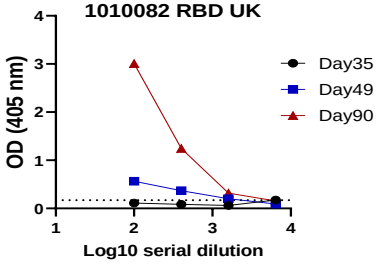
	Day35	Day49	Day90
Total Area	385.4	512.9	526.8



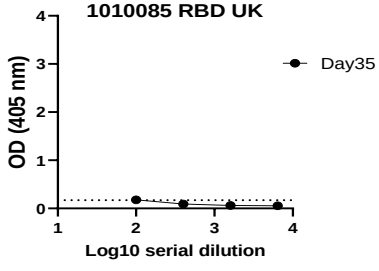
	Day35	Day49	Day90
Total Area	364.2	671.4	510.0



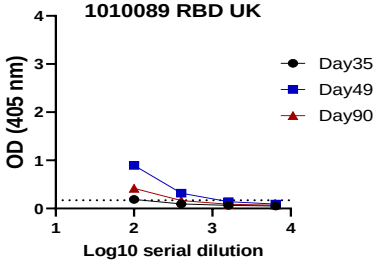
	Day35	Day49	Day90
Total Area	683.4	1183	2717



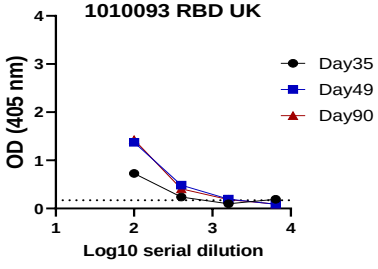
	Day35
Total Area	413.6



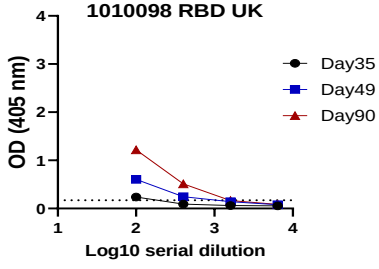
	Day35	Day49	Day90
Total Area	413.0	1014	615.6



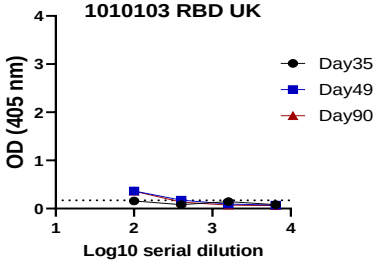
	Day35	Day49	Day90
Total Area	1039	1367	1298



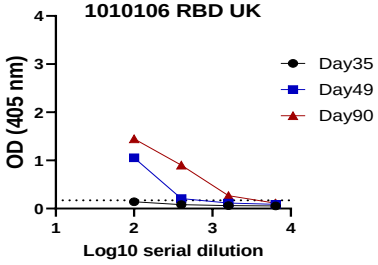
	Day35	Day49	Day90
Total Area	425.7	892.2	1264



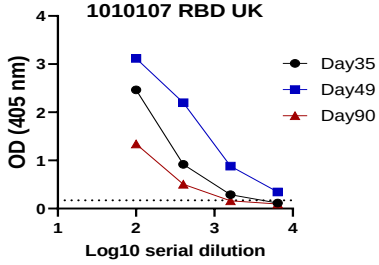
	Day35	Day49	Day90
Total Area	710.0	643.2	520.8



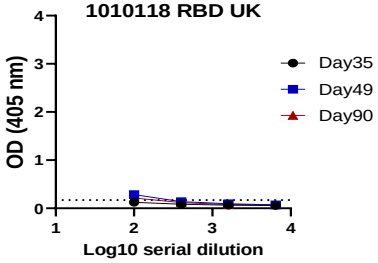
	Day35	Day49	Day90
Total Area	403.5	871.4	1961



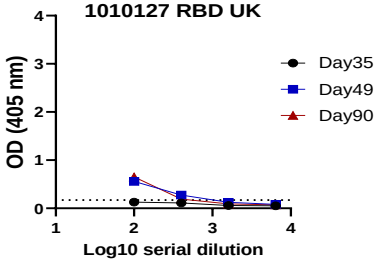
	Day35	Day49	Day90
Total Area	2202	5590	1297



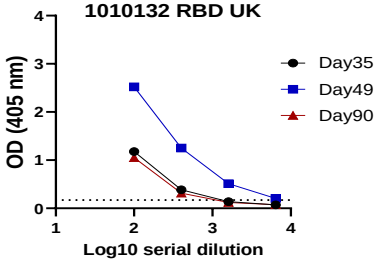
	Day35	Day49	Day90
Total Area	413.7	606.5	527.4



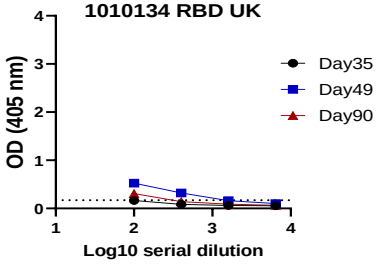
	Day35	Day49	Day90
Total Area	408.0	863.3	689.9



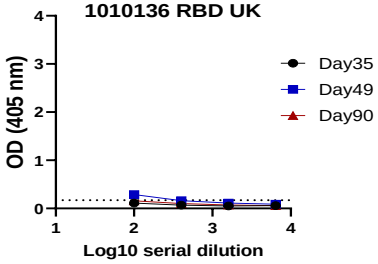
	Day35	Day49	Day90
Total Area	1046	3340	939.8



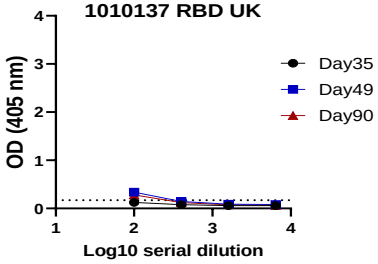
	Day35	Day49	Day90
Total Area	411.8	1047	570.5



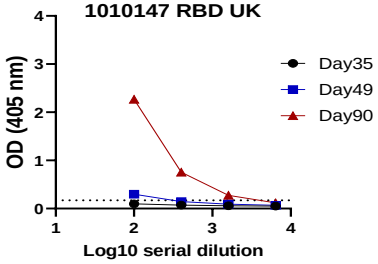
	Day35	Day49	Day90
Total Area	363.3	715.2	457.2



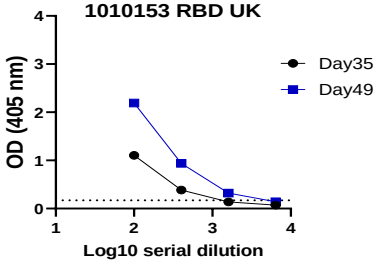
	Day35	Day49	Day90
Total Area	398.4	623.3	507.6



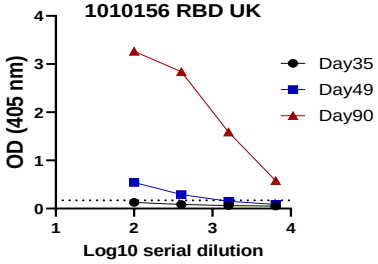
	Day35	Day49	Day90
Total Area	373.4	594.2	2020



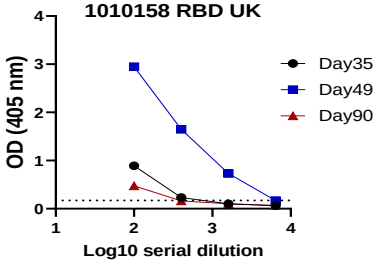
	Day35	Day49
Total Area	1037	2337



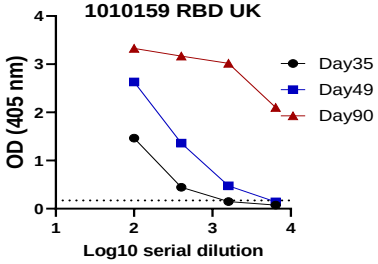
	Day35	Day49	Day90
Total Area	386.9	963.3	8774



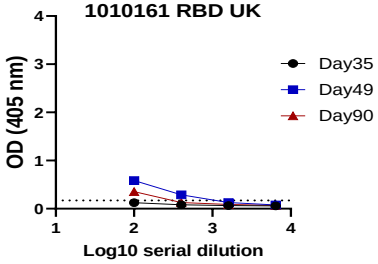
	Day35	Day49	Day90
Total Area	759.8	4276	656.7



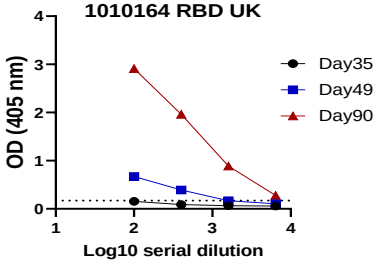
	Day35	Day49	Day90
Total Area	1172	3180	16978



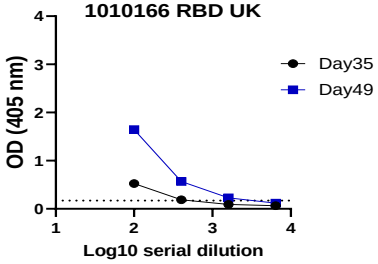
	Day35	Day49	Day90
Total Area	411.5	875.0	576.6



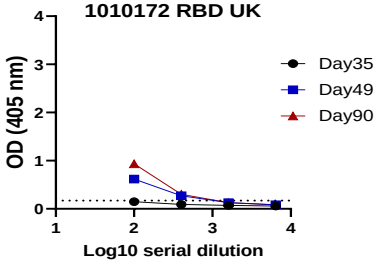
	Day35	Day49	Day90
Total Area	428.4	1148	5243



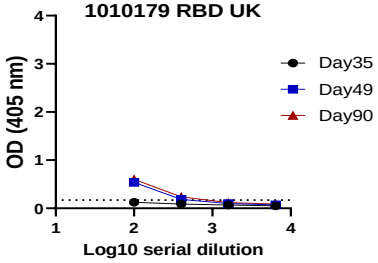
	Day35	Day49
Total Area	658.1	1649



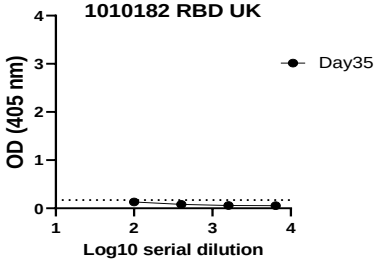
	Day35	Day49	Day90
Total Area	437.4	880.2	943.1



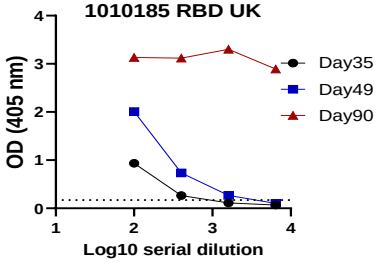
	Day35	Day49	Day90
Total Area	415.4	691.5	838.1



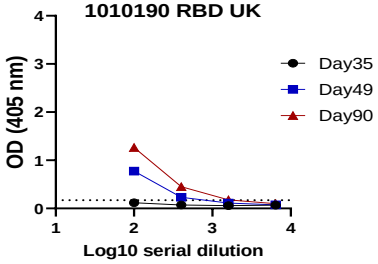
	Day35
Total Area	391.7



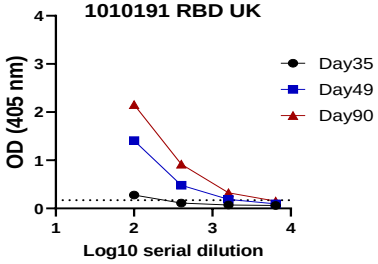
	Day35	Day49	Day90
Total Area	838.1	1893	19648



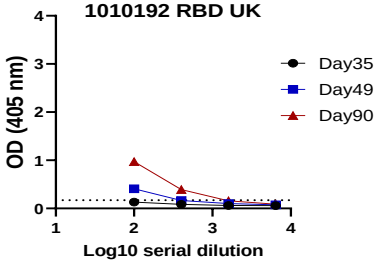
	Day35	Day49	Day90
Total Area	414.2	810.8	1305



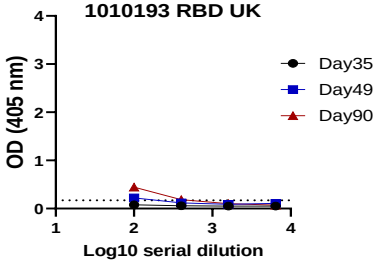
	Day35	Day49	Day90
Total Area	483.6	1368	2356



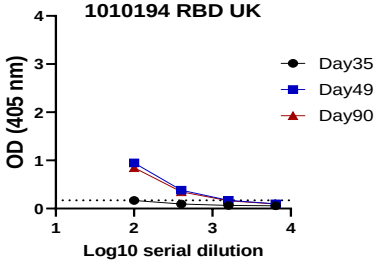
	Day35	Day49	Day90
Total Area	408.3	668.6	1127



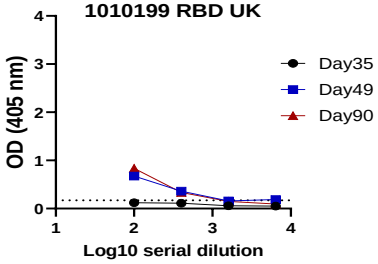
	Day35	Day49	Day90
Total Area	339.8	651.8	684.9



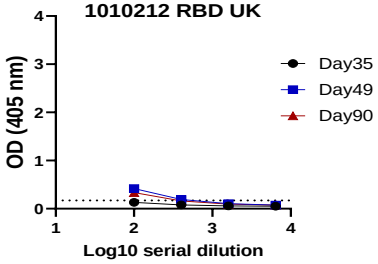
	Day35	Day49	Day90
Total Area	430.1	1182	1101



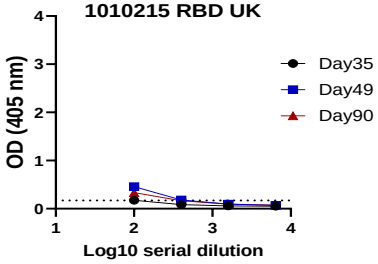
	Day35	Day49	Day90
Total Area	405.6	1298	1049



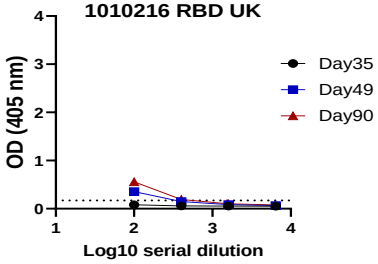
	Day35	Day49	Day90
Total Area	382.2	702.6	637.4



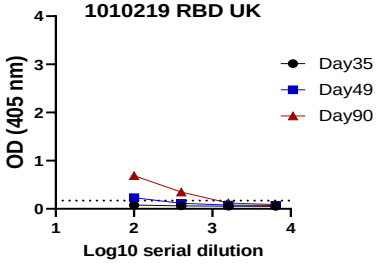
	Day35	Day49	Day90
Total Area	385.7	654.9	639.8



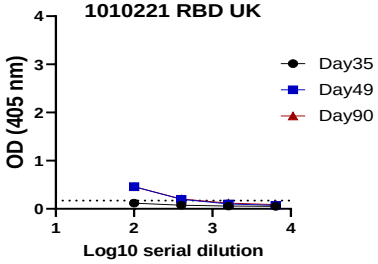
	Day35	Day49	Day90
Total Area	347.9	575.0	714.9



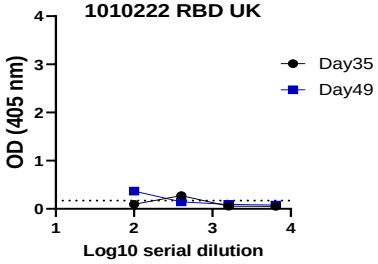
	Day35	Day49	Day90
Total Area	344.3	528.0	943.8



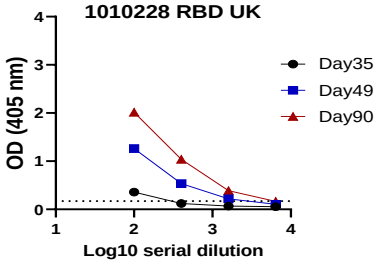
	Day35	Day49	Day90
Total Area	372.8	696.0	792.3



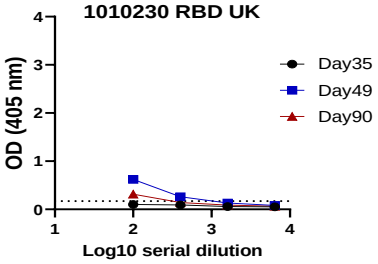
	Day35	Day49
Total Area	512.7	621.6



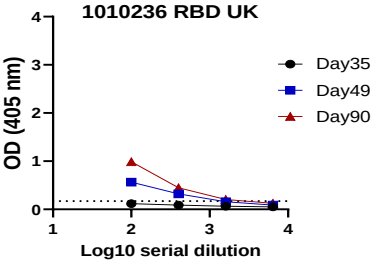
	Day35	Day49	Day90
Total Area	479.1	1496	2640



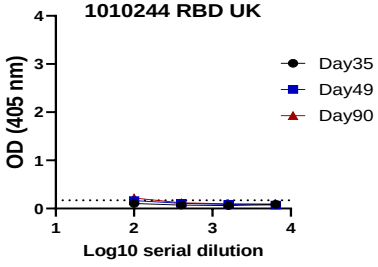
	Day35	Day49	Day90
Total Area	386.4	883.2	579.9



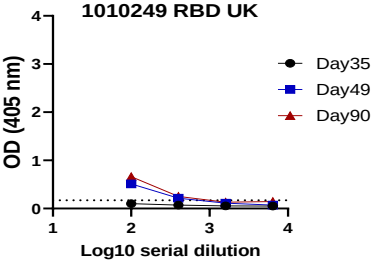
	Day35	Day49	Day90
Total Area	398.9	1014	1393



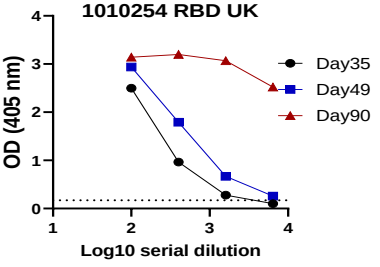
	Day35	Day49	Day90
Total Area	475.4	533.1	639.5



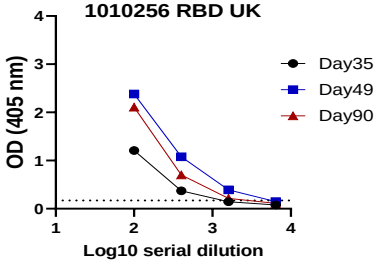
	Day35	Day49	Day90
Total Area	350.0	739.8	1031



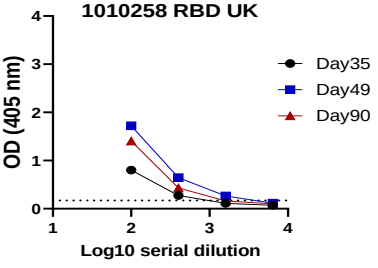
	Day35	Day49	Day90
Total Area	2176	4408	18123



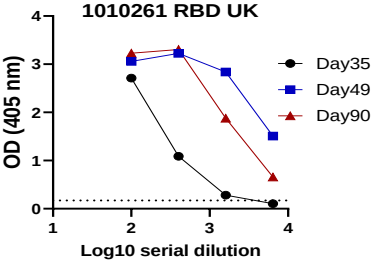
	Day35	Day49	Day90
Total Area	1083	2696	1757



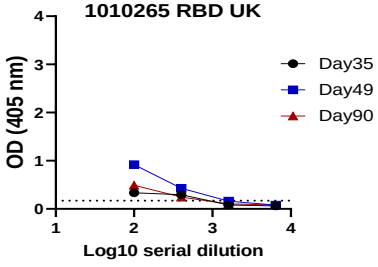
	Day35	Day49	Day90
Total Area	832.7	1813	1260



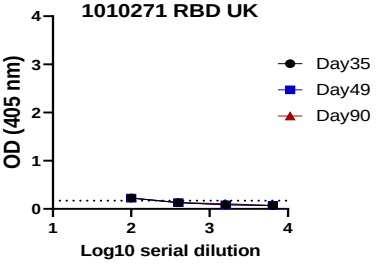
	Day35	Day49	Day90
Total Area	2326	15013	10175



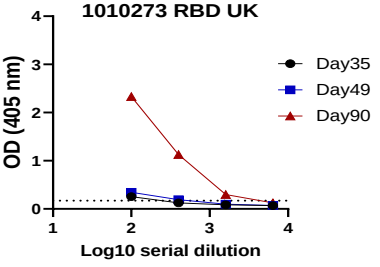
	Day35	Day49	Day90
Total Area	660.2	1134	769.5



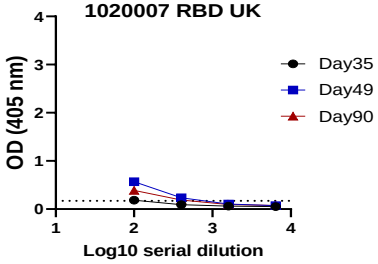
	Day35	Day49	Day90
Total Area	559.8	561.2	623.9



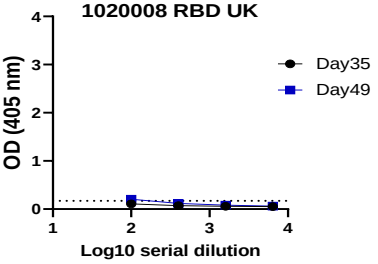
	Day35	Day49	Day90
Total Area	551.1	663.8	2396



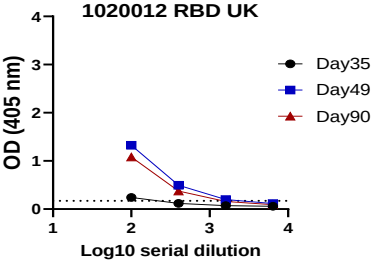
	Day35	Day49	Day90
Total Area	411.5	749.3	664.1



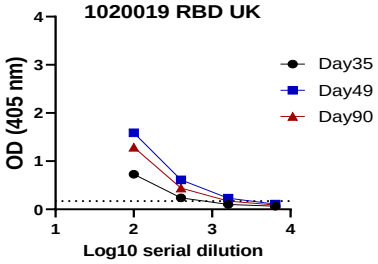
	Day35	Day49
Total Area	369.8	505.8



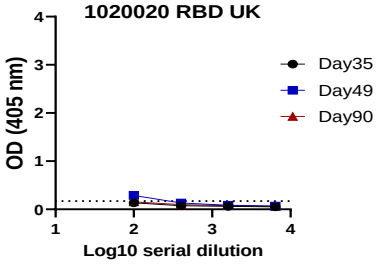
	Day35	Day49	Day90
Total Area	480.5	1441	1136



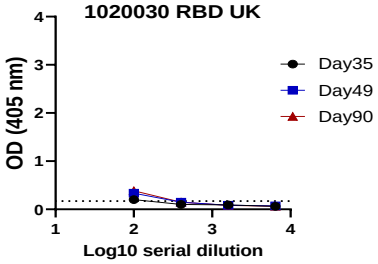
	Day35	Day49	Day90
Total Area	747.6	1655	1257



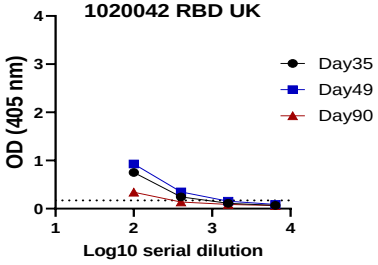
	Day35	Day49	Day90
Total Area	384.3	566.1	468.3



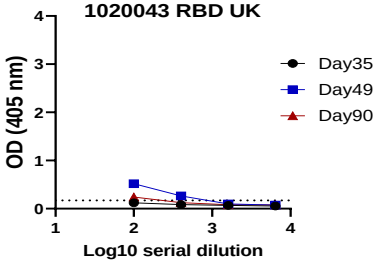
	Day35	Day49	Day90
Total Area	531.5	594.6	574.1



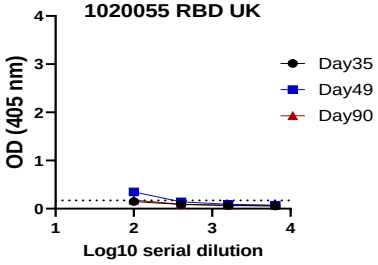
	Day35	Day49	Day90
Total Area	789.6	1080	568.5



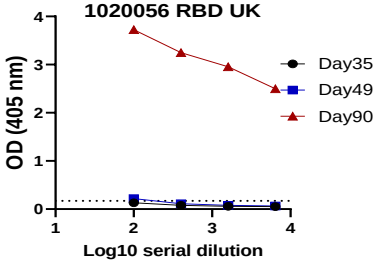
	Day35	Day49	Day90
Total Area	416.0	745.1	566.6



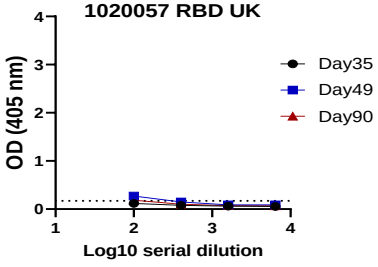
	Day35	Day49	Day90
Total Area	417.2	606.8	459.3



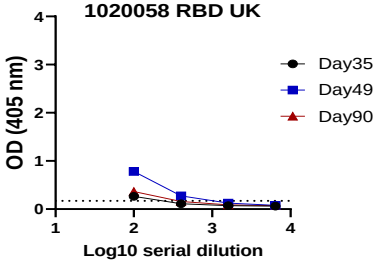
	Day35	Day49	Day90
Total Area	385.7	503.9	17858



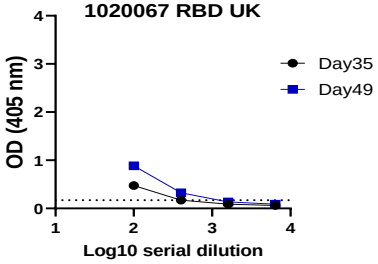
	Day35	Day49	Day90
Total Area	395.9	638.3	484.5



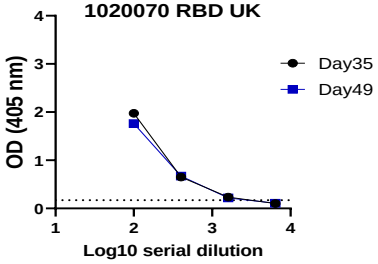
	Day35	Day49	Day90
Total Area	492.3	887.1	611.9



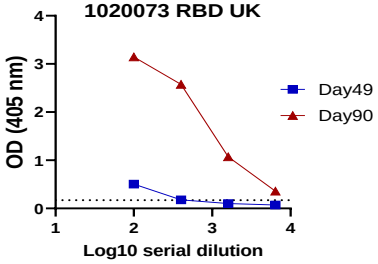
	Day35	Day49
Total Area	615.3	995.0



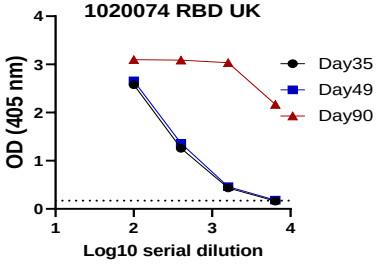
	Day35	Day49
Total Area	1729	1682



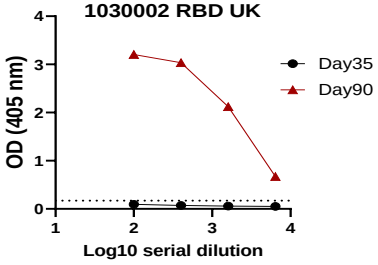
	Day49	Day90
Total Area	688.1	6486



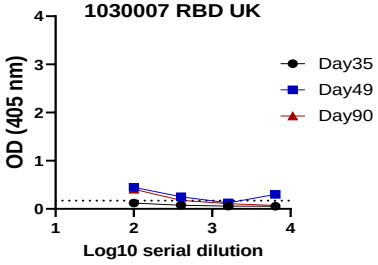
	Day35	Day49	Day90
Total Area	3023	3247	17093



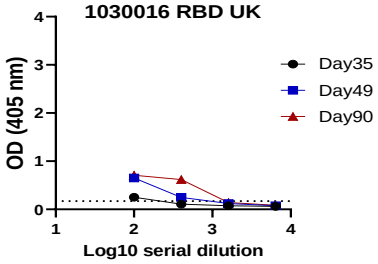
	Day35	Day90
Total Area	366.9	10728



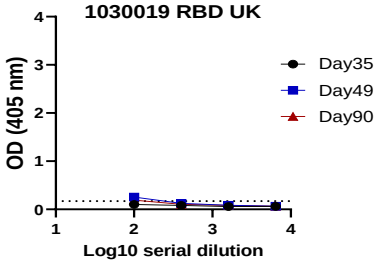
	Day35	Day49	Day90
Total Area	384.9	1351	698.6



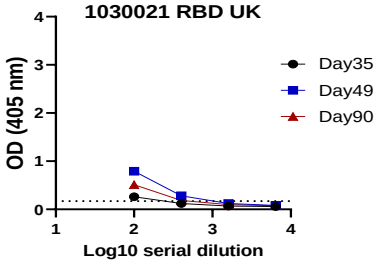
	Day35	Day49	Day90
Total Area	489.2	831.6	1205



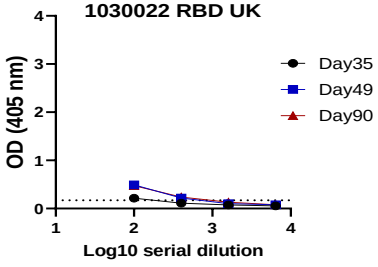
	Day35	Day49	Day90
Total Area	399.6	545.4	508.7



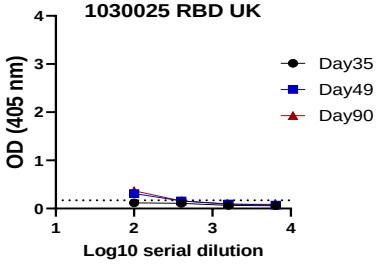
	Day35	Day49	Day90
Total Area	482.7	889.8	683.1



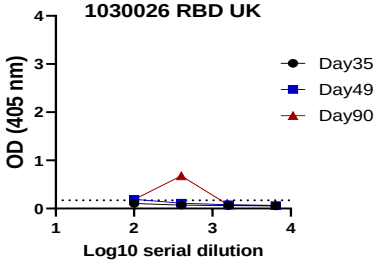
	Day35	Day49	Day90
Total Area	471.0	733.4	833.9



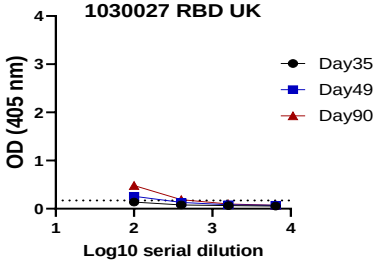
	Day35	Day49	Day90
Total Area	426.8	623.4	648.3



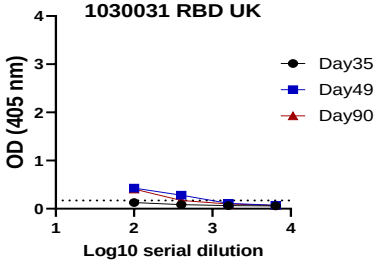
	Day35	Day49	Day90
Total Area	386.9	496.5	911.1



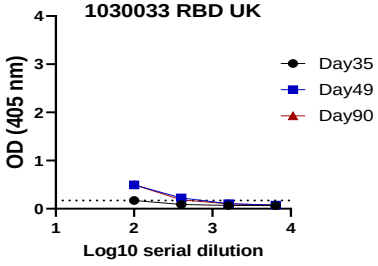
	Day35	Day49	Day90
Total Area	412.2	548.7	677.0



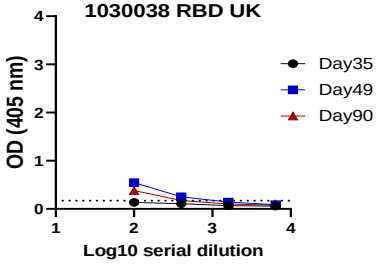
	Day35	Day49	Day90
Total Area	418.8	782.3	653.0



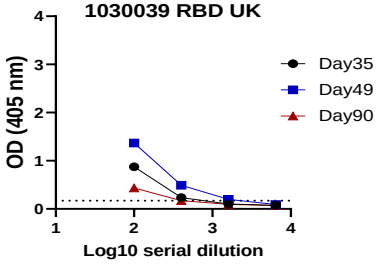
	Day35	Day49	Day90
Total Area	453.3	744.2	703.2



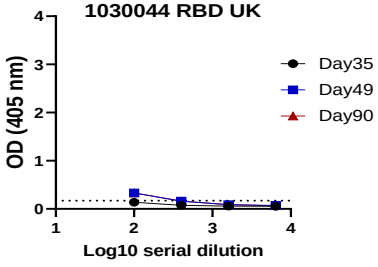
	Day35	Day49	Day90
Total Area	444.9	907.2	675.6



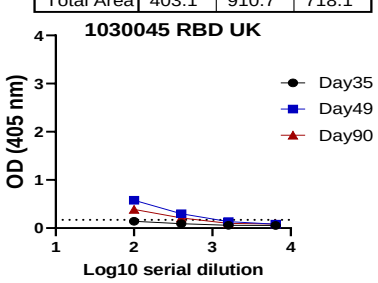
	Day35	Day49	Day90
Total Area	799.7	1388	643.2



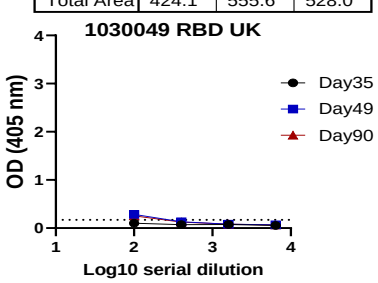
	Day35	Day49	Day90
Total Area	384.3	602.4	593.9



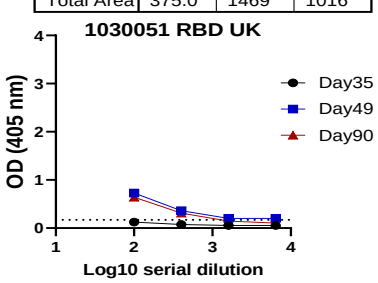
	Day35	Day49	Day90
Total Area	403.1	910.7	718.1



	Day35	Day49	Day90
Total Area	424.1	555.6	528.0



	Day35	Day49	Day90
Total Area	375.0	1469	1016



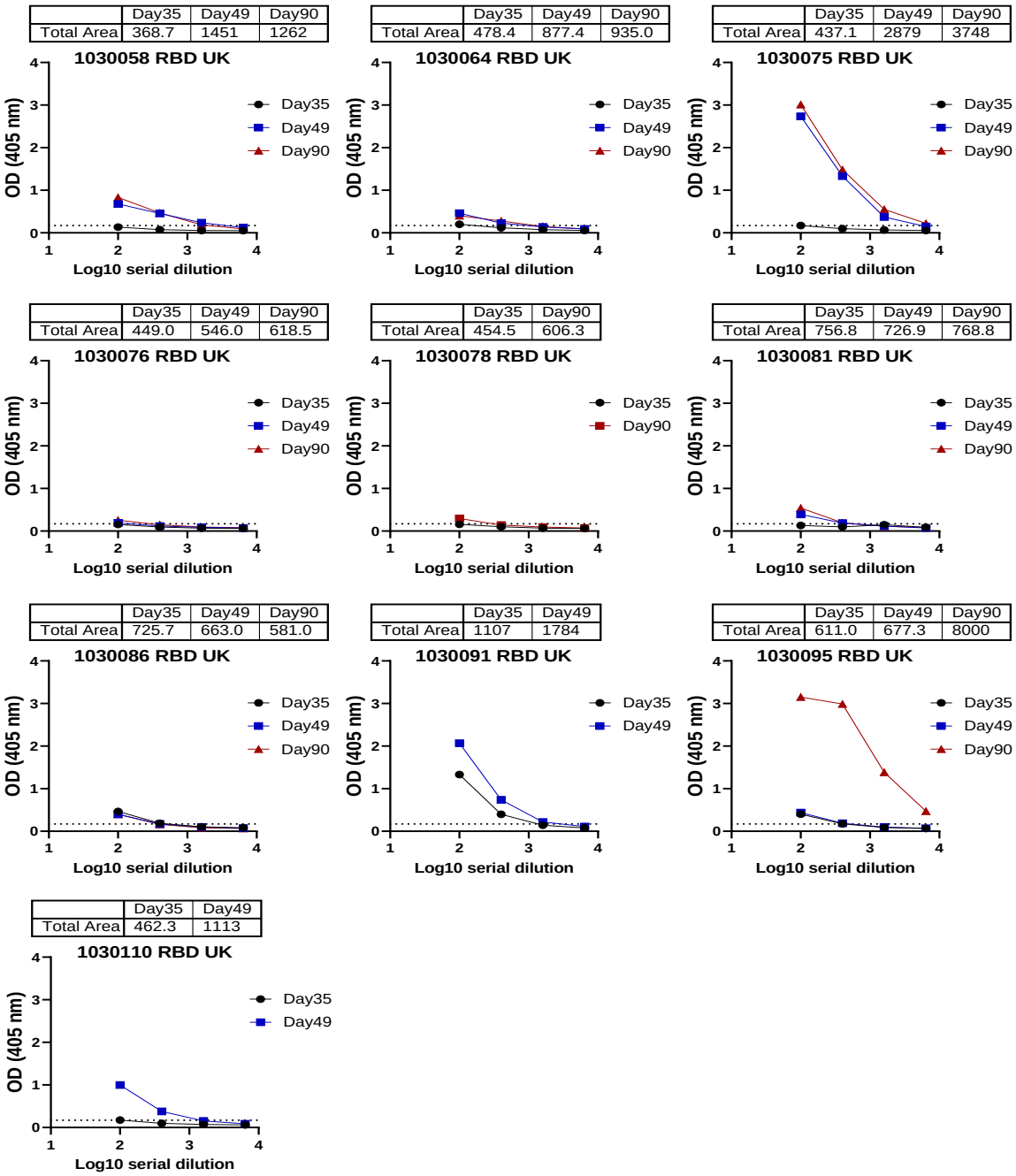
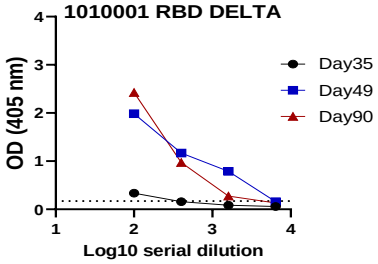
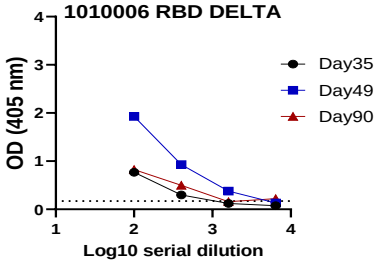


Figure A.4. The IgG responses of the volunteers against recombinant RBD UK protein were assessed by ELISA. 2HB ELISA plates were coated 1 ug/ml of recombinant RBD UK protein and following overnight incubation and blocking steps, the human sera collected at days 35, 49, and 90 were added to the wells. The sera were initially prepared in 1:100 ratio and then serially diluted fourfold for 3 times. After overnight incubation, the plates were treated with anti-human IgG prepared in 1:1000 ratio and the OD405 values were recorded following treatment with PNPP substrate solution. OD405 values for each volunteer are demonstrated in each graph with area under the curve values presented in the tables.

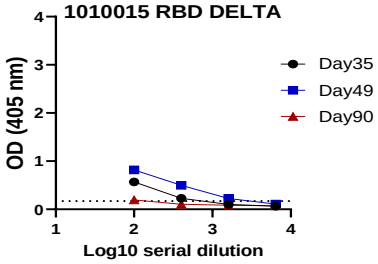
	Day35	Day49	Day90
Total Area	564.9	3922	2238



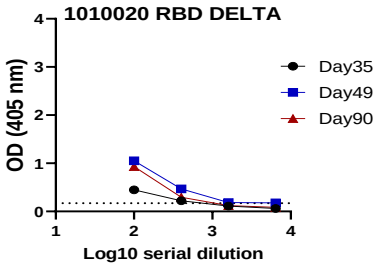
	Day35	Day49	Day90
Total Area	883.8	2432	1499



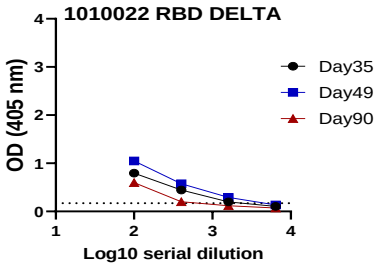
	Day35	Day49	Day90
Total Area	718.8	1434	538.2



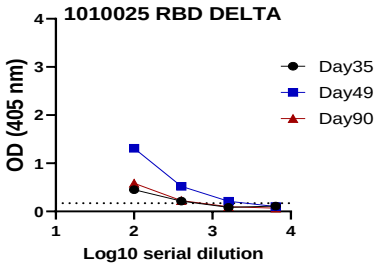
	Day35	Day49	Day90
Total Area	714.8	1490	932.6



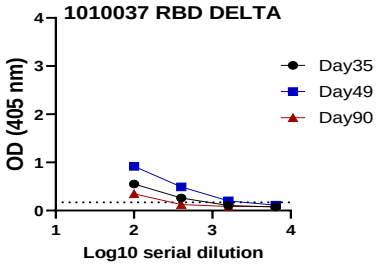
	Day35	Day49	Day90
Total Area	1303	1789	771.6



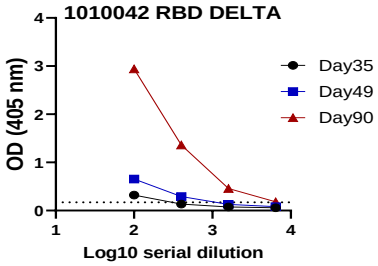
	Day35	Day49	Day90
Total Area	751.8	1475	717.6



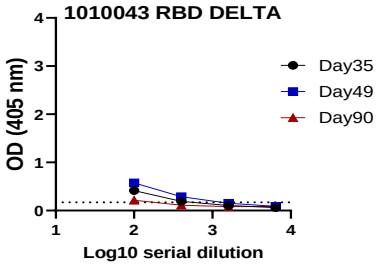
	Day35	Day49	Day90
Total Area	777.0	1378	589.8



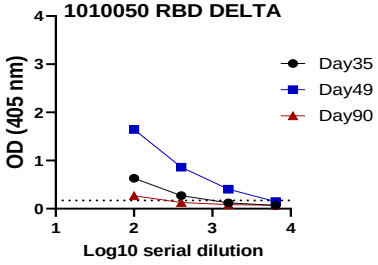
	Day35	Day49	Day90
Total Area	512.9	896.4	3268



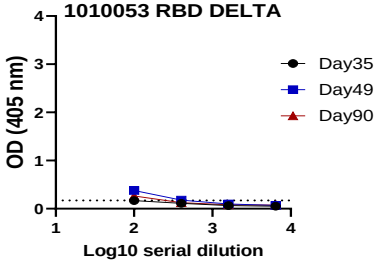
	Day35	Day49	Day90
Total Area	671.0	976.5	565.4



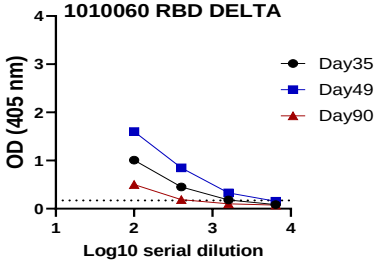
	Day35	Day49	Day90
Total Area	829.1	2471	556.4



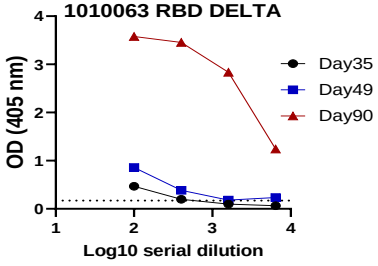
	Day35	Day49	Day90
Total Area	435.0	653.4	555.0



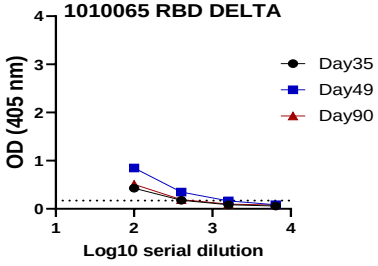
	Day35	Day49	Day90
Total Area	1238	2236	693.9



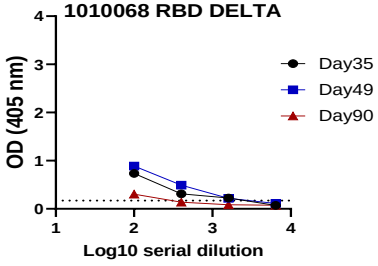
	Day35	Day49	Day90
Total Area	665.6	1531	14618



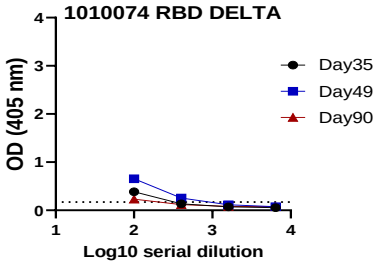
	Day35	Day49	Day90
Total Area	597.9	1088	694.7



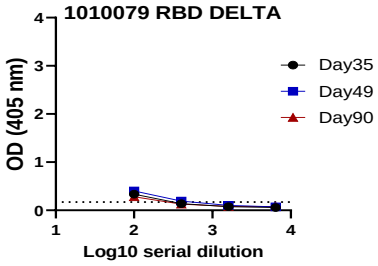
	Day35	Day49	Day90
Total Area	1190	1420	582.0



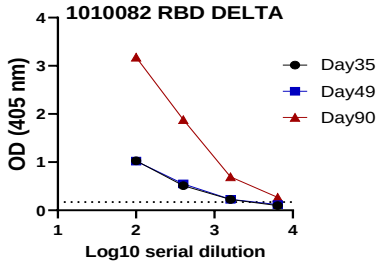
	Day35	Day49	Day90
Total Area	510.2	814.5	549.2



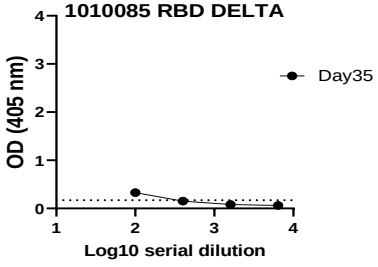
	Day35	Day49	Day90
Total Area	511.8	679.1	574.4



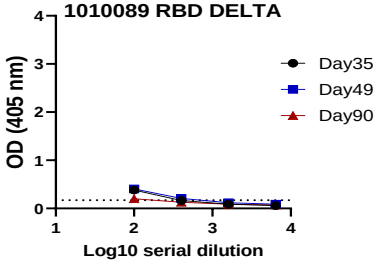
	Day35	Day49	Day90
Total Area	1444	1537	4616



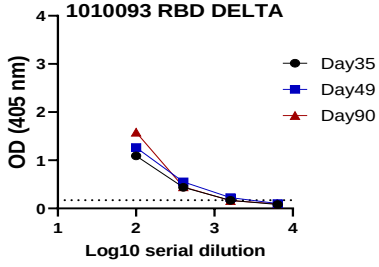
	Day35
Total Area	559.2



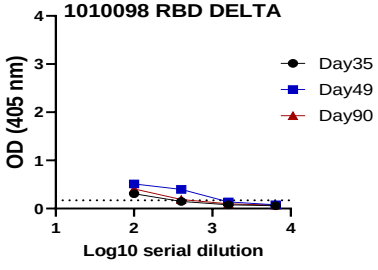
	Day35	Day49	Day90
Total Area	583.7	785.0	554.7



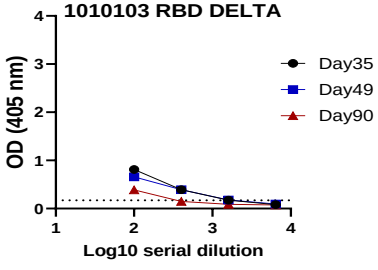
	Day35	Day49	Day90
Total Area	1191	1521	1290



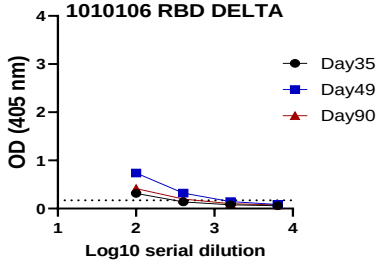
	Day35	Day49	Day90
Total Area	535.2	979.5	667.7



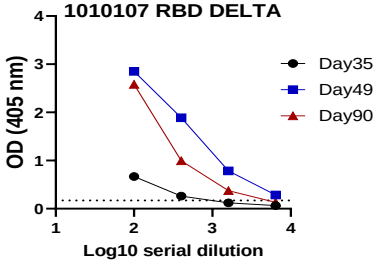
	Day35	Day49	Day90
Total Area	1139	1149	620.9



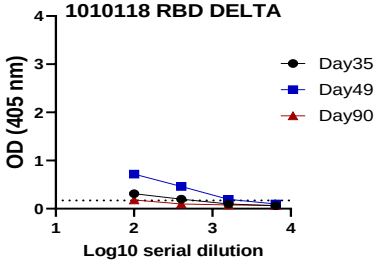
	Day35	Day49	Day90
Total Area	518.0	990.8	692.4



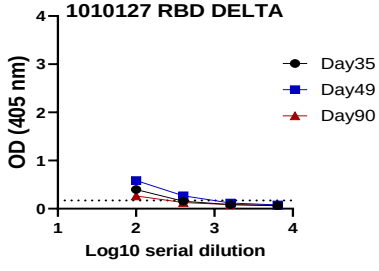
	Day35	Day49	Day90
Total Area	812.6	4888	2568



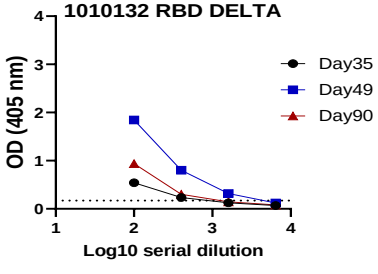
	Day35	Day49	Day90
Total Area	640.5	1275	497.6



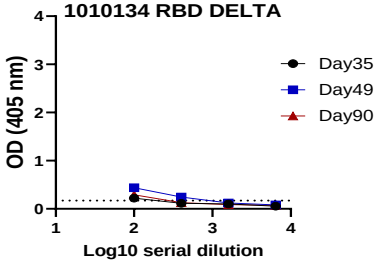
	Day35	Day49	Day90
Total Area	573.6	831.8	556.4



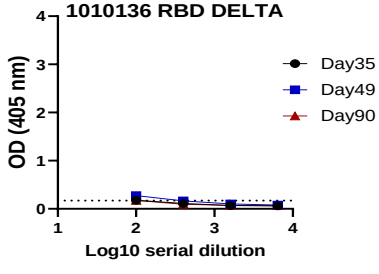
	Day35	Day49	Day90
Total Area	797.9	2121	996.8



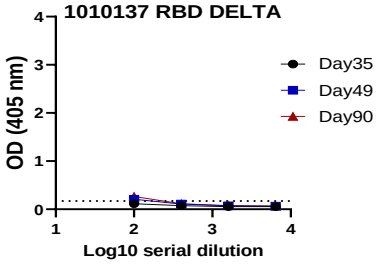
	Day35	Day49	Day90
Total Area	560.3	809.4	576.6



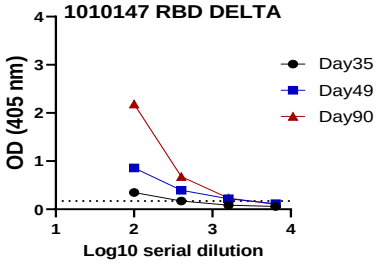
	Day35	Day49	Day90
Total Area	463.5	654.8	471.0



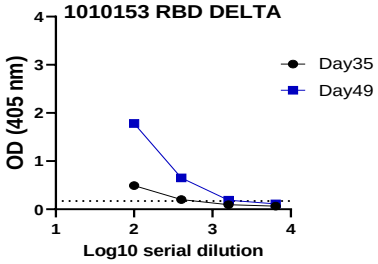
	Day35	Day49	Day90
Total Area	370.7	478.8	505.2



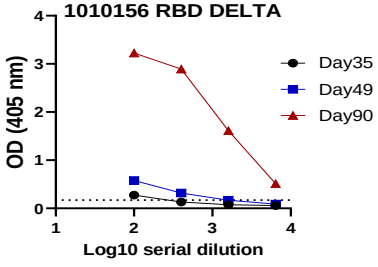
	Day35	Day49	Day90
Total Area	583.5	1352	1771



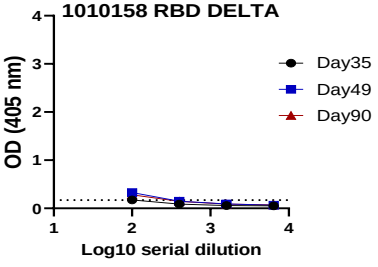
	Day35	Day49
Total Area	662.7	1591



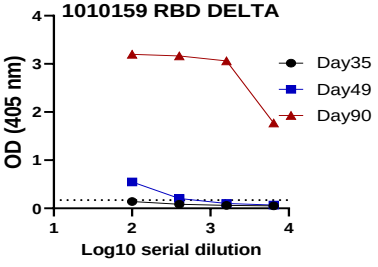
	Day35	Day49	Day90
Total Area	508.1	1044	8708



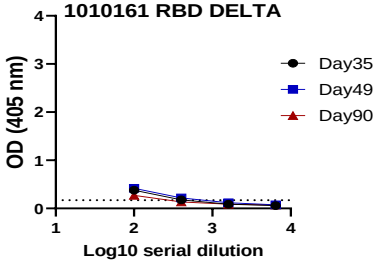
	Day35	Day49	Day90
Total Area	397.2	595.4	590.0



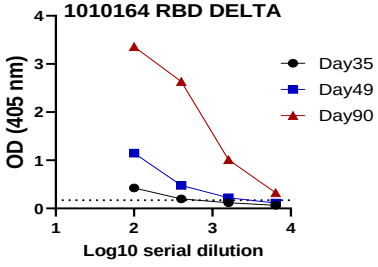
	Day35	Day49	Day90
Total Area	391.8	705.9	16288



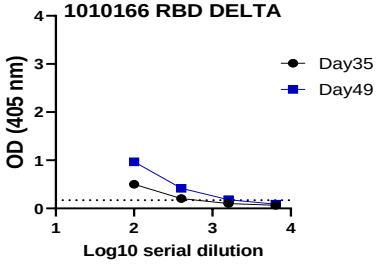
	Day35	Day49	Day90
Total Area	598.7	762.6	582.8



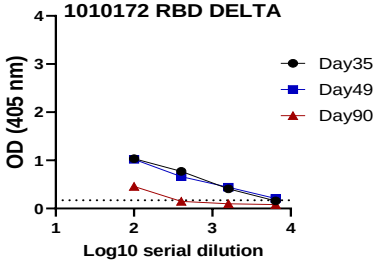
	Day35	Day49	Day90
Total Area	720.8	1469	6299



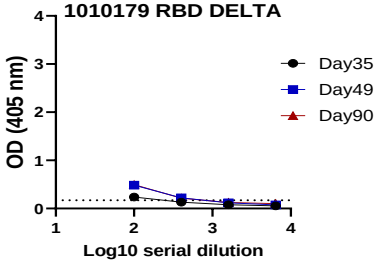
	Day35	Day49
Total Area	689.4	1225



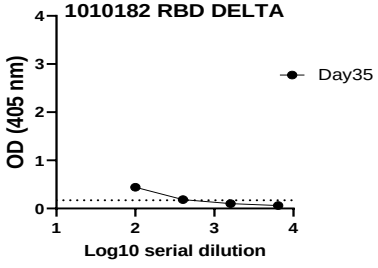
	Day35	Day49	Day90
Total Area	2336	2474	666.8



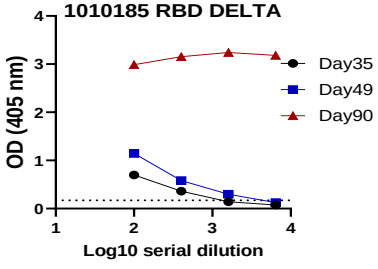
	Day35	Day49	Day90
Total Area	493.8	775.4	849.2



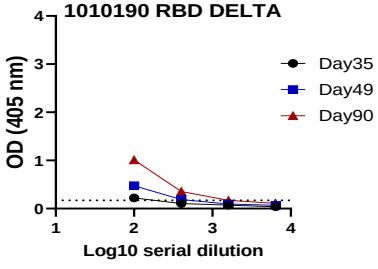
	Day35
Total Area	656.0



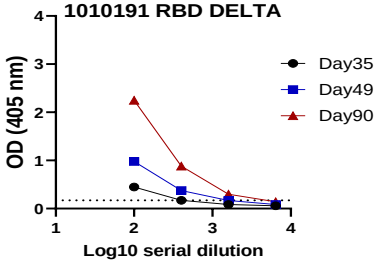
	Day35	Day49	Day90
Total Area	986.1	1803	20175



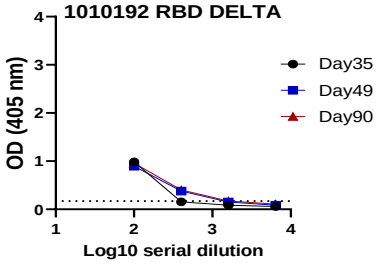
	Day35	Day49	Day90
Total Area	414.9	661.8	1185



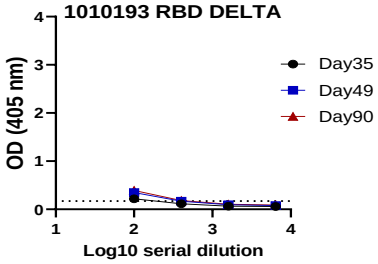
	Day35	Day49	Day90
Total Area	592.2	1130	2229



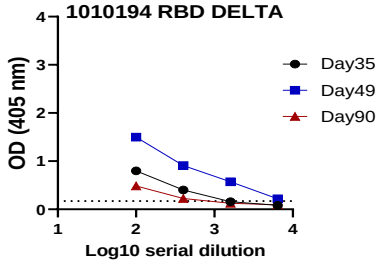
	Day35	Day49	Day90
Total Area	666.2	1079	1216



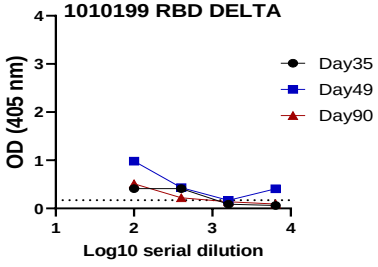
	Day35	Day49	Day90
Total Area	452.6	644.9	725.6



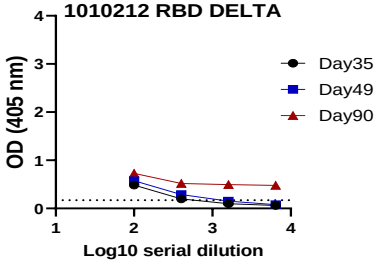
	Day35	Day49	Day90
Total Area	1094	3148	846.3



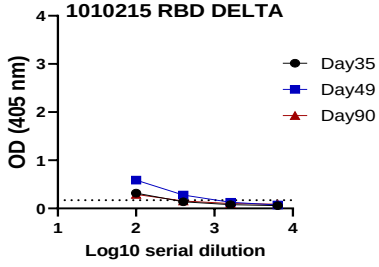
	Day35	Day49	Day90
Total Area	788.9	1951	879.0



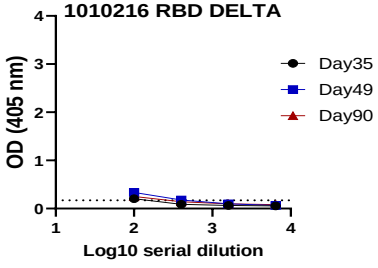
	Day35	Day49	Day90
Total Area	664.2	941.4	3131



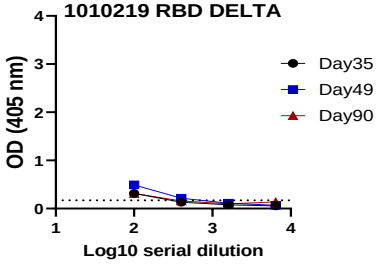
	Day35	Day49	Day90
Total Area	526.7	854.0	676.7



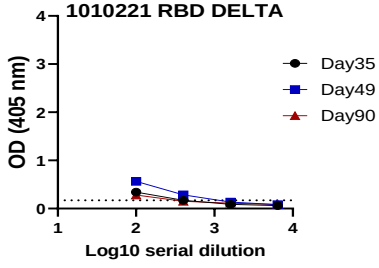
	Day35	Day49	Day90
Total Area	422.0	637.5	631.7



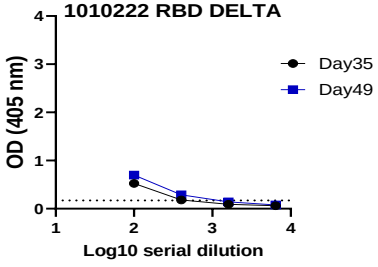
	Day35	Day49	Day90
Total Area	511.5	729.8	785.7



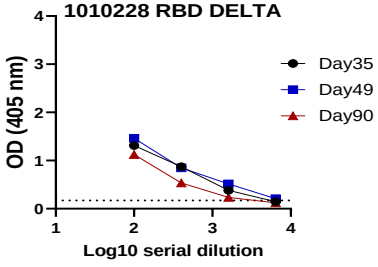
	Day35	Day49	Day90
Total Area	586.2	899.1	695.1



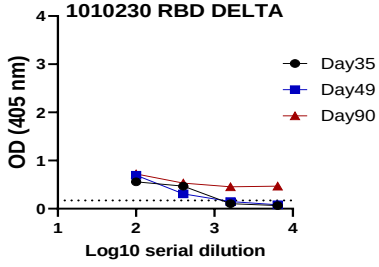
	Day35	Day49
Total Area	643.1	937.2



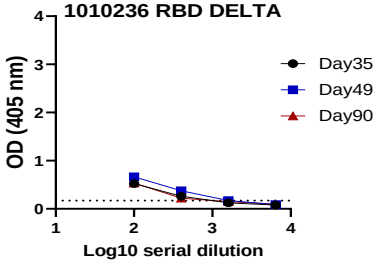
	Day35	Day49	Day90
Total Area	2348	2898	1569



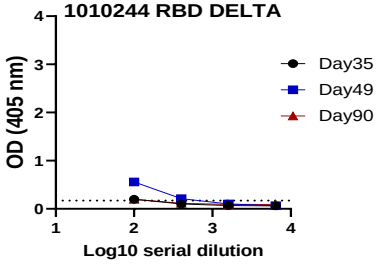
	Day35	Day49	Day90
Total Area	905.3	978.3	2990



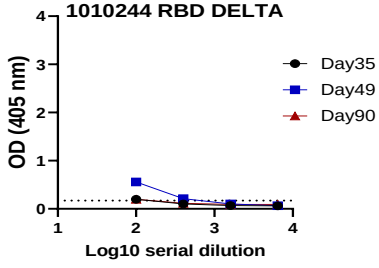
	Day35	Day49	Day90
Total Area	833.6	1105	929.0



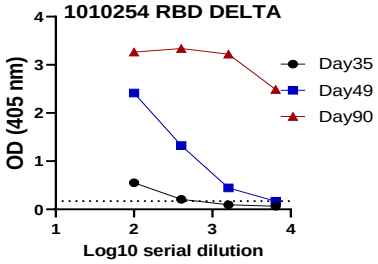
	Day35	Day49	Day90
Total Area	462.9	707.0	607.5



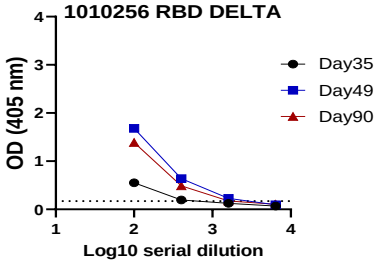
	Day35	Day49	Day90
Total Area	462.9	707.0	607.5



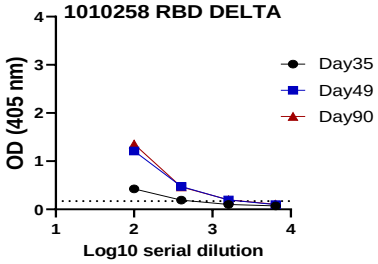
	Day35	Day49	Day90
Total Area	685.2	3096	18636



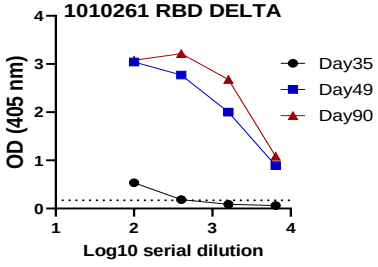
	Day35	Day49	Day90
Total Area	767.1	1643	1350



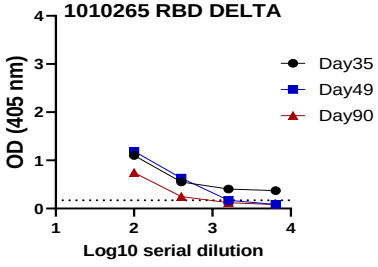
	Day35	Day49	Day90
Total Area	682.5	1356	1400



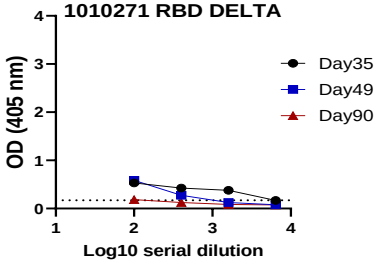
	Day35	Day49	Day90
Total Area	639.5	10673	13509



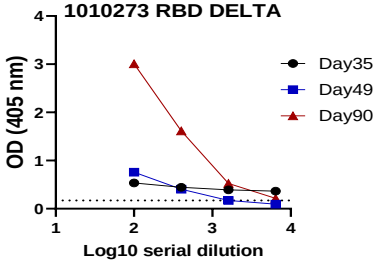
	Day35	Day49	Day90
Total Area	2686	1367	865.4



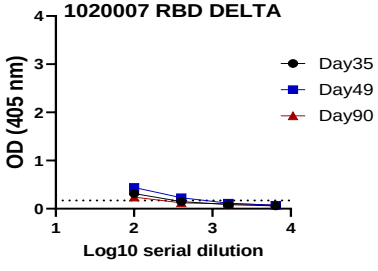
	Day35	Day49	Day90
Total Area	1931	850.8	554.0



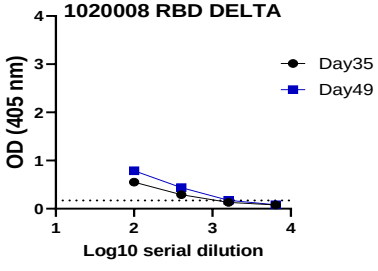
	Day35	Day49	Day90
Total Area	2466	1165	3760



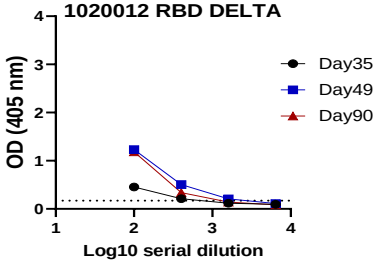
	Day35	Day49	Day90
Total Area	560.9	755.9	623.4



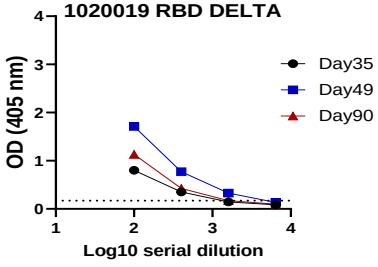
	Day35	Day49
Total Area	885.2	1171



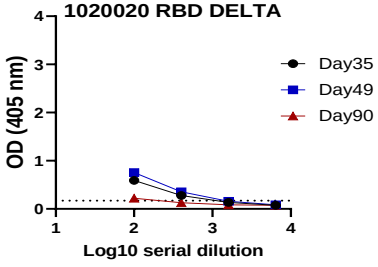
	Day35	Day49	Day90
Total Area	814.1	1452	1066



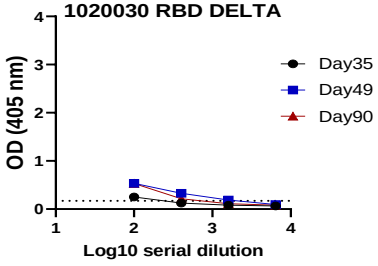
	Day35	Day49	Day90
Total Area	1020	2143	1235



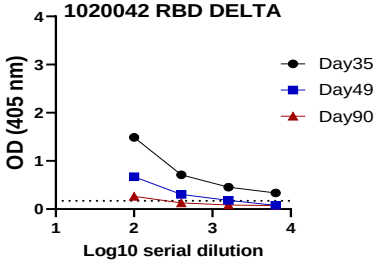
	Day35	Day49	Day90
Total Area	879.3	1058	566.1



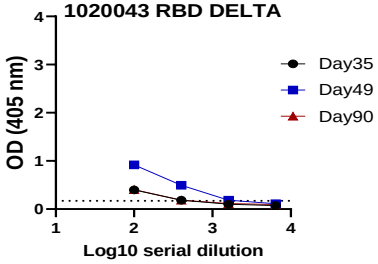
	Day35	Day49	Day90
Total Area	529.1	1121	765.6



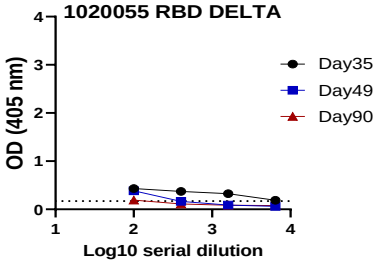
	Day35	Day49	Day90
Total Area	2923	1057	561.2



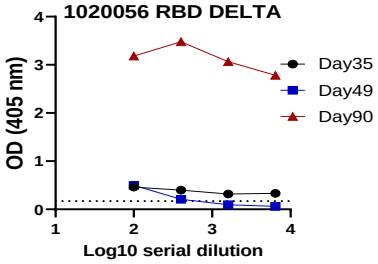
	Day35	Day49	Day90
Total Area	679.4	1334	778.7



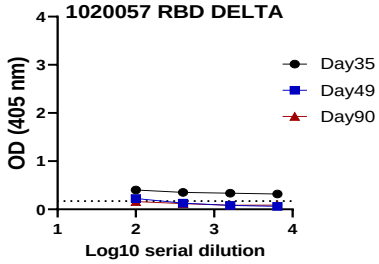
	Day35	Day49	Day90
Total Area	1765	593.6	553.1



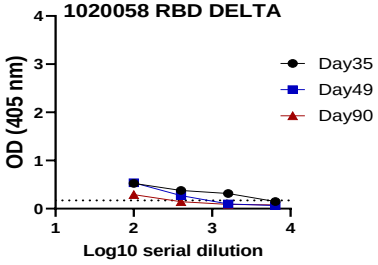
	Day35	Day49	Day90
Total Area	2119	668.4	18958



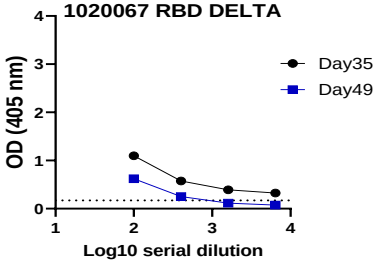
	Day35	Day49	Day90
Total Area	2093	522.3	579.2



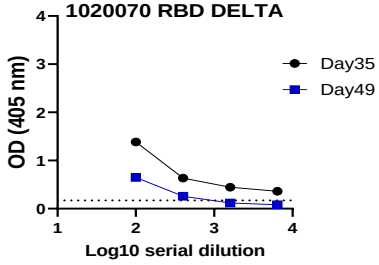
	Day35	Day49	Day90
Total Area	1670	733.7	606.9



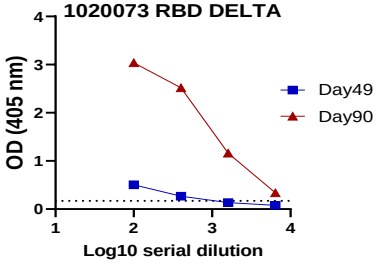
	Day35	Day49
Total Area	2557	804.2



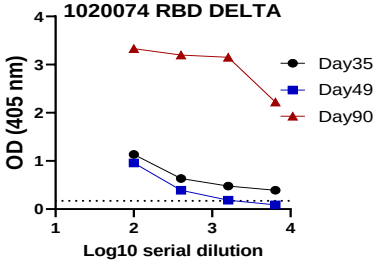
	Day35	Day49
Total Area	2891	843.5



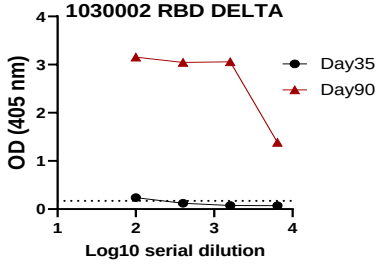
	Day49	Day90
Total Area	873.6	6641



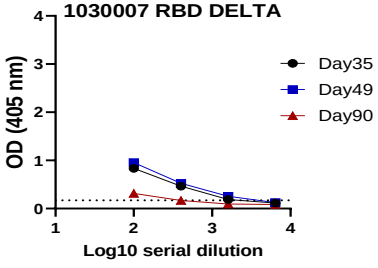
	Day35	Day49	Day90
Total Area	3024	1200	17685



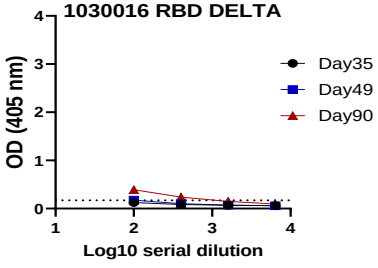
	Day35	Day90
Total Area	522.3	15253



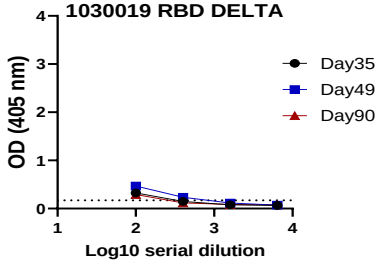
	Day35	Day49	Day90
Total Area	1319	1601	661.5



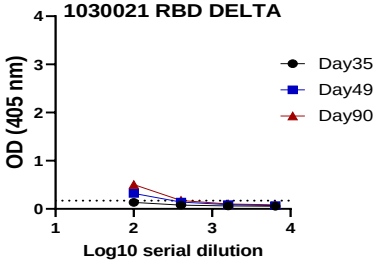
	Day35	Day49	Day90
Total Area	430.7	465.2	908.6



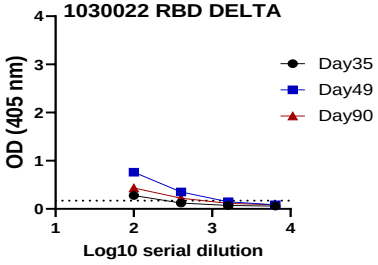
	Day35	Day49	Day90
Total Area	551.3	768.3	581.4



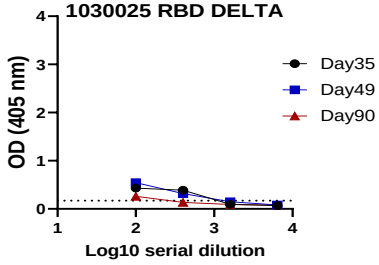
	Day35	Day49	Day90
Total Area	392.1	578.0	714.0



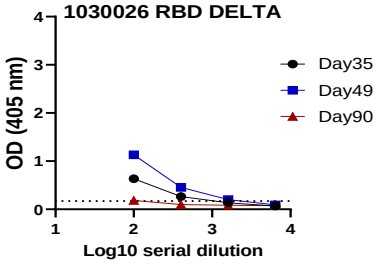
	Day35	Day49	Day90
Total Area	489.6	1026	783.2



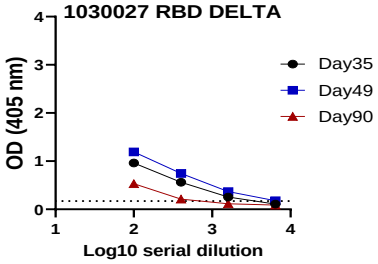
	Day35	Day49	Day90
Total Area	804.0	956.3	601.2



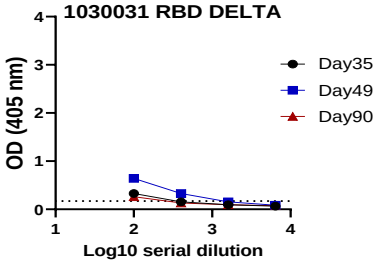
	Day35	Day49	Day90
Total Area	863.7	1335	538.7



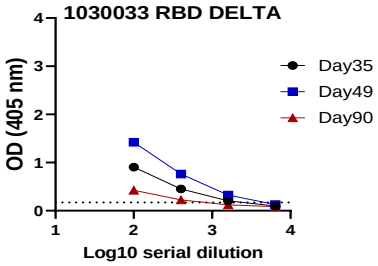
	Day35	Day49	Day90
Total Area	1588	2266	788.6



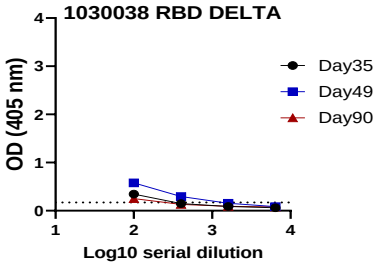
	Day35	Day49	Day90
Total Area	609.5	1006	603.9



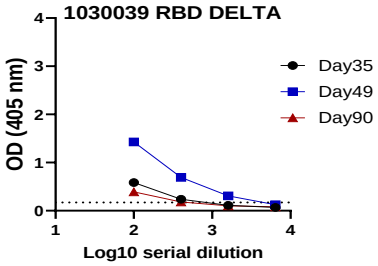
	Day35	Day49	Day90
Total Area	1323	2060	803.4



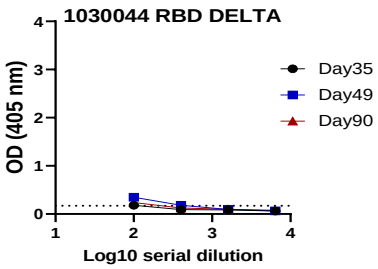
	Day35	Day49	Day90
Total Area	572.6	977.9	603.2



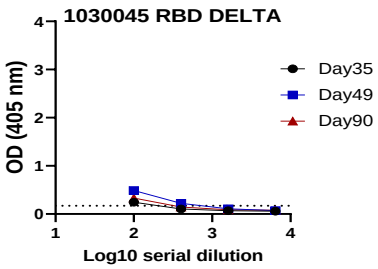
	Day35	Day49	Day90
Total Area	760.4	1952	696.3



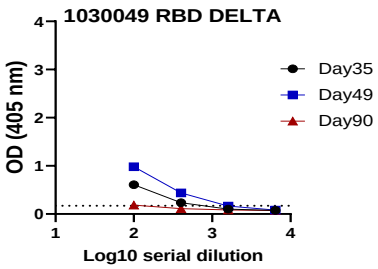
	Day35	Day49	Day90
Total Area	496.5	624.3	611.1



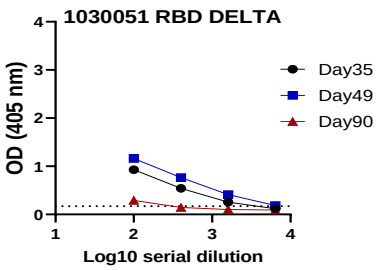
	Day35	Day49	Day90
Total Area	466.5	728.9	613.5



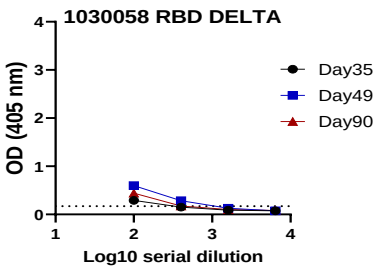
	Day35	Day49	Day90
Total Area	759.0	1167	541.1



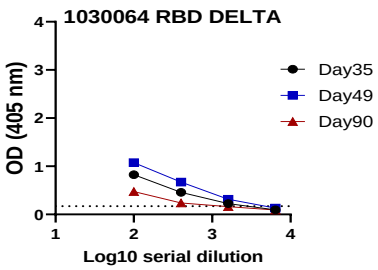
	Day35	Day49	Day90
Total Area	1599	2425	676.7



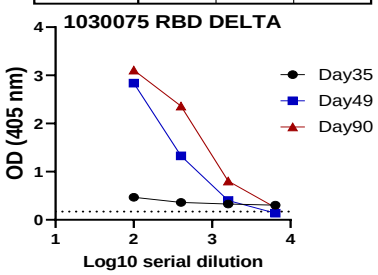
	Day35	Day49	Day90
Total Area	604.8	873.5	700.1



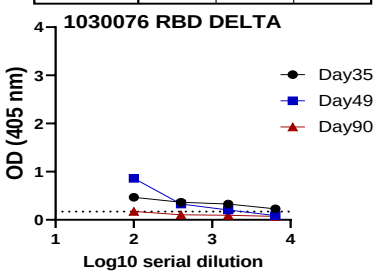
	Day35	Day49	Day90
Total Area	1372	1933	955.2



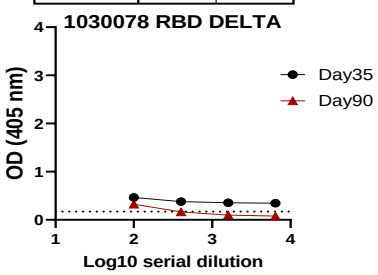
	Day35	Day49	Day90
Total Area	2061	2959	5268



	Day35	Day49	Day90
Total Area	1877	1205	568.2



	Day35	Day90
Total Area	2242	660.0



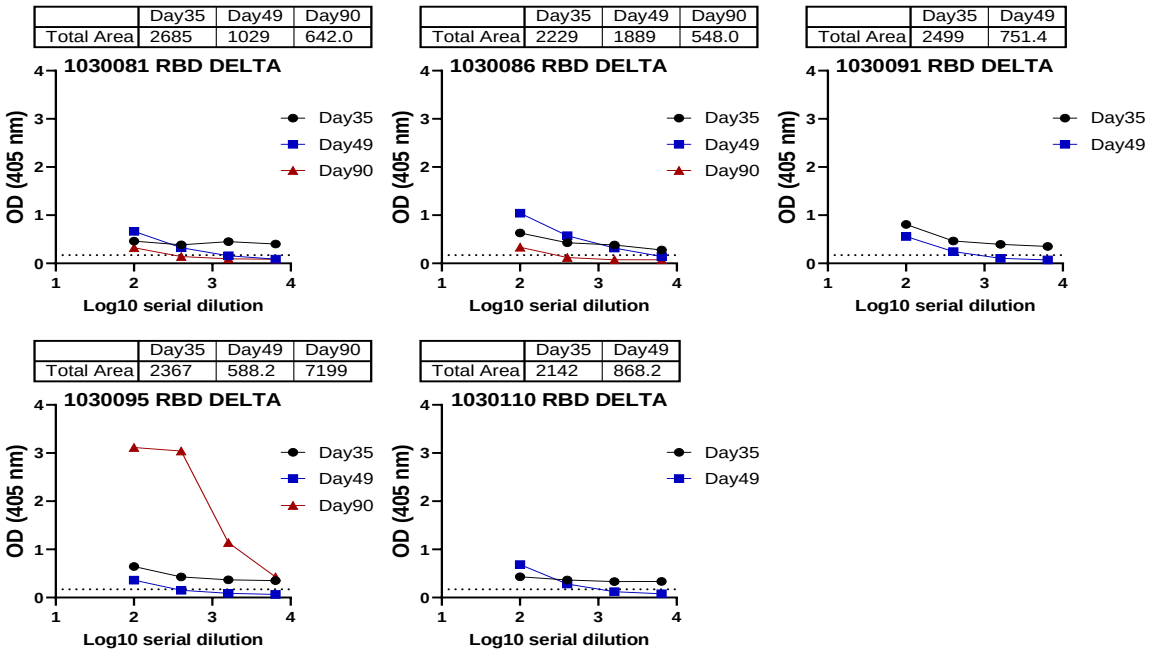
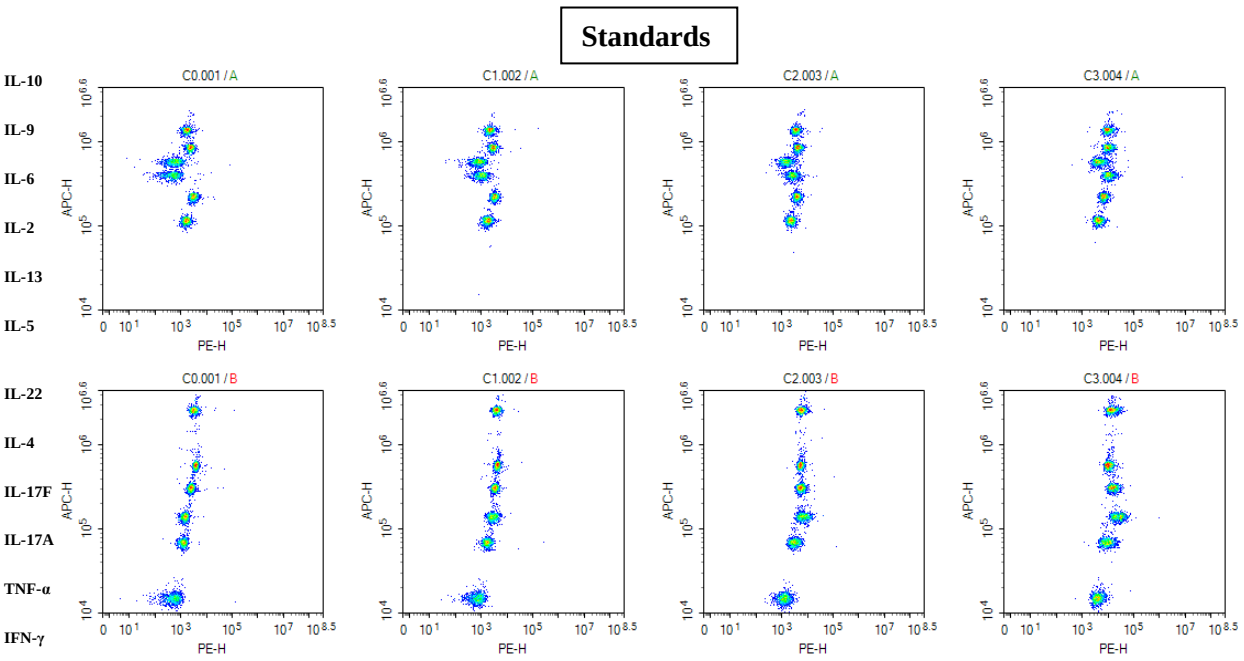
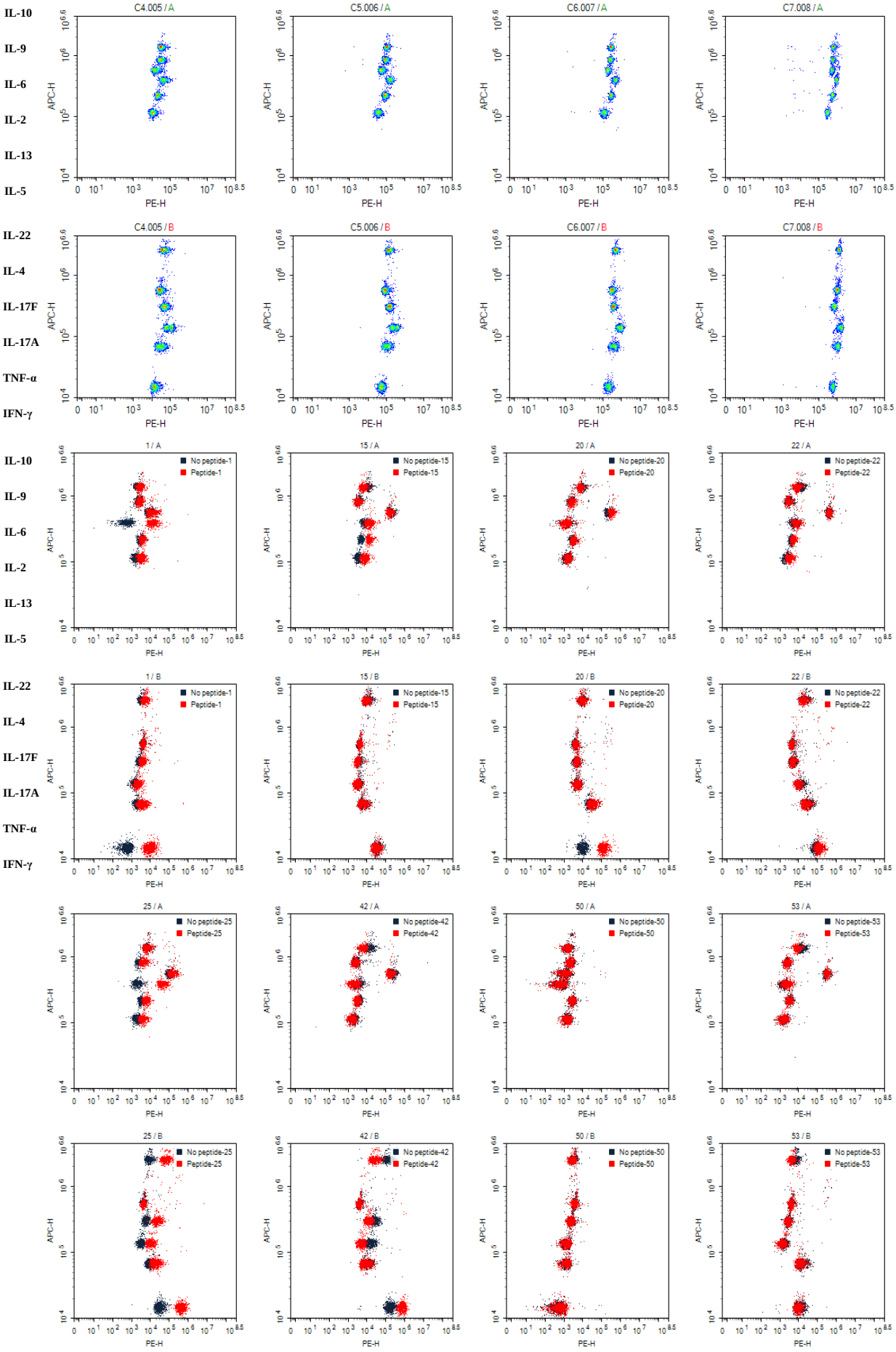
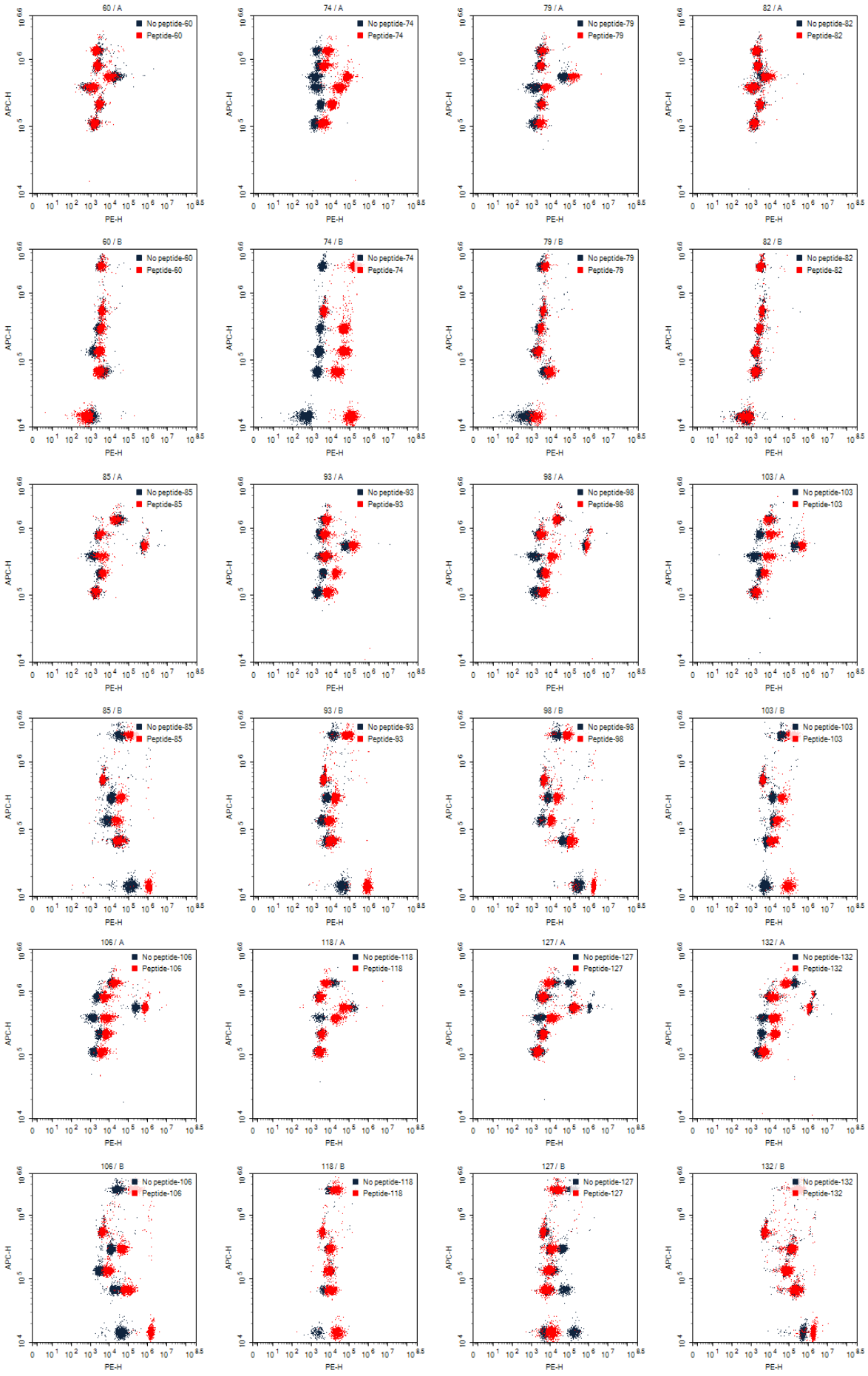
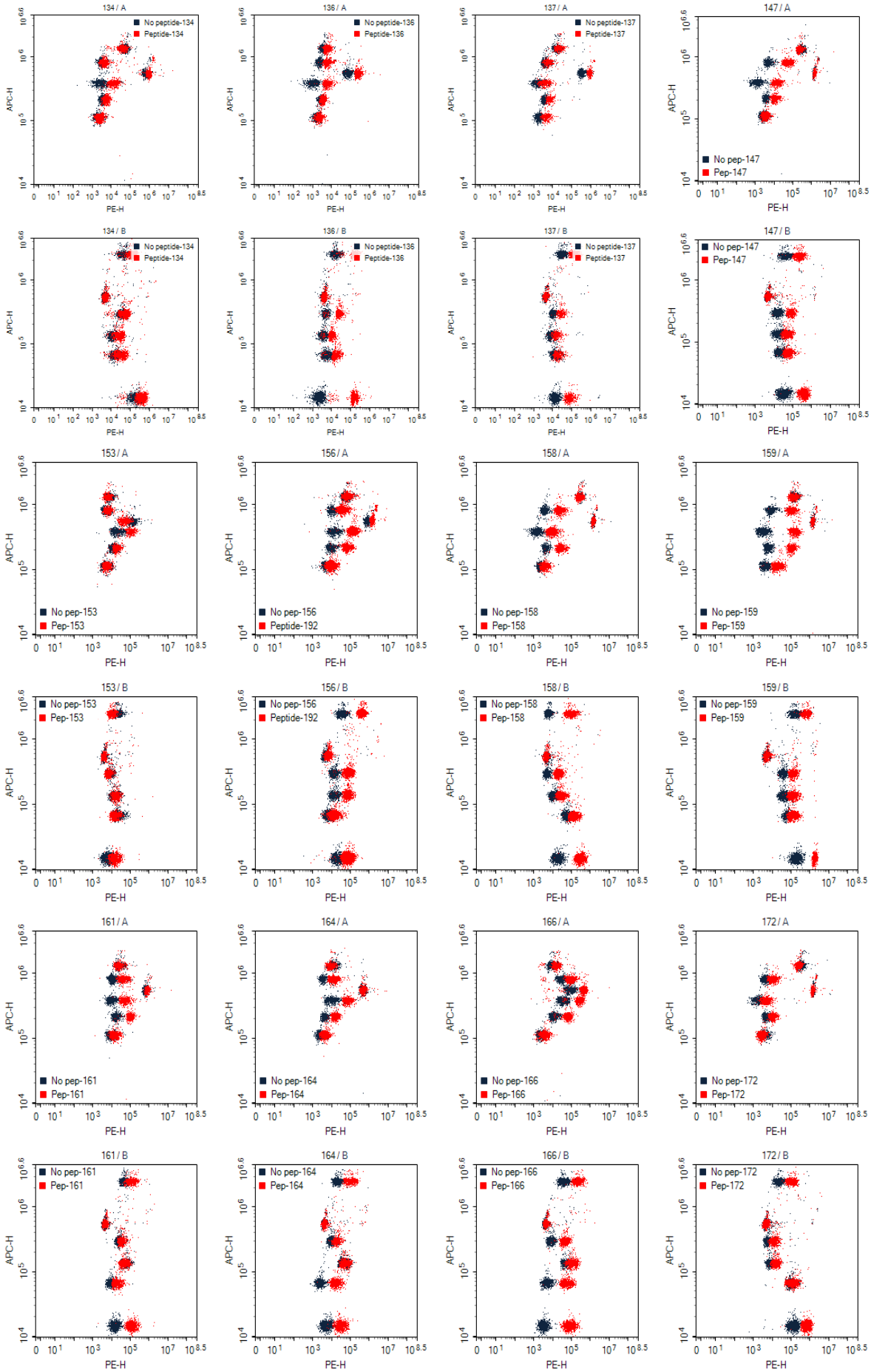


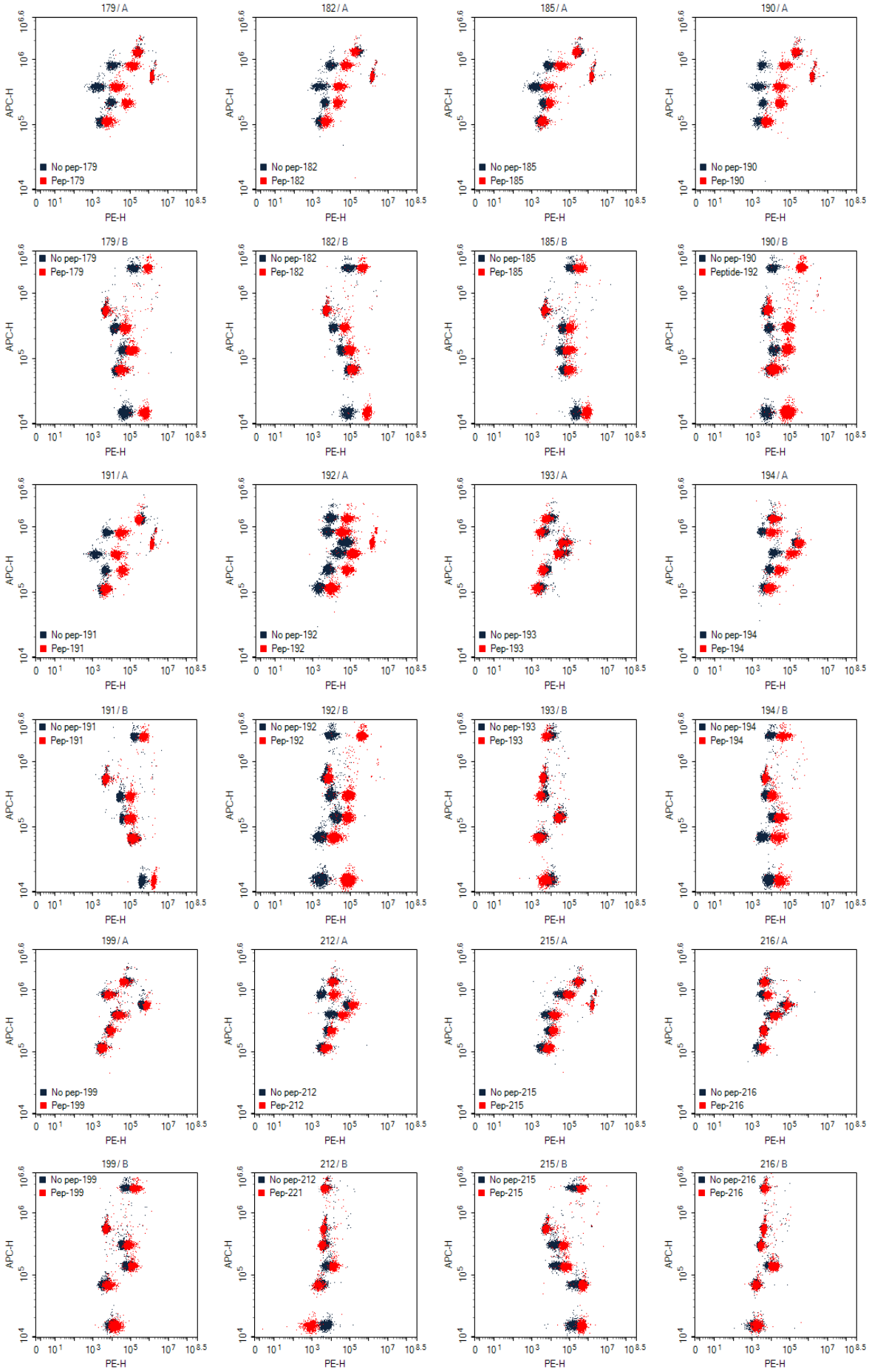
Figure A.5. The IgG responses of the volunteers against recombinant RBD Delta protein were assessed by ELISA. 2HB ELISA plates were coated 1 ug/ml of recombinant RBD Delta protein and following overnight incubation and blocking steps, the human sera collected at days 35, 49, and 90 were added to the wells. The sera were initially prepared in 1:100 ratio and then serially diluted fourfold for 3 times. After overnight incubation, the plates were treated with anti-human IgG prepared in 1:1000 ratio and the OD405 values were recorded following treatment with PNPP substrate solution. OD405 values for each volunteer are demonstrated in each graph with area under the curve values presented in the tables.

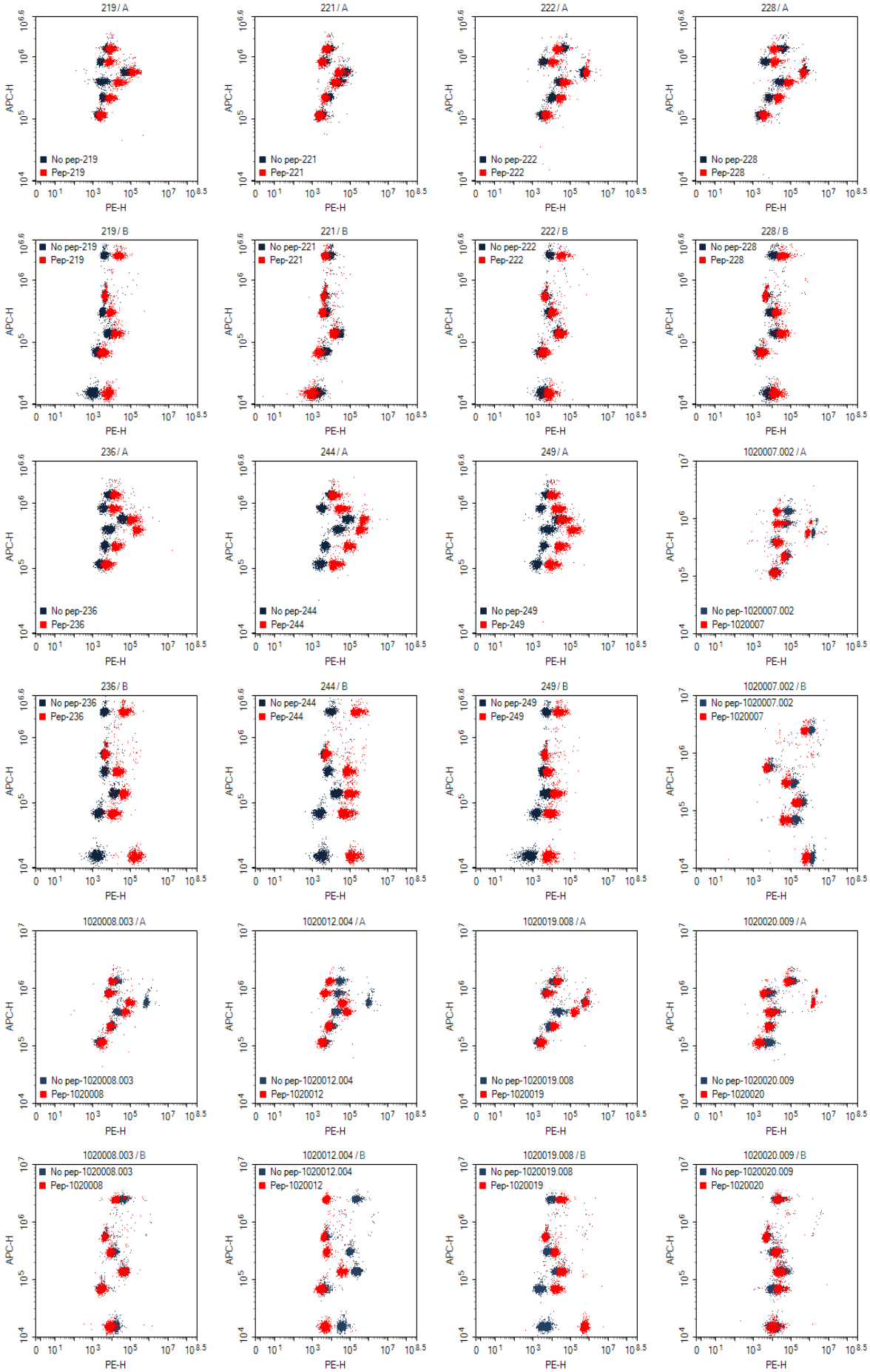


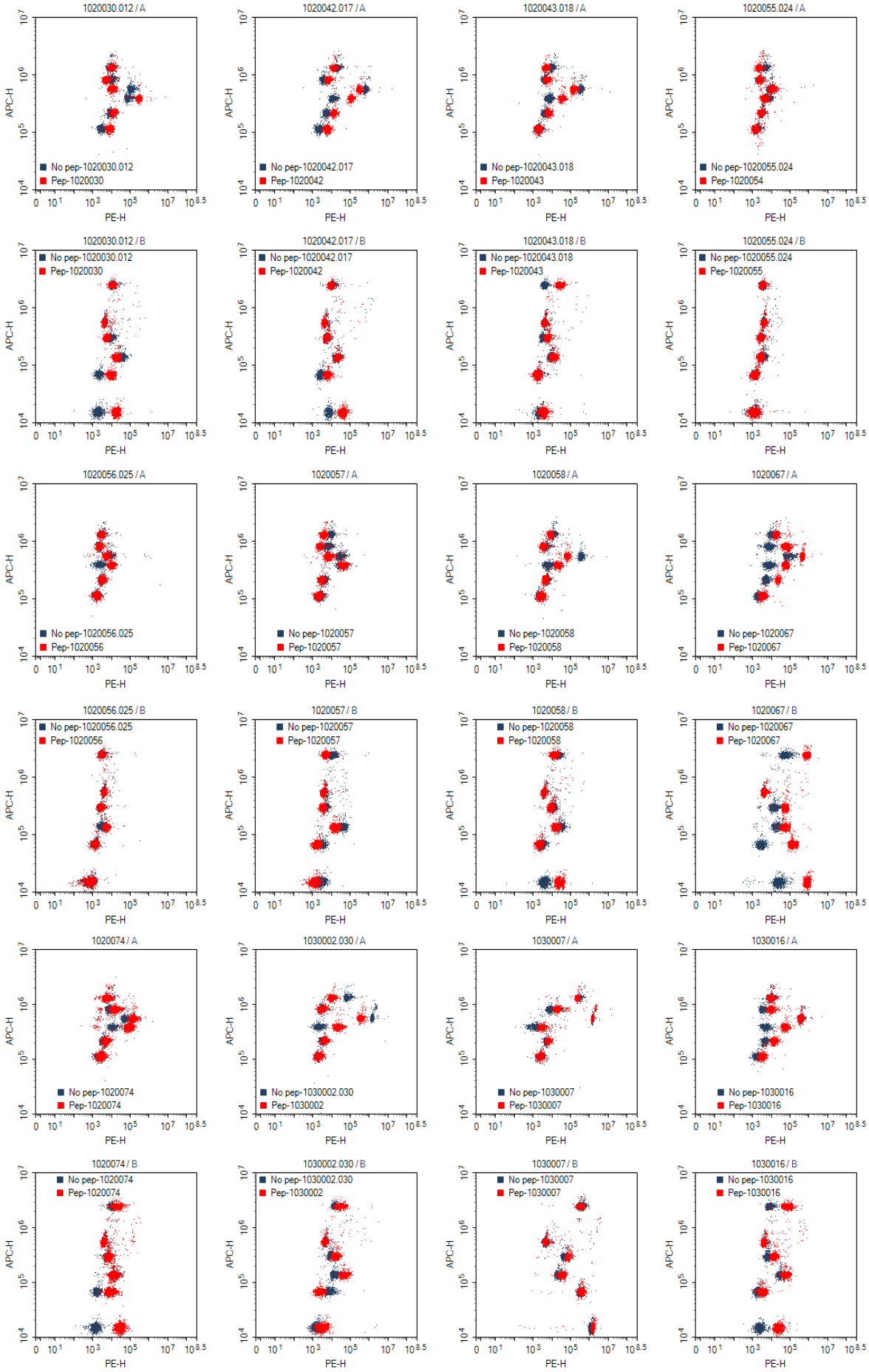

IL-10
IL-9
IL-6
IL-2
IL-13
IL-5
C4.005 / A
C5.006 / A
C6.007 / A
C7.008 / A
IL-22
IL-4
IL-17F
IL-17A
TNF-α
IFN-γ
C4.005 / B
C5.006 / B
C6.007 / B
C7.008 / B
1 / A
15 / A
20 / A
22 / A
No peptide-1
Peptide-1
No peptide-15
Peptide-15
No peptide-20
Peptide-20
No peptide-22
Peptide-22
1 / B
15 / B
20 / B
22 / B
25 / A
42 / A
50 / A
53 / A
No peptide-25
Peptide-25
No peptide-42
Peptide-42
No peptide-50
Peptide-50
No peptide-53
Peptide-53
25 / B
42 / B
50 / B
53 / B
APC-H
PE-H

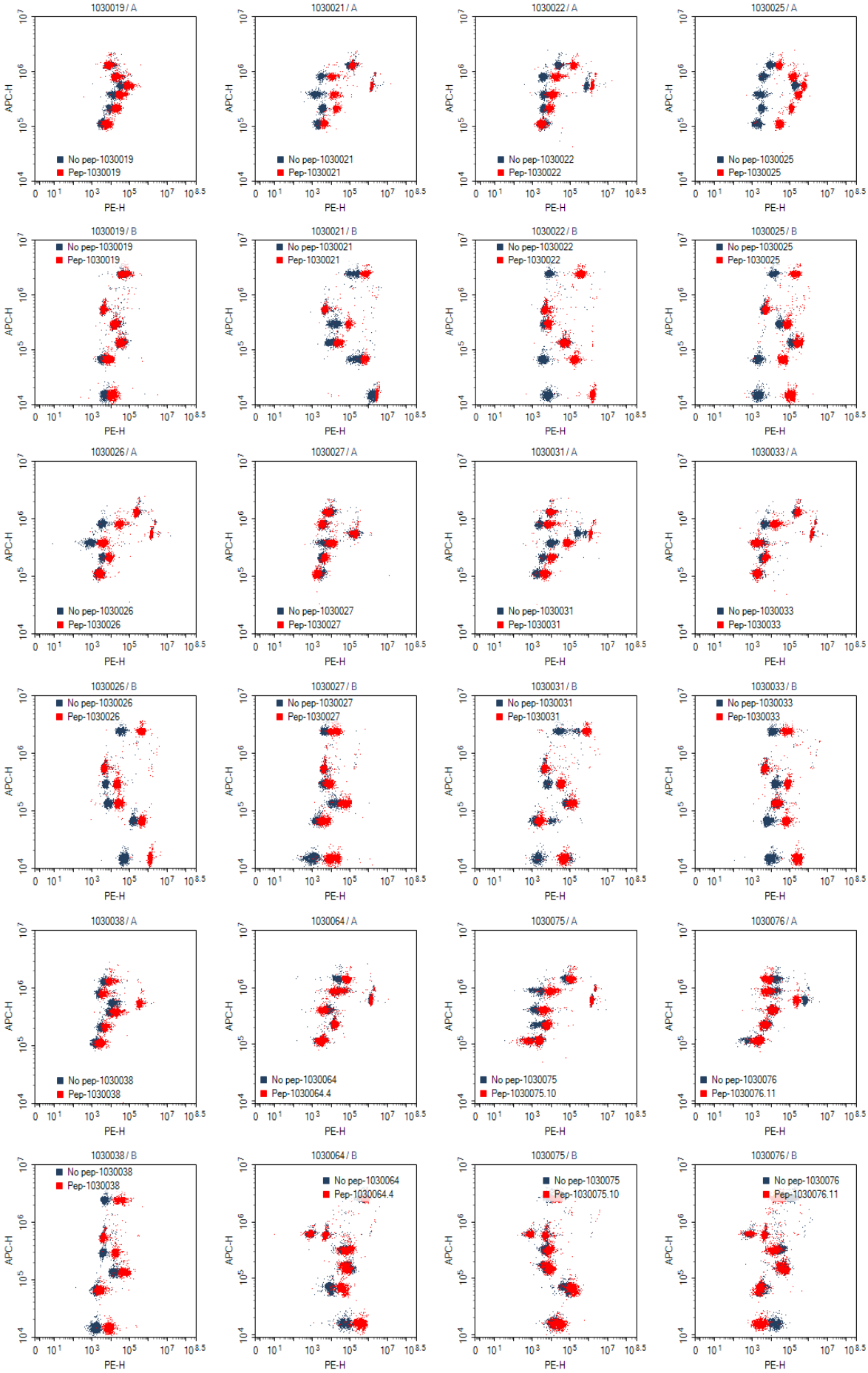

60 / A
No peptide-60
Peptide-60
74 / A
No peptide-74
Peptide-74
79 / A
No peptide-79
Peptide-79
82 / A
No peptide-82
Peptide-82
60 / B
No peptide-60
Peptide-60
74 / B
No peptide-74
Peptide-74
79 / B
No peptide-79
Peptide-79
82 / B
No peptide-82
Peptide-82
85 / A
No peptide-85
Peptide-85
93 / A
No peptide-93
Peptide-93
98 / A
No peptide-98
Peptide-98
103 / A
No peptide-103
Peptide-103
85 / B
No peptide-85
Peptide-85
93 / B
No peptide-93
Peptide-93
98 / B
No peptide-98
Peptide-98
103 / B
No peptide-103
Peptide-103
106 / A
No peptide-106
Peptide-106
118 / A
No peptide-118
Peptide-118
127 / A
No peptide-127
Peptide-127
132 / A
No peptide-132
Peptide-132
106 / B
No peptide-106
Peptide-106
118 / B
No peptide-118
Peptide-118
127 / B
No peptide-127
Peptide-127
132 / B
No peptide-132
Peptide-132
APC-H
PE-H


134 / A
No peptide-134
Peptide-134
136 / A
No peptide-136
Peptide-136
137 / A
No peptide-137
Peptide-137
147 / A
No pep-147
Pep-147
134 / B
No peptide-134
Peptide-134
136 / B
No peptide-136
Peptide-136
137 / B
No peptide-137
Peptide-137
147 / B
No pep-147
Pep-147
153 / A
No pep-153
Pep-153
156 / A
No pep-156
Peptide-192
158 / A
No pep-158
Pep-158
159 / A
No pep-159
Pep-159
153 / B
No pep-153
Pep-153
156 / B
No pep-156
Peptide-192
158 / B
No pep-158
Pep-158
159 / B
No pep-159
Pep-159
161 / A
No pep-161
Pep-161
164 / A
No pep-164
Pep-164
166 / A
No pep-166
Pep-166
172 / A
No pep-172
Pep-172
161 / B
No pep-161
Pep-161
164 / B
No pep-164
Pep-164
166 / B
No pep-166
Pep-166
172 / B
No pep-172
Pep-172
APC-H
PE-H


179 / A
No pep-179
Pep-179
182 / A
No pep-182
Pep-182
185 / A
No pep-185
Pep-185
190 / A
No pep-190
Pep-190
179 / B
No pep-179
Pep-179
182 / B
No pep-182
Pep-182
185 / B
No pep-185
Pep-185
190 / B
No pep-190
Peptide-192
191 / A
No pep-191
Pep-191
192 / A
No pep-192
Pep-192
193 / A
No pep-193
Pep-193
194 / A
No pep-194
Pep-194
191 / B
No pep-191
Pep-191
192 / B
No pep-192
Pep-192
193 / B
No pep-193
Pep-193
194 / B
No pep-194
Pep-194
199 / A
No pep-199
Pep-199
212 / A
No pep-212
Pep-212
215 / A
No pep-215
Pep-215
216 / A
No pep-216
Pep-216
199 / B
No pep-199
Pep-199
212 / B
No pep-212
Pep-221
215 / B
No pep-215
Pep-215
216 / B
No pep-216
Pep-216
APC-H
PE-H


219 / A
No pep-219
Pep-219
221 / A
No pep-221
Pep-221
222 / A
No pep-222
Pep-222
228 / A
No pep-228
Pep-228
219 / B
No pep-219
Pep-219
221 / B
No pep-221
Pep-221
222 / B
No pep-222
Pep-222
228 / B
No pep-228
Pep-228
236 / A
No pep-236
Pep-236
244 / A
No pep-244
Pep-244
249 / A
No pep-249
Pep-249
1020007.002 / A
No pep-1020007.002
Pep-1020007
236 / B
No pep-236
Pep-236
244 / B
No pep-244
Pep-244
249 / B
No pep-249
Pep-249
1020007.002 / B
No pep-1020007.002
Pep-1020007
1020008.003 / A
No pep-1020008.003
Pep-1020008
1020012.004 / A
No pep-1020012.004
Pep-1020012
1020019.008 / A
No pep-1020019.008
Pep-1020019
1020020.009 / A
No pep-1020020.009
Pep-1020020
1020008.003 / B
No pep-1020008.003
Pep-1020008
1020012.004 / B
No pep-1020012.004
Pep-1020012
1020019.008 / B
No pep-1020019.008
Pep-1020019
1020020.009 / B
No pep-1020020.009
Pep-1020020
APC-H
PE-H


1020030.012 / A
No pep-1020030.012
Pep-1020030
1020042.017 / A
No pep-1020042.017
Pep-1020042
1020043.018 / A
No pep-1020043.018
Pep-1020043
1020055.024 / A
No pep-1020055.024
Pep-1020054
1020030.012 / B
No pep-1020030.012
Pep-1020030
1020042.017 / B
No pep-1020042.017
Pep-1020042
1020043.018 / B
No pep-1020043.018
Pep-1020043
1020055.024 / B
No pep-1020055.024
Pep-1020055
1020056.025 / A
No pep-1020056.025
Pep-1020056
1020057 / A
No pep-1020057
Pep-1020057
1020058 / A
No pep-1020058
Pep-1020058
1020067 / A
No pep-1020067
Pep-1020067
1020056.025 / B
No pep-1020056.025
Pep-1020056
1020057 / B
No pep-1020057
Pep-1020057
1020058 / B
No pep-1020058
Pep-1020058
1020067 / B
No pep-1020067
Pep-1020067
1020074 / A
No pep-1020074
Pep-1020074
1030002.030 / A
No pep-1030002.030
Pep-1030002
1030007 / A
No pep-1030007
Pep-1030007
1030016 / A
No pep-1030016
Pep-1030016
1020074 / B
No pep-1020074
Pep-1020074
1030002.030 / B
No pep-1030002.030
Pep-1030002
1030007 / B
No pep-1030007
Pep-1030007
1030016 / B
No pep-1030016
Pep-1030016
APC-H
PE-H


1030019 / A
No pep-1030019
Pep-1030019
1030021 / A
No pep-1030021
Pep-1030021
1030022 / A
No pep-1030022
Pep-1030022
1030025 / A
No pep-1030025
Pep-1030025
1030019 / B
No pep-1030019
Pep-1030019
1030021 / B
No pep-1030021
Pep-1030021
1030022 / B
No pep-1030022
Pep-1030022
1030025 / B
No pep-1030025
Pep-1030025
1030026 / A
No pep-1030026
Pep-1030026
1030027 / A
No pep-1030027
Pep-1030027
1030031 / A
No pep-1030031
Pep-1030031
1030033 / A
No pep-1030033
Pep-1030033
1030026 / B
No pep-1030026
Pep-1030026
1030027 / B
No pep-1030027
Pep-1030027
1030031 / B
No pep-1030031
Pep-1030031
1030033 / B
No pep-1030033
Pep-1030033
1030038 / A
No pep-1030038
Pep-1030038
1030064 / A
No pep-1030064
Pep-1030064.4
1030075 / A
No pep-1030075
Pep-1030075.10
1030076 / A
No pep-1030076
Pep-1030076.11
1030038 / B
No pep-1030038
Pep-1030038
1030064 / B
No pep-1030064
Pep-1030064.4
1030075 / B
No pep-1030075
Pep-1030075.10
1030076 / B
No pep-1030076
Pep-1030076.11
APC-H
PE-H

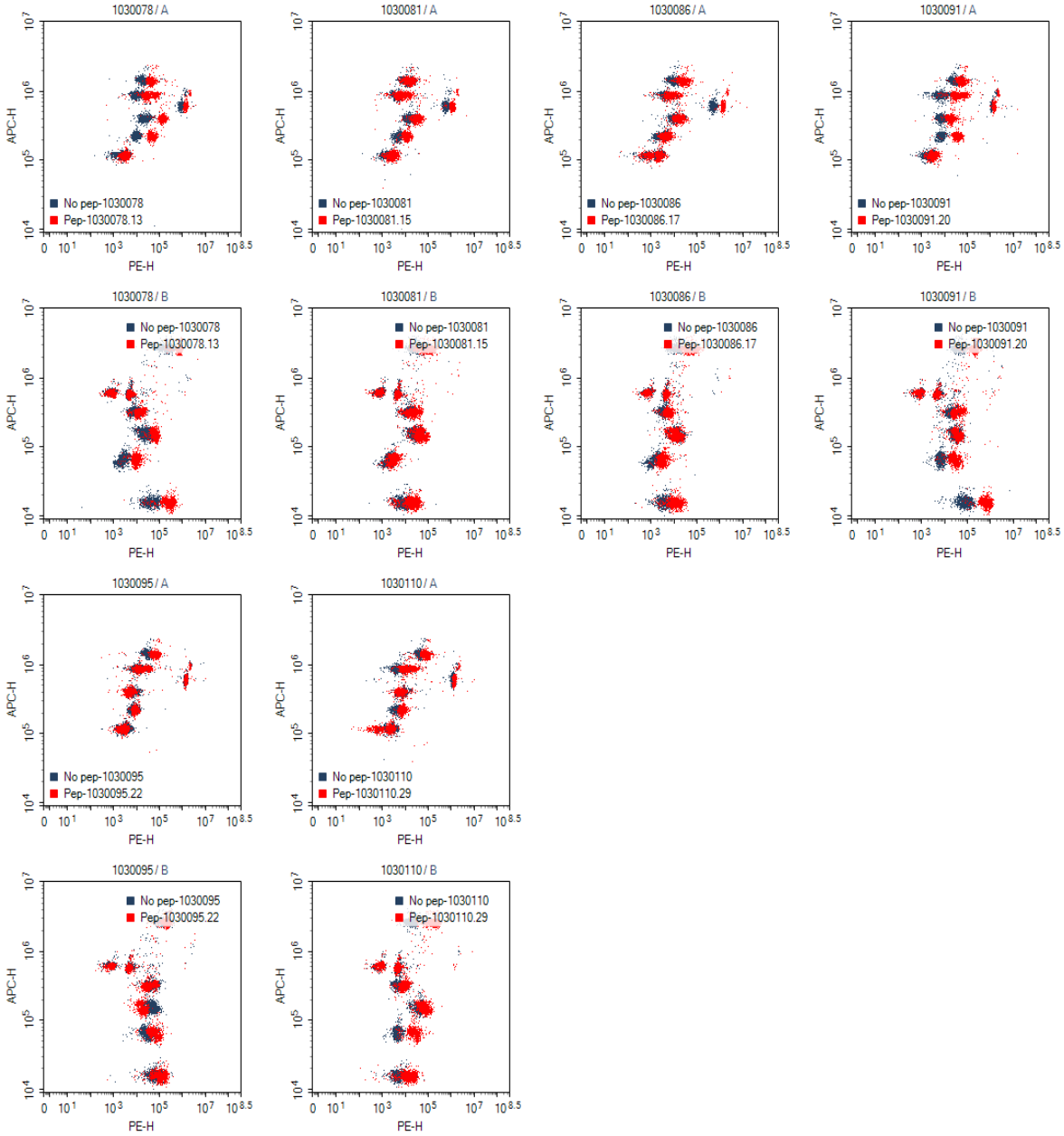


Figure A.6. The PBMCs of the volunteers collected at day 35 after first injection were treated and not treated with SMNO peptide pool for 48 hours and the secretion of IL-10, IL-9, IL-6, IL-2, IL-13, IL-5, IL-22, IL-4, IL-17F, IL-17A, TNF-α and IFN-γ were quqantified using LEGENDplex™ HU Th Cytokine Panel (12-plex) w/ VbP V02 kit. The CBA dot plot overlays for the standards and each volunteer are presented in the figure. The secreted IL-10, IL-9, IL-6, IL-2, IL-13, IL-5 are presented in the A panel while the secreted IL-22, IL-4, IL-17F, IL-17A, TNF-α and IFN-γ are presented in the B panel for each volunteer. The secretion of the respective cytokines for the no peptide treated cells are demonstrated with black while that of peptide treated group is demonstrated with red in each plot.

COPYRIGHT PERMISSIONS

Copy right permission for Figure 1.1

SPRINGER NATURE LICENSE

TERMS AND CONDITIONS

Aug 24, 2022

This Agreement between Miss. Kadriye Tuğçe Bildik ("You") and Springer Nature ("Springer Nature") consists of your license details

and the terms and conditions provided by Springer Nature and Copyright Clearance Center.

License Number 5375491449345

License date Aug 24, 2022

Licensed Content

Publisher

Springer Nature

Licensed Content

Publication

Nature Reviews Immunology

Licensed Content Title The history of Toll-like receptors — redefining innate immunity

Licensed Content Author Luke A. J. O'Neill et al

Licensed Content Date May 17, 2013

Type of Use Thesis/Dissertation

Requestor type non-commercial (non-profit)

Format print and electronic

Portion figures/tables/illustrations

Number of

figures/tables/illustrations

1

High-res required no

Will you be translating? no

Circulation/distribution 200 - 499

Author of this Springer

Nature content

no

Title INVESTIGATION OF CELLULAR AND HUMORAL IMMUNE RESPONSES INDUCED BY SARSCoV-2 VLP VACCINE IN PRE-CLINICAL AND CLINICAL STUDIES

Institution name Bilkent University

Expected presentation

date

Aug 2022

Portions Figure 1: Mammalian TLR signalling pathways.

Requestor Location Miss. Kadriye Tuğçe Bildik

Bilkent University, Science Building

SB Building, 2nd Floor, Department of

Molecular Biology and Genetics

Ankara, 06800

Turkey

Attn: Miss. Kadriye Tuğçe Bildik

Total 0.00 USD

Copyright permission for Figure 1.5

SPRINGER NATURE LICENSE

TERMS AND CONDITIONS

Aug 24, 2022

This Agreement between Miss. Kadriye Tuğçe Bildik ("You") and Springer Nature ("Springer Nature") consists of your license details

and the terms and conditions provided by Springer Nature and Copyright Clearance Center.

License Number 5375500415622

License date Aug 24, 2022

Licensed Content

Publisher

Springer Nature

Licensed Content

Publication

Nature Reviews Molecular Cell Biology

Licensed Content Title Mechanisms of SARS-CoV-2 entry into cells

Licensed Content Author Cody B. Jackson et al

Licensed Content Date Oct 5, 2021

Type of Use Thesis/Dissertation

Requestor type non-commercial (non-profit)

Format print and electronic

Portion figures/tables/illustrations

Number of

figures/tables/illustrations

1

High-res required no

Will you be translating? no

Circulation/distribution 200 - 499

Author of this Springer

Nature content

no

Title INVESTIGATION OF CELLULAR AND HUMORAL IMMUNE RESPONSES INDUCED BY SARSCoV-2 VLP VACCINE IN PRE-CLINICAL AND CLINICAL STUDIES

Institution name Bilkent University

Expected presentation

date

Aug 2022

Portions Fig. 3: Two distinct SARS-CoV-2 entry pathways.

Requestor Location Miss. Kadriye Tuğçe Bildik

Bilkent University, Science Building

SB Building, 2nd Floor, Department of

Molecular Biology and Genetics

Ankara, 06800

Turkey

Attn: Miss. Kadriye Tuğçe Bildik

Total 0.00 USD

Copyright permission for Figure 1.6

ELSEVIER LICENSE

TERMS AND CONDITIONS

Aug 24, 2022

This Agreement between Miss. Kadriye Tuğçe Bildik ("You") and Elsevier ("Elsevier") consists of your license details and the terms

and conditions provided by Elsevier and Copyright Clearance Center.

License Number 5375500614887

License date Aug 24, 2022

Licensed Content

Publisher

Elsevier

Licensed Content

Publication

Cell Host & Microbe

Licensed Content Title Antibody and B cell responses to SARS-CoV-2 infection and vaccination

Licensed Content Author Katharina Röltgen,Scott D. Boyd

Licensed Content Date Jul 14, 2021

Licensed Content Volume 29

Licensed Content Issue 7

Licensed Content Pages 13

Start Page 1063

End Page 1075

Type of Use reuse in a thesis/dissertation

Portion figures/tables/illustrations

Number of

figures/tables/illustrations

1

Format both print and electronic

Are you the author of this

Elsevier article?

No

Will you be translating? No

Title INVESTIGATION OF CELLULAR AND HUMORAL IMMUNE RESPONSES INDUCED BY SARSCoV-2 VLP VACCINE IN PRE-CLINICAL AND CLINICAL STUDIES

Institution name Bilkent University

Expected presentation

date

Aug 2022

Portions Figure 1. Overview of the humoral immune response to SARS-CoV-2

Requestor Location Miss. Kadriye Tuğçe Bildik

Bilkent University, Science Building

SB Building, 2nd Floor, Department of

Molecular Biology and Genetics

Ankara, 06800

Turkey

Attn: Miss. Kadriye Tuğçe Bildik

Publisher Tax ID GB 494 6272 12

Total 0.00 USD